

**STUDIES ON RADIATION INDUCED SYNTHESIS, THERMAL
BEHAVIOR AND APPLICATIONS OF
POLYDIALYLDIMETHYLAMMONIUM CHLORIDE SYSTEM**

By

SANJU FRANCIS

Enrolment No.: CHEM01200604033

Bhabha Atomic Research Centre

Mumbai, India

*A thesis submitted to the
Board of Studies in Chemical Sciences*

*In partial fulfillment of requirements
For the Degree of*

**DOCTOR OF PHILOSOPHY
Of
HOMI BHABHA NATIONAL INSTITUTE**



June, 2014

Homi Bhabha National Institute

Recommendations of the Viva Voce Committee

As members of the Viva Voce Committee, we certify that we have read the dissertation prepared by **Sanju Francis** entitled “**Studies on radiation induced synthesis, thermal behavior and applications of polydiallyldimethylammonium chloride system**” and recommend that it may be accepted as fulfilling the thesis requirement for the award of Degree of Doctor of Philosophy.

Chairman: Prof. R. C. Bindal

Date:

Guide / Convener: Prof. Lalit Varshney

Date:

External Reviewer: Prof. T. K. Chaki, IIT Kharagpur

Date:

Member 1: Prof. Manmohan Kumar

Date:

Member 2: Prof. D. B. Naik:

Date:

Final approval and acceptance of this thesis is contingent upon the candidate's submission of the final copies of the thesis to HBNI.

I/We hereby certify that I/we have read this thesis prepared under my/our direction and recommend that it may be accepted as fulfilling the thesis requirement.

Date:

Signature

Place:

Guide

STATEMENT BY AUTHOR

This dissertation has been submitted in partial fulfillment of requirements for an advanced degree at Homi Bhabha National Institute (HBNI) and is deposited in the Library to be made available to borrowers under rules of the HBNI.

Brief quotations from this dissertation are allowable without special permission, provided that accurate acknowledgement of source is made. Requests for permission for extended quotation from or reproduction of this manuscript in whole or in part may be granted by the Competent Authority of HBNI when in his or her judgment the proposed use of the material is in the interests of scholarship. In all other instances, however, permission must be obtained from the author.

Sanju Francis

DECLARATION

I, hereby declare that the investigation presented in the thesis has been carried out by me. The work is original and has not been submitted earlier as a whole or in part for a degree / diploma at this or any other Institution / University.

Sanju Francis

List of Publications arising from the thesis

Journals

1. "Size tunable synthesis of gold nanoplates by gamma irradiation in presence of polydiallyldimethylammonium chloride as the capping agent", Sanju Francis, J. Nuwad, Alka Gupta, J. K. Sainis, R. Tewari, Nidhi Gupta, D. Mitra and Lalit Varshney, *J. Nano. Res.* (2013) 23: 57.
2. "Sunlight mediated synthesis of PDDA protected concave gold nanoplates", Sanju Francis, J. Nuwad, Alka Gupta, J. K. Sainis, R. Tewari, D. Mitra, Lalit Varshney, *J. Nanopart Res.* (2013) 15:1482.
3. "Radiation-induced grafting of diallyldimethylammonium chloride onto acrylic acid grafted polyethylene", Sanju Francis, B.R. Dhanawade, D.Mitra, Lalit Varshney, Sunil Sabharwal *Radiation Physics and Chemistry* (2009) 78: 42.
4. "Poly(DADMAC) encapsulation in PES microcapsules utilizing gamma radiation", Sanju Francis, Lalit Varshney, Keesari Tirumalesh, Sunil Sabharwal, *Radiation Physics and Chemistry* (2009) 78: 57.
5. "Thermogravimetric Approach for Determining the Degree of Conversion in Radiation-Polymerized DADMAC", Sanju Francis, Lalit Varshney, Debasish Mitra, Sunil Sabharwal *Journal of Applied Polymer Science*, (2009) 111: 668.
6. "Thermal degradation behavior of radiation synthesized polydiallyldimethylammonium chloride", Sanju Francis, Lalit Varshney, Sunil Sabharwal, *European Polymer Journal* (2007) 43: 2525.

Conferences

1. “Gamma radiolytic synthesis of gold nanoplates in presence of polydiallyldimethylammonium chloride as the capping agent”, Sanju Francis, J. Nuwad , Alka Gupta , J. K. Sainis, D. Mitra, Lalit Varshney, NSRP 2013, March 20-22, Shillong.
2. “A new thermogravimetric approach for determining the degree of conversion in radiation polymerized DADMAC”, Sanju Francis, Lalit Varshney, Debasish Mitra, Sunil Sabharwal, THERMANS 2008, February 4-7, IGCAR, Chennai.
3. “Radiation synthesis and characterization of polydiallyldimethylammonium chloride”, Sanju Francis, Lalit Varshney and Sunil Sabharwal, NSRP 2007, January 29-31, University of Madras, Chennai.
4. “Radiation cyclopolymerization of diallyldimethylammonium chloride”, Sanju Francis, Lalit Varshney and Sunil Sabharwal, PHOTORADCHEM 2007, February 8-11, Mahatma Gandhi University, Kottayam, Kerala.

Dedicated to my Family

ACKNOWLEDGEMENTS

I express my sincere gratitude to my research guide Dr. Lalit Varshney, Professor HBNI and Head, Radiation Technology Development Division, Bhabha Atomic Research Centre, for his valuable guidance, keen interest and good wishes not just during the course of the thesis work but throughout my entire research career. During the last year or so, when things started slowing down considerably, Prof. Varshney was a steady source of motivation much needed to put the pieces of the work together in the final shape, within the time limit. I also thank him for critically reviewing the thesis and making it better by suggesting relevant changes.

Deepest gratitude is also due to the members of the supervisory committee Dr. Manmohan Kumar and Dr. D. B. Naik for providing suggestions to improve the thesis. I wish to thank Dr. Sunil Sabharwal, former Head of the Division, for constantly supporting and encouraging the work, during his tenure in B.A.R.C.

I thank all my colleagues of the division and ISOMED, especially Dr. Y. K. Bhardwaj, D. Mitra, Dr. A. K. Dubey, Dr. Virendra Kumar, B. R. Dhanawade, N. K. Goel, Amit Srivastav and J. R. Rathod for the support and assistance rendered from time to time.

I owe a lot to my parents for the support and unconditional love bestowed on me that has gone a long way in helping me achieve many milestones in life; this thesis for doctorate is one of them.

I thank my wife Shilpa, for being by my side all along, through thick and thin and; thanks to my kids, Aditya and Atulya for being a great source of joy every day.

CONTENTS

	Page No.
SYNOPSIS	xv-xxx
LIST OF FIGURES	xxxi-xxxvii
LIST OF TABLES	xxxviii
LIST OF SCHEMES	xxxix
Chapter 1: INTRODUCTION AND LITERATURE SURVEY	1-34
1.1 General Introduction	1
1.2 Interaction of ionizing radiation with matter	4
1.2.1 Interaction of electromagnetic radiation	4
1.2.2 Interaction of charged particles	6
1.2.2.1 Electrons	6
1.2.2.2 Heavy charged particles	7
1.2.3 Interaction of Neutrons	7
1.2.4 Distribution of active species in the system – track structure	8
1.2.5 Radiation-chemical yield	9
1.2.6 Radiation dosimetry	9
1.2.7 Absorbed dose in samples	10
1.3 Radiation chemistry of water	10
1.3.1 Primary yields	13
1.3.2 Important reducing radicals in aqueous solutions	13
1.3.3 Important oxidizing radicals in aqueous solutions	15
1.4 Radiation effect on monomers	16
1.5 Radiation effects on polymers	18
1.5.1 Crosslinking and degradation of polymers	18
1.5.2 Radiation induced graft polymerization	19

1.5.2.1	Types of radiation induced grafting polymerization	20
1.5.2.2	Advantages of radiation grafting over other grafting techniques	21
1.6	Polyelectrolytes	21
1.7	Techniques for studying transient species	22
1.8	Principle of pulse radiolysis	23
1.9	Radiolytic synthesis of nanoparticles	24
1.9.1	Role of capping agent in stabilization of nanoparticle colloid system	25
1.9.1.1	Types of Stabilization	26
1.9.1.2	Size and shape control of nanoparticles	27
1.10	Thermal analysis and characterization of polymer	27
1.10.1	Thermogravimetric analysis	28
1.10.2	Differential scanning calorimetry	29
1.11	Literature review	29
1.12	Thesis Overview	31
	Chapter 2: EXPERIMENTAL	35-65
2.1	Introduction	35
2.2	Gamma radiation sources	35
2.2.1	Gamma radiation dosimetry	37
2.3	Pulse radiolysis setup	39
2.3.1	LINAC	40
2.3.2	Kinetic spectrophotometer	41
2.3.3	Analysis of the recorded signal	42
2.3.4	Dosimetry for Pulse radiolysis	42
2.4	Transmission electron microscopy	44
2.4.1	Selected Area Electron Diffraction	45

2.5 Scanning electron microscopy	46
2.5.1 Scanning and image formation	47
2.6 Energy-dispersive X-ray spectroscopy	48
2.7 X-Ray Diffraction	50
2.8 Atomic force microscopy	52
2.8.1 Imaging modes	53
2.8.1.1 Contact mode	53
2.8.1.2 Non-contact mode	54
2.8.1.3 Tapping mode	55
2.9 UV-Visible Absorption Spectroscopy	55
2.10 Fourier transform infrared spectroscopy	57
2.11 Ion chromatography	59
2.12 Differential scanning calorimetry	61
2.13 Thermogravimetric analysis	64
Chapter 3: Radiation synthesis of PDADMAC and its characterization	66-92
3.1 Introduction	66
3.2 Pulse radiolysis studies of DADMAC and PDADMAC	70
3.2.1 Kinetic treatment of the experimental pulse radiolysis data	71
3.2.2 Pulse radiolysis of DADMAC in aqueous solutions	73
3.2.2.1 Reaction of OH radical with DADMAC	74
3.2.2.2 Reaction of e_{aq}^- with DADMAC	77
3.2.3 Pulse radiolysis of PDADMAC in aqueous solution	78
3.2.3.1 Reaction of OH radical with PDADMAC	78
3.2.3.2 Reaction of e_{aq}^- with PDADMAC	79
3.3 Steady state irradiation of DADMAC solution	79
3.3.1 Effect of radiation dose on the polymerization of DADMAC	80
3.3.2 Determination of molecular weight of PDADMAC	81

3.3.3 Cyclopolymerization	83
3.3.4 Characterization of PDADMAC	85
3.3.4.1 FTIR Spectroscopy	86
3.3.4.2 UV-Visible spectroscopy	87
3.3.4.3 H-NMR analysis of PDADMAC	87
3.3.4.4 ¹³ C-NMR analysis of PDADMAC	88
3.4 Conclusions	91
Chapter 4: Thermal analysis of DADMAC, PDADMAC and method to determine the degree of conversion of DADMAC to PDADMAC	93-119
4.1 Introduction	93
4.2. Experimental	94
4.2.1 Materials	94
4.2.2 Thermogravimetric analysis	94
4.2.3 Differential scanning calorimetry	95
4.3 Part I: Thermal degradation behavior of radiation synthesized PDADMAC	96
4.3.1 Kinetic analysis	96
4.3.2 TG and DTG analysis	98
4.3.3 DSC evaluation	100
4.3.4 Comparison of TG and DSC results	103
4.3.5 TG and DSC simulation	104
4.4 Part II: Thermogravimetric method for determining the degree of conversion in radiation polymerized DADMAC	107
4.4.1 Calibration Curve	108
4.4.2 Results and discussion	109
4.4.2.1 DSC Analyses	109
4.4.2.2 TG Analyses	111

4.5. Conclusions	118
Chapter 5: Immobilization of PDADMAC by radiation induced grafting and radiolytic encapsulation in microcapsules	120-146
5.1 Introduction	120
5.2. Part I: Radiation induced grafting of PDADMAC onto polyethylene	121
5.2.1 Experimental	122
5.2.1.1 Materials	122
5.2.1.2 Grafting procedure	122
5.2.1.2.1 Acrylic acid grafting onto PE	123
5.2.1.2.2 Diallyldimethylammonium chloride grafting onto AA-g-PE (DADMAC-g-AA-g-PE)	124
5.2.2 Characterization	124
5.2.2.1 Grafting Yield	124
5.2.2.2 Equilibrium degree of swelling	124
5.2.2.3 Thermogravimetric analysis	125
5.2.2.4 FT-IR spectra of the films	125
5.2.3 Results and discussion	125
5.2.3.1 Grafting yield	127
5.2.3.2 Degree of conversion of the carboxyl group to its carboxylate anion and DADMAC grafting	129
5.2.3.3 Swelling studies	131
5.2.3.4 Effect of dose rate	132
5.2.3.5 FT-IR of the films	133
5.2.3.6 Thermogravimetric analysis	134
5.3 Part II: Gamma radiolytic encapsulation of PDADMAC in PES microcapsules	136
5.3.1 Experimental	137

5.3.1.1 Material	137
5.3.1.2 Degree of conversion	138
5.3.1.3 Molecular weight determination	138
5.3.1.4 Instrumentation	138
5.3.2 Results and discussion	139
5.4 Conclusions	145
Chapter 6: PDADMAC as the capping agent for synthesis of gold nanoplates	147-177
6.1 Introduction	147
6.2 Experimental	151
6.3 Part I: Size tunable synthesis of gold nanoplates by gamma irradiation in presence of PDADMAC as the capping agent	151
6.3.1 Synthesis of gold nanoplates	152
6.3.2 Results and discussion	153
6.3.3 Probable mechanism of nanoplate formation	160
6.4 Part II: Photochemical synthesis of concave gold nanoplates employing PDADMAC as the capping agent	165
6.4.1. Synthesis of concave gold nanoplates	167
6.4.2. Results and discussion	167
6.4.2 Probable mechanism of concave nanoplate formation	174
6.5 Conclusions	177
REFERENCES	178-191

SYNOPSIS

Polyelectrolytes are polymers which possess ionizable groups that develop substantial charge when dissolved or swollen in a highly polar solvent like water. In recent years, polyelectrolytes have been subject of increased research efforts due to their versatile commercial applications in various fields. Among the polyelectrolytes, polydiallyldimethylammonium chloride (PDADMAC), a cationic polyelectrolyte and its copolymers have found lot of practical utility and applications [1-5], for instance; it is used as flocculant and coagulant in water treatment, as ion exchange resin, in cosmetic and personal care industries, biology and medicine, in food industry and in membrane technology. Another interesting aspect of DADMAC is the mode by which it undergoes polymerization to form the polymer. Allyl monomers are generally considered as poor monomers for radical polymerization, since chain transfer reactions take place readily by abstraction of allylic hydrogens of the monomer by the propagating radical which leads to the formation of a resonance-stabilized radical species, decreasing the polymerization efficiency and the molecular weight of the polymer. However, in contrast to monoallyl monomers, free radical polymerization of diallyl monomers like DADMAC proceeds efficiently via intra-intermolecular polymerization, which is now referred to as cyclopolymerization, to yield a water soluble linear polymer. The polymer formed contains almost exclusively five-membered rings despite the fact that these five-membered rings are thermodynamically less stable than six-membered rings [6-8].

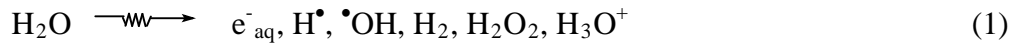
Radiation processing is now a well established commercial method for precisely modifying the properties of polymers and polymeric composites systems [9, 10]. Using ionizing radiation for processing polymers has some unique benefits over conventional chemical processes which mainly rely on heat treatment. In chemical processing, most of the

time the formulations used contains additives which may adversely affect the environment. In contrast, radiation processing of polymers is a green technology because no catalyst or additives are required and the process takes place conveniently at room temperature. Ionizing radiation initiated chemical reactions in polymers like crosslinking, chain scission, oxidation and grafting have resulted in many useful applications in a great variety of polymeric materials [11] such as hydrogels for wound dressing, crosslinked wires and cables, heat shrinkable materials with shape memory effect, polyethylene foams, polymer grafted membranes and conducting polymers. Ionizing radiation significantly improves or modifies important properties of polymers, such as mechanical strength, thermal stability, processability, chemical resistance, surface properties etc. and due to these advantages industries have adopted this technology on large scale.

Although a large number of polymers are processed by radiation for various applications, there is very little information available about the interaction of high energy radiation with DADMAC or PDADMAC and most of the reported work is limited to conventional chemical modification or processing. Considering the interesting chemical structure of DADMAC, its polymerization chemistry and scope for novel applications, it is essential to understand the effects of ionizing radiation to make significant progress in radiation processing of this system. In the thesis, gamma radiation effect on DADMAC and its polymer, immobilization of PDADMAC for potential applications and PDADMAC assisted synthesis of gold nanoplates were investigated. Detailed thermal characterization of DADMAC and radiation synthesized PDADMAC were also carried out. Efforts have been made to get an insight about the underlying mechanisms and develop processes and products having prospective applications.

Water is the most important common solvent for highly polar polymers like PDADMAC and its monomer. When dilute aqueous solution of monomer or polymer is

exposed to radiation, since water is the major component, energy of the ionizing radiation is absorbed predominantly by water molecules and the effects produced are indirectly caused by the transient species (Eqn. 1) generated by the radiolysis of water rather than the direct effect of radiation on the dissolved species.



The transient species generated are important because they initiate polymerization of monomers and in case of polymers, crosslinking and degradation is also brought about by the mediation of these transients. Since the lifetime of the transients are extremely short, their reactivity with solutes needs to be studied by fast monitoring techniques like pulse radiolysis [12]. Although, the concentration of monomer/ polymer used for polymerization or crosslinking is different than that employed for pulse radiolysis, the technique gives fairly good idea about the kinetics of polymerization and crosslinking/ degradation behavior of the polymer. The work described in this thesis includes the pulse radiolysis study of DADMAC and PDADMAC in aqueous solutions wherein the reactivity of e^-_{aq} and $\bullet\text{OH}$ with the monomer and polymer was studied. In addition to the reactions of the transients during irradiation, it is also essential to understand the ultimate effect produced on the monomer/ polymer system after exposure to radiation. Therefore, the polymerization of DADMAC in aqueous solutions was investigated under steady state conditions using gamma radiation.

PDADMAC contains the quaternary ammonium group which is known to exhibit excellent ion exchange capacity for anions in solution. However, it is practically difficult to separate the polymer from the solution after ion exchange reactions because of its exceptionally high water solubility. This limitation can be circumvented or avoided if a water insoluble matrix like PDADMAC hydrogel, PDADMAC grafted membranes or PDADMAC encapsulated polymer beads are employed for ion exchange. Radiation induced grafting [13,

14] is a simple, effective and promising technique for the development of novel materials for a variety of applications. In this process, ionizing radiation produces macro radicals on the base polymer which subsequently initiates the growth of polymer chains with desired functional characteristics. The base polymer provides appropriate dimensional, physical and chemical stability to the matrix under the conditions of actual use. A part of the thesis investigates the radiation induced grafting of PDADMAC onto the surface of polyethylene (PE). Mutual radiation induced grafting studies of DADMAC onto PE surface did not give satisfactory results even when grafting enhancing additives was used. Therefore a novel radiolytic approach was developed and adopted which consisted of two grafting steps. In the process, first of all PE film was modified by grafting acrylic acid (AA) through mutual radiation grafting method and the film thus obtained was subjected to analogous grafting reaction of DADMAC, to give a DADMAC-g-AA-g-PE film. The grafted film due to the presence of quaternary ammonium group may find application for extraction and separation of ions.

Polymers in the form of microcapsules have interesting characteristics and have found various applications in medicine, pharmaceuticals and engineering [15-17]. Microcapsules containing extracting agents are being tried for new applications like ion extraction because of enhanced efficiency and better extraction kinetics. A radiolytic procedure was developed for immobilization of PDADMAC in the core of poly ether sulfone (PES) microcapsule for use as an ion exchanger. Ion chromatography study of the PDADMAC loaded microcapsules revealed that the microcapsules could extract and exchange representative anions such as F⁻, Cl⁻, Br⁻, NO₃²⁻ and SO₄²⁻ at relatively low concentration indicating its potential for large scale ion exchange applications.

Gold nanoparticles are of great scientific interest because of their unique physical and chemical properties, biocompatibility, as well as promising applications in diverse areas like

biology, medicine, plasmonics, electronics and catalysis. Nanoparticles of the same composition but having different shapes exhibit significantly different chemical reactivity and physical properties [18]. Therefore, controlling the shape is very important and provides an additional dimension to fine tune the properties of nanoparticles. Polymeric capping agents, apart from stabilizing the nanoparticle colloidal system, exert a profound influence on the size and shape of the nanoparticles by selectively interacting on the surface of the seeds through certain functional groups during the growth process. In this thesis, the possibility of employing PDADMAC as a capping agent for the size and shape selective synthesis of gold nanoparticles was explored. PDADMAC, the capping agent employed in the study contains the quaternary ammonium group which can interact on the {111} facet of the growing seed. By judiciously tuning the experimental conditions gold nanoplates having triangular and hexagonal morphology could be synthesized in abundant yield with good control over the size distribution. These nanoplates find applications in various fields like catalysis, biosensors, bio-diagnostics, photoluminescence, surface enhanced Raman scattering and imaging [19, 20]. A photochemical method was also developed for the synthesis of gold nanoplates using PDADMAC as the shape controlling capping agent. In addition to the regular nanoplates, rare concave gold nanoplates were also synthesized in high yield by adjusting the reaction conditions. These concave nanoplates are reported to show enhanced catalytic activity compared to their flat counterparts.

The thermal behavior of a polymer is one of the important criterions that decide the choice of a polymer for a particular application. The melting point of a polymer, decomposition temperature, glass transition temperature etc. are of some of the main characteristic of the polymer that determines the usable temperature range of the polymer. Therefore, the determination of these parameters is essential from a practical point of view and thermal analysis is one of the best techniques which provide accurate and reliable

information about the parameters. A detailed thermal analysis is useful for accurate estimation of polymer in a composite or a blend formulation and can also provide insights into the decomposition kinetics and predict the lifetime of the material at different temperatures. In this study, thermal investigation was carried out on radiation polymerized PDADMAC and important kinetic parameters like order of reaction, activation energy and pre-exponential factor was determined. Based on the insight gained from the above study, a thermogravimetric method was developed to determine the degree of conversion of DADMAC to PDADMAC during the gamma radiation induced polymerization.

The thesis is divided into six chapters and brief chapter wise description of the work is as follows:

Chapter 1: INTRODUCTION

In the chapter a brief introduction of polymers with special mention about polyelectrolytes is given. The fundamentals of radiation chemistry of water and interaction of radiation with matter are discussed with an emphasis laid on the interaction of radiation with monomers and polymers. The principle of pulse radiolysis, a fast monitoring technique used for studying the basic reactions of transients formed on radiolysis of water, is briefly discussed. The basic aspects of radiation induced grafting procedures and their advantages over conventional methods are included in the chapter. Radiolytic process for synthesis of nanoparticles, the role of capping agent for stabilization of the system and its importance in controlling the size and shape of nanoparticles is discussed. The importance of thermogravimetric analysis (TGA) and differential scanning calorimetry (DSC) in the analysis of polymers are also discussed.

Chapter 2: EXPERIMENTAL

The principles and instrumentation of the various techniques and facilities employed in the present studies is described in this chapter. These include description and use of ^{60}Co gamma radiation chamber for steady-state irradiation studies and pulse radiolysis technique for characterization of transients generated as a result of water radiolysis. Many techniques employed for the characterization of nanoparticles like transmission electron microscopy (TEM), scanning electron microscopy (SEM), energy dispersive X-rays analysis (EDX), atomic force microscopy (AFM) and X-ray diffraction (XRD) are described in the chapter. Other techniques such as Fourier transform infrared spectroscopy (FTIR), ion chromatography, UV-visible spectroscopy, DSC and TGA are also described in this chapter.

Chapter 3: Radiation synthesis of PDADMAC and its characterization

Nanosecond pulse radiolysis technique was employed for investigating the reactions of radiolytic products of water (e_{aq}^- and $\bullet\text{OH}$) with the DADMAC and PDADMAC during early stages of reaction. The rate constant for reaction with hydrated electrons (e_{aq}^-) was calculated by following the decay of hydrated electron at 700 nm, at different concentrations of the solute, while, rate constants for the reactions of OH radical with the monomer and polymer were evaluated by competition kinetics method, using SCN^- as a reference solute because the transient formed in reaction of $\bullet\text{OH}$ with DADMAC and PDADMAC did not show absorbance above 270 nm. The reaction of e_{aq}^- with DADMAC was studied by pulse radiolysing the N_2 saturated aqueous solution of $1.0 \times 10^{-3} \text{ mol dm}^{-3}$ DADMAC at near neutral pH containing 0.3 mol dm^{-3} *t*-butanol using 50 ns electron pulse. From the decay rate of e_{aq}^- at 700 nm in the presence of solute, the bimolecular rate constant for the reaction was found to be $3.4 \times 10^9 \text{ dm}^3 \text{ mol}^{-1} \text{ s}^{-1}$. Similarly the bimolecular rate constant for the reaction of e_{aq}^- with PDADMAC was determined to be $4.4 \times 10^{10} \text{ dm}^3 \text{ mol}^{-1} \text{ s}^{-1}$. The rate constant of $\bullet\text{OH}$ with DADMAC and PDADMAC was calculated to be $7.4 \times 10^9 \text{ dm}^3 \text{ mol}^{-1} \text{ s}^{-1}$ and $8.1 \times 10^{10} \text{ dm}^3 \text{ mol}^{-1} \text{ s}^{-1}$ respectively.

It was observed that the monomer undergoes radiation induced polymerization to yield PDADMAC under steady state conditions and the extent of polymerization was determined gravimetrically by precipitating and weighing the polymer. The % polymerization of the DADMAC increases steadily with the increase in the radiation dose up to a dose of about 40 kGy (80 -90 %) after which it levels off. The molecular weight of the synthesized polymer was determined by viscometry. Intrinsic viscosity of the polymers measurements were carried out in 1 M NaCl solution and the viscosity-average molecular weights were calculated using the Mark – Houwink – Sakurada equation. The molecular weight (M_v) was found to increase from 2.57×10^4 (at 5.5 kGy) to 4.65×10^4 (at 27.8 kGy). The molecular weight of the polymer synthesized was found to be an order of magnitude lower than that of commercially available polymer. This is probable because at high absorbed dose degradation of the polymer may predominate even though both crosslinking and degradation occurs simultaneously in the system. The purified polymer was also characterized by IR, $^1\text{H-NMR}$ and $^{13}\text{C-NMR}$ techniques which confirmed the formation of five membered rings in the polymer structure.

Chapter 4: Thermal analysis of DADMAC, PDADMAC and method to determine the degree of conversion of DADMAC to PDADMAC

This chapter is divided into two parts. The first part deals with the TGA and DSC investigations on DADMAC and radiation polymerized PDADMAC. The second part describes a thermogravimetric method for determining the degree of conversion of monomer to polymer.

4.1. Thermal degradation behavior of radiation synthesized PDADMAC

Some applications of polymer may require its use at a temperature lower or higher than room temperature. The determination of kinetic parameters associated with the degradation has a lot of practical significance as the evaluation of the parameters helps in

predicting the thermal behavior of a polymer at other temperatures. In this chapter, the kinetic parameters (order of the reaction, activation energy and the pre-exponential factor) of PDADMAC degradation was evaluated from a single Thermogravimetric (TG) or differential scanning calorimetric (DSC) scan. The polymer was found to undergo thermal degradation in two stages. The first stage showed a weight loss of 33 % and the second stage showed a weight loss of 67 %. The DSC thermogram shows two endothermic peaks corresponding to the two stages in the TG thermogram and the experimental enthalpy change associated with the first and second stages were 650 Jg^{-1} and 129.5 Jg^{-1} respectively. The n^{th} order kinetic parameters (order of the reaction, activation energy and the pre-exponential factor) were determined from a single dynamic DSC or TG thermoanalytical curve. Theoretical TG and DSC thermograms derived from the calculated kinetic parameters were in good agreement with the experimental ones at the heating rate employed.

4.2. A thermogravimetric method for determining the degree of conversion in radiation polymerized DADMAC

Although, PDADMAC is one of the most commercially important quaternary ammonium polymers, not many methods have been reported for determining the degree of conversion in DADMAC polymerization. The degree of conversion of DADMAC is usually studied by classical gravimetry or by using the ^1H NMR technique.⁶ In gravimetry, the polymer is precipitated by adding a non solvent, preferably acetone or isopropanol and the polymer is separated, dried and weighed but the method is prone to experimental error. ^1H NMR gives accurate and reproducible results, but requires expensive instruments and careful sample preparation in D_2O . Also the rate of polymerization of the monomer may differ in D_2O and H_2O .

In this chapter, a convenient method to determine the degree of conversion of DADMAC to PDADMAC using dynamic thermogravimetry is reported. The monomer

solution, exposed to different radiation dose (different degree of conversion), was removed from the radiation field and TGA runs were taken. The conversion degree of the monomer to the polymer was determined from a calibration plot generated previously using different known DADMAC/ PDADMAC ratios. One of the main advantage of the method is that the concentration of the polymer or monomer could be directly determined without their separation. The concentration of monomer and polymer in the mixture was estimated by measuring the weight loss corresponding to the steps involved in the thermograms. By employing the method, polymerization of DADMAC as a function of irradiation dose was studied. The degree of conversion of DADMAC increases considerably during the initial stages of irradiation, up to a dose of 40 kGy, after which the conversion is not significant.

Chapter 5: Immobilization of PDADMAC by radiation induced grafting and radiolytic encapsulation in microcapsules

Two different procedures were adopted for the immobilization of PDADMAC and are described below:

5.1. Radiation induced grafting of PDADMAC onto polyethylene

Part of this chapter discusses gamma radiation induced grafting of DADMAC onto polyethylene (PE). The direct grafting of DADMAC onto the surface of PE in the presence of different additives like salts (NaCl, ZnCl₂ and LiCl), ammonia, acids, surfactants, Mohr's salt etc were tried, but no noticeable grafting was observed even at high absorbed dose (> 50 kGy). Therefore, an indirect approach was adopted wherein grafting was carried out in two steps. PE film was initially functionalized by grafting acrylic acid (AA), through a mutual radiation grafting method. The AA-g-PE film thus obtained was subjected to an analogues radiation grafting reaction of DADMAC, to give a DADMAC-g-AA-g-PE film. The influence of different parameters, such as the extent of acrylic acid grafting, DADMAC

concentration, absorbed dose and dose rate on the grafting yield of DADMAC was investigated. Grafting was confirmed by gravimetry and under optimized conditions; DADMAC could be grafted to a maximum extent of 30 %. The grafted samples were characterized by IR spectroscopy, TGA and DSC.

5.2. Gamma radiolytic encapsulation of PDADMAC in PES microcapsules

In second part of this chapter, a radiolytic method for encapsulating PDADMAC in the core of a preformed hollow polyether sulfone (PES) microcapsule, for the extraction of anions from aqueous solutions is described. DADMAC monomer was introduced inside the porous microcapsules by equilibrating in excess 3 M monomer solution and then polymerization was initiated by irradiation (8.8 kGy), to trap the polymer formed inside the capsule. The hollow capsules are permeable to water, ions and low molecular weight monomers but impermeable to high molecular weight polymers. When the Stokes radius of the polymer formed is more than the pore size of the microcapsule, it remains trapped in the core of the microcapsule. The microcapsules were washed in deionized water to remove unreacted DADMAC and low molecular weight PDADMAC. The polymer in the core was converted to its hydroxide form (PDADMA-OH) by equilibrating in excess of NaOH solution and used for the anion exchange studies. Ion chromatography studies showed that the resultant microcapsule was able to take up and exchange some anions (F^- , Cl^- , Br^- , NO_3^{2-} and SO_4^{2-}) at relatively low concentrations. The viscosity average molecular weight of PDADMAC formed in the core of the PES microcapsule was determined to be 2.8×10^4 and the degree of conversion of the monomer was gravimetrically determined to be 0.4 (40 %).

Chapter 6: PDADMAC as the capping agent for synthesis of gold nanoplates

In this chapter, two methods for the synthesis of gold nanoplates using PDADMAC as a capping agent are described.

6.1. Size tunable synthesis of gold nanoplates by gamma irradiation in presence of PDADMAC as the capping agent

The synthesis of nanoparticles by gamma irradiation is a simple green process because external reducing agents are not required and the reduction is brought about by the transient species, e^-_{aq} and $H\cdot$, generated by radiolysis of water. However, it is difficult to control the shape of the nanoparticles and usually spherical or irregular nanoparticles are produced. In the first part of this chapter, we report a gamma irradiation strategy for the synthesis of single crystal gold nanoplates by employing PDADMAC as the capping agent. The capping agent is believed to play a crucial role in controlling the shape of nanoparticles by adsorbing preferentially or selectively on particular facets of the growing seeds and PDADMAC, used in our study is reported to preferentially adsorb on the {111} surface of gold with its quaternary ammonium head group [21-23]. It binds to the {111} plane of the radiolytically generated seeds and blocks access to this surface and hence, further reduction of Au^{3+} or growth has to take place along other directions, mainly $\langle 110 \rangle$, resulting in the formation of nanoplates. SEM and TEM investigations revealed that the nanoplates had hexagonal and triangular shapes. XRD pattern of the nanoplates showed an extremely strong diffraction peak at 38.2° . No other peaks were observed in the entire scanning range suggesting that the nanoplates are single crystal fcc gold bound by {111} lattice planes. SAED pattern obtained by aligning the electron beam perpendicular to the plane of a hexagonal nanoplate confirmed that the gold nanoplates are single crystals with fcc structure and which are bound by {111} lattice planes on the top and bottom. The nanoplates were also characterized by EDX and XPS. The method reported herein, does not require seeds or surfactants and the reduction occurs at room temperature. Importantly, the size of the nanoplates could be controlled from 500 nm to 5 μm by adjusting the concentration of Au^{3+} and PDADMAC in the solution. Also,

the dose rate was found to significantly affect the shape of the gold nanoparticles, with low dose rate favoring the formation of nanoplates.

6.2. Photochemical synthesis of concave gold nanoplates employing PDADMAC as the capping agent

Concave nanoplates reveal fascinating properties and shows immense potential for applications, especially in the field of catalysis [24, 25]. However, it is difficult to produce nanoplates in an oxidative environment because the twinned seeds or seeds with stacking faults, considered crucial for the formation of nanoplates, have lower stability and undergoes oxidative dissolution very easily in the solution. In second part of this chapter, a method is described to circumvent this limitation by using a suitable capping agent that selectively protects the twinned seeds and facilitates its anisotropic growth. A photochemical (sunlight) irradiation strategy was developed for the synthesis of concave gold nanoplates, employing PDADMAC as the capping agent. By using sunlight as a reducing agent, and thereby eliminating the use of chemical reducing agents, we are at least a step closer to a green synthetic procedure for preparing nanocrystals. As mentioned before, PDADMAC selectively binds to the {111} facet of the twinned seeds and directs or controls the growth anisotropically, while the Cl^- released from PDADMAC, along with the dissolved oxygen present in the solution, aids oxidative etching resulting in the formation of nanoplates with concave surfaces. SEM and TEM studies revealed that the nanoplates had hexagonal and triangular shapes with an edge length of about 15 μm . The contrast of the electron microscope images suggested a thickness gradient across the nanoplate which was confirmed by AFM imaging. The thickness at the edge was about 40 nm, which progressively decreased towards the centre where the thickness was about 10 nm. The fcc structure of the nanoplates were confirmed from XRD and SAED studies. The elemental composition of the nanoplates determined by EDX revealed that the nanoplates are entirely composed of Au and are

stabilized by PDADMAC. The nanoplates were also characterized by XPS, which indicated the complete reduction of gold.

Summary

This thesis reports the effect of ionizing radiation on DADMAC/ PDADMAC system with a focus on the development of process or product having prospective applications in various fields. The fundamental effect of radiation in generating the transient species of water radiolysis and the subsequent reactions of the transients with DADMAC and PDADMAC were investigated. The radiation induced cyclopolymerization of DADMAC in aqueous system was also confirmed by analyzing and characterizing the polymer synthesized under the conditions of the experiment. The immobilization of PDADMAC for potential applications like ion exchange was achieved by two techniques, namely, radiation induced grafting and radiolytic encapsulation in polymer microcapsules. DADMAC was successfully grafted onto PE by employing a two step procedure and many of the parameters that exert a strong influence on the grafting yield were investigated. A radiolytic process was also developed for immobilization of PDADMAC in the core of preformed PES microcapsule and the resultant microcapsule was able to take up and exchange some anions at relatively low concentrations. A gamma irradiation method was developed for synthesis of 'excellent' size tunable gold nanoplates employing PDADMAC as the capping agent, without the need of any chemical reducing agent. The size of the nanoplates could be easily controlled by varying the ratio of gold precursor and PDADMAC in solution. Using PDADMAC as the capping agent, a novel photochemical method was also developed for synthesis of *concave* nanoplates which could have potential applications in catalysis. The thesis provides an insight about the underlying mechanism of the various processes mentioned above. Thermal behavior of DADMAC and gamma radiation synthesized PDADMAC were investigated using TGA and DSC techniques. Besides estimation of shelf life of the polymer at different temperature, a

convenient thermogravimetric method was developed to determine the degree of conversion of DADMAC to PDADMAC during the gamma radiation induced polymerization.

References

- [1] Menlo Park. (1983) Chemical economics handbook. Stanford Research Institute, 581.
- [2] Ottenbrite R.M, Ryan W.S Jr. (1980) Ind Engng Chem Prod Res Dev., 528.
- [3] Butler G.B. (1992) Cyclopolymerization and Cyclocopolymerization. New York: Marcel Dekker.
- [4] McCormick C.L. (1996) J Polym Sci., 34, 913.
- [5] Wandrey C, Hunkeler D. (1999) Adv .Polym. Sci. 145, 123.
- [6] Butler G.B. (2000) J Polym Sci Part A: Polym Chem., 38, 3451.
- [7] Matsumoto A. (2001) Prog.Polym. Sci., 26, 189.
- [8] Hoover M.F. (1970) J Macromol Sci Chem A., 4, 1327.
- [9] Makuuchi K, Cheng S. (2011) Radiation Processing of Polymer Materials and Its Industrial Applications. John Wiley and Sons, New York.
- [10] Andrzej G.C, Mohammad H.S, Shamshad A. (2005) NimB. 236, 44.
- [11] Wood R.J, Pikaev A.K. (1994) .Applied radiation chemistry: Radiation processing, John Wiley & Sons Inc.
- [12] Tabata Y. (Eds.) (1991) Pulse radiolysis. CRC Press, Boca Raton.
- [13] Bhattacharya A, Misra B.N. (2004) Prog.Polym. Sci., 29 767.
- [14] Garnett J.L. (1979) Radiat. Phys. Chem.,. 14, 79.

- [15] Benita S. (1996) *Microencapsulation: Methods and Industrial Applications*. Marcel Dekker, New York.
- [16] Kondo A. (1979) *Microcapsule Processing and Technology*. Marcel Dekker, New York.
- [17] Chang T.M.S. (1964) *Science*. 146, 524.
- [18] Andrea R.T, Habas S, Yang P.D. (2008) *Small*. 4, 310.
- [19] Haes A.J, Van Duyne R.P. (2002) *J. Am. Chem. Soc.*, 124, 10596.
- [20] Imura K, Nagahara T, Okamoto H. (2006) *Appl. Phys. Lett.*, 88, 23104.
- [21] Li C, Cai W, Cao B, Sun F, Li Y, Kan C, Zhang L. (2006) *Adv. Funct. Mater.* 16, 83.
- [22] Swallow A.J. (1973) *Radiation chemistry: An introduction*, Wiley, New York.
- [23] Link S, El-Sayed M.A. (1999) *J. Phys. Chem. B*. 40, 4212.
- [24] Tian N, Zhou Z.Y, Sun S.G. (2008) *J Phys Chem C*. 112,19801.
- [25] Lee S.W, Chen S.O, Sheng W.C, Yabuuchi N, Kim Y.T, Mitani T, Vescovo Shao-Horn Y. (2009) *J Am Chem Soc*. 131, 15669.

LIST OF FIGURES

	Page No.
Fig. 1.1: Distribution of ions and excited species along the track of fast electron	8
Fig. 1.2: Sequence of events in water radiolysis and formation of primary species from 10^{-16} to 10^{-7} second	11
Fig. 1.3: Preparation scheme of graft adsorbent by post-irradiation grafting	20
Fig. 1.4: Block diagram of pulse radiolysis technique with optical detection	24
Fig. 2.1: Decay scheme for ^{60}Co	36
Fig. 2.2: Gamma Chamber 5000	37
Fig. 2.3: Pulse Radiolysis Set-up with optical detection system	41
Fig. 2.4: Schematic of a TEM	45
Fig. 2.5: Schematic of a SEM	48
Fig. 2.6: Principle of EDS	49
Fig. 2.7: Schematic of a XRD instrument	51
Fig. 2.8: Schematic of an AFM	53
Fig. 2.9: Schematic of UV- visible spectrophotometer	56
Fig. 2.10: Correlation table of IR bands	57
Fig. 2.11: Schematic diagram of a Michelson interferometer configured for FTIR	58

Fig. 2.12:	The Fourier transform	59
Fig. 2.13:	Schematic diagram of ion chromatography	60
Fig. 2.14:	Schematic of DSC measuring cell	62
Fig. 2.15:	Temperature difference between sample and reference (ΔT) versus time	63
Fig. 2.16:	Schematic diagram of TGA set up	64
Fig. 3.1:	Determination of rate constant for the reaction of $\bullet\text{OH}$ radical with DADMAC by competition kinetics using KSCN as reference solute; absorbance due $(\text{SCN})_2\bullet^-$ measured at 500nm	76
Fig. 3.2:	Typical decay trace of e_{aq}^- at 700 nm in the presence of DADMAC	77
Fig. 3.3:	Determination of rate constant for the reaction of $\bullet\text{OH}$ radical with PDADMAC by competition kinetics using KSCN as reference solute; absorbance due $(\text{SCN})_2\bullet^-$ measured at 500 nm	79
Fig. 3.4:	% Polymerization as a function of absorbed dose	81
Fig. 3.5:	Variation in the molecular weight of PDADMAC with increase in gamma radiation dose	82
Fig. 3.6:	FT-IR spectrum of PDADMAC in KBr pellet	86
Fig. 3.7:	Absorption spectrum of DADMAC and PDADMAC in water	87
Fig. 3.8:	H-NMR of PDADMAC in D_2O	88

Fig. 3.9:	^{13}C -NMR of PDADMAC in D_2O	89
Fig. 3.10:	Cis and Trans forms of PDADMAC	89
Fig. 3.11:	Cyclopolymerization of DADMAC initiated by gamma irradiation	91
Fig. 4.1:	TG and DTG curve of PDADMAC in nitrogen atmosphere at a heating rate of $10\text{ }^\circ\text{C min}^{-1}$	99
Fig. 4.2:	DSC and DTG curve of PDADMAC in nitrogen atmosphere at a heating rate of $10\text{ }^\circ\text{C min}^{-1}$	101
Fig. 4.3:	Comparison of experimental DSC curve with theoretically generated curve by the method of least squares. Inset: DSC curve recorded at heating rate of $50\text{ }^\circ\text{C min}^{-1}$ for determination of glass transition	102
Fig. 4.4:	Comparison of experimental DTG curve with theoretically generated curve by the method of least squares	105
Fig. 4.5:	Degree of conversion versus time plot for the first decomposition step ($223 - 391\text{ }^\circ\text{C}$) of PDADMAC in nitrogen atmosphere	106
Fig. 4.6:	Degree of conversion versus time plot for the second decomposition step ($391 - 730\text{ }^\circ\text{C}$) of PDADMAC in nitrogen atmosphere	107
Fig. 4.7:	DSC curve of DADMAC solution in nitrogen atmosphere at a heating rate of $10\text{ }^\circ\text{C min}^{-1}$	110
Fig. 4.8:	TG curve of DADMAC and PDADMAC solutions in nitrogen atmosphere at a heating rate of $10\text{ }^\circ\text{C min}^{-1}$	112

Fig. 4.9:	Experimental TG curves of DADMAC-PDADMAC mixtures of various compositions	113
Fig. 4.10:	Percentage weight loss of DADMAC step M1 versus PDADMAC weight percentage in the mixture	114
Fig. 4.11:	Percentage weight loss of the PDADMAC step P2 versus PDADMAC weight percentage in the mixture	115
Fig. 4.12:	Experimental TG curves of the DADMAC irradiated to different absorbed doses	116
Fig. 4.13:	Degree of conversion of DADMAC as a function of radiation dose, calculated from classical gravimetry and TGA	117
Fig. 5.1:	Grafting percentage of AA onto PE films as a function of absorbed dose at an AA concentration of 20 % and dose rate of 3.8 kGy	126
Fig. 5.2:	Grafting percentage of DADMAC onto AA-g-PE (30 % AA grafted) films as a function of absorbed dose at various DADMAC monomer concentration	128
Fig. 5.3:	Grafting percentage of DADMAC onto AA-g-PE films of different initial AA grafted composition, at a fixed absorbed dose of 15 kGy	129
Fig. 5.4:	Grafting percentage of DADMAC as a function of conversion degree of the carboxyl group to its carboxylate anion at an irradiated to dose of 7.6 kGy in 20 % DADMAC solution	130

Fig. 5.5:	Equilibrium degree of swelling of DADMAC grafted films as a function of irradiation dose	131
Fig. 5.6:	Grafting yield of DADMAC, as a function of irradiation dose, at dose rates of (a) 0.26 kGy and (b) 3.8 kGy	132
Fig. 5.7:	FT-IR spectra of (a) PE, (b) AA-g-PE, (c) pure PDADMAC and (d) DADMAC-g-AA-g-PE	133
Fig. 5.8:	TGA profiles of the original PE film, pure PAA and PDADMAC	134
Fig. 5.9:	TGA profiles of (a) original PE film, (b) AA-g-PE film and (c) DADMAC-g-AA-g-PE film	135
Fig. 5.10:	Typical optical image of the microcapsules	141
Fig. 5.11:	SEM image of a cross-section of the microcapsule showing a core-shell morphology	142
Fig. 5.12:	DTG plots of (a) the pure PES microcapsule and (b) the microcapsule containing the monomer and polymer after gamma irradiation	143
Fig. 5.13:	Ion chromatograph for the typical mixed fluoride and nitrate ion standards	145
Fig. 6.1:	The different facets of Au nanocube and Au octahedron	148
Fig. 6.2:	UV-Visible spectrum of the gold nanoparticles synthesized at different Au^{3+} /PDADMAC ratios	154

Fig. 6.3:	Electron microscopy images of gold nanoparticles synthesized at different Au ³⁺ /PDADMAC ratios. (a) SEM image at R=1:3; (b) SEM image at R=1:4; (c) TEM image at R=1:5; (d) TEM image at R=1:10	156
Fig. 6.4:	XRD pattern of gold nanoparticles synthesized at different Au ³⁺ /PDADMAC ratios	157
Fig. 6.5:	EDX spectra of the nanoplates synthesized at R=1:4, deposited on a silicon wafer	158
Fig. 6.6:	XPS spectrum of gold nanoplates deposited on a silicon wafer	159
Fig. 6.7:	SAED pattern obtained by aligning the electron beam perpendicular to the plane of a hexagonal nanoplate	160
Fig. 6.8:	Truncated octahedron showing the {111} and {100} facets	161
Fig. 6.9:	Growth of octahedral seed along the <111> and <100> directions	162
Fig. 6.10:	Plate like seed showing the concave (A) and convex (B) sides	163
Fig. 6.11:	Schematic illustration of facet blocking and lateral growth of gold nanoplates	164
Fig. 6.12:	Effect of dose rate on the shape of the nanoparticles (a) Spherical nanoparticles formed at 2.2 kGyh ⁻¹ and (b) Nanoplates formed at 0.2 kGyh ⁻¹	165

Fig. 6.13:	(a) Spectrum of the freshly prepared solution; (b) Spectrum of the solution exposed to sunlight for six hours; (c) Spectrum of the solution kept in dark for six hours	168
Fig. 6.14:	(a) Optical microscope images of the concave nanoplates using 100 X objective lens (b) SEM image of the nanoplates (c) and (d) TEM image the nanoplates	170
Fig. 6.15:	(a) 3D AFM image of a truncated nanotriangle (b) section analysis across the nanoplate from one edge to the opposite edge	171
Fig. 6.16:	XRD pattern of gold nanoplates	173
Fig. 6.17:	SAED pattern recorded from a single hexagonal nanoplate (inset)	173
Fig. 6.18:	EDX spectra of the nanoplates deposited on a silicon wafer	172
Fig. 6.19:	XPS spectrum of gold nanoplates	174
Fig. 6.20:	Schematic presentation of the oxidative etching process on the {111} surface of gold nanoplates	175
Fig. 6.21:	SEM images of the nanoplates synthesized at different concentrations of Au and PDADMAC. (a) 100 uM Au and 1 mM PDADMAC; (b) 200 uM Au and 2 mM PDADMAC	176

LIST OF TABLES

	Page No.
Table 1.1: Spur Reactions in Water	12
Table 1.2: Properties of e_{aq}^-	14
Table 1.3: Properties of H^\bullet atom	15
Table 1.4: Properties of $\bullet OH$ radical	15
Table 3.1: Some neutral monomers	67
Table 3.2: Some ionic and polyfunctional monomers	68
Table 3.3: Summary of the ^{13}C -NMR chemical shift data of PDADMAC	90
Table 3.4: Kinetic parameters of the various reactions of the transient species	91
Table 4.1: TG / DTG analysis of PDADMAC at a heating rate of $10\text{ }^\circ\text{C min}^{-1}$ in nitrogen atmosphere	99
Table 4.2: DSC analysis of PDADMAC at a heating rate of $10\text{ }^\circ\text{C min}^{-1}$ in nitrogen atmosphere	102
Table 4.3: Evaluation of glass transition temperature of PDADMAC by different methods	103
Table 4.4: Evaluation of kinetic parameters from TGA and DSC using the method of least squares	104
Table 4.5: Composition of the ternary solution (for 100 g)	109
Table 5.1: Anion uptake by the microcapsule from mixed anion standards	144
Table 5.2: Fluoride and Nitrate uptake by the microcapsule (separately)	144

LIST OF SCHEMES

	Page No.
Scheme 3.1: Reaction mechanism for the polymerization of DADMAC to form the six-member piperidine ring system	84
Scheme 3.2: Reaction mechanism for the polymerization of DADMAC to form the five-member pyrrolidone ring system.	85
Scheme 5.1: Grafting of DADMAC onto PE employing a two stage procedure	123
Scheme 5.2: Different reaction modes of DADMAC	127
Scheme 5.3: The radiolytic encapsulation process	140

Chapter 1: INTRODUCTION AND LITERATURE SURVEY

1.1 General Introduction

Radiation chemistry is a branch of chemistry that studies chemical transformations in materials exposed to high-energy electromagnetic radiations (γ -rays, X-rays), charged particles (electrons, protons, deuterons, α -particles) or uncharged particle (neutron), termed as “ionizing radiation”, with energy in the range of 100 eV to 10 MeV. Ionizing radiation as the name implies causes ionization and excitation of various types of molecules and atoms present in the medium in many possible ways resulting in the formation of a variety of reactive species. This is a non-selective process which is different from photochemistry where one can selectively excite, ionize or break a particular bond in a given molecule by choosing the energy of a photon. Radiation chemistry does not deal with radioactive elements but these elements are used as a source of radiation. The origins of radiation chemistry can be traced back to the end of the 19th century, just after the discovery of X-rays in 1895. However, early attempts to understand the nature of chemical reactions induced by radiation were hindered by the non availability of sufficiently strong radiation sources to produce changes and also due to the lower sensitivity of analytical techniques existing at that time to track the changes produced. Radiation chemistry as a new discipline was only recognized in the early 1940s when radiation and nuclear sciences went through rapid developments and numerous breakthroughs. Machines that produce radiation and radioactive isotope sources were produced with outputs not even dreamed of before. An important achievement was the discovery of the most powerful chemical reducing agents, known as solvated electrons. This species play a very significant role in the radiation induced physical and chemical changes in materials especially in aqueous systems. The arrival of a technique known as pulse radiolysis in the 1960s extended frontiers of chemical kinetics even

farther and the fastest diffusion-controlled reactions were directly observed. This rate information is very much important to researchers applying radiation in studies of environmental and biological problems, radio therapy, modeling problems in industrial processing and reactor technology.

The important advantage of radiation chemistry lies in its ability to produce and study many reactive species playing a part in chemical reactions, synthesis, industrial processes, or in biological systems. The techniques are applicable to gaseous, liquid, solid, and heterogeneous systems. By combining different techniques of radiation chemistry with analytical chemistry, kinetics of chemical reactions can be studied and reaction mechanisms may be proposed. Radiation chemistry has now evolved into a broad discipline of chemistry. The methods employed and knowledge acquired has a broad range of applications which extends to other scientific disciplines and industries including health care, food and agriculture, modification of polymers, surface coating, manufacturing, and radiation sterilization.

A polymer is a large molecule composed of many repeating subunits, known as monomers. Natural and synthetic polymers play an essential and ubiquitous role in everyday life because of their almost limitless range of properties. Natural biopolymers like DNA, proteins and carbohydrates are basic building blocks which are essential for the very existence of plant and animal life. Other naturally occurring polymers like wool, silk, rubber and many others have been in use for centuries. However, it is only in the last few decades that a wide range of scientific studies were carried out to understand the molecular structure of these materials and the relationship that exists between structural properties and function. With the new understanding, scientists and technologists have been able to use natural polymers more effectively by modifying its properties and have also been able to design new synthetic materials to replace them. After World War II, a vast range of entirely new

polymeric materials such as plastics, elastomers and fibers were synthesized, many of which have properties different and superior than the existing natural polymers. Today, these substances are truly indispensable to mankind and are being increasingly employed in engineering, transportation, communication, clothing, shelter and other conveniences of modern living.

The irradiation of polymeric materials with ionizing radiation, notably gamma rays and electron beams can lead to changes in physical and chemical properties that make it more beneficial from an application point of view. The degree of these transformations depends on the structure of the polymer and the conditions of treatment before, during and after irradiation at a given dose. Good control of all these important factors facilitates the modification of polymers by radiation processing. Therefore, radiation processing has opened up new avenues to tune the properties of polymeric system. It has emerged as a commercially viable technology to produce polymeric materials of high performance such as crosslinked wire and cables, heat shrinkable materials, polythene foams, radiation synthesized hydrogel for wound dressing, battery separator membranes and different kinds of surface coatings.

This chapter covers important concepts and areas in radiation chemistry which may be considered as a prerequisite for better understanding of the investigations carried out and reported in later chapters of the thesis. This includes interaction of radiation with matter, radiation chemistry of water, radiation effect on monomers and polymers and radiolytic synthesis of nanoparticles. Towards the end of this chapter, a brief section highlights the significance of thermal analysis for the study of polymeric materials. In the final and concluding section, an “overview of the thesis” is incorporated which describes, in a nutshell, the complete work carried out and reported in the thesis.

1.2 Interaction of ionizing radiation with matter

To understand the radiation chemical effects on a system, it is necessary to have a thorough knowledge of the processes by which ionizing radiation interacts with matter. It is the absorbed energy which finally results in the observed chemical changes. The extent and process of energy absorption depends upon the nature of radiation, state and properties of the material. The important parameters on which the interaction will depend are energy, mass and charge of the radiation, and atomic number and electron density of the material [1]. Mechanisms of interaction of (i) Electromagnetic radiation (ii) Electrons (iii) Heavy charged particles and (iv) Neutrons, which are of relevance in radiation chemistry are explained briefly in the following sections.

1.2.1 Interaction of electromagnetic radiation

Electromagnetic radiations of wavelength less than 100 \AA belong to the class of ionizing radiation. They are usually called X-rays (extra nuclear origin) or γ rays (produced from the atomic nuclei). The gamma rays emitted by radioactive isotopes are mono-energetic, possessing one or more discrete energies, for example ^{60}Co emits γ -photons of energy 1.332 MeV and 1.173 MeV. For a narrow beam, the intensity of gamma radiation transmitted through an absorber is given by Eqn. 1.1.

$$I = I_0 e^{-\mu x} \quad (1.1)$$

Where I_0 is the incident radiation intensity, x is the thickness of material through which radiation has traversed and μ is the linear attenuation coefficient, which is the sum of a number of partial coefficients representing different processes occurring inside the absorber. These are (i) photoelectric effect, (ii) Compton scattering, (iii) Pair production (iv) Coherent scattering and (v) Photonuclear reactions. The relative importance of each process depends on the photon energy and the atomic number of the absorbing material. Coherent scattering is of importance for low energy photons ($<0.1 \text{ MeV}$), photonuclear reactions are possible with

photons of energies in the range of 2 to 8 MeV for low Z materials and in the region of 7-20 MeV for high Z materials. Thus, for gamma radiation emitted by ^{60}Co source, only the first three processes are of importance and are discussed below briefly.

(i) Photoelectric effect: This process is the principal interaction process at low photon energies. In photoelectric process photon interacts with a bound electron in an atom and transfers all its energy to eject it from the atom. The energy of the ejected electron “ E_e ” is equal to the difference between the energy of the photon “ E_o ” and the binding energy of the electron “ E_b ” (Eqn. 1.2).

$$E_e = E_o - E_b \quad (1.2)$$

(ii) Compton scattering: Compton scattering occurs when a photon with energy E_o interacts with a loosely bound or free electron. The resulting photon is deflected with reduced energy E_T at an angle θ to the direction of the incident photon and the electron gets accelerated at an angle ϕ with recoil energy E_e . The relation between the various parameters is given by Eqn. 1.3. The energy of recoil electron is given by the Eqn. 1.4.

$$E_T = \frac{E_o}{1 + (E_o / m_e c^2)(1 - \cos\theta)} \quad (1.3)$$

$$E_T = E_o - E_e \quad (1.4)$$

Compton scattering predominates for photon energies between 30 keV to 20 MeV for low Z materials like water and polymeric materials.

(iii) Pair production: This process is the reverse of electron-positron annihilation phenomenon and involves the complete absorption of a photon in the vicinity of an atomic nucleus resulting in the formation of two particles, an electron and a positron. This is an example of a physical process in which energy is converted into mass (Eqn. 1.5). Since the

rest mass of an electron or positron is 0.511 MeV, for pair production to occur, minimum photon energy must be 1.02 MeV (i.e. $2m_e c^2$)

$$E_0 = E_e + E_{e^+} + 2m_e c^2 \quad (1.5)$$

Depending on the incident photon energy, the photon gets attenuated and the total linear attenuation coefficient (μ) is given by Eqn. 1.6.

$$\mu = \tau + \sigma + \kappa \quad (1.6)$$

Where τ , σ , κ are the linear attenuation coefficient of photoelectric, Compton and pair production process respectively.

1.2.2 Interaction of charged particles

1.2.2.1 Electrons

Electron interacts with matter via four processes namely, emission of Bremsstrahlung radiation, inelastic collision, elastic collision and Cerenkov emission. The relative importance of these processes depends mostly on the energy of the electrons and to a lesser extent on the nature of the absorbing material.

(i) Bremsstrahlung: High energy electrons passing close to the nucleus of an atom are decelerated due to their interaction with the electric field of the nucleus and radiate electromagnetic radiation called bremsstrahlung radiation. Bremsstrahlung emission is negligible below 100 KeV but increases rapidly with increasing energy and is the dominant process at electron energy between 10-100 MeV.

(ii) Inelastic collision: This is the major process for electrons having energy more than that at which bremsstrahlung emission occurs. The average amount of kinetic energy lost per unit length by electron through coulomb interaction with atomic electrons in a medium is defined as the specific energy loss or stopping power (S) of the medium and is defined by the Bethe's equation (Eqn. 1.7).

$$S = -\frac{dE}{dx} = \frac{2\pi e^4 N_o Z}{m_o v^2} \left[\ln \frac{m_o v^2 E}{2I^2 (1-\beta^2)} - (2\sqrt{1-\beta^2} - 1 + \beta^2) \ln 2 + 1 - \beta^2 + \frac{1}{8}(1-\sqrt{1-\beta^2})^2 \right] \quad (1.7)$$

Where “e” and “ m_0 ” represents the charge and rest mass of electron respectively, “v” is the velocity of electron, “ N_0 ” is the number of atoms cm^{-3} in the medium, “Z” is the atomic number and “ I ” is the mean excitation potential of the electrons in the stopping material, “ β ” is the ratio of “v” to the speed of light “c” and is given by Eqn. 1.8.

$$\beta = \sqrt{1 - \{m_0 c^2 / (E - m_0 c^2)\}^2} \quad (1.8)$$

(iii) Elastic collision: This is a frequent phenomenon because of the small mass of electrons and happens when electrons get deflected by the electrostatic field of an atomic nucleus. This essentially leads to a change in the direction of motion of electrons and is more probable for electrons with low energy and target with high atomic number.

(iv) Cerenkov emission: Electrons with velocity higher than that of light in a particular medium interacts and emits electromagnetic radiation, called Cerenkov radiation. This phenomenon is responsible for the blue glow observed around high intensity γ -sources stored under water.

1.2.2.2 Heavy charged particles

The interaction of heavy charged particles with matter is the same as that of electrons, i.e., Bremsstrahlung emission, inelastic collision and elastic scattering. The most important among these processes by which charged particle interact with matter is inelastic collision. As heavy charged particles have higher mass than electrons, for a given energy, they have a much higher linear energy transfer (LET), which give rise to high local concentration of primary species and leads to recombination in spurs to yield molecular products.

1.2.3 Interaction of Neutrons

Neutrons do not produce ionization directly in matter but interact almost exclusively with the atomic nuclei of the material. The main processes by which neutron interacts with matter are: elastic scattering, inelastic scattering, nuclear reaction and capture. The products

of neutron interactions often cause ionization and thus produce typical radiation chemical changes. The main products of neutron interactions are protons and heavy positive ions but the chemical effects of neutron interactions are similar to those of charged particles.

1.2.4 Distribution of active species in the system – track structure

The electrons from Compton scattering of ^{60}Co γ -rays have an average energy of 440 keV. These electrons, also termed as δ -rays, bring about further ionization and excitation. Such events along the main track or the δ -ray branch track are called isolated spurs. In water, the isolated spurs contain on an average ~ 6 active species and ~ 100 eV energy is involved. When δ -ray electron energy is < 5 keV, its penetration becomes very less and the spurs formed in close vicinity, overlap and take cylindrical shape, known as short tracks. As the electron energy becomes less than 500 eV, even denser regions of ionization, which look like large spurs, called as blobs, are produced (Fig. 1.1).

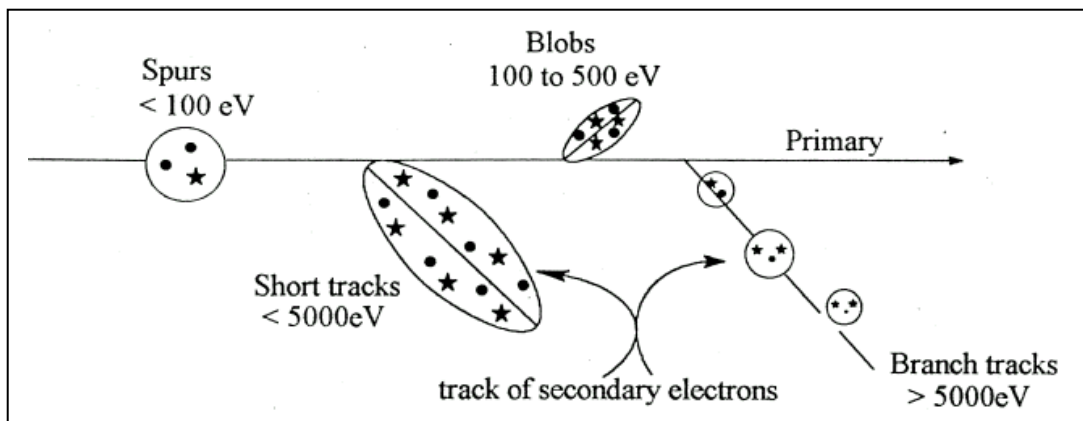


Fig. 1.1: Distribution of ions and excited species along the track of fast electron; (•) represents the ions and (*) represents the excited species

The typical energy distribution ratio for a 440 keV electron in water is spur (64%), short tracks (25%) and blobs (11%). In contrast to this, for heavy charged particles (high LET), more energy will be deposited in blobs and short tracks than in isolated spurs.

1.2.5 Radiation-chemical yield

Radiation chemical yields is usually reported in terms of G values, which represents the number of molecules of the product formed or changed per 100 eV of energy absorbed [2]. The SI unit of radiation chemical yield is defined as change in the number of moles of material formed or decomposed by energy absorption of 1 Joule [3]. G-values reported in terms of number of species formed per 100 eV can be converted to SI units using Eqn. 1.9

$$G (\text{mol J}^{-1}) = G (\text{as 100 eV}) \times 1.036 \times 10^{-7} \quad (1.9)$$

1.2.6 Radiation dosimetry

To gain an understanding of the physical, chemical or biological changes produced by ionizing radiation, it is necessary to estimate the amount of energy absorbed per unit mass of the absorber and also the distribution of absorbed energy in the material. Radiation dosimetry constitutes determination of these quantities.

(i) Absorbed dose: The absorbed dose is the amount of energy absorbed per unit mass of the irradiated material. The SI unit for the absorbed dose is Joules per kilogram (J kg^{-1}), which is also known as gray (Gy). The old unit is rad (1 rad = 0.01 Gy).

(ii) Absorbed dose rate: The absorbed dose rate is the absorbed dose per unit time.

1.2.6.1 Primary and secondary dosimeters

Dosimeters can be classified into two categories viz. primary dosimeters and secondary dosimeters. Primary dosimeters utilize a physical measurement such as temperature rise in a calorimeter, ionization produced in a gas or the charge carried by a beam of charged particles of known energy [4, 5]. Secondary dosimeters are those dosimeters whose response to radiation has to be calibrated against a primary dosimeter. These include Fricke dosimeter, nylon film dosimeter, solutions of various dyes, perspex dosimeters [6]. The choice of a dosimeter for a particular application depends on many factors namely, (i) state of the system, (ii) dose range to be monitored and (iii) nature of radiation.

1.2.7 Absorbed dose in samples

The absorbed dose measured by the dosimeter will represent the dose absorbed by the sample only when the following conditions are satisfied: (i) the dosimeter as well as the sample is homogeneous, (ii) both have same size, density and atomic composition, and (iii) both are irradiated under same conditions. The simple and widely used method to achieve these conditions is to use equal volumes of dilute solutions of both sample and dosimeter, and irradiated them in turn using the same container at the same position in the radiation field. Therefore, experimental conditions must be suitably controlled for accurate measurement of the absorbed dose in the sample.

For electromagnetic radiation like ^{60}Co γ -rays, the absorbed dose in the dosimeter (D_D) and sample (D_S) are related by Eqn. 1.10.

$$D_S = D_D \times (Z/A)_S / (Z / A)_D \quad (1.10)$$

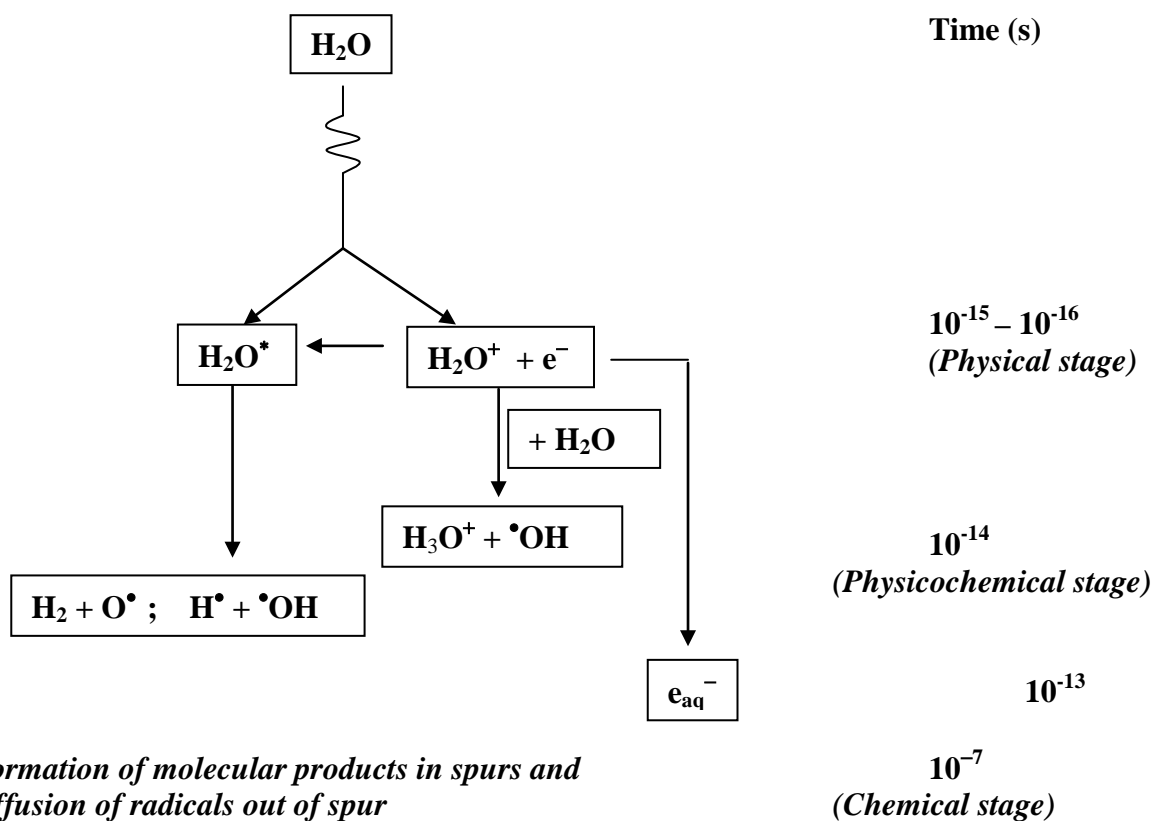
where Z/A is the ratio of the atomic number (Z) to the atomic weight (A) for an element and the ratio of the sum of the atomic numbers of the element present to the molecular weight for a compound.

1.3 Radiation chemistry of water

Understanding the radiation chemistry of water is of great significance as water is present in most biological and chemical systems. For water, the sequence of events like formation and solvation of the primary species, and the time scale of events initiated either by fast electrons from an accelerator or by ^{60}Co gamma-rays is illustrated in Fig. 1.2 [7]. High energy radiation deposits energy in 10^{-16} seconds in the spurs forming positively charged ions, electrons and excited species. Energetically unstable positively charged ions (H_2O^+) undergo ion-molecule reaction in 10^{-14} seconds producing $\bullet\text{OH}$ radicals [8].

The excited water molecules decompose in 10^{-14} seconds yielding H^\bullet and $\bullet\text{OH}$ radicals. The electron released during ionization can also bring about further ionization provided it has

sufficient kinetic energy. Eventually, its energy will fall below the ionization threshold of water and then it dissipates rest of its energy by exciting vibrational and rotational modes of the solvent molecules. Finally, it would be localized in a potential energy well long enough to become solvated as a result of molecular dipoles rotating under the influence of the negative charge, and thus get stabilized [9]. The electrons get thermalized in about 10^{-13} seconds and subsequently get hydrated or solvated in less than 10^{-12} seconds and these are called hydrated electron (e_{aq}^-) [10].



Formation of molecular products in spurs and diffusion of radicals out of spur

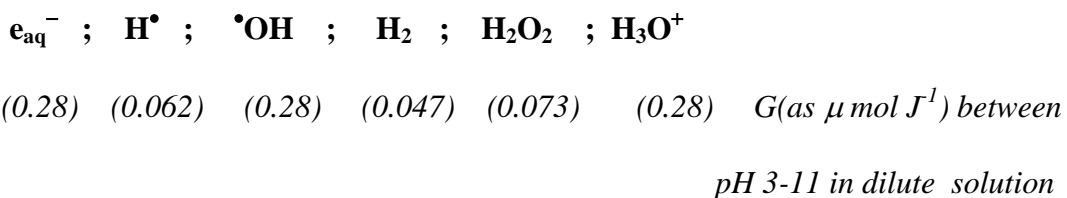


Fig. 1.2: Sequence of events in water radiolysis and formation of primary species from 10^{-16} to 10^{-7} second

Hydrated electrons, hydrogen atoms and hydroxyl radicals are formed in the spurs can react with one another to reform water or molecular products, H₂ and H₂O₂, while the remaining escape into the bulk solution. This spur expansion is complete in about 10⁻⁷ seconds. The reactions occurring during spur expansion are listed in Table 1.1. After about 10⁻⁷ seconds the species are homogeneously distributed and are known as primary species.

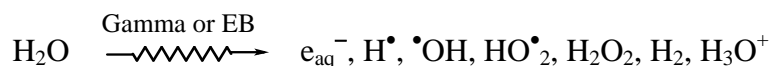
Table 1.1: Spur Reactions in Water

Reactions	k x 10 ⁻¹⁰ (dm ³ mol ⁻¹ s ⁻¹)
e _{aq} ⁻ + e _{aq} ⁻ → H ₂ + 2•OH	0.55
e _{aq} ⁻ + •OH → OH ⁻	3.0
e _{aq} ⁻ + H ₃ O ⁺ → H• + H ₂ O	2.3
e _{aq} ⁻ + H• → H ₂ + OH ⁻	2.5
H• + H• → H ₂	1.3
•OH + •OH → H ₂ O ₂	0.53
•OH + H• → H ₂ O	3.2
H ₃ O ⁺ + OH ⁻ → 2 H ₂ O	14.3

In the nanosecond time scale, different processes ultimately produce hydrated electrons (e_{aq}⁻), •OH, H• and molecular products H₂ and H₂O₂. These species can subsequently react with solutes present in the system. In water, 10⁻⁷ seconds is the lifetime of the radicals reacting at a diffusion-controlled rate with a solute whose concentration is 10⁻³ mol dm⁻³. Under these conditions the G-values of e_{aq}⁻, H• and •OH radicals at 10⁻⁷ second are shown in the Fig. 1.2. Under these conditions classical kinetics is generally valid.

1.3.1 Primary yields

Primary yields are the yields of the species remaining when all spur reactions are complete, that is about 10^{-7} seconds after the ionization event. At this time the radiolytic change in water is represented by:



and the material balance Eqns. are:

$$\begin{aligned} G(-\text{H}_2\text{O}) &= 2 G(\text{H}_2) + G(\text{H}^\bullet) + G(e_{\text{aq}}^-) - G(\text{HO}_2^\bullet) \\ &= 2 G(\text{H}_2\text{O}_2) + G(\bullet\text{OH}) + 2G(\text{HO}_2^\bullet) \end{aligned} \quad (1.11)$$

or if HO_2^\bullet is neglected, which is justified for low LET radiation

$$\begin{aligned} G(-\text{H}_2\text{O}) &= 2 G(\text{H}_2) + G(\text{H}^\bullet) + G(e_{\text{aq}}^-) \\ &= 2 G(\text{H}_2\text{O}_2) + G(\bullet\text{OH}) \end{aligned} \quad (1.12)$$

Primary yields were measured particularly for low LET radiations using scavengers in dilute solutions. In very dilute solutions the radical and molecular yields are constant, but in the presence of a reactive solute at concentrations more than $10^{-2} \text{ mol dm}^{-3}$, the yields of H_2 and H_2O_2 decrease and radical yields increase due to spur scavenging by the solute molecules [11].

1.3.2 Important reducing radicals in aqueous solutions

The hydrated electron, e_{aq}^- , and the hydrogen atom (H^\bullet) are the primary reducing radicals produced by the radiolysis of water. The redox-potential value $\xi^\circ = -2.9 \text{ V}$ vs NHE for e_{aq}^- proves that they are powerful reducing agents (Table 1.2). Its reactions with solutes are best understood in terms of availability of a suitable vacant orbital in the solute molecule (S) for the electron to get localized. A typical reaction is represented by Eqn. 1.13 where n represents the positive charge on the solute.



The rate constant values for typical hydrated electron reactions support the above requirement. For water, the rate constant, k is only $16 \text{ dm}^3 \text{ mol}^{-1} \text{ s}^{-1}$ as a low-lying vacant orbital is absent in water. It also explains the sufficiently long half-life of e_{aq}^- in water. With solutes having low lying π^* orbital, the k value approaches the diffusion controlled limit.

Table 1.2: Properties of e_{aq}^-

Radius of charge distribution	0.25-0.30 nm
Diffusion coefficient	$4.9 \times 10^{-5} \text{ cm}^2 \text{ s}^{-1}$
Spectral characteristics	e_{aq}^- , $\lambda_{\text{max}} = 715 \text{ nm}$, $\epsilon = 1.85 \times 10^4 \text{ dm}^3 \text{ mol}^{-1} \text{ cm}^{-1}$
Redox potential (Vs NHE)	$\xi^\circ (e_{\text{aq}}^- + \text{H}^+ \rightarrow \frac{1}{2} \text{H}_2 + \text{H}_2\text{O}) - 2.9 \text{ V}$
Half life: pH ≥ 7.0	6.6×10^{-4} seconds.

In neutral and acidic pH, H^\bullet is an important reducing species with its redox potential value, $\xi^\circ = -2.3 \text{ V}$ vs NHE (Table 1.3). It can be thought of as a weak acid with pK_a of 9.6. While it readily reduces substrates with more positive redox potential, the corresponding rates are slower than for e_{aq}^- reactions. With substrate having center of unsaturation, it is known to add readily to form H-adduct.

From a solute devoid of π electrons, it abstracts hydrogen atom giving rise to a solute transient radical. Optical absorption of H^\bullet lies around 200 nm with very low extinction coefficient, which is normally not accessible with the available experimental facilities. Thus, measurements of H^\bullet reaction parameters are made by competition kinetics method or from the transient formation kinetics.

Table 1.3: Properties of H• atom

Diffusion constant	$8.0 \times 10^{-5} \text{ cm}^2 \text{ s}^{-1}$
Spectral characteristics	H^\bullet , $\lambda_{\text{max}} = 200 \text{ nm}$
Reduction potentials (vs. NHE)	$\xi^\circ (\text{e}_{\text{aq}}^- + \text{H}_3\text{O}^+ \rightarrow \text{H} + \text{H}_2\text{O}) - 2.3 \text{ V}$
pK _a :	9.6

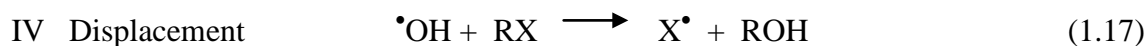
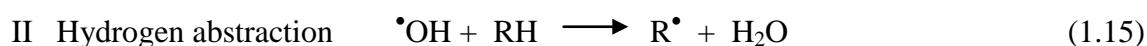
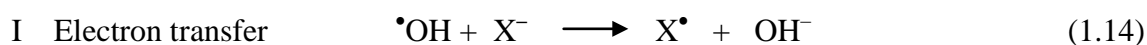
1.3.3 Important oxidizing radicals in aqueous solutions

Hydroxyl radical ($\bullet\text{OH}$) is a strong oxidizing radical ($\xi^\circ = 2.8 \text{ V}$ vs NHE) and since its absorption lies in the far UV region of the spectrum the kinetic parameters are estimated by competition kinetics or transient formation kinetics. In strongly basic solution ($\text{pH} > 11.9$), it is deprotonated to give O^\bullet . The properties of $\bullet\text{OH}$ radical are listed in Table 1.4.

Table 1.4: Properties of $\bullet\text{OH}$ radical

Diffusion constant	$2.2 \times 10^{-5} \text{ cm}^2 \text{ s}^{-1}$
Spectral characteristics	$\bullet\text{OH}$, $\lambda_{\text{max}} = 235 \text{ nm}$, $\epsilon = 530 \text{ dm}^3 \text{ mol}^{-1} \text{ cm}^{-1}$
Reduction potentials (vs. NHE)	$\xi^\circ (\text{e}^- + \bullet\text{OH} + \text{H}^+ \rightarrow \text{H}_2\text{O}) + 2.8\text{V}$, acid
	$(\text{e}^- + \bullet\text{OH} \rightarrow \text{OH}^-) + 1.8 \text{ V}$, alkali
pK _a :	$(\bullet\text{OH} \rightleftharpoons \text{O}^\bullet + \text{H}^+) \quad 11.9$

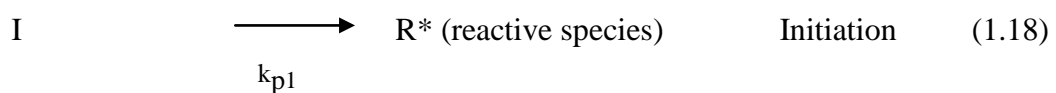
With organic compounds the hydroxyl radical can undergo mainly four types of reactions:

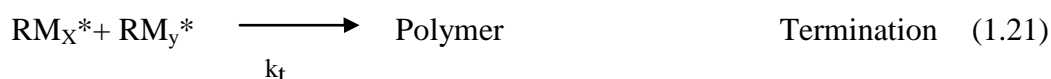


1.4 Radiation effects on monomers

When a monomer is subjected to ionizing radiation, the initial physical processes are similar to that occur in organic molecules i.e. ionization and excitation of the monomer molecules. The external energy required for the initiation step in radiation polymerization is supplied by the ionizing radiation. After initiation further processes of propagation and termination (by combination and disproportionation) go on according to conventional free radical polymerization. The radiation chemical act is merely limited to the primary events, which lead to the production of free radicals and to a few specific secondary effects. The radiation polymerization process depends on experimental variables like dose rates, viscosity of the polymerization medium, type of the polymerization medium and reaction temperature and pressure. In certain specific cases, ionizing radiation can also initiate ionic chain reactions [12].

Chain polymerization is initiated by an initiator which generates a reactive species like free radical, cation or anion. The polymerization then proceeds by the propagation of the reactive species by successive rapid addition of the monomer. Finally, chain termination occurs either by combination or disproportionation. Termination in radical polymerization occurs when the free radicals combine and end the polymerization process. The various steps involved in the polymerization process are given below;





If R_i is the rate of initiation (Eqn. 1.18), R_p and R_t are the rates of propagation and termination respectively. k_p and k_t are the rate constants for the propagation (Eqn. 1.19 & Eqn. 1.20) and termination (Eqn. 1.21). If it is assumed that the different propagation steps k_{p1} , k_{p2} and k_{pj} etc. are independent of the chain length, then;

$$k_p = k_{p1} = k_{p2} = k_{pj} \text{ etc.} \quad (1.22)$$

The general propagation reaction can be written as;



And rate of propagation as

$$R_p = k_p \cdot [\text{RM}_n^*] \cdot \text{M} \quad (1.24)$$

From Eqn. 1.21, rate of termination can be written as

$$R_t = k_t \cdot [\text{RM}_n^*]^2 \quad (1.25)$$

Now using steady state approximation, i.e. rate of initiation is equal to rate of termination

$$R_i = R_t \quad (1.26)$$

And substituting R_t from Eqn. 1.25, we can obtain (RM_n^*) .

$$[\text{RM}_n^*] = [R_i/k_t]^{1/2} \quad (1.27)$$

Assuming all of the monomer consumed is converted into the polymer, the rate of propagation is equal to rate of polymerization or rate of monomer consumption.

$$-d(\text{M})/dt = R_p = k_p \cdot [\text{RM}_n^*] \cdot \text{M} \quad (1.28)$$

On substituting $[\text{RM}_n^*]$ from Eqn. 1.27

$$R_p = (k_p/k_t^{1/2}) \cdot (R_i)^{1/2} \cdot [\text{M}] \quad (1.29)$$

This equation (Eqn. 1.29) is called the polymerization rate equation. The exponent of R_i in the rate equation is $1/2$ because a bimolecular termination was assumed i.e. the reaction

of two propagating species. The exponent of R_i gives an indication of the termination step. The exponent between 1 and $1/2$ suggests the presence of unimolecular termination like impurity termination. If the exponent is less than $1/2$ it indicates the presence of premature termination which is possible at very high rates of initiation.

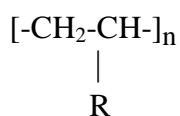
1.5 Radiation effects on polymers

When a polymer is subjected to ionizing radiation the chemical reactions that occur depend upon many factors such as nature of the polymer, ambient condition and irradiation conditions, absorbed dose and dose rate. The important chemical changes produced in a polymer due to irradiation are: formation of intermolecular and intramolecular bonds (crosslinking), scission of bonds in the main polymer chain (degradation), formation of gaseous products like H_2 , CH_4 , CO , oxidation reactions in the presence of air or oxygen, changes in unsaturation and formation of trapped ions and radicals in polymer matrix. The yields of different reactions depend upon the chemical nature, physical state and morphology of the polymer. Radiation induced changes can lead to beneficial effects in many polymers, for instance, crosslinking of polyethylene imparts high temperature dimensional stability and induces "memory effect" to the polymer which makes it useful for high temperature applications and for producing heat shrinkable materials respectively. Similarly, radiation degradation of polytetrafluoroethylene (PTFE or Teflon) results in the formation of low molecular weight powder, which has immense commercial applications. Formation of trapped radicals/ ions in polymers has been used for initiating grafting reactions, which can help in designing and synthesizing polymers having desired properties.

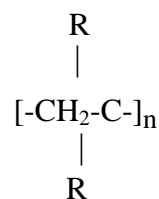
1.5.1 Crosslinking and degradation of polymers

Crosslinking and degradation are two important radiation induced processes that occur simultaneously in a polymeric system, although, one of the processes may predominate depending upon the chemical structure and physical state of the polymer and irradiation

conditions. Polymers are generally divided into crosslinking type (which predominantly crosslink) and degrading type (which predominantly undergo chain scission). It has been observed that if each carbon atom of the polymer chain has at least one hydrogen atom (as in the structure I), the polymer crosslinks and if a tetra-substituted carbon atom is present in the repeat unit (as in the structure II), the polymer degrades predominantly.



Structure I (crosslinking)



Structure II (degrading)

For example, polyethylene and polystyrene are crosslinking type of polymers, while polymethyl methacrylate and polytetrafluoroethylene are degrading type of polymers. In general, crosslinking reactions in polymers are favoured by the presence of unsaturated groups particularly vinyl groups, absence of oxygen, high chain mobility and molecular entanglements. Chain scission on the other hand is favoured by restrictions to chain rotation i.e. glassy state, high levels of crystallinity and presence of oxygen. Usually radiation stability of the polymer increases in the presence of aromatic ring in its structure.

Crosslinking reaction transforms a linear polymer into a single three-dimensional molecule with significantly different properties. The crosslinked structure has ultra high molecular mass, is practically insoluble in any solvent and has improved mechanical properties. Degradation on the other hand results in a reduction of molecular mass as chains are fractured and results in a general degradation of the physical properties of the polymer.

1.5.2 Radiation induced graft polymerization

Grafting is an important process to modify the properties of polymeric materials. In radiation induced grafting, radical sites are generated on the trunk polymer by irradiating it with ionization radiation (gamma rays or electron beams). Then a polymer branch with

desired functional capabilities is grafted onto the trunk polymer [13]. The role of the trunk polymer is to provide an appropriate practical shape and dimension and to maintain physical and chemical stability, whereas, the grafted polymer branch exhibits various properties for different applications such as ion exchange separation of metal ions, dyes, catalytic and antibacterial properties.

1.5.2.1 Types of radiation induced grafting polymerization

There are mainly two categories of radiation grafting technique which are commonly employed [14];

- (i) **Simultaneous or mutual irradiation grafting:** Here, the trunk polymer and a monomer in contact are irradiated simultaneously. The method is simple and straight forward but since the monomer is also exposed to radiation, there is possibility of homopolymerization which needs to be controlled.
- (ii) **Post-irradiation grafting:** In this method, the trunk polymer is first irradiated to generate reactive radical sites and subsequently it is brought into contact with the monomer. Since the monomer is not exposed to radiation, homopolymerization of the monomer does not occur. Fig. 1.3 shows the schematic of post irradiation grafting procedure followed by the functionalization of the grafted chains for metal adsorption.

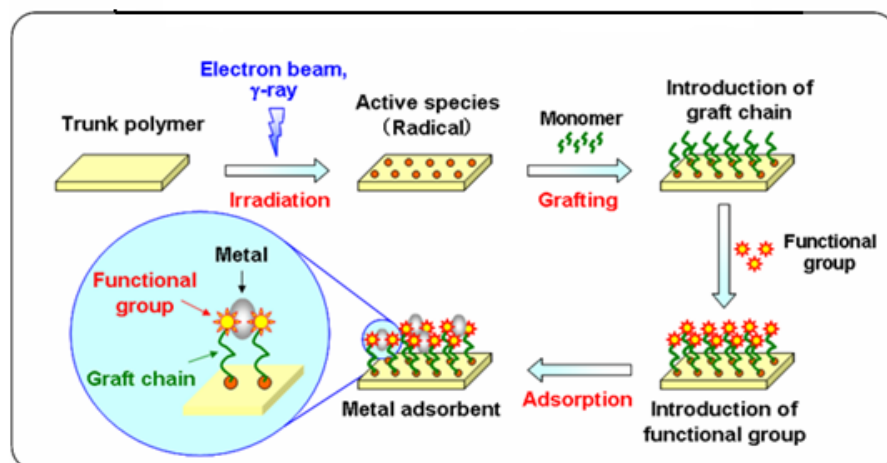


Fig. 1.3: Preparation scheme of graft adsorbent by post-irradiation grafting

1.5.2.2 Advantages of radiation grafting over other grafting techniques

Radiation-grafting is a room temperature process which does not require any additives unlike photo grafting or thermal grafting methods. Therefore, radiation-grafting method can be used for grafting on temperature sensitive polymer backbones which is not possible by thermal chemical methods. Since additives are avoided, high purity modified polymer are produced which have vast applications in biomedical field. Some polymers such as solid fiber which are difficult to be grafted by chemical initiators can be easily grafted by gamma radiation or high-energy electrons because of its good penetrating power. Radiation induced grafting methods are limitless owing to the unselective absorption of radiation energy in matter, which in principle may be used to prepare any desired combination of polymers. Unlike conventional grafting methods, radiation grafting reaction can either be conducted homogeneously throughout bulk of polymers or limited to the surface. This depends upon the type of radiation, the total energy absorbed, the depth of penetration and radiation sensitivity of trunk polymer and monomer. The product quality can be precisely and easily controlled by adjusting the process parameters such as total dose, dose rate, concentration of monomer and nature of solvents.

1.6 Polyelectrolytes

A polyelectrolyte is a polymeric material in which the monomer units possess ionizable groups that develop substantial charge when dissolved or swollen in a highly polar solvent such as water. If the extent of dissociation of an electrolyte's ionic groups depends on solution conditions, the polyelectrolyte is labeled as "weak"; otherwise, the polyelectrolyte is labeled as "strong". Polyelectrolytes may be anionic or cationic depending on the charge they carry. Electrostatic interactions between the ionized groups, as well as the presence of small electrolyte ions in the nearby solution, convey to polyelectrolyte system a host of properties distinct from those displayed by neutral polymer systems. Polyelectrolytes show features of

both electrolytes and linear polymers hence they have been subject of investigation by electrochemists [15] as well as polymer chemists [16]. The physical properties of polyelectrolyte solutions are usually strongly affected by this degree of ionization. Since the polyelectrolyte dissociation releases counter-ions, this affects the solution's ionic strength which in turn affects other properties, such as electrical conductivity. Industrial applications and academic interests lead to more studies on the polyelectrolyte behavior in solutions, gels, adsorbed layers, and grafted brushes. Many biological molecules like polypeptides, glycosaminoglycans and DNA are polyelectrolytes that play a major role in biology and biochemistry.

1.7 Techniques for studying transient species

Radiation induced chemical processes generates highly reactive intermediate species termed as transients that have extremely short lifetimes ranging from 10^{-12} to 10^{-3} s. During the course of reaction from the energy absorption by the medium to the appearance of stable products several transient species maybe involved in sequence or in parallel. The lifetime of transients depends upon their nature and the reaction conditions. Some information about the nature of transients may be inferred from the results of the steady-state experiments. However, detailed identification and characterization of these species necessitates either the ability to enhance their lifetimes by reducing their reactivity or to monitor their behavior with a degree of precision over extremely short intervals. The two most important methods that have been employed to study the transient intermediates are matrix isolation method and time-resolved methods. In matrix isolation method, lifetime of the transient species is increased by reducing their mobility by glass formation at extremely low temperatures. In time-resolved methods, two ultra-fast techniques, namely, pulse radiolysis and laser flash photolysis have provided major breakthrough in detection of many transients [17, 18].

1.8 Principle of pulse radiolysis

The block diagram of pulse radiolysis technique with optical detection system is shown in Fig. 1.4. An intense ultra-short pulse of high energy electrons, typically a few MeV, is delivered to the system to create a non-equilibrium situation in which a significant concentration of the transient species is produced. The characteristics of the transient species are monitored by following the change in their properties such as optical absorption [19], electric conductivity [20], electron spin resonance [21] or light scattering [22]. Assuming that the monitoring technique used is capable of following the transient species formed, a limit on the time resolution of the measurement is set by the duration of electron pulse. When the pulse is long as compared to the relaxation time of the system, the concentration of the transient species available for the measurement will be insufficient for any meaningful results. Ideally, the pulse duration should be very short as compared to the relaxation time so that transient species are produced instantaneously and the kinetic analysis is only dependent on the subsequent chemical reactions. A more detailed description of pulse radiolysis is given in Chapter 2.

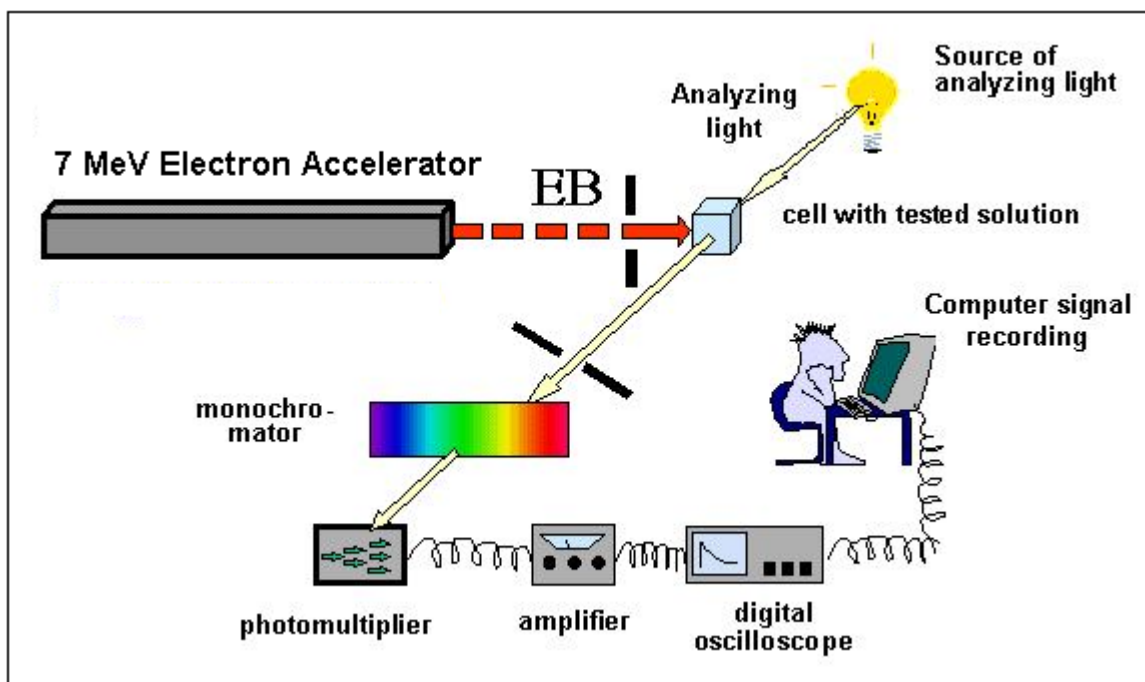


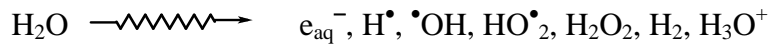
Fig. 1.4: Block diagram of pulse radiolysis technique with optical detection

1.9 Radiolytic synthesis of nanoparticles

There are several methods developed for the synthesis of nanoparticles but the most commonly employed procedure is the wet chemical synthesis wherein the nanoparticle precursor, usually in the form of salts, are reduced by a chemical reducing agent in presence of capping agents. The capping agent used is usually a surfactant or polymer which prevents the aggregation of particles and imparts stability to the colloidal system. The radiolytic method is a versatile and powerful method to synthesize a variety of metallic and inorganic nanoparticles with good control of size and size distribution [23-26]. Here the reaction proceeds at room temperature in the absence of extraneous reagents and leads to homogeneous reduction and nucleation in the bulk brought about by solvated electrons and other reducing species generated by the radiolysis of the solvent.

As mentioned before, the primary effects of the interaction of high-energy radiation such as particle beams, X-rays or gamma photons with a solution of metal ions are the

excitation and the ionization of the solvent. In aqueous solutions radiolysis produces the following transient species;



The hydrated electron, e_{aq}^- , and the hydrogen atom (H^\bullet) are the primary reducing radicals. The redox-potential value $\xi^\circ = -2.9 \text{ V vs NHE}$ for e_{aq}^- and $\xi^\circ = -2.3 \text{ V vs NHE}$ for H^\bullet shows that they are powerful reducing agents which can bring about the reduction of many metal ions. However, hydroxyl radicals (HO^\bullet) is a strong oxidative species ($\xi^\circ = +2.34 \text{ V vs NHE}$ at pH 7) and to avoid competitive oxidation reactions which may limit or even prevent metal reduction, hydroxyl scavengers are added in solution prior to irradiation. Among these scavengers, primary or secondary alcohols such as isopropanol are generally used. Isopropanol scavenges both H^\bullet and HO^\bullet and in turn is converted into isopropyl radical which is also a good reducing radical ($\xi^\circ = -1.8 \text{ V vs NHE}$). All these radicals can reduce the metal precursor to the zerovalent state (Eqn. 1.30) which then undergoes coalescence (Eqn. 1.31) to form the metal nanoparticle.



1.9.1 Role of capping agent in stabilization of nanoparticle colloid system

Nanoparticles have a particular tendency to lower their very high surface energy, which is the origin of their thermodynamic instability. Bare nanoparticles tend to stabilize themselves either by sorption of molecules from the surroundings or by lowering the surface area through coagulation and agglomeration. Colloidal nanoparticles in a dispersion medium always undergo Brownian motion and hence collide with each other frequently. The stability of colloids is thus determined by the interaction between the particles during such a collision. There are two basic interactions: one being attractive and the other repulsive. When attraction dominates, the particles will adhere with each other and finally the entire dispersion may

coalesce or aggregate. When repulsion dominates, the system will be stable and remain in a dispersed state [27]. Van der Waals forces are the primary source of attraction between colloidal particles that are always present between particles of similar composition. Therefore, a colloidal dispersion is stable only when a sufficiently strong repulsive force counteracts the Van der Waals attraction. The capping agent introduced in the system provides this repulsive force necessary for the stability of the nanocolloid.

1.9.1.1 Types of Stabilization

Stability can be imparted to the colloidal system by surrounding particles with an electrical double layer (electrostatic or charge stabilization) or by chemically attaching polymeric molecules (steric stabilization). Combination of the above two stabilization mechanisms is known as electrosteric stabilization.

i) Electrostatic stabilization

An effective way to counterbalance the Van der Waals attraction between colloidal particles in polar liquids is to provide the particles with Coulombic repulsion. In liquid dispersion media, ionic groups can adsorb to the surface of a colloidal particle through different mechanisms to form a charged layer. To maintain electroneutrality, an equal number of counter ions with the opposite charge will surround the colloidal particles and give rise to overall charge-neutral double layers. Due to electrostatic repulsion between particles they remain stable without coagulation. Charge stabilization is widely used in stabilizing dispersions in aqueous media however the disadvantage is its great sensitivity to the ionic strength of the dispersion medium.

ii) Polymeric stabilization

Steric stabilization consists in covering the particles with polymers to prevent the particle from getting close in the range of attractive forces. As long as these polymer molecules generate repulsion, they can be used to impart colloid stability [28].

1.9.1.2 Size and shape control of nanoparticles

Under a given set of experimental conditions it is possible to control the size of nanoparticles by choosing an appropriate ratio of metal precursor to the capping agent. It has been observed that for a fixed concentration of the precursor, when relatively high concentration of capping agent is used, small, nanoparticles are produced. Conversely, large nanoparticles are formed when lower concentration of capping agents is employed. Therefore, adjusting the ratio of precursor to capping agent provides an exquisite way to control the size of nanoparticles. In addition to controlling the size of nanoparticles and imparting stability to the colloidal system some of the capping agents play a vital role in controlling or directing the shape of the nanoparticles. For example, capping agents like polyvinyl pyrrolidone, cetyltrimethylammonium bromide, citrate etc. have been employed for the synthesis of nanoparticles of various shapes [29-31]. There are several hypothesis put forth to explain the synthesis of non- spherical nanoparticles. Among these, the most widely accepted view is that the capping agents containing certain functional groups selectively adhere to some facets of the growing nanocrystals and retard or inhibit growth on these surfaces while permitting unhindered growth on other facets. The preferential growth along specific directions results in anisotropic nanocrystals of various shapes. It may be mentioned that apart from the proper choice of capping agents other parameters such as kinetics of reduction, concentration of metal precursor and ratio of metal precursor to the capping agent profoundly influences the nucleation and growth process which ultimately dictates the final morphology or shape of the nanocrystals. The various factors that affect the shape of nanoparticles are more elaborately discussed in chapter 5.

1.10 Thermal analysis and characterization of polymer

Thermogravimetric analysis and Differential scanning calorimetry are two of the most useful thermal analysis techniques for the characterization of polymers.

1.10.1 Thermogravimetric analysis (TGA)

Thermogravimetry analysis is the branch of thermal analysis which measures the weight change of a sample as a function of temperature or time. Weight loss or gain of the samples occurs as a result of some important process which include desorption, absorption, sublimation, vaporization, oxidation, reduction and decomposition. TGA is used to characterize the decomposition and thermal stability of materials under a variety of conditions and to examine the kinetics of the physicochemical processes occurring in the sample. It is especially useful for the study of polymeric materials like thermoplastics, thermosets, elastomers, composites, films, fibers, coatings and paints. The principal applications of TGA in polymers are (1) determination of the thermal stability of polymers, (2) compositional analysis, and (3) identification of polymers from their decomposition pattern. TGA curves are also used to determine the kinetics of thermal decomposition of polymers and the kinetics of cure where weight loss accompanies the cure reaction (eg, as in condensation polymerizations, such as cure of phenolic resins). TGA decomposition information can also be used to approximately predict the useful product lifetimes of some polymeric materials, such as the coatings for electrical or telecommunication cables.

One good example demonstrating the application of TGA is in the rubber industry to determine the composition of a rubber formulation, either cured or uncured. The standard test method for compositional analysis by TGA provides a method for determining four components: (1) highly volatile matter, (2) matter of medium volatility, (3) combustible material, and (4) ash, left after oxidative decomposition of inorganic components. The success of the method depends on each component having a different thermal stability range in an inert atmosphere and in an oxidizing atmosphere.

1.10.2 Differential scanning calorimetry (DSC)

Differential Scanning Calorimetry is a thermal analysis technique that monitors heat absorbed or generated in a material as a function of temperature or time. A sample of known mass is heated or cooled in a programmed manner and the changes in heat flow are tracked. DSC is used in many industries including pharmaceuticals, polymers, food, paper, printing, manufacturing, agriculture, semiconductors, and electronics as most materials exhibit some sort of transitions. It is widely used for examining polymeric materials to determine the thermal transitions like melting, crystallization and glass transition. Melting points and glass transition temperatures for most polymers are available from standard compilations and therefore determination of these parameters help in identifying the polymer. The percent crystalline content of a polymer can be estimated from the crystallization/melting peaks of the DSC thermogram by comparing with the reference values given in the literature. DSC can also be used to study thermal degradation of polymers using an approach such as Oxidative Onset Temperature/Time (OOT). The biggest advantage of DSC is the ease and speed with which it can be used to observe transitions in materials.

1.11 Literature review

The use of ionizing radiation for inducing chain polymerization of vinyl monomers were initiated in the late 1930s [32-34] and by the late fifties, radiation polymerization of many common synthetic water soluble monomers such as acrylamide [35], methacrylic acid [36], vinyl pyrrolidone [37] and others were reported. Since radiation-initiated polymerization of vinyl monomers in aqueous solution is a clean process, it also provides a method for investigating primary events associated with the radiolysis of water and the subsequent reaction of the transient species with the monomer.

The effect of radiation on polymers has also been studied since a long time. The earliest report on the effect of radiation on polymers in solution was by Khenokh in 1941,

who subjected solutions of natural polymers like gelatin and starch to gamma rays in order to gain information about the effect of radiation on proteins and carbohydrates respectively [38, 39]. First investigations on the radiolysis of synthetic polymer, poly(methacrylic acid), in aqueous solutions were reported in the early 1950s by Alexander and Fox who studied the X-ray induced degradation of polymer in aqueous solution [40-42]. Charlesby and Alexander also studied the effect of radiation on a number of water soluble polymers and showed that, depending on their chemical structure and irradiation conditions, these polymers either degrade or crosslink on irradiation [43]. Radiation effects on different polymers have been investigated by a large number of research workers and are well documented in literature [44-47].

Radiation interaction with polyelectrolytes, like polydiallyldimethylammonium chloride investigated in the thesis, may lead to materials or products with interesting properties and applications. For example, irradiation of polyacrylic acid leads to the formation of hydrogels (crosslinked polymeric network) with tremendous swelling capacities [48]. These are known as Superabsorbents and a few grams of the material can absorb several hundred grams of water making them useful in applications such as personal hygiene products, agriculture, spillage control etc. Other applications include radiation synthesis of polyampholyte hydrogel by using a combination of oppositely charged polyelectrolytes [49]; radiation grafting of polyelectrolyte brushes to certain substrates for use as ion exchange resins [50], removal of organic dyes from effluents [51] and for protein separation [52]. Our group has investigated the radiation effect on certain polyelectrolytes like polystyrenesulfonate [53, 54], polyvinylbenzyltrimethylammonium chloride [55, 56] and 2-(methacryloyloxy) ethyl trimethylammonium chloride [57, 58].

Radiation-induced grafting technique has been studied for many applications like purification of proteins [59], immobilization of enzymes [60] and extraction of uranium from

sea water [61]. Many of the technologies have been successfully commercialized for the production of ion-exchange membranes, battery separators, fiber membranes for micro-filtration of proteins solutions and ion exchange non-woven fabrics for removal of trace amounts of gases from ultra clean rooms [62, 63]. Therefore, one can easily and effectively incorporate the desired properties onto a polymer backbone using graft polymerization by selecting suitable monomer without destroying or affecting the basic properties of the of the trunk polymer like crystallinity, melting point or mechanical properties [64-65].

In this thesis, the radiation induced changes in polydiallyldimethylammonium chloride (PDADMAC) a polyelectrolyte and its monomer is investigated and reported. In addition to exploration of fundamental effects, this study also comprises the investigations on radiation processing of this polymeric system for the design and development of procedures or protocols for synthesis of materials exhibiting potential applications.

1.12 Thesis Overview

Polydiallyldimethylammonium chloride (PDADMAC), a cationic polyelectrolyte has generated immense interest because of its unique polymerization chemistry which is relevant to academics and also due to many industrial applications. It is used as a flocculation aid in water treatment, as ion exchange resin, in cosmetic and personal care industry, biology and medicine, in food industry and in membrane technology [66-70]. Most of the process or products developed and research work reported however pertains to conventional processing with practically no information available about the consequence of radiation interaction with PDADMAC or its monomer diallyldimethylammonium chloride (DADMAC). Understanding the effects of ionizing radiation on PDADMAC system may lead to advancement in radiation processing of the system like better technologies and newer materials for industrial applications.

In the thesis, the chemical changes produced as a result of gamma radiation interactions with DADMAC and its polymer PDADMAC was investigated. In the nanosecond timescale, the reactions of the transient species produced by radiolysis of water, namely e_{aq}^- and $\bullet OH$, with DADMAC and PDADMAC were studied by means of pulse radiolysis technique. The steady state behavior or the final effect produced on this system after radiation exposure was also investigated under gamma irradiation conditions. Polymerization of DADMAC was initiated by gamma radiation and the various parameters affecting yield of the polymer were evaluated. Molecular weight is one of the most important characteristics of any polymer. In the present work, the molecular weight of the synthesized polymer was determined by the viscometric method and further characterization was done by various spectroscopic techniques such as UV-Visible, FT-IR, 1H -NMR and ^{13}C -NMR. Based on the structural analysis of the polymer a mechanistic pathway for its formation is suggested.

There are few analytical techniques available to characterize bulk polymeric properties and thermodynamic/thermal stability studies essential for developing applications. Thermal behavior of DADMAC and radiation synthesized PDADMAC were studied using advanced TGA and DSC techniques and important kinetic parameters associated with the various phase transitions and decompositions of the polymer were evaluated. This helps in approximately predicting the behavior of the system at a different temperature. Based on the knowledge acquired by using these techniques, a convenient thermogravimetric method was developed to determine the degree of conversion of DADMAC to PDADMAC during polymerization.

PDADMAC contains the quaternary ammonium group which is known to exhibit excellent ion exchange capacity, flocculation ability and bactericidal activity. However, to realize this potential for practical applications it is necessary to immobilize PDADMAC on

an inert support. This objective was achieved by two techniques, namely, radiation induced grafting and radiolytic encapsulation in polyethersulfone microcapsules. DADMAC was successfully grafted onto polyethylene by employing a two step grafting procedure and many of the parameters that exert a strong influence on the grafting yield were investigated in detail. For immobilization of PDADMAC in the core of polyethersulfone microcapsule, a radiolytic process was developed and it was demonstrated that the functionalized microcapsule could absorb and exchange anions such as F^- , Cl^- , Br^- , NO_3^{2-} and SO_4^{2-} at ppm level concentration.

The quaternary ammonium group of PDADMAC is reported to interact with the surface of nanoparticles and impart stability to the colloidal system. In a part of the study, PDADMAC was employed as a capping agent for the synthesis of gold nanoparticles, under gamma radiolytic conditions. In presence of this capping agent, very stable spherical gold nanoparticles with relatively narrow distribution could be synthesized easily. Further, by tweaking the experimental conditions, gold nanoparticles having triangular and hexagonal shapes could be synthesized in abundant yield. These nanoparticles known as nanoplates, exhibits physical and chemical properties vastly different from their spherical counterparts and finds applications in specialized fields like plasmonics, catalysis and Surface Enhanced Raman Scattering phenomenon. A photochemical method similar to the radiolytic method was developed where PDADMAC was utilized as a shape controlling capping agent. This method, in addition to producing the usual gold nanoplates, could afford the synthesis of *concave* nanoplates by subtle variation in the process conditions. These nanoplates are reported to be effective catalyst for various organic oxidation reactions.

Overall, the thesis provides an insight about the underlying mechanism of the various processes and products described using DADMAC and PDADMAC, especially the formation of encapsulated/grafted ion exchangers and gold nanoplates. The study would be helpful in

laying a foundation for further research and development of newer applications in the field of radiation processing of similar polymeric system.

Chapter 2: EXPERIMENTAL

2.1 Introduction

The basic principles and instrumentation of the various techniques and facilities employed in the present studies is described in this chapter. The schematic layouts of the instruments used are included for better clarity. The techniques include description and use of ^{60}Co gamma radiation chamber for steady-state irradiation studies and Pulse radiolysis technique for characterization of transients generated as a result of water radiolysis. Common analytical techniques such as Fourier transform infrared spectroscopy (FTIR), Ion chromatography, UV-visible spectroscopy, Differential scanning calorimetry (DSC) and Thermogravimetric analysis (TGA) are discussed here. Many techniques employed for the characterization of nanoparticles like Transmission electron microscopy (TEM), Scanning electron microscopy (SEM), Energy dispersive X-rays analysis (EDX), Atomic force microscopy (AFM) and X-ray diffraction (XRD) are also described in the chapter.

2.2 Gamma radiation sources

Gamma Chamber (GC 5000) used for gamma irradiation of the samples was procured from BRIT, INDIA. The gamma source used in the chamber is ^{60}Co radioisotope which is produced by irradiating natural cobalt (^{59}Co) in the form of pellets, small slugs or thin disks in nuclear reactor by the $^{59}\text{Co} (n,\gamma) ^{60}\text{Co}$ reaction to give a uniformly active material. ^{60}Co emits two γ -rays of energies 1.33 MeV and 1.17 MeV according to the decay scheme shown in Fig. 2.1 below;

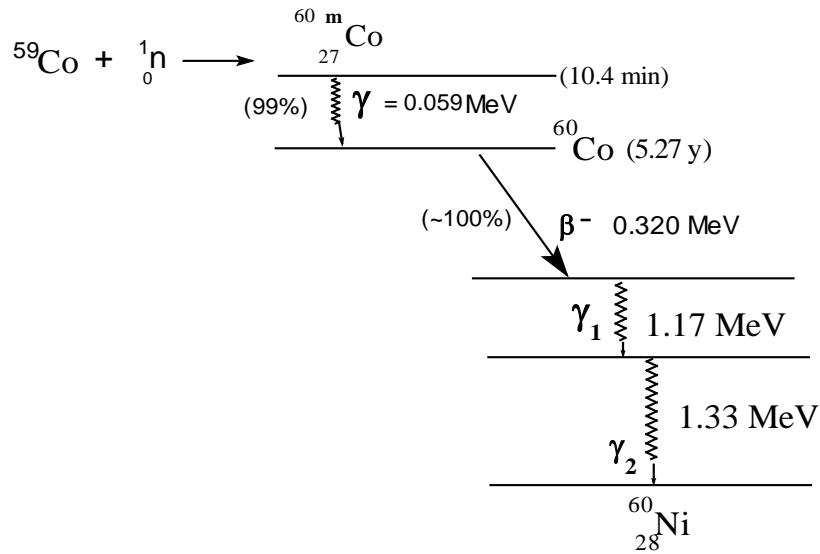


Fig. 2.1: Decay scheme for ^{60}Co

The stationary ^{60}Co source is placed in a cylindrical enclosure surrounded by a lead shield to keep external radiation field well within permissible limits. The material for irradiation is placed in a vertical drawer inside the lead flask that can be moved up and down with the help of a system of motorized drive, which enables precise positioning of the irradiation chamber at the center of the radiation field. The walls of the metal container serve to filter out β radiation emitted by the ^{60}Co source. The gamma chamber used for our studies is shown in. Fig. 2.2.

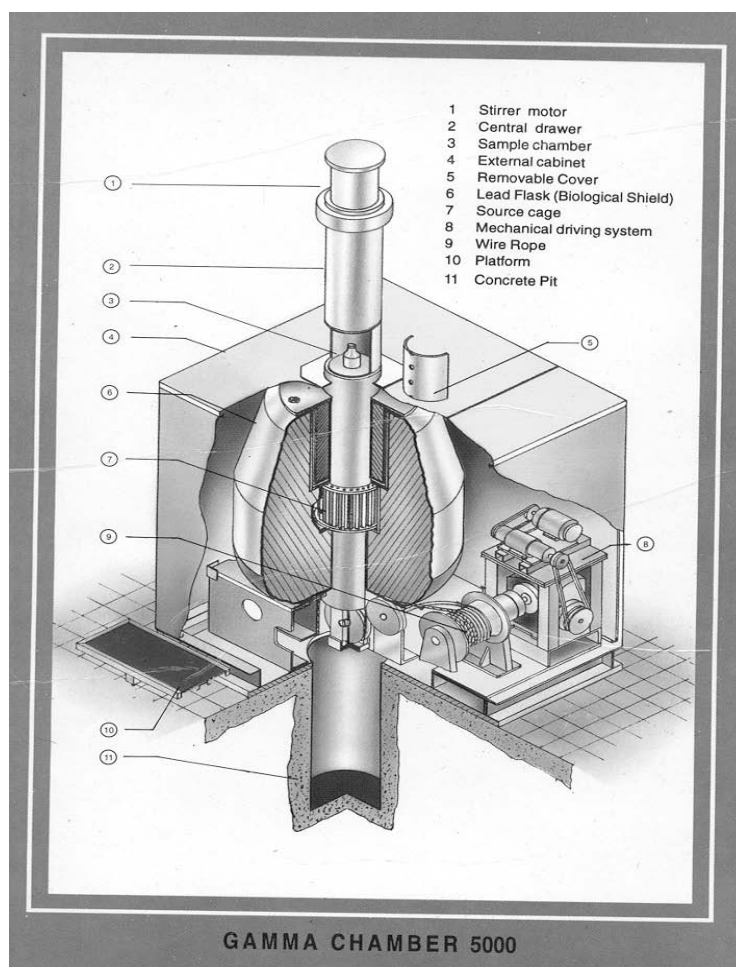


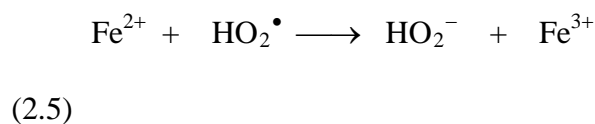
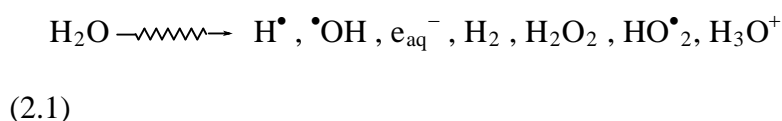
Fig. 2.2: Gamma chamber 5000

2.2.1 Gamma radiation dosimetry (Fricke Dosimeter)

The dose rate of the gamma chamber was determined using Fricke dosimeter which is based on radiation induced oxidation of the ferrous ions [72, 73] to the ferric ions in aqueous solutions. The standard Fricke dosimeter consists of an aerated solution of $1.0 \times 10^{-3} \text{ mol dm}^{-3}$ ferrous ammonium sulphate, $1.0 \times 10^{-3} \text{ mol dm}^{-3}$ NaCl and 0.4 mol dm^{-3} sulphuric acid [74]. The yield of Fe^{3+} ions produced is determined by absorption spectrophotometry employing Beer's law ($\Delta A = \Delta \epsilon \cdot c \cdot l$) at 304 nm with $\epsilon(\text{Fe}^{3+}) = 220.5 \pm 0.3 \text{ m}^2 \text{ mol}^{-1}$ and $\epsilon(\text{Fe}^{2+}) = 0.1 \text{ m}^2 \text{ mol}^{-1}$ at 25°C. The $G(\text{Fe}^{3+}) \cdot \epsilon$ value accepted for electron and photon radiation in the range 1

to 30 MeV is $3.52 \times 10^4 \text{ m}^2 \text{ J}^{-1}$ at 25°C [75]. The Fricke dosimeter can be used to accurately determine dose only up to 400 Gy because of depletion of dissolved oxygen. Fricke dosimeter is independent of dose rate between 0.2 to $2.0 \times 10^6 \text{ Gy s}^{-1}$.

The reaction involved in the Fricke dosimeter is the radiation-induced oxidation of ferrous ion to ferric ion at low pH and in the presence of oxygen in accordance with the series of reactions (Egns. 2.1 to 2.7) [76-79].



The yield of ferric ion is related to the primary radical and molecular yields by Eqn. 2.8.

$$G(\text{Fe}^{3+}) = 2G(\text{H}_2\text{O}_2) + 3[G(e_{\text{aq}}^-) + G(\text{H}^\bullet) + G(\text{HO}_2^\bullet)] + G(\bullet\text{OH}) \quad (2.8)$$

Since each molecule of hydrogen peroxide oxidizes two ferrous ions according to Eqn. 2.4 and then Eqn. 2.7, while the reducing radicals each oxidize three ferrous ions by sequential reactions involving HO_2^\bullet , H_2O_2 and $\bullet\text{OH}$ respectively. Substituting the G values

of various species in equation 2.26, the $G(\text{Fe}^{3+})$ has been found to be $1.61 \mu\text{mol J}^{-1}$ [80, 81].

Absorbed dose can be determined in Grays using Eqn. 2.9.

$$D_D = 2.77 \Delta A/l \quad (2.9)$$

Where ΔA is change in the absorption (at 304 nm) of solution and l is the path length in meters.

2.3 Pulse radiolysis setup

The intermediates produced by radiolysis are very reactive and has very short lifetimes in most environments. The ability to monitor transient behavior with a degree of precision over extremely short time scale is necessary for identification and characterization of these intermediate. Since the concentration of such intermediates is very low detection, very sensitive techniques are required for characterization of the transient behavior. In pulse radiolysis a very intense pulse of electrons is given to a system to achieve a non-equilibrium condition in which significant concentration of transient species is produced in a short time interval. These transient species are monitored by following the changes in their characteristic properties such as optical absorption, electrical conductivity or electron spin resonance. In pulse radiolysis, very short (i.e., short with respect to the life time of the species under observation) pulses of radiation with sufficiently high energy is used to produce an adequate concentration of chemical species homogenously in the system. Energy should not be too high to induce radioactivity in the target. For 5-7 MeV electrons passing through unit density material like water, the energy deposited is uniform over at least 1 cm depth [82].

The pulse radiolysis set up used in this thesis is shown schematically in Fig. 2.3. **It consists of a linear electron accelerator (LINAC)** as a radiation source, and a **kinetic spectrophotometer** as an analyzing unit. The LINAC delivers electron pulses of 7 MeV energy and the pulse duration can be varied from 25 ns to 2 μs in steps with intermediate time

scales of 50 ns to 500 ns. The sample solutions are irradiated in $1 \times 1 \text{ cm}^2$ suprasil quartz cuvettes kept at a distance of about 12 cm from the electron beam exit window. The beam diameter at 12 cm is approximately 1 cm. The absorbance of the solution is monitored with the help of a collimated light beam from a pulsed 450 W Xenon arc lamp. The monitoring light after passing through the sample cell is directed to the detection room through a tunnel with the help of fused silica lenses and aluminum-coated mirrors. Finally, the light beam is focused on the entrance slit of a grating monochromator, whose exit slit is connected to a photo multiplier tube. The output signal from photo multiplier is digitized and read on an oscilloscope. Traces are conveniently transferred to a computer for data storage and analysis [83]. The accelerator, sample cell and monitoring light source are housed in a shielded cave with 5 feet concrete walls and roof for protection from radiation. The details of the LINAC assembly are discussed in the following section.

2.3.1 LINAC

The LINAC assembly was supplied by M/s Forward Industries Ltd, UK (formerly M/s Viritech Ltd and M/s Radiation Dynamics). The important features of the machine are described below.

(i) Electron gun: A tungsten electrode in the pellet form is heated continuously by electrons from the filament of the gun. 43 keV electron pulse of 2 μs duration is initially produced which is then focused by electromagnetic lenses into a deflector chamber and finally into a corrugated cylindrical wave-guide.

(ii) Wave guide: A synchronous traveling R.F. field of 2 μs pulse width, produced by a 3 GHz, 1.8 MW peak power magnetron is fed into the wave guide, The electrons from the gun assembly entering in the correct phase of the RF field are accelerated in vacuum (10^{-8} mbar, achieved by using ion pumps) to the energy of 7 MeV, by the time they reach to the other end

of the wave guide. The accelerated electrons are focused by electromagnetic coils to obtain a well defined uniform beam of about 1 cm diameter, which comes out of the wave guide through a thin titanium window.

2.3.2 Kinetic spectrophotometer

The indigenously assembled kinetic spectrophotometer set up consists of (i) a pulsed xenon lamp as the analyzing light source; (ii) optical arrangement comprising electro-mechanical shutter, lenses, mirrors, monochromator, appropriate light filters and a suitable photomultiplier detector, (iii) amplifier, (iv) oscilloscope and (v) a computer. These units are shown in Fig. 2.3.

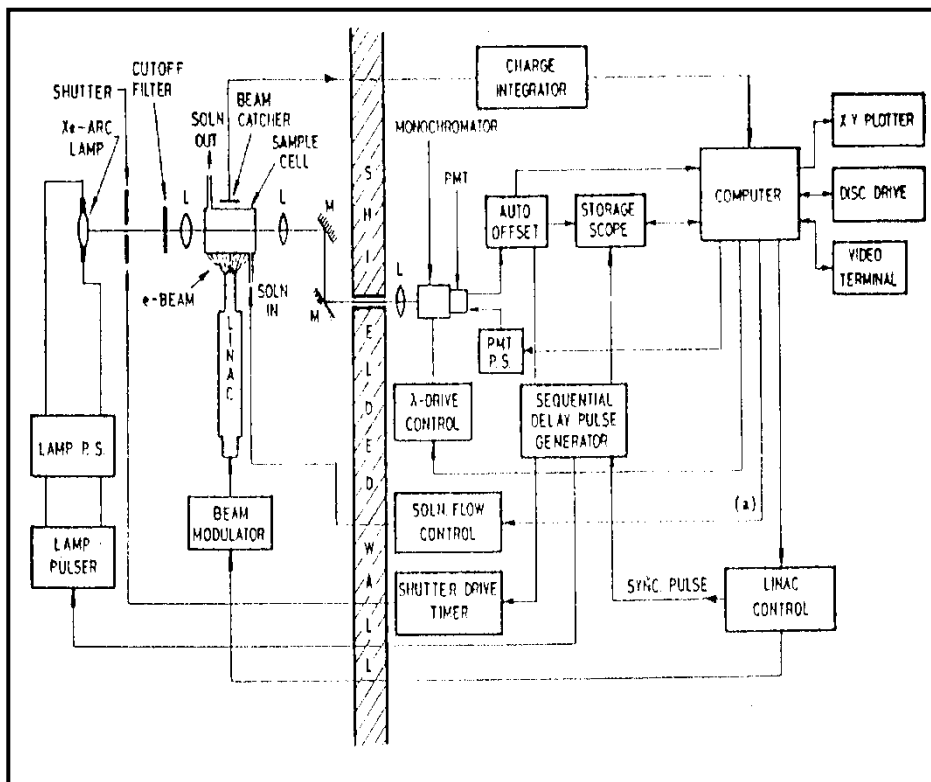


Fig. 2.3: Pulse Radiolysis Set-up with optical detection system

2.3.3 Analysis of the recorded signal

The transient signals obtained are plot of signal (mV), which is proportional to intensity of the absorbed light (I_{abs}), versus time. These signals are converted into optical density (O.D.) using Eqn. 2.10.

$$\text{O.D.} = \log \{ [\text{DC(mV)}] / [\text{DC(mV)} - \text{Signal(mV)}] \} \quad (2.10)$$

where DC(mV) is the difference of the PMT output under identical conditions with and without the analyzing light and is proportional to incident light intensity (I_0). The denominator is proportional to the intensity of the transmitted light (I_{tr}). To obtain the absorption spectrum of a transient species, the absorbance (O.D.) value at a selected time, after the end of the electron pulse, is plotted as a function of the wavelength of the analyzing light. The time- resolved spectra of the transient species could be obtained by reading the absorbance values of signals at different selected time intervals and plotting them as a function of wavelength.

2.3.4 Dosimetry for Pulse radiolysis

The main difference between steady-state gamma radiolysis using radioisotopes and pulse radiolysis using EB accelerator lies in the large difference in the dose rates employed in the two techniques. The typical gamma irradiation dose rates available from radioisotope like ^{60}Co are in the range 0 - 10 Gy s^{-1} , whereas electron beam machines generally deliver much higher dose rates in the range 10^6 to 10^{10} Gy s^{-1} . As a result, much higher concentration of radicals per unit time is generated in pulse radiolysis experiments as compared to the steady-state gamma radiolysis. The radiation chemical yields determined at low dose rates cannot be employed for high-dose rate measurements. For such systems, the possibility of quantitatively detecting the transient radicals or ions, having lifetime of the order of 10^{-6} to

10^{-3} s offers a convenient method of dose determination. Thiocyanate (SCN^-) dosimeter is commonly used in pulse radiolysis experiment which is based on the measurement of transient species produced by the intense electron beam pulse.

Thiocyanate dosimeter consists of a neutral aerated aqueous solution of 1.0×10^{-2} mol dm^{-3} solution of potassium thiocyanate. After delivery of the pulse, $\bullet\text{OH}$ produced in solution react with SCN^- to produce $(\text{SCN})_2^{\bullet-}$ according to following reactions Eqn. 2.10 and Eqn. 2.11.



The $G [(\text{SCN})_2^{\bullet-}].\epsilon$ is reported to be $2.23 \times 10^{-4} \text{ m}^2\text{J}^{-1}$ at 500 nm and this value is generally employed for dose determination [84]. From the measured O.D. values, the absorbed dose per pulse is computed using the following expression.

$$\text{Dose absorbed} = (\text{O.D.}/G.\epsilon) \times (N/1000) \times 100 \text{ eV cm}^{-3} \quad (2.13)$$

where N is the Avogadro's number. Substituting the appropriate values of $G.\epsilon$ and N , Eqn. 2.12 can be simplified to Eqn. 2.13.

$$\text{Dose absorbed} = \text{O.D.} \times 2.8 \times 10^{18} \text{ eV cm}^{-3} \quad (2.14)$$

Absorbed dose in the units of Gy is computed by multiplying the O.D. value by a factor of 448.6. The absorbed dose employed for various experiments reported in the present thesis were of the order of ~ 15 Gy per pulse.

2.4 Transmission electron microscopy (TEM)

The maximum theoretical resolution, d , that can be obtained with a light microscope is limited by the wavelength of the photons that are used to probe the sample, λ and the numerical aperture (NA) of the system (Eqn. 2.15).

$$d = \frac{\lambda}{2 n \sin \alpha} = \frac{\lambda}{2 NA} \quad (2.15)$$

TEMs are capable of imaging at a significantly higher resolution than light microscopes, owing to the small de Broglie wavelength of electrons which is related to their kinetic energy [85, 86]. In modern TEMs accelerating voltage of ~100-1500 keV are used and the wavelength of electrons at these voltages is in pico meters, therefore TEM can in principle image lattice planes. Electrons are usually generated by thermionic emission from a filament like tungsten or alternatively by field electron emission. The electrons are then accelerated by an electric potential (measured in volts) and focused by electrostatic and electromagnetic lenses onto the sample. The transmitted beam contains information about electron density, phase and periodicity and is used to form an image. The image is magnified and focused onto an imaging device, such as a fluorescent screen or to be detected by a sensor such as a CCD camera. Transmission electron microscopy of our samples was carried out using **Zeiss Libra 120 electron microscope** at an accelerating voltage of 120 keV. A typical schematic layout of the microscope is shown in Fig. 2.4.

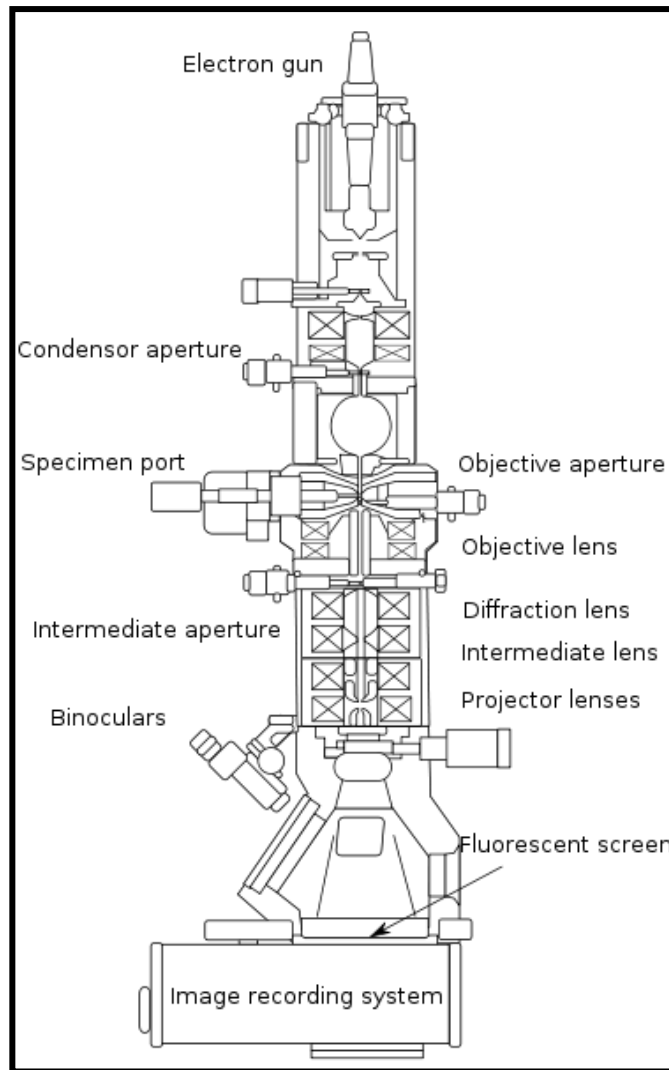


Fig. 2.4: Schematic of a TEM

2.4.1 Selected Area Electron Diffraction (SAED)

Apart from imaging mode, TEM instrument can also be used to obtain electron diffraction patterns which occur due to elastic scattering of electrons in crystalline samples. In a crystalline sample presence of long range order gives rise to rings or spots arising from constructive interference of scattering from different planes. The angular position of spots or rings is related to crystalline structure or symmetry. In a particular crystalline sample there will be several ring or spots placed radially from the central point or undiffracted beam. The rings that are seen consist of large number of merged spots. The spots arise from diffraction from a particular plane of a crystallite. The radial distance from the centre is related to the

lattice spacing and TEM parameters. Since the magnification parameters of TEM are known, lattice spacing can be obtained. Selected area electron diffraction (SAED) pattern of the samples were obtained using **JEOL (Model: 200 FX) transmission electron microscope**.

2.5 Scanning electron microscopy (SEM)

SEM produces images of a sample by scanning it with a focused beam of electrons [87, 88]. The electrons interact with atoms in the sample, producing various signals that contain information about the sample's surface topography and composition. The electron beam is generally scanned in a raster scan pattern and the beam's position is combined with the detected signal to produce an image. Specimens can be observed in high vacuum, in low vacuum or without vacuum in wet conditions (environmental SEM). The types of signals produced by SEM arises due to secondary electrons (SE), back-scattered electrons (BSE), light (cathodoluminescence), specimen current and transmitted electrons. Secondary electron detectors are standard equipment in all SEMs and the signals result from interactions of the electron beam with atoms at or near the surface of the sample. In the secondary electron imaging mode, the SEM can produce very high-resolution images of a sample surface. Due to the very narrow electron beam, SEM micrographs have a large depth of field yielding a characteristic three-dimensional appearance useful for understanding the surface structure of a sample.

Back-scattered electrons (BSE) are electrons that are reflected from the sample by elastic scattering. BSE are often used in analytical SEM because the intensity of the BSE signal is strongly related to the atomic number of the specimen. BSE images can provide information about the distribution of different elements in the sample. Characteristic X-rays are emitted when the electron beam removes an inner shell electron from the sample, causing a higher-energy electron to fill the shell and release energy. These characteristic X-

rays are used to identify the composition and measure the abundance of elements in the sample.

2.5.1 Scanning and image formation

In a typical SEM, an electron beam is thermionically emitted from an electron gun fitted with a tungsten filament cathode. Tungsten is normally used in thermionic electron guns because it is relatively cheap, has the highest melting point and lowest vapour pressure of all metals, thereby allowing it to be heated for electron emission. Lanthanum hexaboride (LaB_6) is another electron emitter which can be used in a standard tungsten filament SEM if the vacuum system is upgraded. The electron beam which typically has an energy ranging from 0.2 keV to 40 keV is focused by one or two condenser lenses to a spot about 0.4 nm to 5 nm in diameter. The beam passes through pairs of scanning coils or pairs of deflector plates in the electron column, typically in the final lens, which deflect the beam in the x and y axes so that it scans in a raster fashion over a rectangular area of the sample surface.

When the primary electron beam interacts with the sample, the electrons lose energy by repeated random scattering and absorption within a teardrop-shaped volume of the specimen known as the interaction volume, which extends from less than 100 nm to approximately 5 μm into the surface. The size of the interaction volume depends on the electron's energy, the atomic number of the specimen and the specimen's density. The energy exchange between the electron beam and the sample results in the reflection of high-energy electrons by elastic scattering, emission of secondary electrons by inelastic scattering and the emission of electromagnetic radiation, each of which can be detected by specialized detectors. The beam current absorbed by the specimen can also be detected and used to create images of the distribution of specimen current. Electronic amplifiers of various types are used to amplify the signals, which are displayed as variations in brightness on a computer monitor.

Each pixel of computer video memory is synchronized with position of the beam on the specimen in the microscope, and the resulting image is therefore a distribution map of the intensity of the signal being emitted from the scanned area of the specimen. **SEM images were recorded using SERON Technologies Inc. (Model: AIS 2100)** operating at an accelerating voltage of 20 keV. A typical schematic layout of the microscope is shown in Fig. 2.5.

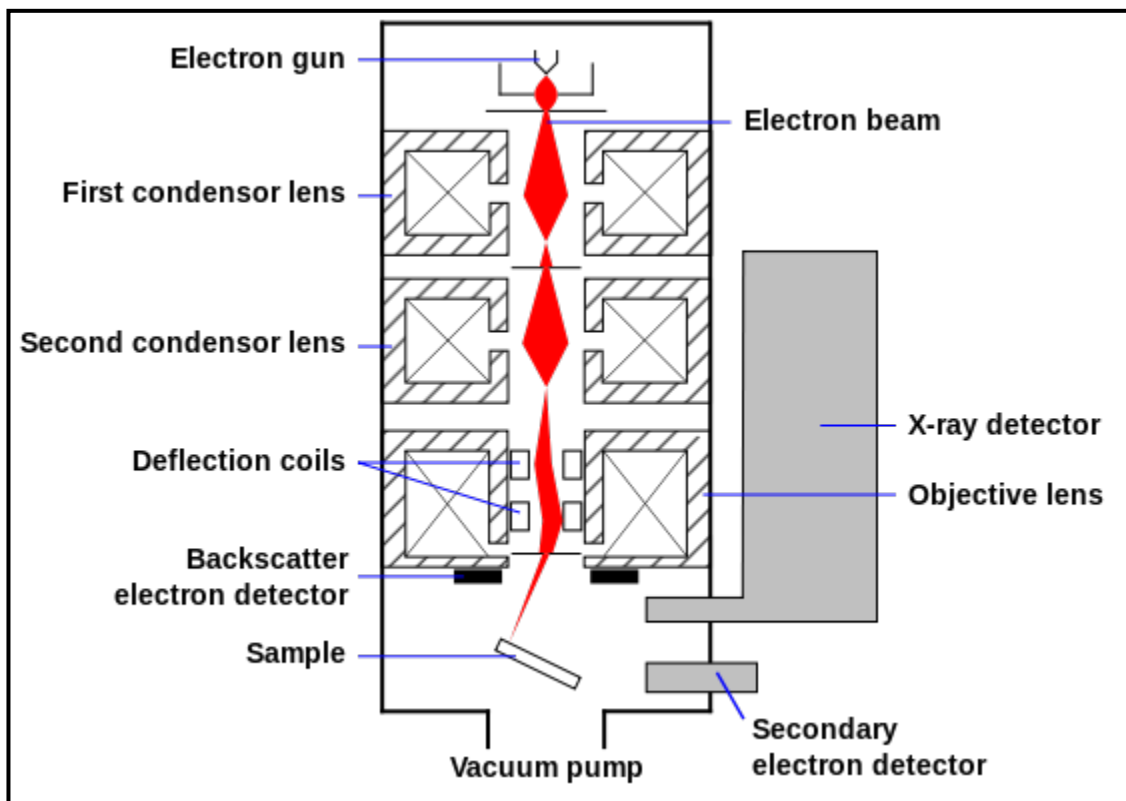


Fig. 2.5: Schematic of a SEM

2.6 Energy-dispersive X-ray spectroscopy

Energy-dispersive X-ray spectroscopy (EDS, EDX, or XEDS) is an analytical technique used for the elemental analysis or chemical characterization of a sample. Its characterization capabilities are due in large part to the fundamental principle that each element has a unique atomic structure allowing unique set of peaks on its X-ray spectrum [89]. To stimulate the emission of characteristic X-rays from a specimen, a high-energy beam

of charged particles such as electrons or protons or a beam of X-rays, is focused into the sample being studied. At rest, an atom within the sample contains ground state (or unexcited) electrons in discrete energy levels or electron shells bound to the nucleus. The incident beam may excite an electron in an inner shell, ejecting it from the shell while creating an electron hole where the electron was. An electron from an outer, higher-energy shell then fills the hole, and the difference in energy between the higher-energy shell and the lower energy shell may be released in the form of an X-ray. The number and energy of the X-rays emitted from a specimen can be measured by an energy-dispersive spectrometer. As the energy of the X-rays is characteristic of the difference in energy between the two shells, and of the atomic structure of the element from which they were emitted, this allows the elemental composition of the specimen to be measured. The phenomenon is depicted in Fig. 2.6.

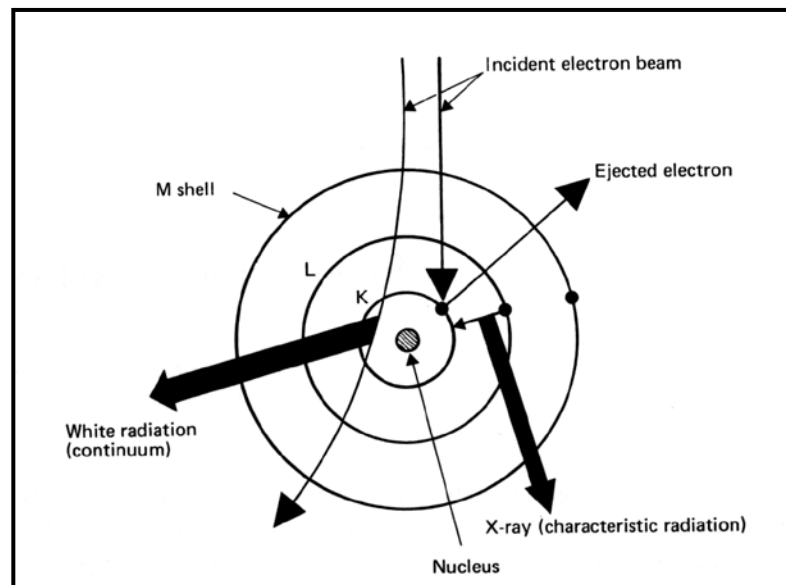


Fig. 2.6: Principle of EDS

Electron beam excitation is used in SEM and scanning transmission electron microscopes (STEM). A detector is used to convert X-ray energy into voltage signals and this information is sent to a pulse processor, which measures the signals and passes them onto an analyzer for data display and analysis. The SEM although primarily used for producing

electron images can also be used for element mapping if an X-ray spectrometer is added. There is thus a considerable overlap in the functions of these instruments and usually EDX is added as an accessory to the SEM. Energy-dispersive X-ray (EDX) analysis of the samples was performed with **Oxford Instruments (Model: INCA E350)** coupled to the SEM (SERON Technologies).

2.7 X-Ray Diffraction

In this technique, X-rays are used to obtain the diffraction pattern from a sample and helps in identifying crystallinity and different polymorphs present in a specimen [90, 91]. The diffraction from a sample with random orientation of crystal planes appear at different angles which forms the basis for identification of different phases. The angle of diffraction is clearly indicative of distances between the planes. The relationship between lattice plane spacing and angle of diffraction is given by Bragg's law.

$$n\lambda = 2d \sin\theta \quad (2.16)$$

Where n is the order of diffraction; θ is diffraction angle; d is the lattice spacing. Another important factor which helps in indexing an XRD pattern is the intensity of diffraction. The intensity is also a function of atomic scattering factors and miller indices of the planes. The atomic scattering factors influences intensity as the scattering centers in atoms are electrons. Therefore higher the number of electrons, greater is scattering from that particular atom. Phase characterization can be done just by comparing the diffraction pattern obtained for samples with that of previously reported patterns given in database from by Joint Committee on Powder Diffraction Standards (JCPDS) [92].

Fig. 2.7 shows a schematic of XRD instrument. The first step is creation of X-Rays which is accomplished by bombarding high energy electrons on a metal target. In this process, apart from broad distribution of X-rays created due to deceleration of electrons

(Bremsstrahlung) sharp lines are also created which are superimposed on the broad distribution. These sharp lines arise from characteristic X-ray coming from knocking down of core electrons creating a “hole” and subsequent filling of higher electrons. Performing a diffraction experiment requires intense sharp X-ray as the diffraction angle is also dependent on x-ray energies; therefore a broad distribution is ineffective for performing diffraction. The mainly used targets are metals like copper, molybdenum, chromium etc. The filtering of broad distribution is accomplished by using a filter which has a 1 unit atomic number less than the target material. The resultant beam is further monochromatised by using a single crystal monochromator. In a powder XRD, the samples in powdered form are spread over an amorphous substrate (generally glass slides) in presence of a binder like colloiddion in amyl alcohol. The detector is generally scintillation counter which is scanned at different angles and intensities are plotted with respect to angles. The peak position observed are angle where Bragg condition is satisfied. X-ray powder diffraction patterns of the samples were recorded with the help of **Philips X-ray diffractometer (Model PW 1729)** using Cu Ka radiation.

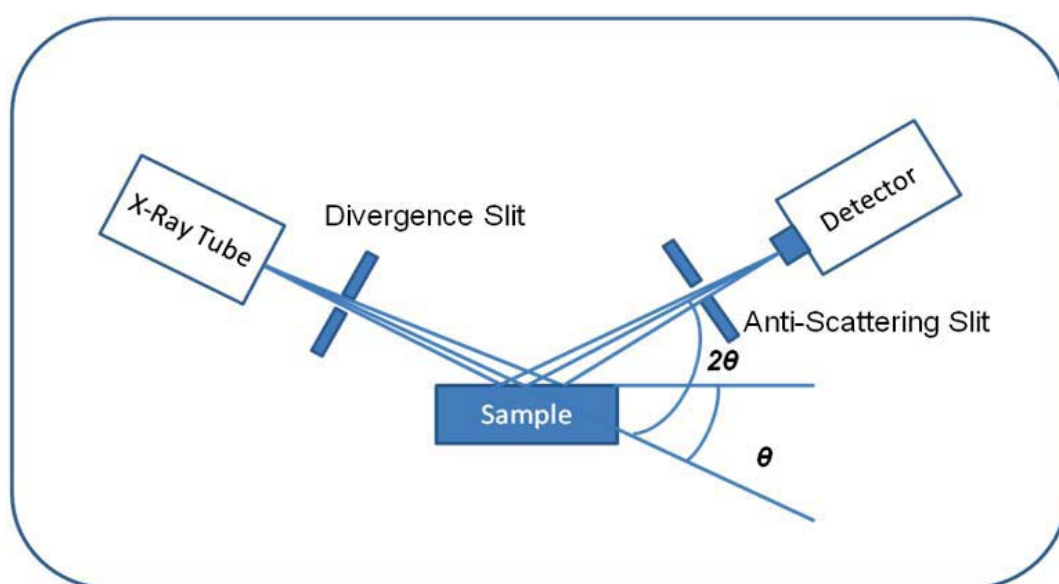


Fig. 2.7: Schematic of a XRD instrument

2.8 Atomic force microscopy (AFM)

AFM is a very high-resolution type of scanning probe microscopy and is one of the foremost tools for imaging, measuring, and manipulating matter at the nanoscale, with demonstrated resolution on the order of fractions of a nanometer [93]. The information is gathered by "feeling" the surface with a mechanical probe. Piezoelectric elements that facilitate tiny but accurate and precise movements enable the very precise scanning. In some variations, electric potentials can also be scanned using conducting cantilevers. AFM images of our samples were recorded by **NT-MDT Solver Next** at a scanning rate of 0.5 Hz in semicontact mode.

The AFM consists of a cantilever with a sharp tip (probe) at its end that is used to scan the specimen surface. The cantilever is typically silicon or silicon nitride with a tip radius of curvature on the order of nanometers. When the tip is brought into proximity of a sample surface, forces between the tip and the sample lead to a deflection of the cantilever. Depending on the situation, forces that are measured in AFM include mechanical contact force, van der Waals forces, capillary forces, chemical bonding, electrostatic forces, magnetic forces, Casimir forces, solvation forces, etc. Typically, the deflection is measured using a laser spot reflected from the top surface of the cantilever into an array of photodiodes. Schematic of an AFM is shown in Fig. 2.8.

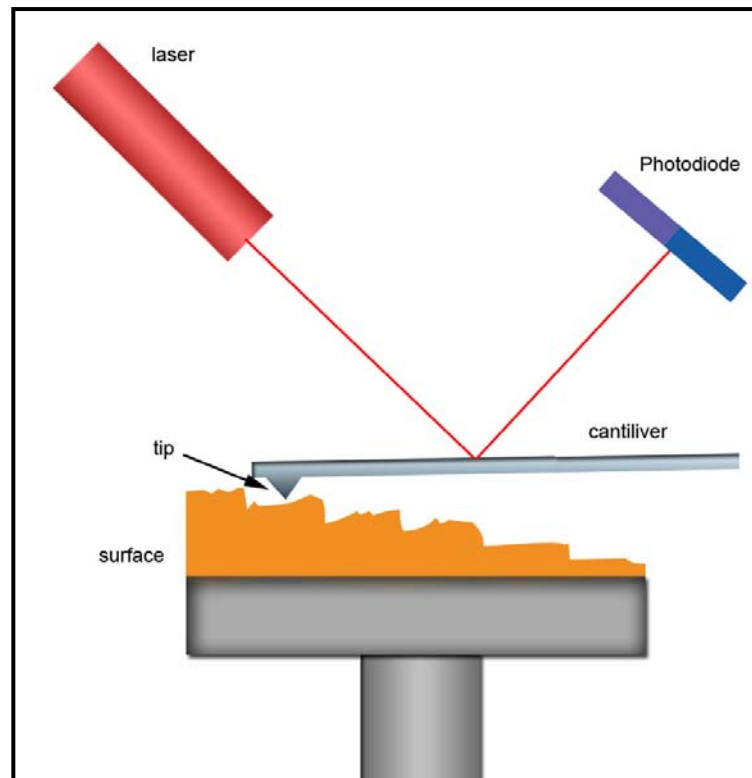


Fig. 2.8: Schematic of an AFM

2.8.1 Imaging modes

The primary modes of operation for an AFM are static mode and dynamic mode. In static mode the cantilever is "dragged" across the surface of the sample and contours of the surface are measured directly using the deflection of the cantilever. In the dynamic mode, the cantilever is externally oscillated at or close to its fundamental resonance frequency or a harmonic. The oscillation amplitude, phase and resonance frequency are modified by tip-sample interaction forces. These changes in oscillation with respect to the external reference oscillation provide information about the sample's characteristics.

2.8.1.1 Contact mode

In the static mode operation, the static tip deflection is used as a feedback signal. Since the measurement of a static signal is prone to noise and drift, low stiffness cantilevers

are used to boost the deflection signal. However, close to the surface of the sample, attractive forces can be quite strong, causing the tip to "snap-in" to the surface. Thus static mode AFM is almost always done in contact where the overall force is repulsive. Consequently, this technique is typically called "contact mode". In contact mode, the force between the tip and the surface is kept constant during scanning by maintaining a constant deflection.

2.8.1.2 Non-contact mode

In this mode, the tip of the cantilever does not contact the sample surface. The cantilever is instead oscillated at either its resonant frequency (frequency modulation) or just above (amplitude modulation) where the amplitude of oscillation is typically a few nanometers (<10 nm) down to a few picometers. The van der Waals forces, which are strongest from 1 nm to 10 nm above the surface, or any other long range force which extends above the surface acts to decrease the resonance frequency of the cantilever. This decrease in resonant frequency combined with the feedback loop system maintains a constant oscillation amplitude or frequency by adjusting the average tip-to-sample distance. Measuring the tip-to-sample distance at each (x,y) data point allows the scanning software to construct a topographic image of the sample surface. Non-contact mode AFM does not suffer from tip or sample degradation effects that are sometimes observed in contact AFM. This makes non-contact AFM preferable to contact AFM for measuring soft samples, e.g., biology sample and organic thin film. In the case of rigid samples, contact and non-contact images may look the same. However, if a few monolayers of adsorbed fluid are lying on the surface of a rigid sample, the images may look quite different. An AFM operating in contact mode will penetrate the liquid layer to image the underlying surface, whereas in non-contact mode an AFM will oscillate above the adsorbed fluid layer to image both the liquid and surface.

2.8.1.3 Tapping mode

In *tapping mode*, the cantilever is driven to oscillate up and down at near its resonance frequency by a small piezoelectric element mounted in the AFM tip holder similar to non-contact mode. However, the amplitude of this oscillation is greater than 10 nm, typically 100 to 200 nm. The interaction of forces acting on the cantilever when the tip comes close to the surface, Van der Waals forces, dipole-dipole interactions, electrostatic forces, etc. cause the amplitude of this oscillation to decrease as the tip gets closer to the sample. An electronic servo uses the piezoelectric actuator to control the height of the cantilever above the sample. The servo adjusts the height to maintain a set cantilever oscillation amplitude as the cantilever is scanned over the sample. A *tapping AFM* image is therefore produced by imaging the force of the intermittent contacts of the tip with the sample surface. This method of "tapping" lessens the damage done to the surface and the tip compared to the amount done in contact mode. Tapping mode is gentle enough even for the visualization of supported lipid bilayers or adsorbed single polymer molecules (for instance, 0.4 nm thick chains of synthetic polyelectrolytes) under liquid medium. With proper scanning parameters, the conformation of single molecules can remain unchanged for hours.

2.9 UV-Visible Absorption Spectroscopy

Atoms and molecules have discrete electronic levels in the ground state as well as in the excited states and this technique exploits the electronic excitation of chemical species from ground to different excited states using UV or visible light. Since electronic levels in a particular chemical species are unique, these can be used as fingerprint for identification of molecules. The peak height is proportional to concentration of the species, therefore, this technique can be used for both quantitative and qualitative evaluation of a chemical species [94].

The system consists of a calibrated source of incident light of a particular wavelength. When a chemical species absorbs around λ_{\max} , then the intensity of transmitted light at that wavelength decreases. Decrease in intensity of transmitted light is a function of concentration and path length. The relation between the absorbance, concentration and path length is given by Beers-Lambert law;

$$A = \log_{10} \left(\frac{I_0}{I} \right) = \epsilon cl \quad (2.17)$$

In above equation A is the absorbance, I_0 is incident intensity, I is transmitted intensity for a particular wavelength and l is path length, ϵ is extinction coefficient and c is concentration of that species. We assume that decrease in intensity arises from absorption of light by sample and not scattering. Scattering is especially large in cases where solubility of sample is poor. Additionally concentration of samples are expected to be kept low as at higher concentration factors like intermolecular interactions and changes in refractive index affect measurement. The scan over entire UV-Vis region gives rise to absorption spectra which forms the basis of this technique. UV-Visible spectra of the sample solution were recorded using **Thermo, Evolution 300** spectrophotometer. Schematic of UV- visible spectrophotometer is shown in Fig. 2.9.

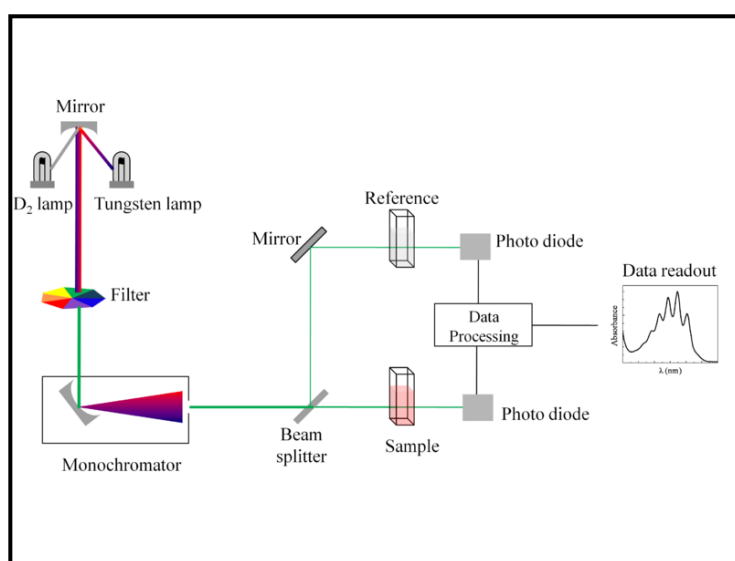


Fig. 2.9: Schematic of UV- visible spectrophotometer

2.10 Fourier transform infrared spectroscopy (FTIR)

Infrared spectroscopy deals with the infrared region of the electromagnetic spectrum and exploits the fact that molecules absorb specific frequencies that are characteristic of their structure. These absorptions are resonant frequencies, i.e. the frequency of the absorbed radiation matches the transition energy of the bond or group that vibrates. In order for a vibrational mode in a molecule to be "IR active," it must be associated with changes in the dipole. A permanent dipole is not necessary, as the rule requires only a change in dipole moment. A molecule can vibrate in many ways, and each way is called a *vibrational mode*. For molecules with N atoms in them, linear molecules have $3N - 5$ degrees of vibrational modes, whereas nonlinear molecules have $3N - 6$ degrees of vibrational modes (also called vibrational degrees of freedom). As an example H_2O , a non-linear molecule, will have $3 \times 3 - 6 = 3$ degrees of vibrational freedom, or modes. Simple diatomic molecules have only one bond and only one vibrational band. If the molecule is symmetrical, e.g. N_2 , the band is not observed in the IR spectrum, but only in the Raman spectrum. Asymmetrical diatomic molecules, e.g. CO , absorb in the IR spectrum. More complex molecules have many bonds, and their vibrational spectra are correspondingly more complex, i.e. big molecules have many peaks in their IR spectra. IR spectroscopy is often used to identify structures because functional groups give rise to characteristic bands both in terms of intensity and position (frequency). The position of these bands is summarized in correlation table shown in Fig. 2.10.

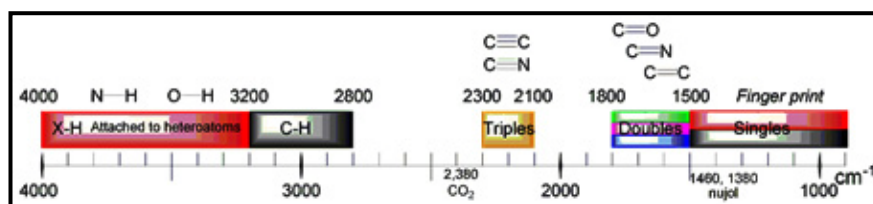


Fig. 2.10: Correlation table of IR bands

One method for taking spectra is the "dispersive" or "scanning monochromator" method where one wavelength at a time passes through the sample. The dispersive method is more common in UV-Vis spectroscopy, but is less practical in the infrared than the FTIR method. The term *Fourier transform infrared spectroscopy* [95, 96] originates from the fact that a Fourier transform (a mathematical process) is required to convert the raw data into the actual spectrum. The main part of the FTIR spectroscope is the "Michelson interferometer" and in this technique infrared light is guided through the interferometer and then through the sample. A moving mirror inside the apparatus alters the distribution of infrared light that passes through the interferometer (Fig. 2.11).

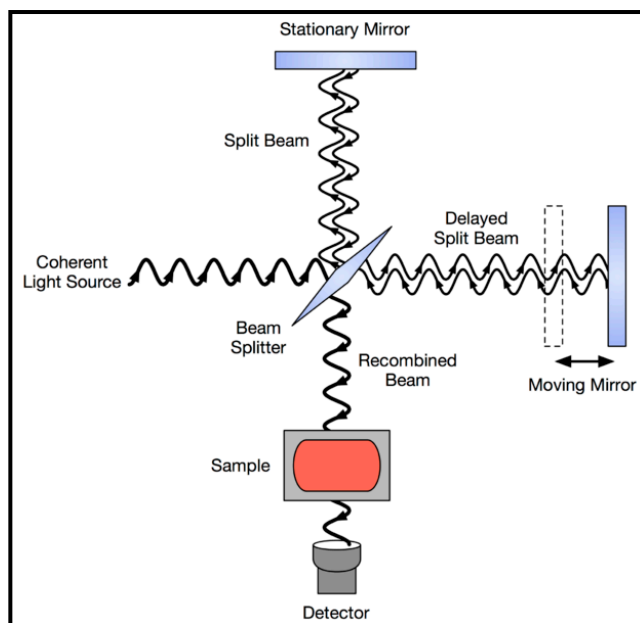


Fig. 2.11: Schematic diagram of a Michelson interferometer configured for FTIR

The signal directly recorded, called an "interferogram", represents light output as a function of mirror position. The Fourier transform (FT) turns this raw data into the desired sample's spectrum as shown in Fig. 2.12.

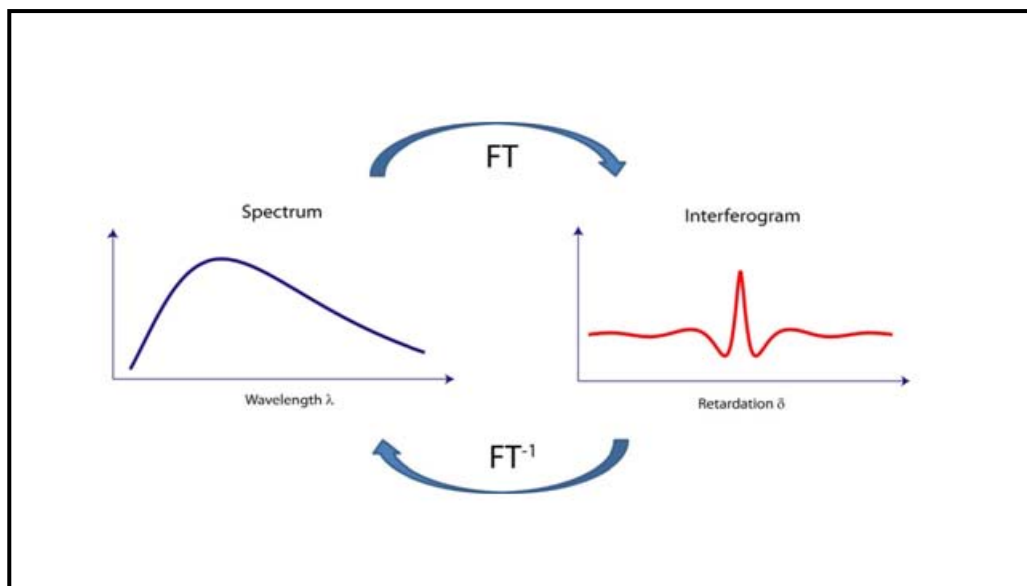


Fig. 2.12: The Fourier transform

In FTIR the information at all frequencies is collected simultaneously, improving both speed and signal-to-noise ratio. This is termed as " Fellgett's advantage" or the "multiplex advantage" Another is called "Jacquinot's Throughput Advantage": A dispersive measurement requires detecting much lower light levels than an FTIR measurement. There are other advantages, as well as some disadvantages, but virtually all modern infrared spectrometers are FTIR instruments. The spectrum of our polymer sample was recorded by **JASCO 660 FTIR** spectrometer. The resolution of the scan was set at 2 cm^{-1} and an average of 16 scans were obtained.

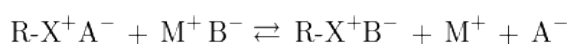
2.11 Ion chromatography

Ion chromatography is a process that allows the separation of ions and polar molecules based on their charge [97, 98]. It can be used for almost any kind of charged molecule including large proteins, small nucleotides and amino acids. Ion-exchange chromatography retains analyte molecules on the column based on coulombic (ionic) interactions. The stationary phase surface displays ionic functional groups (R-X) that interact

with analyte ions of opposite charge. This type of chromatography is further subdivided into cation exchange chromatography and anion exchange chromatography. The ionic compound consisting of the cationic species M^+ and the anionic species B^- can be retained by the stationary phase. Cation exchange chromatography retains positively charged cations because the stationary phase displays a negatively charged functional group:



Anion exchange chromatography retains anions using positively charged functional group:



The ion strength of either C^+ or A^- in the mobile phase can be adjusted to shift the equilibrium position and thus retention time. Fig. 2.13 shows the schematic diagram of ion chromatography.

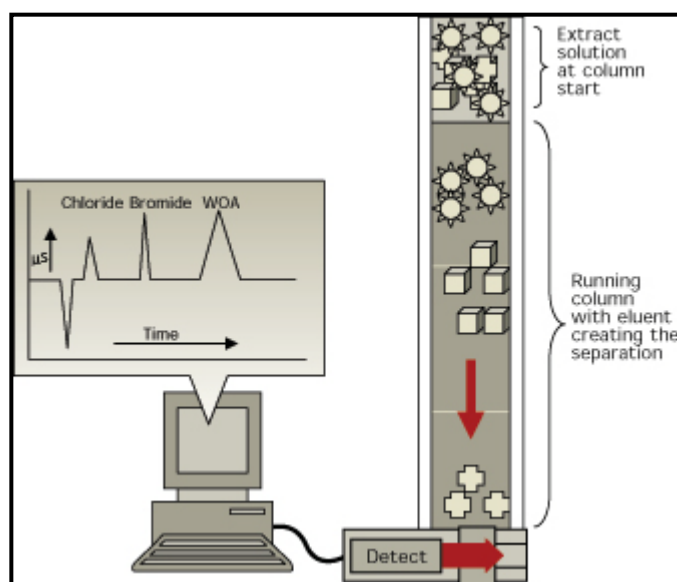


Fig. 2.13: Schematic diagram of ion chromatography

The sample is introduced manually or with an auto sampler into a sample loop of known volume. A buffered aqueous solution known as the mobile phase carries the sample from the loop into a column that contains some form of stationary phase material. This is typically a resin or gel matrix consisting of beads with covalently bonded charged functional groups. The target analytes (anions or cations) are retained on the stationary phase which can be later eluted by increasing the concentration of a similarly charged species that will displace the analyte ions from the stationary phase. For example, in cation exchange chromatography, the positively charged analyte could be displaced by the addition of positively charged sodium ions. The analytes of interest must then be detected by some means, typically by conductivity or UV/Visible light absorbance.

All the sample analyses were conducted on **Dionex ion chromatography equipment (DX-500)** consisting of a gradient pump (GP 40), Rheodyne injection port, anion trap column (ATC), anion guard column (AG 11, 4 mm), anion separating column (AS 11, 4 mm), anion self-regenerating suppressor unit (ASRS-ULTRA, 4 mm), electrochemical detector (ED 40), UV/vis absorbance detector (AD 20) and auto-sampler (AS 40). A Dionex PeakNet (version 5.01) chromatography workstation was used for system control and data collection. Sample loop of 10 ml was used throughout the analyses.

2.12 Differential scanning calorimetry (DSC)

The basic principle underlying differential scanning calorimetry involves measurement of heat absorbed or liberated when the sample undergoes phase transitions under a controlled heating or cooling program [99, 100]. For example, as a solid sample melts to a liquid it will require more heat flowing to the sample to increase its temperature at the same rate as the reference. This is due to the absorption of heat by the sample as it undergoes the endothermic phase transition from solid to liquid. Likewise, as the sample undergoes exothermic processes (such as crystallization) less heat is required to raise the sample

temperature. By observing the difference in heat flow between the sample and reference, differential scanning calorimeters are able to measure the amount of heat absorbed or released during such transitions.

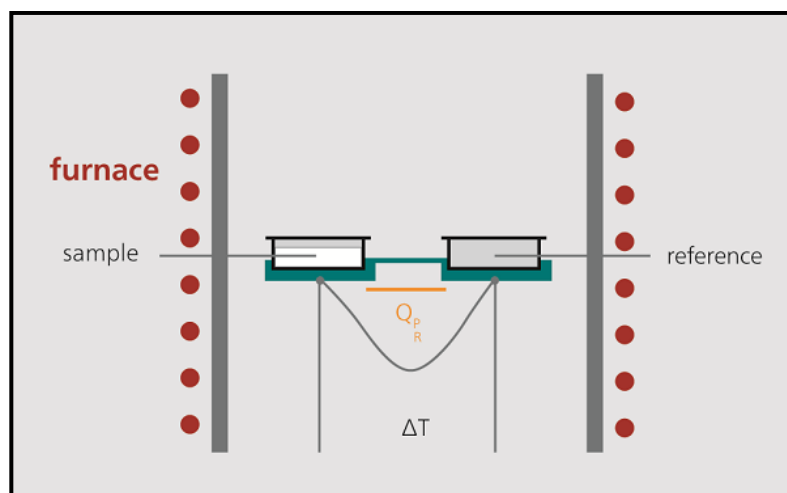


Fig. 2.14: Schematic of DSC measuring cell

The DSC measuring cell consists of a furnace and an integrated sensor with designated positions for the sample and reference pans (Fig. 2.14). The sensor areas are connected to thermocouples which allows the recording of the temperature difference between the sample and reference side and also the temperature of the furnace is closely monitored. A typical temperature difference between sample and reference (ΔT) under controlled heating is shown below (Fig. 2.15);

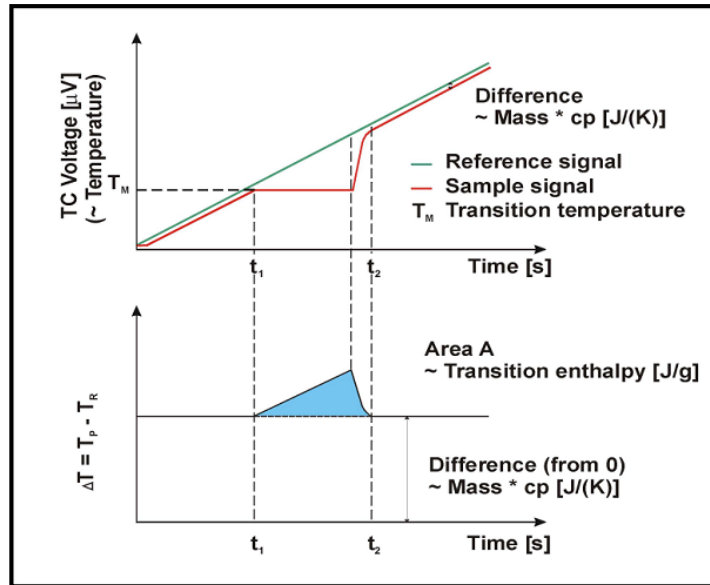


Fig. 2.15: Temperature difference between sample and reference (ΔT) versus time

Due to the heat capacity (c_p) of the sample, the reference side (usually an empty pan) generally heats faster than the sample side during heating of the DSC measuring cell; i.e., the reference temperature (T_R) increases a bit faster than the sample temperature (T_P). The two curves exhibit parallel behavior during heating at a constant heating rate until a sample reaction occurs. In the case shown here, the sample starts to melt at t_1 . The temperature of the sample does not change during melting; the temperature of the reference side, however, remains unaffected and continues exhibiting a linear increase. When melting is completed, the sample temperature also begins to increase again and, beginning with the point in time t_2 , again exhibits a linear increase. The differential signal (ΔT) of the two temperature curves is presented in the lower part of the image. In the middle section of the curve, calculation of the differences generates a peak representing the endothermic melting process. The peak area is correlated with the heat content of the transition (enthalpy in J/g).

As discussed in previous chapter (Introduction) differential scanning calorimetry is used to measure a number of characteristic properties of a sample such as fusion,

crystallization events and glass transition temperatures T_g . Glass transitions appear as a step in baseline of the recorded DSC signal because the sample undergoes only a change in heat capacity rather than a phase transition. DSC can also be used to study oxidation, as well as other chemical reactions. DSC studies were performed using **Mettler-Toledo DSC 823^e** with liquid nitrogen cooling assembly.

2.13 Thermogravimetric analysis (TGA)

In thermogravimetric analysis the change in weight of sample is measured as a function of temperature or time when the substance is subjected to a controlled temperature programme [101, 102]. Thermogravimetric analysis relies on a high degree of precision measurements in mass change and temperature. Therefore, the basic instrumental requirements for TGA are a precision balance with a pan loaded with the sample, and a programmable furnace. The furnace can be programmed for either isothermal or dynamic measurements. The schematic of TGA is shown below;

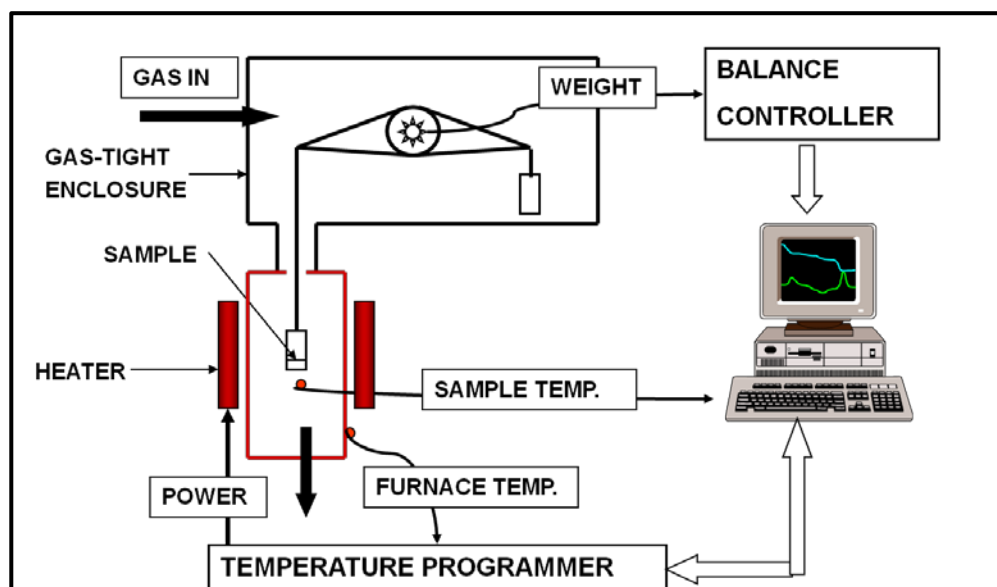


Fig. 2.16: Schematic diagram of TGA set up

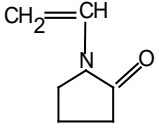
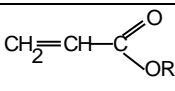
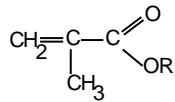
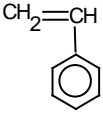
As mentioned in the introductory chapter, TGA is commonly used for characterization of materials that exhibit either mass loss or gain due to decomposition, oxidation, or loss of volatiles (such as moisture). Common applications of TGA are (1) materials characterization through characteristic decomposition pattern recognition, (2) studies of degradation mechanisms and reaction kinetics, (3) determination of organic content in a sample, and (4) determination of inorganic (e.g. ash) content in a sample. The thermogravimetric analyses reported in the thesis were carried out with **Mettler thermogravimetric analyzer (TG 50) coupled with a Mettler TC 10A processor**. The experimental data collected were transferred to a computer and kinetic analyses were carried out by Mettler STAR^e program.

Chapter 3: Radiation synthesis of PDADMAC and its characterization

3.1 Introduction

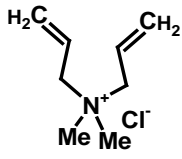
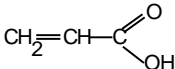
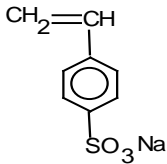
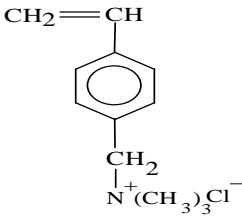
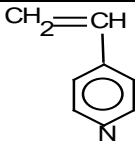
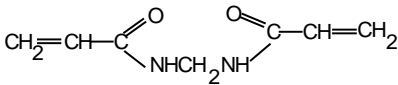
Radiation chemistry has made a profound impact in the field of polymer science and this has resulted in the emergence of a new interdisciplinary branch which may be termed as radiation polymer chemistry. Beneficial effects of radiation polymer chemistry are found along three different lines; (i) radiation-induced polymerization, (ii) radiation induced crosslinking or degradation of polymers and (iii) radiation-induced graft polymerization. Since radiation-initiated polymerization of vinyl monomers in aqueous solution is a clean process, it provides a method for investigating primary events associated with the radiolysis of water and the subsequent reaction of the transient species with the monomer. This was one of the reasons why much effort was initially devoted to the study of radiation polymerization. The desired or targeted properties of polymer can be obtained through copolymerizing a combination of monomers which can be hydrophobic, hydrophilic or ionic in nature. Radiation chemical studies of water soluble monomers that polymerize and subsequently crosslink upon irradiation can be used to synthesize various kinds of crosslinked polymer network or *gel* [103-113]. In cases where crosslinking is retarded, crosslinking agents may be introduced to achieve a crosslinked polymeric system and the extent of crosslinking may be modulated by using the proper type and amount of the crosslinker. Table 3.1 and Table 3.2 list variety of mono-functional monomers: neutral (hydrophilic and hydrophobic), ionic (anionic and cationic) and poly-functional crosslinking monomers.

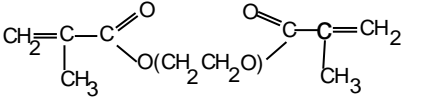
Table 3.1: Some neutral monomers

Monomer	Structure	Type
N-vinyl-2-pyrrolidone		Neutral hydrophilic
Acrylates		Neutral hydrophobic
Methacrylates		Neutral hydrophobic
Styrene		Neutral hydrophobic

where R= alkyl groups

Table 3.2: Some ionic and polyfunctional monomers

Monomer	Structure	Type
Diallyldimethyl ammonium chloride		Ionic (cationic)
Acrylic acid		Ionic (anionic)
p-Sodium styrene sulphonate		Ionic (anionic)
Vinylbenzyltrimethyl ammonium chloride		Ionic (cationic)
Vinyl pyridine		Ionic (cationic)
N,N'-methylene bisacrylamide		Polyfunctional crosslinking monomer

Ethyleneglycol dimethacrylate		Polyfunctional crosslinking monomer
-------------------------------	--	-------------------------------------

The effects produced by the interaction of Ionizing radiation with a monomer or polymer strongly depends on whether the material is irradiated in the pure form (solid / liquid) or in solution. When bulk monomer/ polymer are irradiated in pure state, either in solid state or in liquid state, radicals are generated only by the direct radiation effect and reaction pathways are limited. When polymer or monomer solutions are irradiated, the radicals produced and their subsequent reactions depend to a large extent on the concentration of the species. For dilute aqueous solution, the radicals are predominantly formed by the indirect effect based on the reaction of the products of water radiolysis ($\bullet\text{OH}$, $\text{H}\bullet$ and e^-_{aq}) [1, 12]. On the other hand, irradiation of relatively concentrated monomer or polymer solution results in radiolysis of solvent as well as the monomer/ polymer and therefore the resultant chemical interactions becomes much more complex. Therefore, the mechanism of polymerization, degradation or crosslinking is completely different in solutions than in the solid state or when monomer is used in pure form. It follows that irradiation of an aqueous polymer solution may lead to chemical transformations that do not occur when the polymer is irradiated in bulk. Thus certain degrading type polymers may crosslink when its solution is irradiated, for example, cellulose derivatives which normally degrade on irradiation crosslinks in aqueous solution [114]. Alternatively, for crosslinking type of polymers, the crosslinking reaction may be prevented because radiolytic products of water may quench the polymeric radicals before they can crosslink.

In this chapter pulse radiolysis studies of dilute aqueous solutions of monomer (DADMAC) and polymer (PDADMAC) are discussed which provides useful information regarding the characterization of the transient species generated during the course of irradiation and their subsequent reaction with the monomer or polymer. In addition to studying the fundamental effect of radiation on polymeric systems by pulse radiolysis, for certain technological applications, the monomer needs to be polymerized/ copolymerized, or a polymer crosslinked/degraded to desired extent depending on the use. Therefore, it is important to investigate the effect of various irradiation parameters on the polymerization, crosslinking or degradation behavior of aqueous monomer/polymer solutions. Steady state studies describe the changes produced on materials on exposure to radiation after removal of the sample from the zone of irradiation. The present chapter also describes gamma radiation initiated polymerization of DADMAC under steady state irradiation conditions and characterization of the synthesized polymer by various techniques.

3.2 Pulse radiolysis studies of DADMAC and PDADMAC

The radiolysis of water results in approximately equal concentrations of oxidizing and reducing species which can react with monomer or polymer and result in the formation of transient species. Pulse radiolysis is one of the most powerful techniques to study the reactions of short-lived intermediates in polymerization of synthetic monomers and crosslinking/ degradation of polymer solutions. In order to study reactions due to a particular species with the solute, it is necessary to have either only oxidizing or only reducing species. This can be generally achieved by either converting all the primary radicals into a single type of radical or by converting undesirable primary radicals into unreactive secondary radicals. There are three possible ways of determining rate constants for the reaction of a radiolytic product of water with the solute: (i) by directly monitoring the formation kinetics of the resultant species, (ii) by monitoring decay of the reacting species in the presence of the

monomer/polymer and (iii) by competition kinetic method using a standard reference solute whose rate constant with the reacting species is known.

3.2.1 Kinetic treatment of the experimental pulse radiolysis data

The kinetics of formation and subsequent reactions of the transient species forms an integral and essential part of a pulse radiolysis experiment. The data obtained from oscilloscope is transferred to a computer and detailed kinetic analysis is carried out by using dedicated softwares. Subsequently, the O.D. versus time data can be rearranged for any of the plots of first and second order decay or formation kinetic analysis, as described below;

(i) First order process: The reaction of a transient species R is considered to follow a first order kinetics when its rate of reaction or decay with time follows the following rate expression (Eqn. 3.1).

$$-d[R]/dt = k [R] \quad (3.1)$$

where k is the rate constant or specific rate of reaction, having dimensions time^{-1} . In ideal case, it represents a uni-molecular reaction that does not involve any other chemical species, for example, intra-molecular rearrangement in an ion or radical or rearrangement in an isolated excited molecule. Eqn. 3.1 may be integrated to the form

$$\log [R]_t = \log [R]_o + \{(-kt) / 3.303\} \quad (3.2)$$

where $[R]_o$ represents the initial concentration of the transient and $[R]_t$ = concentration of the transient at any time 't'. Since absorbance (O.D.) is directly proportional to [R]

$$\log (\text{O.D.})_t = \log (\text{O.D.})_o + \{(-kt) / 3.303\} \quad (3.3)$$

The slope of plot of $\log (\text{O.D.})_t$ versus time gives the rate constant k. If the growth of the transient is monitored, a similar expression (3.4) can be used.

$$\log(\text{O.D.}_\infty - \text{O.D.}_t) = \log(\text{O.D.}_\infty - \text{O.D.}_o) + \{(-kt) / 3.303\} \quad (3.4)$$

A bimolecular reaction, equation (3.6), in which the solvent molecule (S) is also involved in the reaction may also show a first order reaction especially in dilute solutions i.e. when $[S] \gg [R]$, concentration of solvent for all practical purposes can be considered constant. Such reactions are termed as *pseudo first order* reactions.



The rate equation for such a reaction is represented by equation (3.6).

$$-d[R] / dt = k [S] [R] = k' [R] \quad [S] \gg [R] \quad (3.6)$$

The rate constant k' is called the pseudo first order rate constant and has dimensions time^{-1} .

The bimolecular rate constant k can be obtained by following Eqn. 3.7.

$$k = k' / [S] \quad (3.7)$$

The bimolecular rate constants for reaction of primary products of water radiolysis (e_{aq}^- , H^\bullet and $\bullet\text{OH}$) with solutes are determined in this manner.

(ii) Second order process: When the transient species is reacting with itself, as shown in Eqn. 3.8.



the decay is truly a second order reaction. The rate constant for such a process is generally defined as $2k$ and its rate equation is represented by Eqn. 3.9.

$$-d[R] / dt = 2k \cdot [R]^2 \quad (3.9)$$

Integrating this equation between time limit '0' and 't', we get

$$1/[R]_t - 1/[R]_0 = 2k.t \quad (3.10)$$

If the species R absorbs at the monitoring wavelength λ , while the product has negligible absorption, the Eqn. 3.10. can be written in terms of the O.D. as shown in Eqn. 3.11.

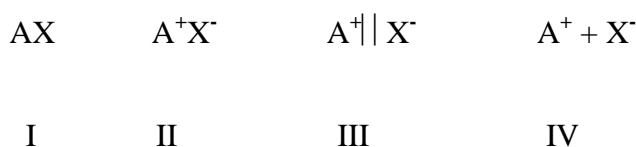
$$[1/\text{O.D.}_t] - [1/\text{O.D.}_o] = 2k.t / \epsilon.l \quad (3.11)$$

where ϵ is the molar extinction coefficient of the species and l is the path length. From the slope of '1/O.D.' versus 't' plot, the value of $2k/\epsilon.l$ can be obtained. However, in order to obtain the absolute value of the rate constant $2k$, it is essential to know the value of the molar absorptivity (ϵ), or the concentration of the transient species at time 't'.

3.2.2 Pulse radiolysis of DADMAC in aqueous solutions

For pulse radiolysis studies, DADMAC solution (~ 65%, Mol wt. 211.74) purchased from Fluka was used without further purification. All other chemicals were of AnalaR grade. Nanopure water (conductivity $0.6 \mu\text{S cm}^{-1}$) was used for preparing all solutions. The pH of solutions was adjusted using HClO_4 , KH_2PO_4 , $\text{Na}_2\text{HPO}_4 \cdot 2\text{H}_2\text{O}$ and NaOH in appropriate quantities. For studying reaction of $\bullet\text{OH}$ radical, solutions were purged with N_2O (Indian Oxygen Ltd., INDIA) and for studying the reaction of e_{aq}^- and H atom, *t*-butanol (IR grade) was used as OH radical scavenger. The transient species formed on irradiation were monitored using a 450 W xenon arc lamp as the light source and a Hamamatsu R-955 photomultiplier as the detector. The photomultiplier output signal was digitized using either a 100 MHz storage oscilloscope (Iwatsu Model 8123) or Larsen and Toubro (Model 4072) and analyzed for kinetic information using an IBM compatible microcomputer. 50 ns/2 μs single pulse of 7 MeV electrons obtained from LINAC (Forward Industries, UK) was used for irradiating the solution in 1 cm square suprasil cuvettes. Dosimetry measurements were carried out using aerated $1.0 \times 10^{-2} \text{ mol dm}^{-3}$ KSCN solution with a value of $G\epsilon = 21,520 \text{ dm}^3 \text{ mol}^{-1} \text{ cm}^{-1}$ at 500 nm [115].

Reactivity of an ionic monomer depends on distribution of electron density on the double bond as well as degree of ionization of the ionogenic group. The different ionic forms of an ionic monomer in salt solution can be represented as



where A^+ is the monomer cation, X^- is the anion and I, II, III and IV represent the non-ionized, the contact ion pair, the solvent-separated ion pair and free ions form of the monomer respectively. Depending on solvating and dissociating capability of the medium, nature of the ions A^+ and X^- , concentration of the monomer, ions added and temperature, the ratios among forms I, II, III, IV may change.

3.2.2.1 Reaction of OH radical with DADMAC

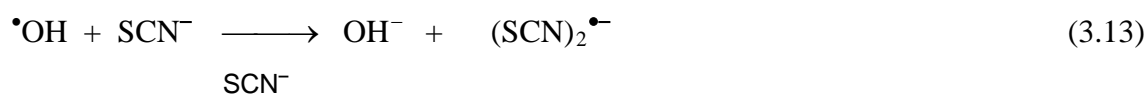
For all the pulse radiolysis experiments, DADMAC solution of concentration $<10^{-2}$ mol dm^{-3} were used. The DADMAC in the text of this chapter indicates the cation moiety generated due to ionization of monomer in aqueous solution, whereas, DADMAC cation ($DADMAC^{\bullet+}$) stands for the DADMAC cation radical generated by reaction of DADMAC with chemically reactive species of water radiolysis. In order to selectively produce $\bullet OH$, solutions were saturated with N_2O prior to pulse irradiation. Under these conditions e_{aq}^- is converted into $\bullet OH$ and the yield of the $\bullet OH$ was 90 % of the total radicals $G(\bullet OH)=6.1$. The remaining 10 % contribution was of H atoms; $G(H)=0.6$



N_2O saturated 1.0×10^{-3} mol dm^{-3} DADMAC aqueous solution was pulse radiolysed at near neutral pH using 50 ns electron pulse. The transient formed in reaction of $\bullet OH$ with

DADMAC does not have absorbance above 270 nm, therefore, the rate of reaction of $\bullet\text{OH}$ with DADMAC was estimated by competition kinetics method. In the competition kinetic study, N_2O saturated aqueous solutions containing $1.0 \times 10^{-4} \text{ mol dm}^{-3}$ KSCN and DADMAC in the concentration range $(0.1-1.0) \times 10^{-4} \text{ mol dm}^{-3}$ were pulsed and the absorbance at 500 nm due to $(\text{SCN})_2^{\bullet-}$ was measured immediately after the electron pulse.

The two competing reactions involved are;



which leads to the relation,

$$A_0/A = 1 + \{k_{\text{DADMAC} + \text{OH}} [\text{DADMAC}] / k_{\text{SCN}^- + \text{OH}} [\text{SCN}^-]\} \quad (3.15)$$

Where A_0 and A are the transient absorbance's of the solutions at 500 nm in the absence and presence of DADMAC respectively. Substituting the value of $k_{\text{SCN}^- + \text{OH}}$ [116] of $1.1 \times 10^{10} \text{ dm}^3 \text{ mol}^{-1} \text{ s}^{-1}$ in the slope obtained from the linear plot (Fig. 3.1) of A_0/A Vs $[\text{DADMAC}]/[\text{SCN}^-]$, the rate constant $k_{\text{DADMAC} + \text{OH}}$ was evaluated to be $7.4 \times 10^9 \text{ dm}^3 \text{ mol}^{-1} \text{ s}^{-1}$.

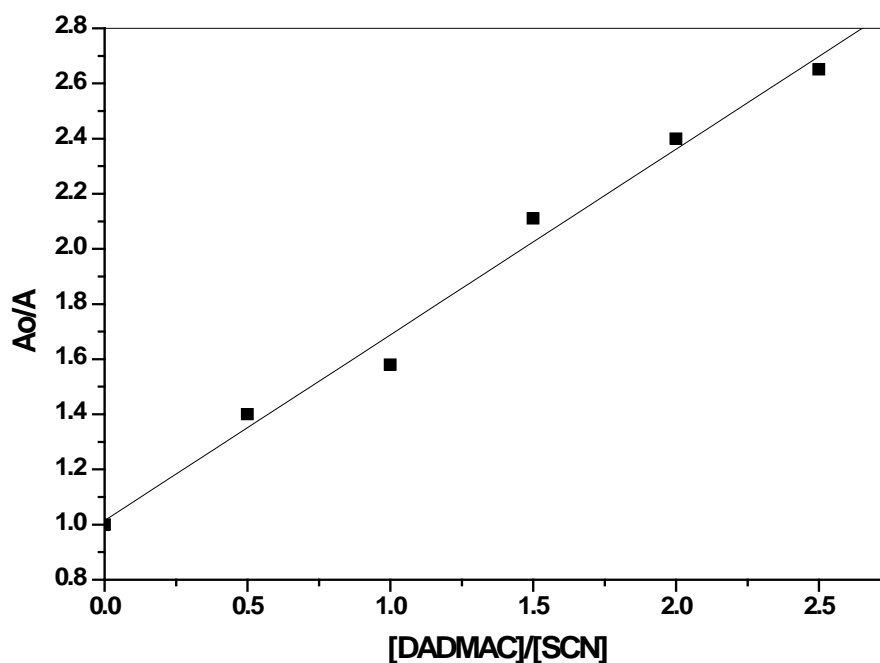
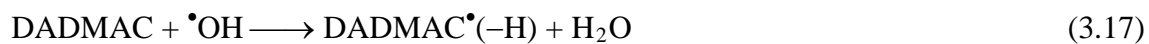


Fig. 3.1: Determination of rate constant for the reaction of $\cdot\text{OH}$ radical with DADMAC by competition kinetics using KSCN as reference solute; absorbance due $(\text{SCN})_2^{\cdot-}$ measured at 500 nm.

$\cdot\text{OH}$ can react with DADMAC mainly via three different ways: (i) addition to double bond (ii) abstraction of H atom and (iii) electron transfer. In the first two cases, neutral radicals are produced, whereas, in the third case a radical cation is formed, as shown in reactions (3.16) to (3.18).



The chemical structures of the possible transient species formed in the reaction of $\bullet\text{OH}$ radical with DADMAC can be obtained by more detailed investigations. However, in this thesis we have restricted our study to the fundamental reactions of $\bullet\text{OH}$ and e_{aq}^- only.

3.2.2.2 Reaction of e_{aq}^- with DADMAC

The reaction of e_{aq}^- with DADMAC was studied by pulse radiolysing the N_2 saturated aqueous solution of $1.0 \times 10^{-3} \text{ mol dm}^{-3}$ DADMAC at near neutral pH containing 0.3 mol dm^{-3} *t*-butanol using 50 ns electron pulse. From the decay rate of e_{aq}^- in the presence of solute, the bimolecular rate constant for the reaction was found to be $3.4 \times 10^9 \text{ dm}^3 \text{ mol}^{-1} \text{ s}^{-1}$. A typical decay trace of e_{aq}^- is shown in Fig. 3.2.

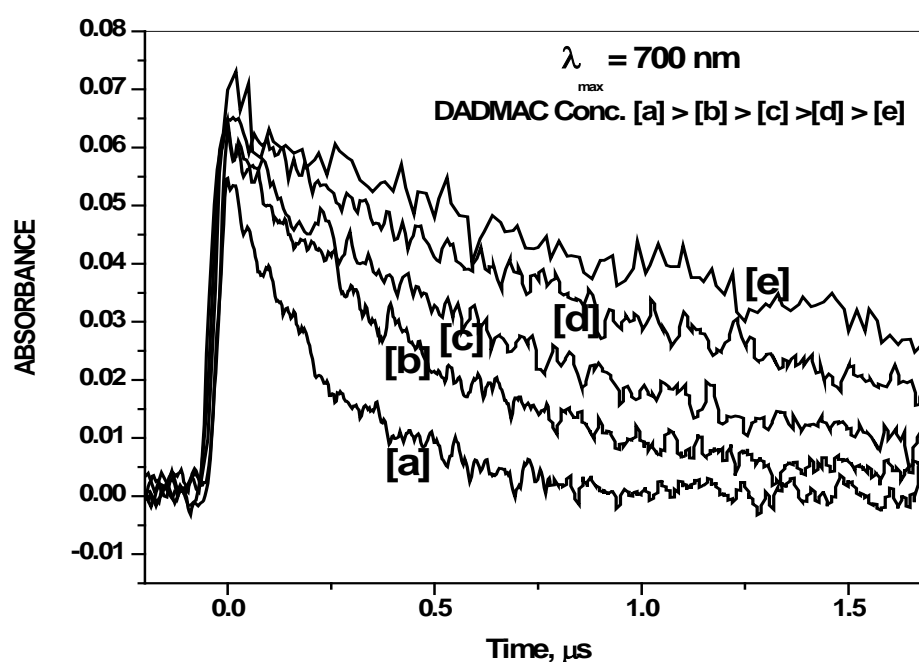


Fig. 3.2: Typical decay trace of e_{aq}^- at 700 nm in the presence of DADMAC

Hydrated electron (e_{aq}^-) adds rapidly to the compounds containing low-lying vacant orbitals such as halides, aldehydes and ketones. In the first instance the reaction of e_{aq}^- is a straightforward addition, but in some cases bond breakage occurs within the time scale of addition, so the reaction can be considered as a dissociative electron capture [117]. The

transient radical formed by the reaction of hydrated electron with DADMAC may react with DADMAC to initiate the polymerization reaction.

3.2.3 Pulse radiolysis of PDADMAC in aqueous solution

Low molecular weight PDADMAC ($M \sim 100,000 - 200,000$, 20 wt % in water) was purchased from Aldrich and used for pulse radiolysis studies without further purification. All other reagents and experimental set up was same as described for the monomer in section 3.2.2.

3.2.3.1 Reaction of OH radical with PDADMAC

As in the case of DADMAC, the transient formed in reaction of $\bullet\text{OH}$ with PDADMAC does not have absorbance above 270 nm therefore the bimolecular rate constant for the reaction of OH radical with PDADMAC was determined by the competition kinetics, using potassium thiocyanate as the reference solute. In the competition kinetics study, using KSCN as a reference solute under suitable conditions as described for DADMAC in section 3.2.2.1, $k_{\text{PDADMAC} + \text{OH}}$ was evaluated to be $8.1 \times 10^{10} \text{ dm}^3 \text{ mol}^{-1} \text{ s}^{-1}$.

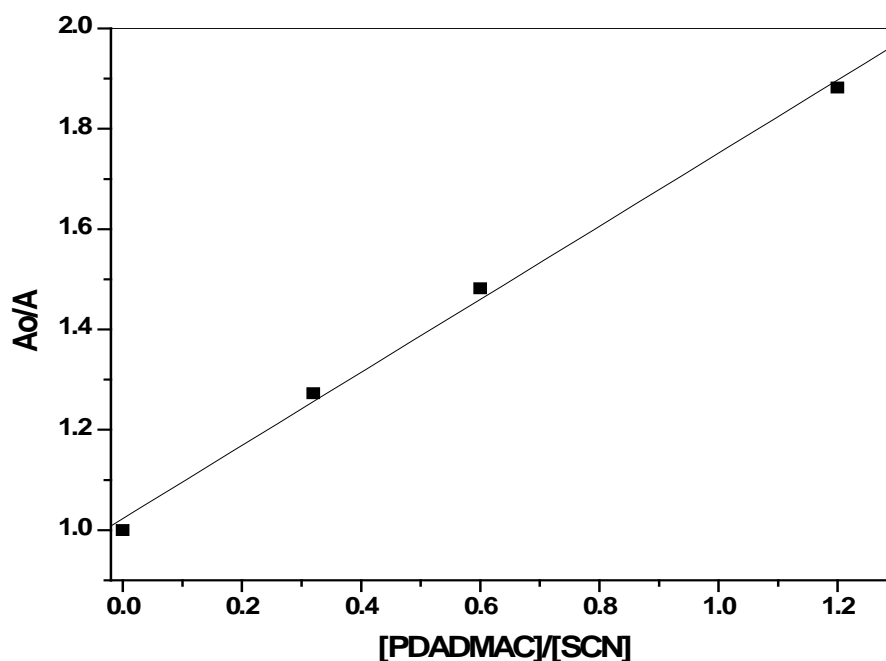


Fig. 3.3: Determination of rate constant for the reaction of $\cdot\text{OH}$ radical with PDADMAC by competition kinetics using KSCN as reference solute; absorbance due $(\text{SCN})_2^{\bullet-}$ measured at 500 nm.

3.2.3.2 Reaction of e_{aq}^- with PDADMAC

The reaction of e_{aq}^- with PDADMAC was studied by pulse radiolysing the N_2 saturated aqueous solution of $1.0 \times 10^{-3} \text{ mol dm}^{-3}$ DADMAC at near neutral pH in presence of 0.3 mol dm^{-3} *t*-butanol using 50 ns electron pulse. From the decay rate of e_{aq}^- in the presence of solute, the bimolecular rate constant for the reaction of e_{aq}^- with PDADMAC was evaluated to be $4.4 \times 10^{10} \text{ dm}^3 \text{ mol}^{-1} \text{ s}^{-1}$.

3.3 Steady state irradiation of DADMAC solution

The actual polymerization mechanism and extent of polymerization depends on several factors like the irradiation conditions, the nature and physical state of monomer, presence of impurities, nature of solvent and relative yields of free radicals and ions. This part of the

study investigates the polymerization behavior of DADMAC in aqueous medium when subjected to gamma irradiation. The PDADMAC synthesized under radiolytic conditions was characterized by a number of techniques and an effort is made to ascertain or establish the mechanism by which it is formed.

3.3.1 Effect of radiation dose on the polymerization of DADMAC

In order to investigate the effect of radiation dose on the polymerization behavior of DADMAC, aqueous solutions of DADMAC (3 mol dm^{-3}) were exposed to gamma radiation for various radiation doses at a dose rate of 3.8 kGy h^{-1} under two conditions, viz; aerated and N_2 purged. When subjected to gamma radiation, an increase in the viscosity of the monomer solution was observed which is attributed to the formation of water soluble PDADMAC. The extent of polymerization was determined gravimetrically by precipitating and separating the polymer formed by the addition of acetone which is a non solvent for many of the hydrophilic polymers. The polymer formed after irradiation was separated and the percentage of polymerization was calculated using Eqn. 3.19 and the results are depicted in Fig. 3.4.

$$\% \text{ Polymerization} = W_p / W_m \times 100 \quad (3.19)$$

Where W_p is the weight of the polymer formed and W_m is the initial weight of the monomer.

In both, aerated and N_2 purged conditions, the polymerization of the DADMAC increases steadily with the increase in the radiation dose up to a dose of about 40 kGy. At this saturation point, about 80 -90 % polymerization could be attained.. However, in the lower dose range (5-10 kGy), the % polymerization for aerated solution was less than that for N_2 purged solution. For example, at 5 kGy, polymer yield was about 10 % for aerated solution while N_2 purged solution polymerized to an extent of approximately 20 %. This clearly indicates that oxygen, which is a very efficient free radical scavenger, affects the polymer

yields at lower doses by scavenging some of the radiolytically generated radical species. It has been reported by earlier workers that in aqueous solution, most of the monomers undergo radiation polymerization via free radical mechanism at dose rate typical of gamma radiation from radionuclide source at room temperature [1].

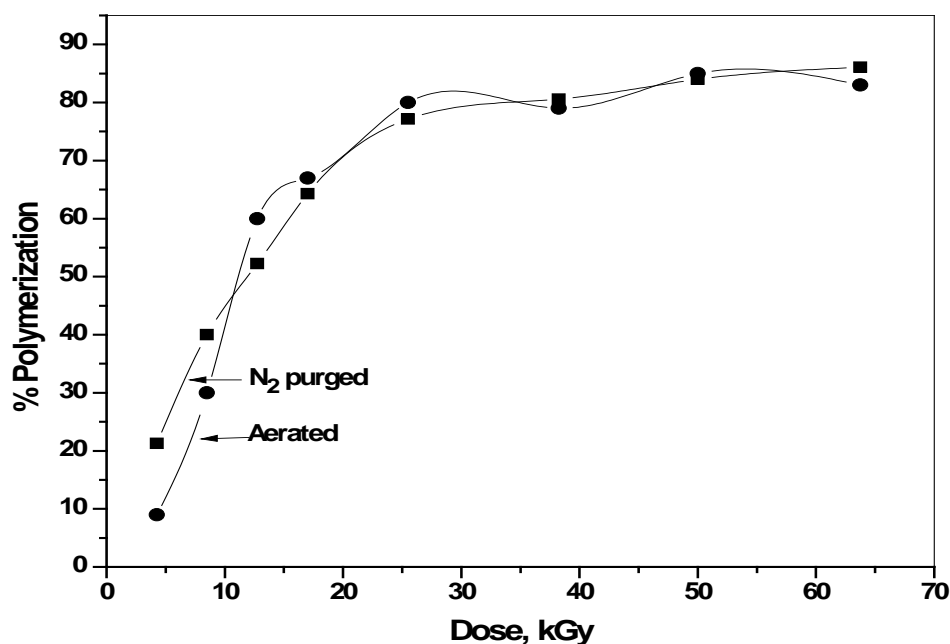


Fig. 3.4: % Polymerization as a function of absorbed dose

3.3.2 Determination of molecular weight of PDADMAC

Viscosity of a polymer solution depends on concentration and molecular weight of the dissolved polymer and therefore by measuring the solution viscosity molecular weight can be calculated. The molecular weight of radiation synthesized PDADMAC was determined by this method. Viscosity measurements were carried out using an ubbelholde viscometer from M/s Scam India, at temperature of $25 \pm 0.5^\circ\text{C}$. Intrinsic viscosity of the polymer measurements were carried out in 1 M NaCl solution and the viscosity-average molecular weights were calculated using the Mark – Houwink – Sakurada relation (Eqn. 3.20).

$$[\eta] = K M_v^a \quad (3.20)$$

Where $[\eta]$ is the intrinsic viscosity and M_v is the molecular weight. 'K' and 'a' are the Mark–Houwink parameters which depend on the particular polymer-solvent system. For PDADMAC in aqueous medium $K = 1.12 \times 10^{-4}$ and $a = 0.82$ [71], therefore the equation can be written as Eqn. 3.21;

$$\eta = 1.12 \times 10^{-4} M_v^{0.82} \quad (3.21)$$

The molecular weight (M_v) was found to increase from 2.57×10^4 to 4.65×10^4 in the 5 kGy to 28 kGy dose range. It may be noted that the molecular weight of the polymer synthesized was found to be an order of magnitude lower than that of commercially available polymer. This is probable because at high absorbed dose degradation of the polymer may predominate even though both crosslinking and degradation occurs simultaneously in the system.

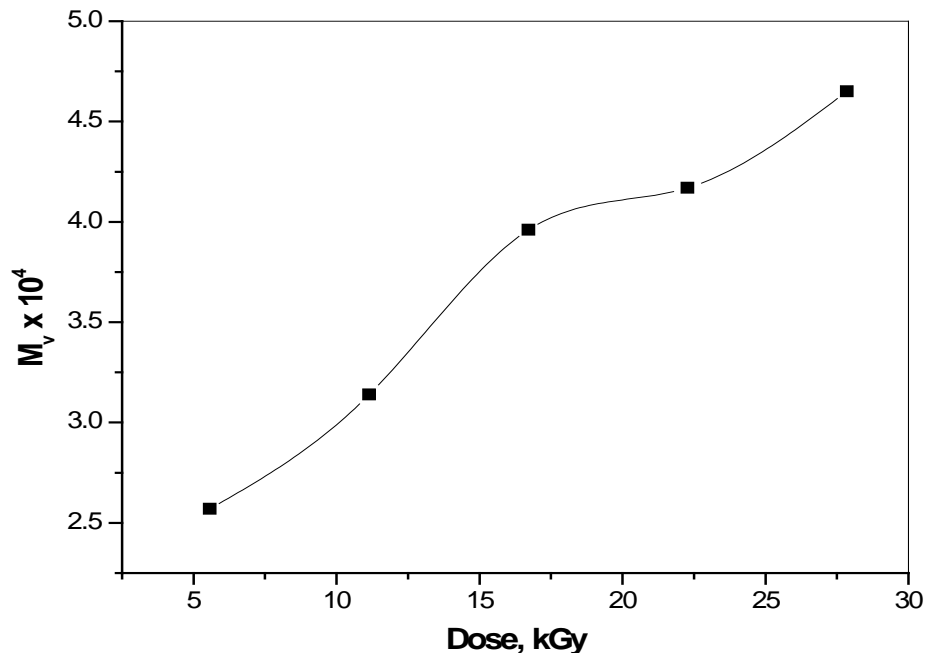


Fig. 3.5: Variation in the molecular weight of PDADMAC with increase in gamma radiation dose.

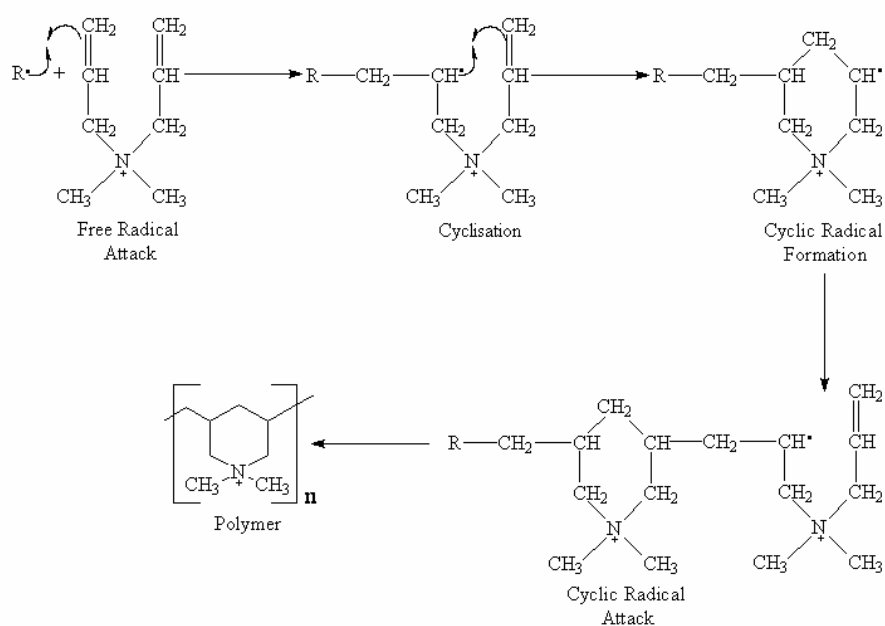
3.3.3 Cyclopolymerization

In modern polymer science, based on the views of Staudinger [118], it was widely believed that polymerization of non conjugated dienes leads to crosslinked nonlinear polymers or copolymers. However, exceptions to this were observed between 1949 and 1957 when studies were conducted on the polymerization of allyl and substituted allyl quaternary ammonium compounds. It was observed that monomers containing two allyl groups produced non-cross-linked polymers that were completely soluble in water, while monomers containing one allyl group did not polymerize at all [119-126]. These findings contradicted the widely accepted view that monomers with one double bond resulted in the formation of linear polymers while monomers with two or more double bonds formed cross-linked polymers possessing no solubility. Allyl monomers are poor monomers for radical polymerization since chain transfer reactions take place readily by abstraction of allylic hydrogens of monomer by the propagating radical [127]. This forms a more stable, resonance-stabilized radical species, decreasing the polymerization efficiency and the molecular weight of the polymer. However, later a cyclopolymerization mechanism was demonstrated [128] which made it possible to synthesize high molecular weight water-soluble polymers from diallyl monomers. Cyclopolymerization is an addition polymerization leading to cyclic structures in the polymer main chain. ie intramolecular cyclization followed by intermolecular propagation. The concept of cyclopolymerization is not limited to polymerizations of divinyl compounds; it extends to polymerizations of other bifunctional monomers, such as dialdehydes, dinitriles, diisocyanates and diepoxides.

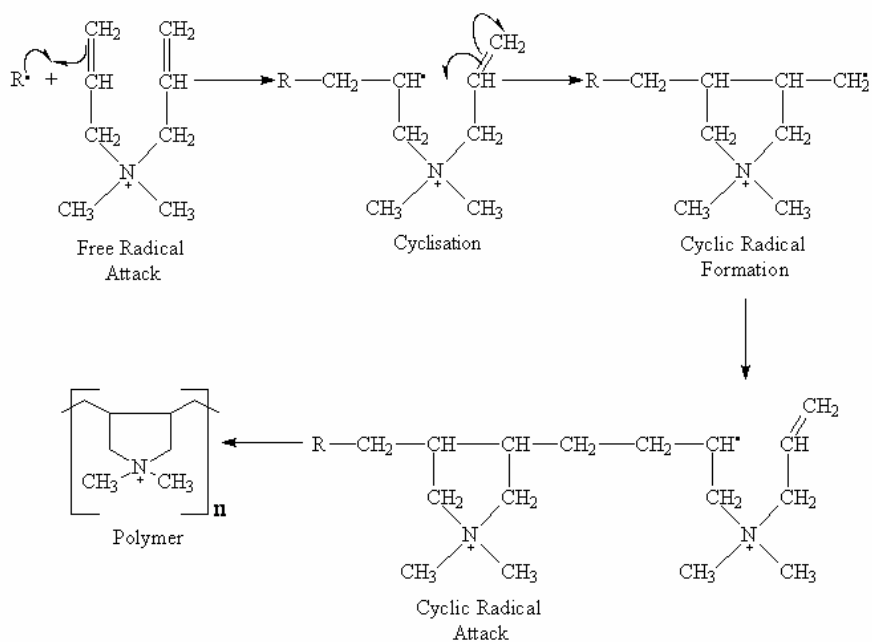
3.3.3.1 The chemical structure of PDADMAC

The generally accepted hypothesis proposed for the radical initiated cyclopolymerization of 1, 6-diene is the formation of six-member structures because of the enhanced stability of the system. However, later studies have shown that there are numerous

cases where cyclopolymerization does not adhere to this hypothesis and cyclic structures are derived by propagation through the less stable intermediate. In this case the cyclopolymerization is said to be under kinetic rather than thermodynamic control. To explain the formation of soluble non-crosslinked polymers such as PDADMAC from its monomer containing two double bonds (DADMAC), a chain propagation mechanism was proposed that involves alternating intra-molecular, followed by inter-molecular, growth steps [120]. The size of the ring structure introduced in the polymer structure depends on the mechanism followed. Under this alternating mechanism there are two reaction pathways that are possible. Scheme 3.1 results in the formation of the six-member piperidine ring system and Scheme 3.2 results in the five-member pyrrolidine ring system.



Scheme 3.1: Reaction mechanism for the polymerization of DADMAC to form the six-member piperidine ring system



Scheme 3.2: Reaction mechanism for the polymerization of DADMAC to form the five-member pyrrolidone ring system.

3.3.4 Characterization of PDADMAC

It has been observed that in many cases, free radical cyclopolymerization of DADMAC results in the formation of five-member pyrrolidone system even though six-member ring system is thermodynamically more stable. This is because in the five member cyclic rings, a more favorable overlap of the reacting centers occurs in the transition state involved [129, 130]. Most of the reports on free radical initiated cyclopolymerization of PDADMAC points to the presence of five-member ring system. In order to confirm the size of ring system formed in radiation synthesized PDADMAC, several techniques were employed to characterize the polymer. Although the intermediates were not isolated or studied, the preferred mechanism of polymerization may be inferred by analyzing the polymer. The polymer produced at an absorbed dose of 27 kGy (M.W $\sim 2.6 \times 10^4$) was arbitrarily chosen and used for characterizing purpose. The molecular weight of the polymer

is immaterial as far as the structural elucidation is concerned because it contains the same functional groups and structural features independent of chain length.

3.3.4.1 FTIR Spectroscopy

Since PDADMAC is highly hygroscopic it is difficult to obtain absolutely dry samples and the spectrum inevitably shows the presence of residual moisture at about 3500 cm^{-1} . In the spectrum shown in Fig. 3.6, the peak assigned to aliphatic secondary amines [131] at 3355 cm^{-1} (1) only appear as small shoulder because of the large absorption by water in this region of the spectrum. The band at 3087 cm^{-1} comes from stretching vibrations of -C-H (2). The signal at 1635 cm^{-1} (3) was also assigned to C-H stretch in PDADMAC [132]. The band at 1473 cm^{-1} (4) appearing in the spectrum indicates a long carbon chain with a high degree of regularity which is contributed by the linear backbone structure of PDADMAC [133]. C-H absorption occurs at 990 cm^{-1} (5) and 887 cm^{-1} (6).

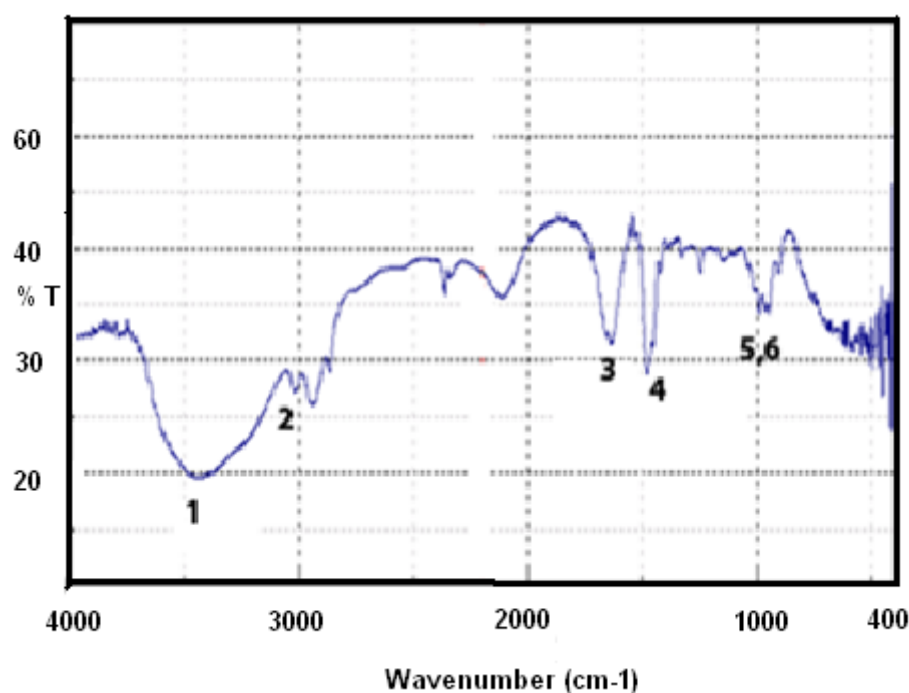


Fig. 3.6: FT-IR spectrum of PDADMAC in KBr pellet

3.3.4.2 UV-Visible spectroscopy

Both DADMAC and PDADMAC form colorless and transparent solution because they do not have any absorption features in the visible region of the spectrum. Fig. 3.7 shows the absorption spectrum of a dilute solution of DADMAC and PDADMAC. DADMAC shows two peaks in the UV region centered at 226 nm and 287 nm whereas the polymer shows only single absorption (λ_{\max}) at 227 nm.

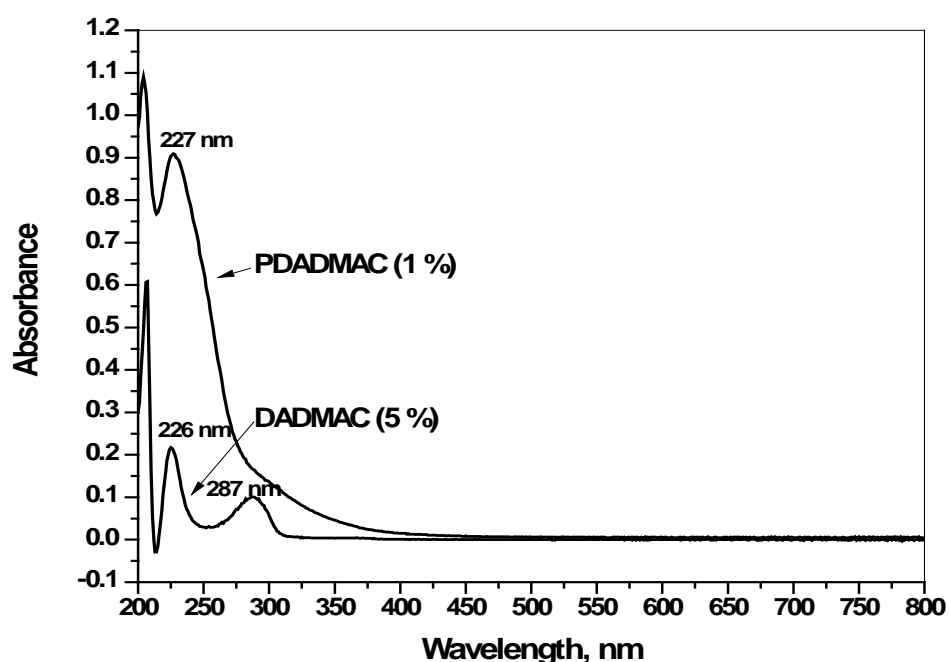


Fig. 3.7: Absorption spectrum of DADMAC and PDADMAC in water

3.3.4.3 H-NMR analysis of PDADMAC

The H-NMR spectrum of PDADMAC is shown in Fig. 3.8. Fig. 3.8 inset gives the position of the protons. The broad doublet peaks at about 1.4 ppm corresponds to the methylene protons (4). The peak at about 2.6 ppm corresponds to the proton attached to the tertiary carbon (3). The multiple resonance peaks at 3.1 ppm (1) and 3.76 ppm (2) are

assigned to methyl and methylene protons bonded to quaternary nitrogen. The peaks detected in the H-NMR spectrum are similar to studies reported in the literature [134].

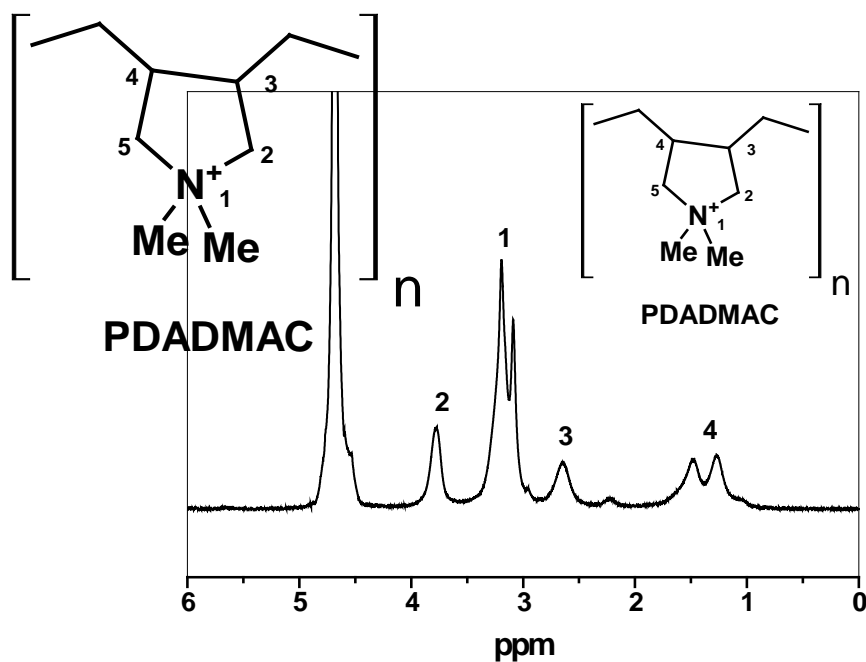


Fig. 3.8: H-NMR of PDADMAC in D₂O

3.3.4.4 ¹³C-NMR analysis of PDADMAC

The ¹³C-NMR spectrum of the polymer depicted in Fig. 3.9 shows both a set of strong and weak lines for each signal. This may be attributed to the formation of isomers which are cis and trans with respect to the inter-connecting rings as shown in Fig. 3.10.

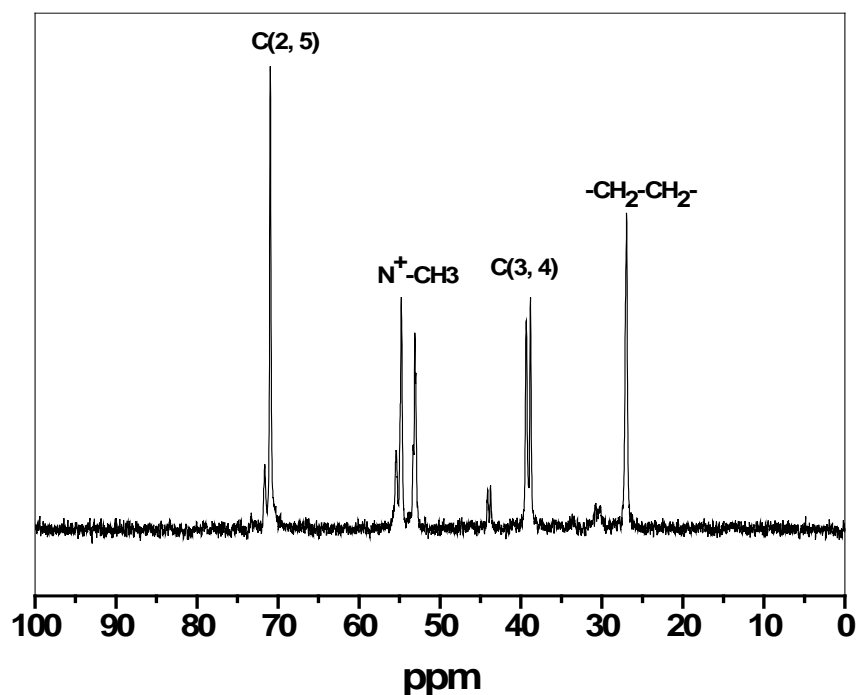


Fig. 3.9: ^{13}C -NMR of PDADMAC in D_2O

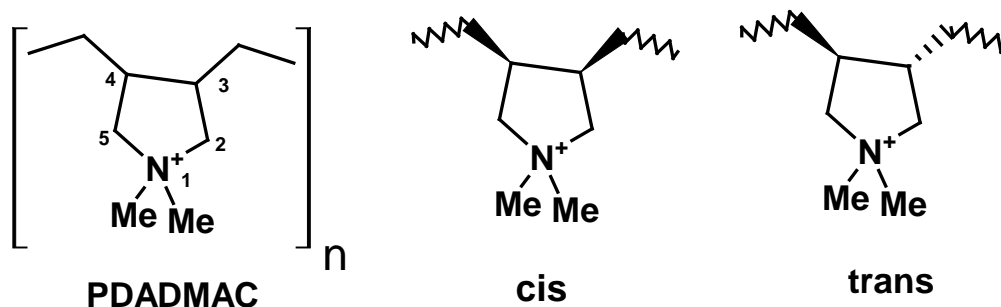


Fig. 3.10: Cis and Trans forms of PDADMAC

In the cis isomer the N^+ -methyl groups are non-equivalent resulting in the formation of two signals in the region 52 to 54 ppm. These signals are further split due to N^+ -C coupling. The N^+ -methyl groups of the trans isomer are equivalent and therefore give rise to a single weak signal at 54.9 ppm. The splitting of the equivalent C3, 4 signal in both isomers into signals of equal intensity at 39 and 43 ppm may be due to steric configurational differences between the inter-connecting rings. The C2, 5 are also equivalent in both isomers and give rise to single

peaks in both instances. Similarly, the $-\text{CH}_2\text{CH}_2-$ carbons are equivalent in both isomers and give rise to a single peak in both cases. If six member cyclic structures are formed then peak corresponding to additional carbon would arise in the spectrum. The absence of any peaks corresponding to additional carbon in the spectrum indicates that the product is not a six-member ring system. A summary of the peak assignments is shown in Table 3.3. which is identical to that described by Lancaster et. al [135] and later confirmed by Assem et al. [136].

Table 3.3: Summary of the ^{13}C -NMR chemical shift data of PDADMAC

Carbon No.	Cis Isomer		Trans Isomer	
	δ Value (ppm)	Comment	δ Value (ppm)	Comment
2, 5	70.5	Equivalent C	71.2	Equivalent C
3, 4	38.8	Equivalent C	43.4	Equivalent C
	38.9	Split Peak	43.7	Split Peak
$-\text{CH}_2-\text{CH}_2-$	26.7	Equivalent C	30.8	Equivalent C
N^+-CH_3	52.4	Non-Equiv. C	54.9	Equivalent C
	54.2	2nd Peak		

^{13}C -NMR, H-NMR and FT-IR analyses confirms that radiation initiated polymerization of DADMAC proceeds according to Scheme 3.2 and results in the formation of PDADMAC contains containing 5 member ring structure as shown in Fig. 3.11.

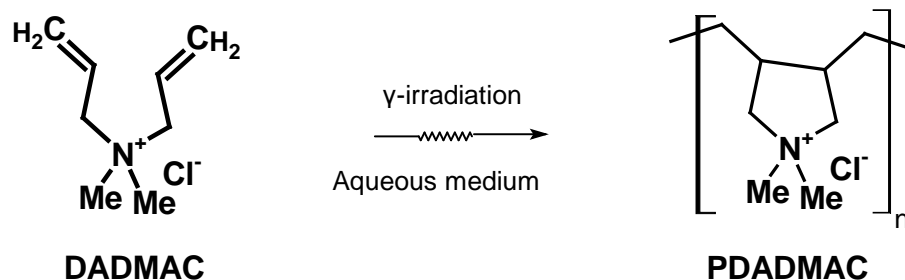


Fig. 3.11: Cyclopolymerization of DADMAC initiated by gamma irradiation.

3.4 Conclusions

The reactions of the transient species produced by the radiolysis of water, namely e_{aq}^- and $\bullet\text{OH}$, with DADMAC and PDADMAC were investigated in the nanosecond timescale by means of pulse radiolysis technique. The rate constant for reaction of hydrated electrons (e_{aq}^-) was calculated directly by following its decay at 700 nm. Since the intermediates formed by the reactions of OH radical with the monomer and polymer did not show absorption features suitable for optical detection, the rate constants were evaluated by competition kinetics method, using SCN^- as a reference solute. The kinetic parameters of the various reactions of the transient species are summarized in Table 3.4.

Table 3.4: Kinetic parameters of the various reactions of the transient species

Solute	Species	Rate constants ($\text{dm}^3\text{mol}^{-1}\text{s}^{-1}$)
DADMAC	e_{aq}^-	3.4×10^9
Poly(DADMAC)	e_{aq}^-	4.4×10^{10}
DADMAC	$\bullet\text{OH}$	7.4×10^9
Poly(DADMAC)	$\bullet\text{OH}$	8.1×10^{10}

The polymerization of DADMAC was conducted in an inert N₂ as well as in aerated condition and it was observed that under both these conditions, the polymerization of the DADMAC increases steadily with the increase in absorbed dose up to a about 40 kGy. At this point it reaches a saturation level and the percentage of polymerization was about 80-90 %. The presence of oxygen, a radical scavenger, suppressed the extent of polymerization only during the initial stage of polymerization. The molecular weight of the polymer synthesized was determined viscometrically by using the Mark – Houwink – Sakurada relation. The molecular weight (M_v) was found to increase from 2.57×10^4 to 4.65×10^4 in the dose range studied (5 kGy to 28 kGy). The radiolytically synthesized PDADMAC was characterized by many techniques and IR, ¹H-NMR and ¹³C-NMR studies confirmed the formation of five member pyrrolidone ring system in the polymer.

Chapter 4: Thermal analysis of DADMAC, PDADMAC and method to determine the degree of conversion of DADMAC to PDADMAC

4.1 Introduction

During the course of the study new methods were developed to characterize DADMAC and radiation synthesized PDADMAC using thermal studies. The thermal behavior of a polymer is one of the important criteria that decide the choice of a polymer for a particular application. The melting point of a polymer; decomposition temperature, glass transition temperature etc. are some of the main characteristics of the polymer that determine the usable temperature range of the polymer. Therefore, the determination of these parameters is essential from a practical point of view and thermal analysis is one of the best techniques which provide accurate and reliable information about the parameters. A detailed thermal analysis is useful for accurate estimation of polymer in a composite or a blend formulation and can also provide insights into the decomposition kinetics and predict the lifetime of the material at different temperatures. In this study, thermal investigation was carried out on radiation polymerized PDADMAC and important kinetic parameters like order of reaction, activation energy and pre-exponential factor were determined. Based on the insight gained from this study, a thermogravimetric method was developed to determine the degree of conversion of DADMAC to PDADMAC during the gamma radiation induced polymerization.

This chapter is divided into two parts. The first part deals with the TGA and DSC investigations on radiation polymerized PDADMAC and the second part describes a thermogravimetric method for determining the degree of conversion of monomer to polymer.

4.2. Experimental

4.2.1 Materials

Aqueous DADMAC solution (~65 %) was purchased from Fluka and used without further purification. PDADMAC used in the study was synthesized by γ -irradiation of DADMAC solution in a ^{60}Co gamma chamber, GC-5000, (BRIT, India) at a dose rate of 3.8 kGy/h. The molecular weight of PDADMAC depends on absorbed radiation, however preliminary investigations revealed that TG profile is not affected by the molecular weight of the polymer in the radiation dose range studied (4 kGy to 70 kGy). Therefore, polymer synthesized at a radiation dose of 27 kGy ($M_v = 4.6 \times 10^4$) was used for all experiments reported herein (Section 3.3.1).

4.2.2 Thermogravimetric analysis (TGA)

The non-isothermal thermogravimetric (TG) measurements were carried out with Mettler thermogravimetric analyzer (TG 50) coupled with a Mettler TC 10A processor. The temperature calibrations were carried according instrument manual [137]. The calibration method was based on the change in magnetic properties of three metal samples (Alumel, Nickel and Trafoperm) at their curie temperatures. The experimental data collected were transferred to a computer and kinetic analyses were carried out by Mettler STAR^e program [138]. For evaluating the kinetic parameters, approximately 15 mg of the polymer samples were taken in an open alumina crucible and the degradation profiles were recorded from 35 °C to 800 °C at a heating rate of 10 °C min⁻¹. A higher sample quantity of about 75 mg was taken to study the degree of conversion of DADMAC to PDADMAC. All the studies were carried out in an inert dynamic atmosphere of high purity nitrogen set at a flow rate of 50 ml min⁻¹.

4.2.3 Differential scanning calorimetry (DSC)

Thermoanalytical thermograms were recorded using Mettler-Toledo DSC 823e with liquid nitrogen cooling assembly. The heat flow and temperature calibrations were carried according to the instrument manual [138]. All the experiments were carried out in an inert dynamic atmosphere of high purity nitrogen set at a flow rate of 50 ml min⁻¹. About 5 mg of the powdered polymer samples were taken in a standard 40 µl aluminum pan. Since the polymer samples were highly hygroscopic in nature, the thermal properties were determined using two scans. The first scan was carried out to eliminate the residual water from the polymer samples. In the first scan the sample was heated from 40 °C to 200 °C at 20 °C min⁻¹ rate, kept isothermally at 200 °C for 10 min and cooled to 0 °C at 10 °C min⁻¹ rate. The second scan was performed from 0 °C to 800 °C at a heating rate of 10 °C min⁻¹ for evaluating the Arrhenius parameters. For the determination of glass transition temperature, the second scan was performed from 0 °C to 500 °C at a higher heating rate of 50 °C min⁻¹. For convenience, only the second scan is shown in the figures. Both TGA and DSC baselines were corrected by subtraction of a prerecorded blank thermogram.

4.3 Part I: Thermal degradation behavior of radiation synthesized PDADMAC

Some applications of polymer may require its use at a temperature lower or higher than room temperature. The determination of kinetic parameters associated with the degradation has a lot of practical significance as the evaluation of the parameters helps in predicting the thermal behavior of a polymer at other temperatures. This part of the chapter discusses the evaluation of kinetic parameters (order of the reaction, activation energy and the pre-exponential factor) of PDADMAC degradation from a single Thermogravimetric (TG) or Differential scanning calorimetric (DSC) scan. Theoretical TG and DSC thermograms derived from the calculated kinetic parameters were in good agreement with the experimental ones at the heating rate employed.

4.3.1 Kinetic analysis

Thermogravimetric analysis (TGA) as a thermal analysis technique, measures the amount and rate of change in the weight of a material as a function of temperature or time in a controlled atmosphere. TGA measurements are used primarily to determine the composition of materials and to predict their thermal stability under elevated temperatures. The weight loss data supplied by the thermogravimetric measurement is completely unspecific and gives no information about the nature of the degradation products. This type of information is only obtained when a TGA instrument is connected via a suitable interface to a device capable of analyzing gases. However, with proper experimental procedures, additional information about the kinetics of decomposition can be obtained from TGA and DSC.

The thermal decomposition of a solid is usually a complex process but can be approximated by the rate equation:



$$\frac{d\alpha}{dt} = k(T)f(\alpha) \quad (4.2)$$

Where α is the degree of conversion, $k(T)$ is a function of temperature and $f(\alpha)$ is a function of conversion. When the n^{th} order model equation is combined with the Arrhenius equation the reaction rate is given:

$$\frac{d\alpha}{dt} = k \exp(-E_a/RT).(1-\alpha)^n \quad (4.3)$$

Where da/dt is the rate of reaction, T is the sample temperature, k is the pre-exponential factor, α is the conversion of the reaction, E_a is the activation energy, n is the order of the reaction and R is the universal gas constant.

To obtain da/dt and α from DSC and TGA, the following equations can be used:

$$\text{DSC:} \quad \frac{d\alpha}{dt} = \frac{H}{A_{\text{tot}}} \quad (4.4)$$

H : DSC signal from baseline (mW)

A_{tot} : Total peak area (mJ)

α : Partial area (mJ)/total peak area (mJ)

$$\text{TGA:} \quad \frac{d\alpha}{dt} = \text{DTG signal (mg s}^{-1}\text{) / total weight stage (mg)} \quad (4.5)$$

α = Partial weight stage (mg) / total weight stage (mg)

There are various methods for the determination of kinetic parameters by thermal analysis depending on the assumptions and approximations involved. Kissinger's method (standard ASTM E 698) [139, 140], Freeman and Carroll (differential method) [141], Coats and Redfern (integral method) [142] etc are some of the commonly used methods. Another popular and frequently used method for determination of the kinetic parameters is non linear regression [143]. Ideally, the kinetic parameters evaluated from multiple TG measurements

are closer to the actual values for a particular reaction, but the determination is inconvenient and time consuming. In the present study, n^{th} order kinetic parameters were determined from a single dynamic TG thermogram and from a single DSC thermogram. Sets of three values T , da/dt and α were taken from the dynamic DSC or TGA thermogram and k , E_a and n were then calculated by the method of least squares. DSC and TG scans were performed in triplicate and the average values of the parameters are reported in this study.

4.3.2 TG and DTG analysis

The TG and DTG thermograms of PDADMAC recorded at a heating rate of $10\text{ }^{\circ}\text{C min}^{-1}$ are shown in Fig. 4.1 and the corresponding data is given in Table.1. Three well defined and resolved stages are seen in the figure. The initial stage (shown as stage 0 in the figure) from $35\text{ }^{\circ}\text{C}$ to around $120\text{ }^{\circ}\text{C}$ is due to the loss of moisture from the polymer sample. This was confirmed from the DSC scan, where an endothermic peak appeared (onset at $\sim 0\text{ }^{\circ}\text{C}$) due to the freezing of residual moisture in the sample. Stage I and stage II in the figure corresponds to the actual polymer degradation. In stage I, the polymer starts decomposing and the decomposition takes place over a broad temperature range of $287\text{ }^{\circ}\text{C}$ (onset) and $355\text{ }^{\circ}\text{C}$ (endset). From the DTG thermogram the maximum rate of weight loss was found to occur at $320\text{ }^{\circ}\text{C}$.

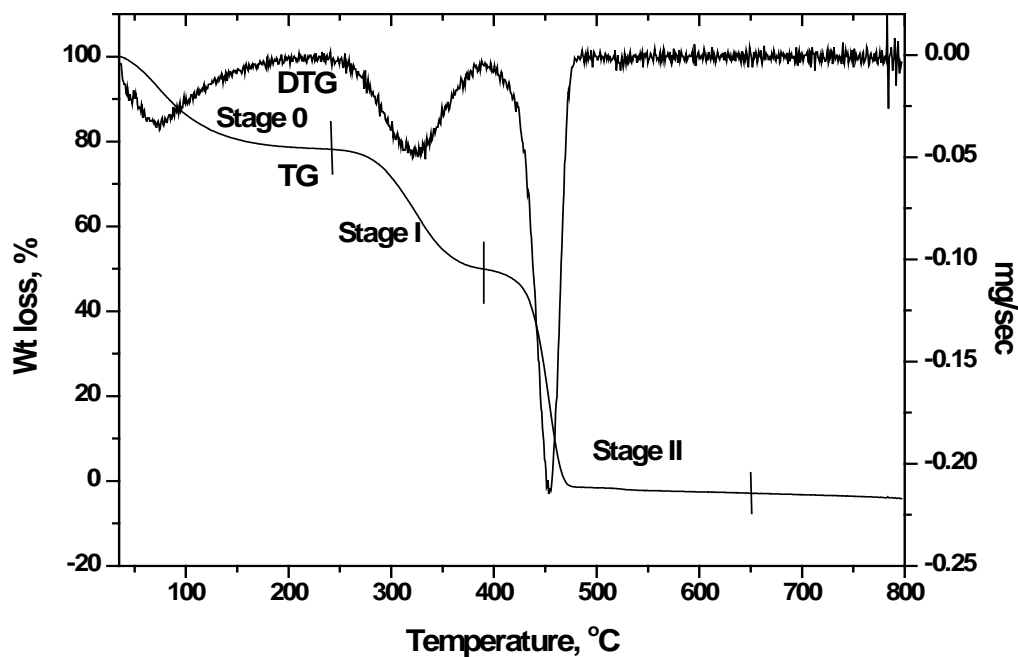


Fig. 4.1: TG and DTG curve of PDADMAC in nitrogen atmosphere at a heating rate of $10\text{ }^{\circ}\text{C min}^{-1}$

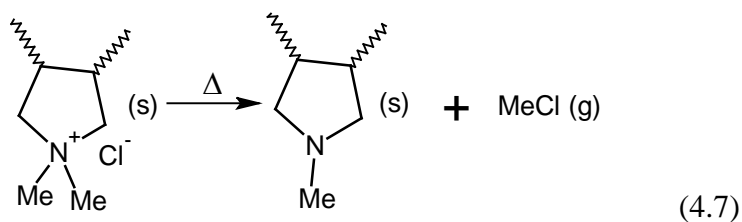
Table 4.1: TG / DTG analysis of PDADMAC at a heating rate of $10\text{ }^{\circ}\text{C min}^{-1}$ in nitrogen atmosphere

	STEP I	STEP II
STEP RANGE (°C)	223 – 391	391 – 730
WEIGHT LOSS (%)	33 ± 2.0	67 ± 2.0
ONSET TEMP (°C)	287	435
ENDSET TEMP (°C)	355	467
DTG PEAK(°C)	320.7 ± 0.4	453.2 ± 0.3

The thermal properties of simple quaternary ammonium salts have been investigated by several workers [144-149]. It was initially suggested and later confirmed that quaternary ammonium salts dissociate with the formation of alkyl halide.



Where X and R indicates a halogen atom and an alkyl or aryl substituent, respectively. By analogy, we can expect PDADMAC to undergo a similar reaction as shown below.



PDADMAC

$$\text{Mw} = 161.68 \quad \text{Mw} = 111.18 \quad \text{Mw} = 50.5$$

Theoretically, the weight loss for the above reaction is 31.24 % and the experimental TG thermogram shows a weight loss (%) of 33.0 ± 2.0 for the first stage. This value corresponds well with the theoretical value and the degradation mechanism of the first stage could be revealed from equation (7). The stage II degradation takes place over a relatively narrow temperature region between 435 °C (onset) and 467 °C (endset) with the DTG peak at 453 °C. The weight loss (%) for Stage II was found to be 67.0 ± 2.0 . The mechanistic details of the decomposition stages can only be obtained when the thermal analysis technique is coupled with other techniques where the evolved gases and/ or the residues are characterized (mass spectrometry, FT-IR, NMR etc)

4.3.3 DSC evaluation

DSC is commonly used to determine the glass transition temperature (T_g) of a polymer. The glass transition is a kinetic phenomenon and is dependent on how the

measurement is made. T_g mainly depends on the thermal history of the sample and also on the heating / cooling rate. The higher the heating rate, the higher is the DSC sensitivity. Hence, for the determination of weak glass transition, a fast heating rate of $50\text{ }^\circ\text{C min}^{-1}$ was preferred. On the contrary, for higher resolution of the peaks and for kinetic parameter calculations, a lower heating rate of $10\text{ }^\circ\text{C min}^{-1}$ was employed. Fig. 4.2 and Fig. 4.3 show the DSC scan of the sample at the heating rate of $10\text{ }^\circ\text{C min}^{-1}$.

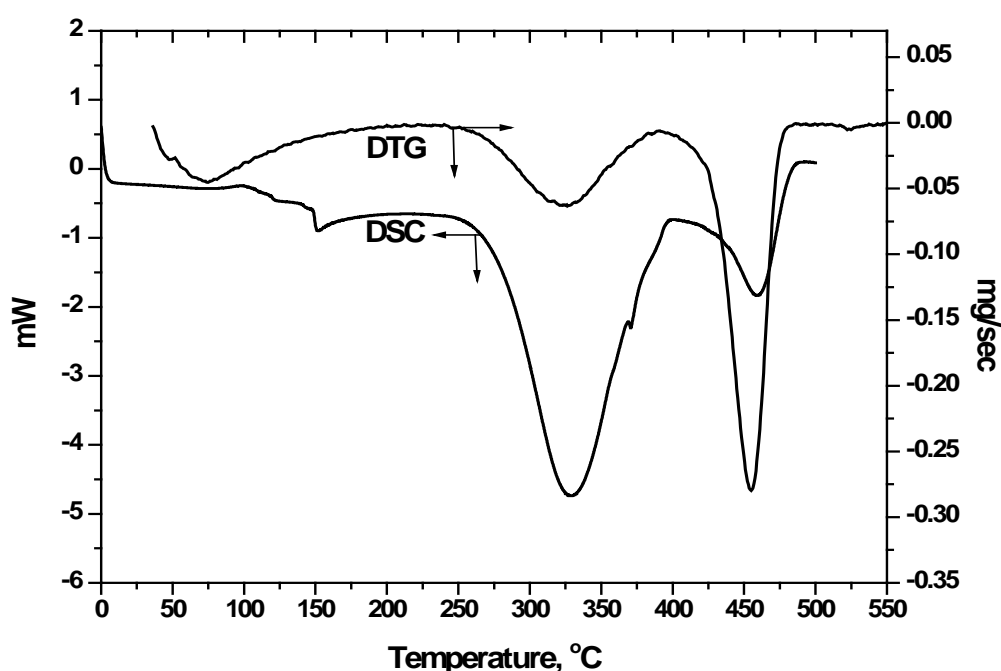


Fig. 4.2: DSC and DTG curve of PDADMAC in nitrogen atmosphere at a heating rate of $10\text{ }^\circ\text{C min}^{-1}$

The DSC thermogram shows two endothermic peaks corresponding to the two stages in the TG thermogram. From Table.4.2, it can be seen that the enthalpy change associated with the first stage (ΔH_I) is 650 Jg^{-1} . The second degradation stage had an enthalpy change (ΔH_{II}) of 129 Jg^{-1} .

Table 4.2: DSC analysis of PDADMAC at a heating rate of 10 °C min⁻¹ in nitrogen atmosphere

	STEP I	STEP II
ONSET TEMP (°C)	275	435
ENDSET TEMP (°C)	349	482
ΔH (Jg ⁻¹)	650.2 ± 40.3	129.5 ± 10.7
DSC PEAK(°C)	329.4 ± 0.2	461.7 ± 0.6

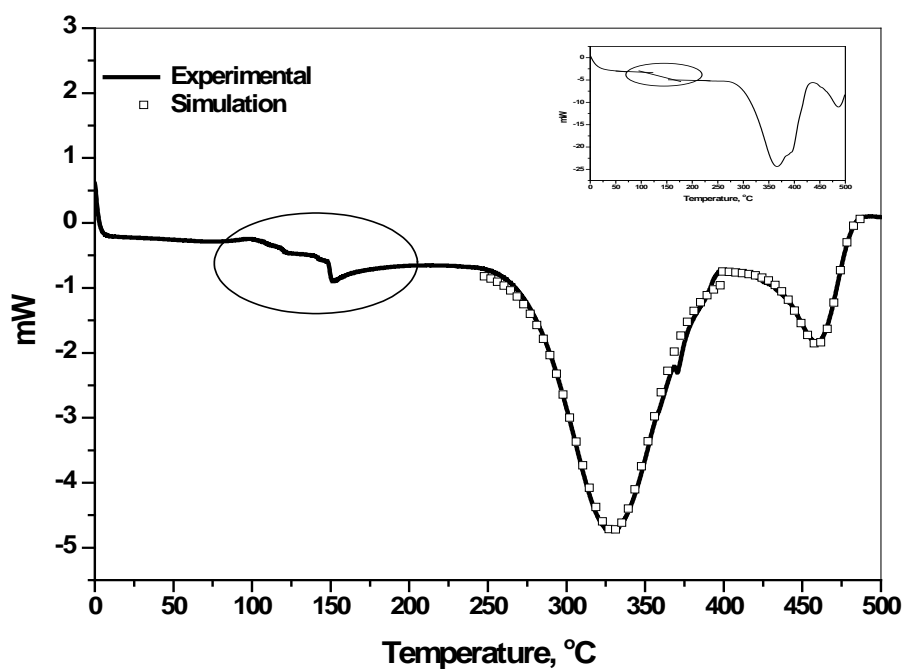


Fig. 4.3: Comparison of experimental DSC curve with theoretically generated curve by the method of least squares. Inset: DSC curve recorded at heating rate of 50 °C min⁻¹ for determination of glass transition

Fig. 4.3 inset shows the DSC scan at a heating rate of 50 °C min⁻¹. For the determination of the glass transition temperature of a polymer, there are different standard evaluation procedures like ASTM [150], DIN [151] and Richardson's method [152]. The glass transition temperature and Δc_p (specific heat capacity) obtained through different methods by the Mettler STAR^e program is shown in Table.3. The ASTM and DIN gave close results (around 150 °C), however the Richardson method revealed a higher value of about 165 °C. At the lower heating rate (10 °C min⁻¹), the glass transition is further resolved into many transitions (α , β , γ etc).

Table 4.3: Evaluation of glass transition temperature of PDADMAC by different methods

	ASTM	DIN	RICHARDSON
Tg (Midpoint)	150.05	148.41	165.85
Δc_p (Jg⁻¹K⁻¹)	0.411	0.586	0.352

4.3.4 Comparison of TG and DSC results

Fig. 4.2 shows the DTG plot along with the DSC thermogram scanned at the same heating rate of 10 °C min⁻¹. From the figure, it can be seen that there is an almost one to one correspondence in the peaks of DTG and DSC. Comparing DTG and DSC data from Table. 4.1 and Table. 4.2, it can be seen that the peak temperatures of the DSC thermogram have higher values (329 °C and 461 °C) than the corresponding DTG thermogram (320 °C and 453 °C). Another interesting observation is that the enthalpy change (DSC) associated with the first stage (650 Jg⁻¹) is considerably higher than that associated with the second stage (129 Jg⁻¹) though the weight loss (TGA) in the first stage is only 33 % of the total weight loss. The

kinetic parameters, activation energy, $\ln k$ and order of the reaction, calculated from the DSC and TG thermograms are shown in Table. 4.4.

Table 4.4: Evaluation of kinetic parameters from TGA and DSC using the method of least squares

	STEP I		STEP II	
Method	TGA	DSC	TGA	DSC
$\ln k$	19.6 ± 2.1	25.2 ± 2.3	67.4 ± 5.4	38.4 ± 3.8
Ea (kJ/mol)	122.1 ± 8.6	150.4 ± 7.2	432.6 ± 15.1	262.6 ± 11.2
n	1.5 ± 0.1	1.7 ± 0.2	1.3 ± 0.1	0.68 ± 0.1
R^2	0.9986	0.9885	0.9967	0.9893

The degree of conversion α was in the range 0.1 to 0.9 for the evaluation. The Arrhenius parameters derived from the DSC measurements are higher than those from the TG measurements for the first degradation stages. On the other hand, for the second degradation stage, the TG analysis yields a higher value for the parameters than the DSC calculations.

4.3.5 TG and DSC simulation

The Mettler STAR^e software enables one to fit or simulate the experimental thermogram over the α range chosen using the method of non linear regression. The actual verification for any kinetic results is to compare the experimental TGA / DTG or DSC thermogram with the theoretically generated thermogram based on any particular model. The shape of the fit is strongly dependent on the pre-exponential factor in the Arrhenius equation although its physical meaning is not clear for a complex degradation mechanism. However,

emphasis is usually given to the determination of the activation energy for the decomposition. The quality of the thermogram fit is expressed by the R^2 values from the least square analysis method. It can be seen from the Fig. 4.3 and Fig. 4.4 and Table. 4.4 (R^2 values) that the agreement between the simulated DSC / DTG thermogram and the experimental thermograms is good.

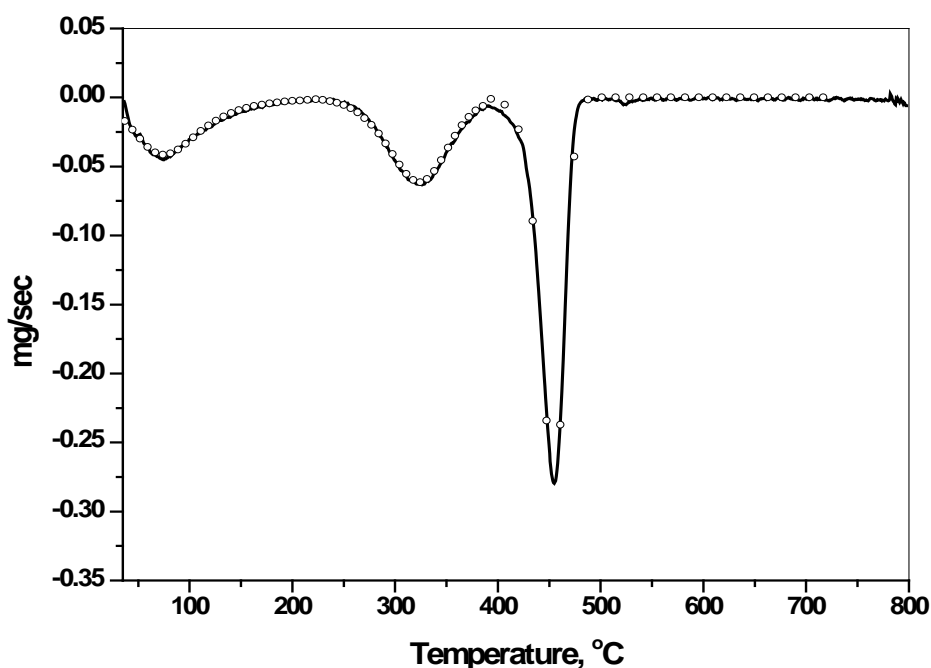


Fig. 4.4: Comparison of experimental DTG curve with theoretically generated curve by the method of least squares

But, as mentioned earlier, the kinetic parameters derived from the DSC and TG is significantly different. If the degradation process takes place in a single stage then the weight loss (TGA) and the enthalpy change (DSC) is directly related to the extent of reaction. Since the TGA and DSC results are different in the present study, the degradation process of the PDADMAC could be complicated and may involve a number of reactions or stages. The TG measurement would follow only the weight loss associated with the decomposition of the

intermediates. The DSC, on the other hand, would follow the weighted sum of the decomposition of the intermediates depending on the change in enthalpy for each stage [153]. In such cases the course of the reaction followed by the TGA and DSC would be different.

With the help of kinetic parameters derived from TGA, it was also possible to predict the thermal behavior of the polymer with respect to the degree of conversion (α). The results are shown in Fig. 4.5 and Fig. 4.6 for the first step and second step respectively. However it should be noted that the extrapolation of the results is only an approximation, especially for degradation of polymers, since the mechanism may be temperature dependent.

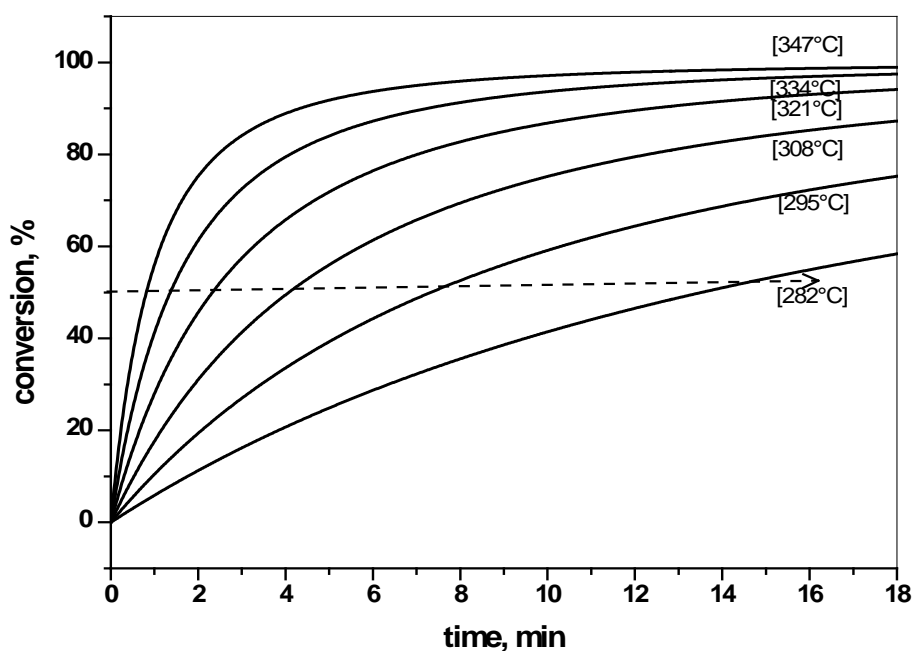


Fig. 4.5: Degree of conversion versus time plot for the first decomposition step (223 – 391 °C) of PDADMAC in nitrogen atmosphere

The horizontal dotted arrows are shown in Fig. 4.5 and Fig. 4.6 to aid in getting an approximate estimate of the percentage conversion for the particular step. For example, in the first step (Fig. 4.5), if the temperature of the sample is maintained 308 °C then it takes about 4

minutes for 50 % conversion. At a lower temperature, say 282 °C the plot predicts that it would take about 15 minutes to reach a conversion of 50 %. In general, the isothermal conversion curves predict increasingly longer times for the decomposition if temperature is decreased. This trend is also true for the second decomposition step shown in Fig. 4.6.

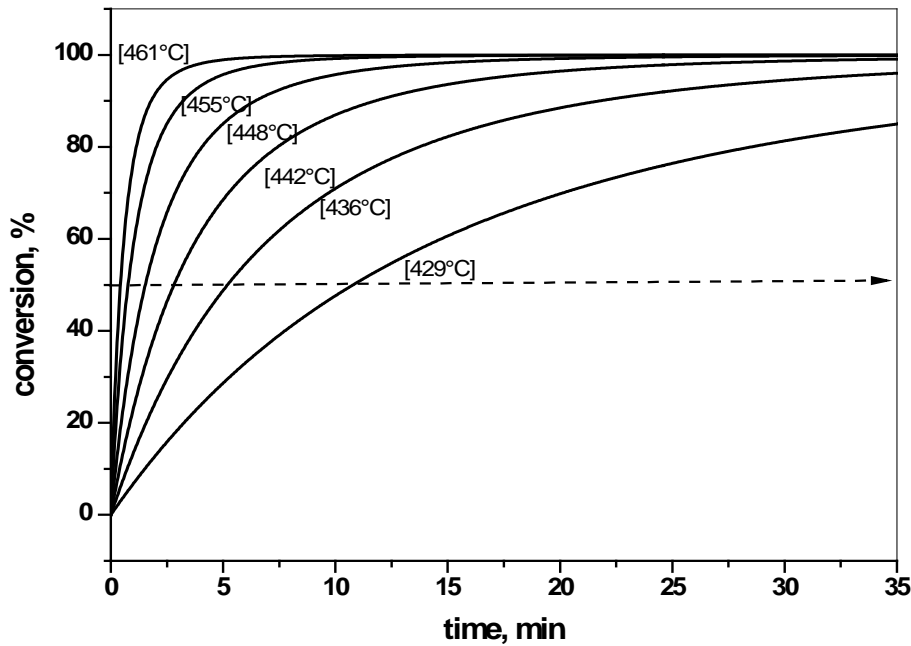


Fig. 4.6: Degree of conversion versus time plot for the second decomposition step (391 – 730 °C) of PDADMAC in nitrogen atmosphere

4.4 Part II: Thermogravimetric method for determining the degree of conversion in radiation polymerized DADMAC

Determining the degree of conversion of a monomer to its corresponding polymer is very important scientifically as well as technologically. For instance, it may offer some details about the mechanistic aspect of polymerization and provide valuable process control information for production of the polymer on an industrial scale. Although PDADMAC is one of the most important commercial polymers, not many methods have been reported for

determining the degree of conversion in DADMAC polymerization. The degree of conversion of DADMAC is usually studied by classical gravimetry or by using the ^1H NMR technique [154]. In gravimetry, the polymer is precipitated by adding a non solvent, preferably acetone or isopropanol and the polymer is separated, dried and weighed but the method is prone to experimental error. ^1H NMR gives accurate and reproducible results, but requires expensive instruments and careful sample preparation in D_2O . Also the rate of polymerization of the monomer may differ in D_2O and H_2O .

In the second part of the chapter, a convenient method to determine the degree of conversion of DADMAC to PDADMAC using dynamic thermogravimetry is reported. The monomer solution, exposed to different radiation dose (different degree of conversion), was removed from the radiation field and TGA runs were taken. The conversion degree of the monomer to the polymer was determined from a calibration plot generated previously using different known DADMAC/ PDADMAC ratios. One of the main advantage of the method is that the concentration of the polymer or monomer could be directly determined without their separation. The concentration of monomer and polymer in the mixture was estimated by measuring the weight loss corresponding to the steps involved in the thermograms. By employing the method, the degree of conversion of DADMAC as a function of absorbed dose was studied from 4 kGy to 70 kGy.

4.4.1 Calibration Curve

Stock solutions of DADMAC (43 wt %) and PDADMAC (43 wt %) were prepared separately in water. Ternary solutions of monomer, polymer and solvent were prepared by mixing the monomer and polymer solutions in appropriate ratios. The compositions of the solutions are given in Table. 4.1. The total concentration (monomer + polymer) in the solution remains 43 wt %. TGA was carried out on the mixture and the percentage weight

loss due to the monomer / polymer determined. A calibration curve was made by plotting the percentage weight loss of DADMAC / PDADMAC as a function of PDADMAC concentration.

Table 4.5: Composition of the ternary solution (for 100 g)

Monomer (g)	Polymer (g)	Monomer + Polymer (g)	Water (g)
4.7	38.3	43	57
9.5	33.5	43	57
11.6	31.4	43	57
17.2	25.8	43	57
22.4	20.6	43	57
25.4	17.6	43	57
34.8	8.2	43	57
38.7	4.3	43	57

4.4.2 Results and discussion

4.4.2.1 DSC Analyses

When a monomer solution is heated, there is possibility for it to undergo polymerization, even in the absence of initiators, depending on its reactivity. For example, vinyl monomers like acrylic acid and acrylamide are known to undergo fast polymerization at elevated temperatures. Allyl monomers, on the contrary, polymerize slowly compared to their vinyl counterparts [155]. However, to rule out the possibility of DADMAC undergoing thermal polymerization, the DSC scan was recorded. Fig. 4.7 shows the DSC thermogram of DADMAC recorded at a heating rate of $10\text{ }^{\circ}\text{C min}^{-1}$. The endothermic peak shown as M1

(centered at 220 °C) corresponds to the monomer decomposition. The preceding peak is due to the evaporation of water from the solution. Previous DSC studies [156] have shown that PDADMAC undergoes decomposition in two steps with endothermic peaks centered at 329 °C and 461 °C. Since no peaks due to the formation of the polymer were observed it may be inferred that heating the monomer solution under the conditions of the experiment does not induce polymerization. This is very important because if the monomer undergoes polymerization during the course of the TGA run, the method is likely to give erroneous results.

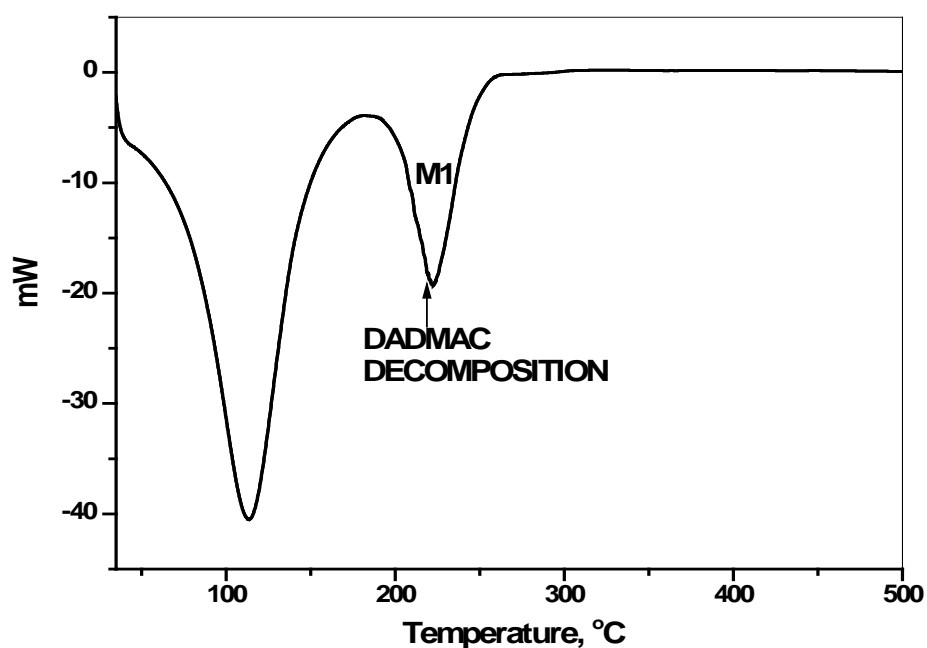


Fig. 4.7: DSC curve of DADMAC solution in nitrogen atmosphere at a heating rate of $10\text{ }^{\circ}\text{C min}^{-1}$

4.4.2.2 TG Analyses

The TG curves of DADMAC recorded at a heating rate of $10\text{ }^{\circ}\text{C min}^{-1}$ are shown Fig. 4.8. The step shown as M1 corresponds to the monomer decomposition. The initial step from $35\text{ }^{\circ}\text{C}$ to around $120\text{ }^{\circ}\text{C}$ is due to the loss of water from the monomer. In step M1, the monomer decomposition takes place over a broad temperature range from $175\text{ }^{\circ}\text{C}$ to $247\text{ }^{\circ}\text{C}$. As discussed before, in our previous study⁷, we investigated the thermal degradation behavior of PDADMAC and found that the polymer undergoes decomposition in two steps. For clarity, the TG of the polymer (in solution) is also shown in the Fig. 4.8. Step P1 and step P2 in the figure corresponds to the polymer degradation. In Step P1, the polymer decomposition takes place over a broad temperature range from $287\text{ }^{\circ}\text{C}$ to $355\text{ }^{\circ}\text{C}$. The step P2 degradation takes place over a relatively narrow temperature region between $435\text{ }^{\circ}\text{C}$ and $467\text{ }^{\circ}\text{C}$. The weight loss for Step I and Step II were found to be 33 % and 67 % respectively (ignoring the step due to water loss).

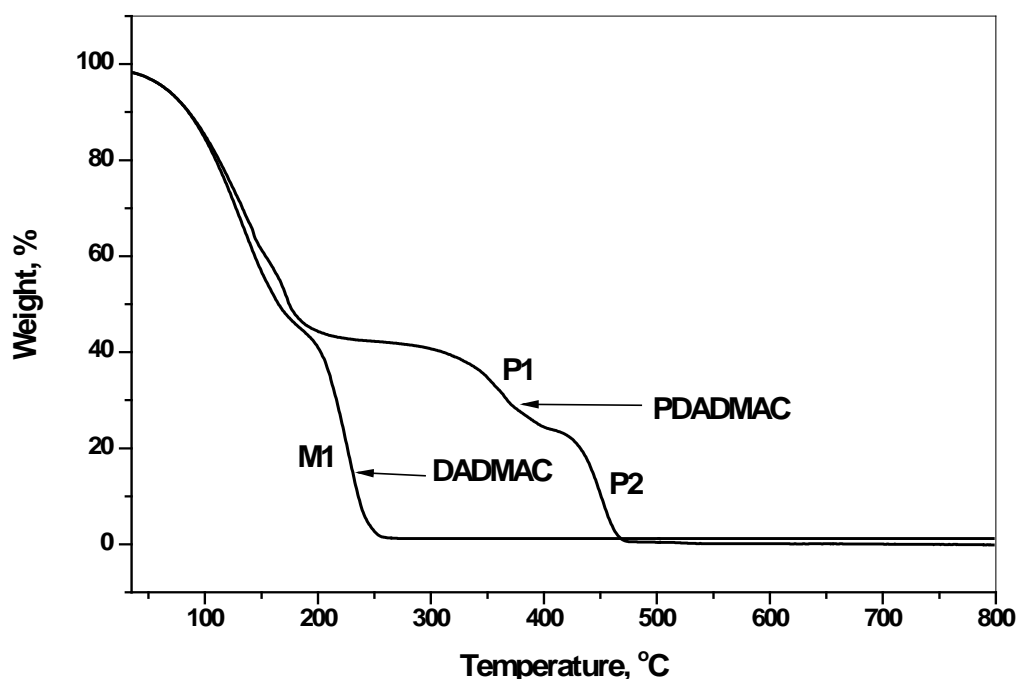


Fig. 4.8: TG curve of DADMAC and PDADMAC solutions in nitrogen atmosphere at a heating rate of $10\text{ }^{\circ}\text{C min}^{-1}$

When polymerization proceeds the concentration of the monomer in the solution decreases while that of the polymer increases which means that theoretically the percentage weight loss due to the monomer should decrease while that due to the polymer should increase. Experimental TGA runs were carried out on the monomer-polymer mixture of different known composition and are shown in Fig. 4.9. The weight loss due to the monomer step M1 decreases with the increase in the polymer concentration, while weight loss due to the polymer steps (P1 and P2) increases with the increase in polymer concentration. The decomposition steps M1 and P2 remains essentially unchanged in the ternary mixture. The monomer decomposition step M1 remains constant in the range $175\text{ }^{\circ}\text{C}$ (onset) to $247\text{ }^{\circ}\text{C}$ (endset) and the polymer step P2 also remain constant in the range $435\text{ }^{\circ}\text{C}$ (onset) and $467\text{ }^{\circ}\text{C}$ (endset). However a clear shift in the polymer step P1 was observed. At relatively lower

concentration of the polymer, the P1 decomposition occurs closer to the M1 step. As the concentration of the polymer increases, the P1 step shifts towards the P2 step.

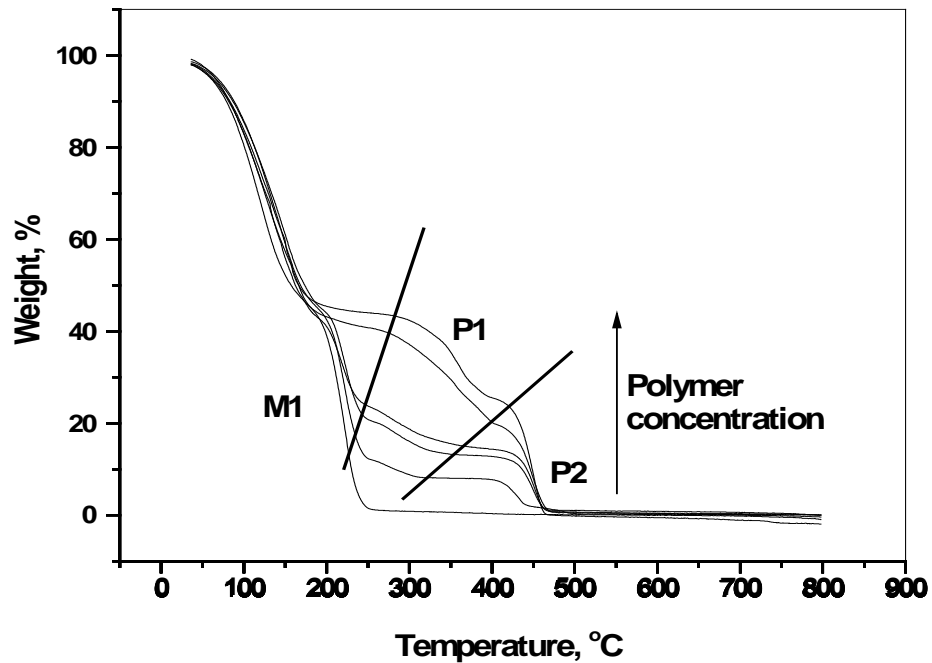


Fig. 4.9: Experimental TG curves of DADMAC-PDADMAC mixtures of various compositions

Also the P1 decomposition occurs over a much broader range as the polymer concentration in the mixture increases. All this indicates that some interaction occurs between the monomer and the polymer under the condition of the experiment. However it is difficult to ascertain the nature of interaction from TGA alone.

From the TG curves shown in Fig. 4.9, a calibration curve for the percentage weight loss of the monomer, step M1, as a function of PDADMAC weight fraction in the mixture was plotted and is shown as Fig. 4.10. The PDADMAC weight percentage is given as; $\text{PDADMAC} / (\text{PDADMAC} + \text{DADMAC}) \times 100$. A good co-linearity was exhibited between the two parameters. The linear correlation factor (R) was found to be 0.9962.

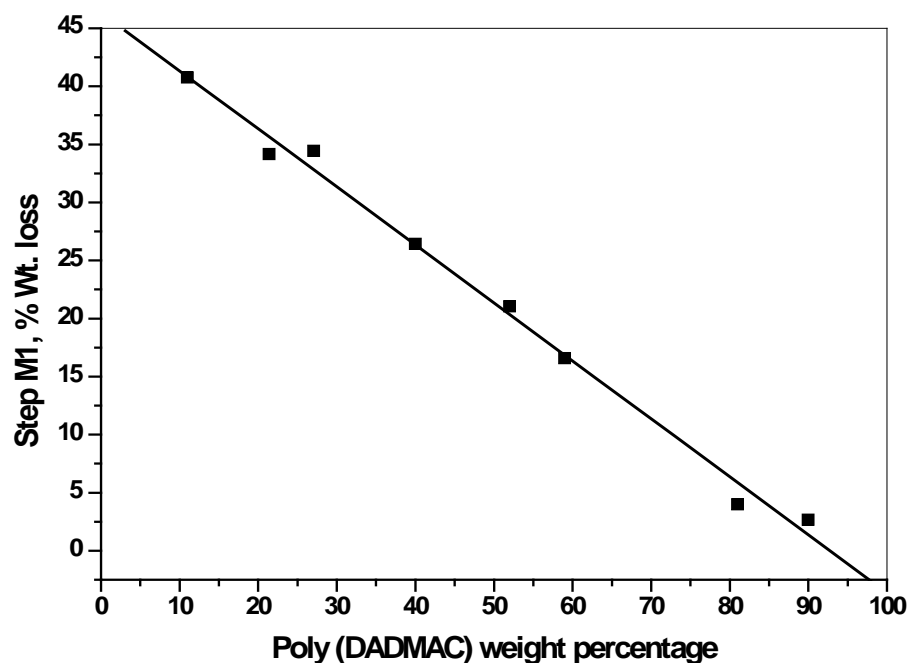


Fig. 4.10: Percentage weight loss of DADMAC step M1 versus PDADMAC weight percentage in the mixture

Similar calibration plot for the polymer decomposition step, P2, shown in Fig. 4.11, yielded a very good R value of 0.9993. The polymer step P1 was not considered for generating a calibration plot because the weight loss in the step P1 is only 33 % of the total weight loss of the polymer. Moreover P1 depends strongly on the composition of the solution and shifts to higher temperature with the increase in polymer content.

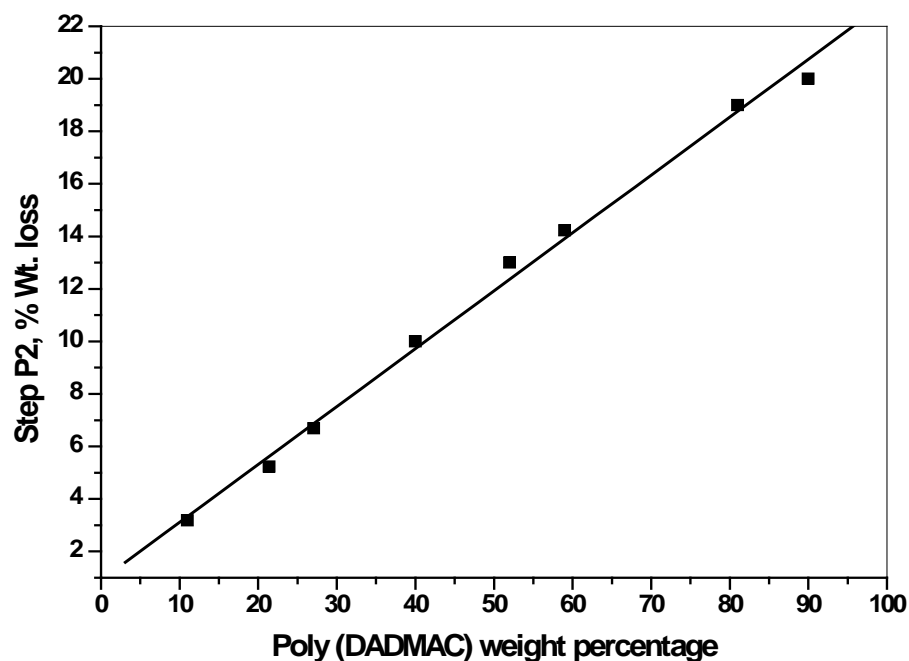


Fig. 4.11: Percentage weight loss of the PDADMAC step P2 versus PDADMAC weight percentage in the mixture

The DADMAC solutions were irradiated from 4 kGy to 70 kGy without the use of any extraneous initiators or crosslinking agents. Since no crosslinking agents were used, gel formation does not take place, and the polymer formed up to the irradiated dose of 70 kGy is entirely soluble in water. After irradiation the solution contains both the monomer and polymer in different ratios depending on the degree of conversion. Fig. 4.12 shows the TGA curves of the irradiated solutions (Monomer + Polymer).

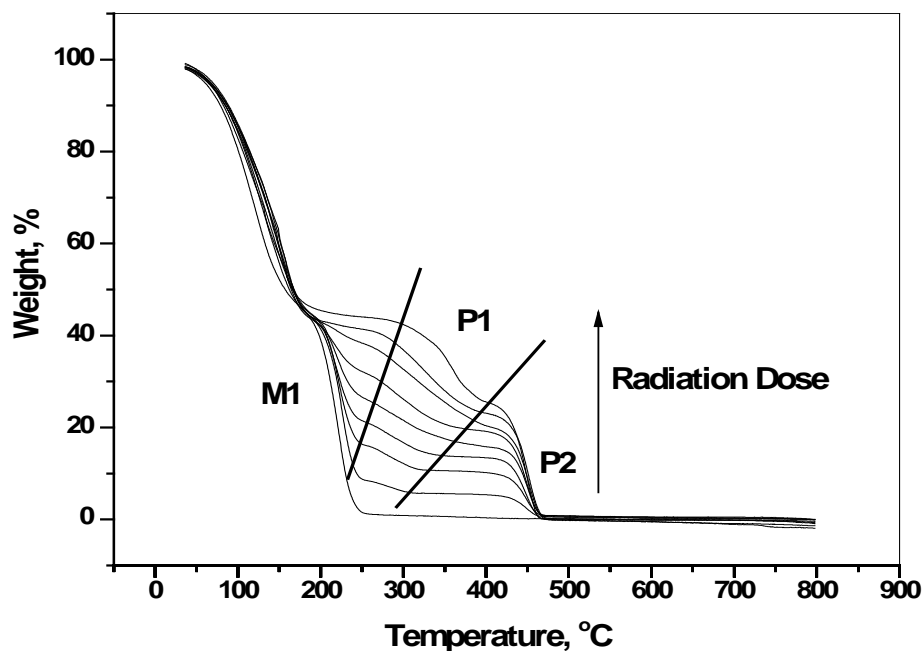


Fig. 4.12: Experimental TG curves of the DADM MAC irradiated to different absorbed doses

The thermal profiles of the samples are similar to that shown in Fig. 4.9. As expected the weight loss due to the monomer decreases and the weight loss associated with the polymer steps (P1 and P2) increases with the increase in irradiation dose. As mentioned earlier, a shift in the polymer step P1 was observed which depended on the concentration of the polymer in the mixture. The P1 decomposition occurs closer to the M1 step at relatively lower concentration of the polymer and shifts towards the P2 step as the concentration of the polymer increases in the mixture. Also a broadening of the P1 step was observed as the polymer concentration in the mixture increases. The weight loss of the monomer step M1 and polymer step P2 were noted and the monomer conversion was calculated from the calibration plot generated previously (Fig. 4.10 and Fig. 4.11). Classical gravimetry studies were carried out to compare the results obtained from TGA studies. In this method, PDADM MAC formed on irradiation was precipitated with excess isopropanol. It was further purified by dissolving

it in minimum amount of water and re-precipitating with isopropanol many times. The polymer samples were dried in air oven at 70 °C till they attained constant weight. The degree of conversion was calculated as:

$$\text{Degree of conversion} = \frac{\text{Weight of polymer precipitated}}{\text{Initial weight of monomer}} \quad (4.8)$$

Fig. 4.13 shows the degree of conversion of the DADMAC to PDADMAC as determined by TGA and classical gravimetry. The monomer conversion values calculated from classical gravimetry was found to correlate with the TGA results within the statistical variation. The TGA measurements had an experimental variation of $\pm 5\%$ while the variation in gravimetric measurements was in the range $\pm 10\%$. Both classical gravimetry and TGA results indicates that the degree of conversion of the DADMAC increases steadily with the increase in the radiation dose up to a dose of about 40 kGy after which it levels off.

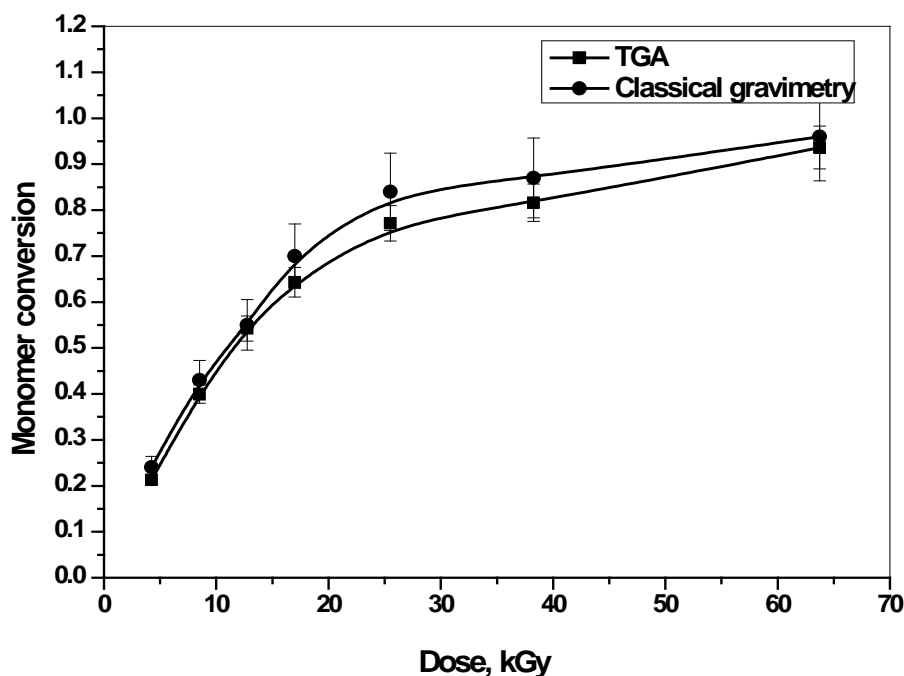


Fig. 4.13: Degree of conversion of DADMAC as a function of radiation dose, calculated from classical gravimetry and TGA

4.5. Conclusions

In first part of the study, the thermal behavior of PDADMAC was studied and the kinetic parameters associated with degradation were determined. TGA and DSC analyses of the polymer revealed that the polymer degrades in two stages; the first stage showing a weight loss of 33 % and the second stage showing a weight loss of 67 %. The DSC thermogram shows two endothermic peaks corresponding to the two stages in the TG thermogram. The experimental enthalpy change associated with the first and second stages were 650 Jg^{-1} and 129.5 Jg^{-1} respectively and the glass transition temperature (T_g) of the polymer was found to be around $150 \text{ }^\circ\text{C}$ depending on the test method employed. The kinetic triplet (order of the reaction, activation energy and the pre-exponential factor) was determined from a single TG measurement and also from a single DSC thermogram. But, the kinetic parameters derived from DSC were significantly different from the parameters derived from TGA. From all the above, the degradation process of the PDADMAC may be complicated involving a number of consecutive or parallel reactions. Since TG measures the loss of sample weight due to thermal degradation, it is a direct technique and gives more reliable information on the degradation kinetics than DSC. From the kinetic parameters calculated, isoconversion plots were generated for the degradation steps which predict the behavior of the polymer at different temperatures.

Based on the understanding gained from studying the thermal behavior of DADMAC and PDADMAC, a thermogravimetric method was developed to determine the degree of conversion of the monomer to polymer during the gamma radiation induced polymerization. The degree of conversion of DADMAC increases considerably during the initial stages of irradiation and at an absorbed dose of 40 kGy the maximum degree of conversion $0.8 - 0.9$ could be achieved. The degree of conversion of the monomer determined by TGA was found to be in good agreement with that obtained using classical gravimetry. In conclusion it may

be inferred that TGA is a convenient and useful method to determine the degree of conversion of DADMAC to PDADMAC as compared to hitherto established methods. This method could perhaps be extended to other monomer system, if the decomposition temperature of the corresponding polymer is well separated.

Chapter 5: Immobilization of PDADMAC by radiation induced grafting and radiolytic encapsulation in microcapsules

5.1 Introduction

The functional group present on a polymer is an important factor that affects its physical and chemical properties to a significant extent and play an important role in deciding the uses and applications on an industrial scale. PDADMAC contains the quaternary ammonium group which exhibit excellent properties such as ion exchange capacity for anions in solution, antibacterial activity and flocculation/ coagulation properties useful for water clarification. For some application like water clarification PDADMAC may be directly used at low concentrations to induce flocculation and coagulation of the undesired ions or impurities in water. Subsequently the flocculate or precipitate may be easily separated by sedimentation or filtration. But, there are applications that demand the immobilization of the polymer on some substrates to impart the desired functionality. For example, although PDADMAC possess ion exchangeable groups it cannot be used directly for separation purpose because of practical difficulty in separating and recovering the polymer from the solution due to its exceptional water solubility. This limitation can be circumvented or avoided if a water insoluble matrix like PDADMAC hydrogel, PDADMAC grafted membranes or PDADMAC encapsulated polymer beads are employed for ion exchange.

Microcapsules have interesting characteristics and have found various applications in medicine, pharmaceuticals and engineering [157-159]. There are many methods reported in the literature [160, 161] for the encapsulation of various functional materials to impart the desired functionality to the microcapsules. Encapsulated beads not only combine the advantages of solvent extraction and ion exchange but also provide benefits with the simplicity of operating condition with solid phase ion exchange process. The advantages of

the use of polymeric beads over other processes extends due to large surface area, minimal use of organic solvents (environment friendly) and absence of phase separation phenomenon.

In this chapter two different procedures adopted for the immobilization of PDADMAC, namely the radiation induced grafting of PDADMAC and radiolytic encapsulation of PDADMAC, are discussed separately. The first part of the chapter investigates the radiation induced grafting of PDADMAC onto the surface of polyethylene (PE) and the second part of the discusses a method for encapsulation of PDADMAC using radiation processing is reported.

5.2. Part I: Radiation induced grafting of PDADMAC onto polyethylene

Grafting of DADMAC onto various polymeric substrates could probably result in materials with newer applications in different areas; however, not many studies have been reported on the radiation induced grafting of DADMAC onto different substrates. In this study, the radiation grafting of DADMAC onto polyethylene (PE) by a two step method or a *double grafting* method is discussed. In the first step, acrylic acid is grafted onto PE by a mutual irradiation technique followed by the second grafting reaction wherein DADMAC is grafted onto the acrylic acid grafted PE. Similar approach has been employed by researchers for the synthesis of modified PTFE [162] and polypropylene [163] films exhibiting pH and thermo responsive behavior. The objective of the present work was to investigate the various factors that affect the grafting yield of DADMAC and also to characterize the grafted films by various analytical techniques.

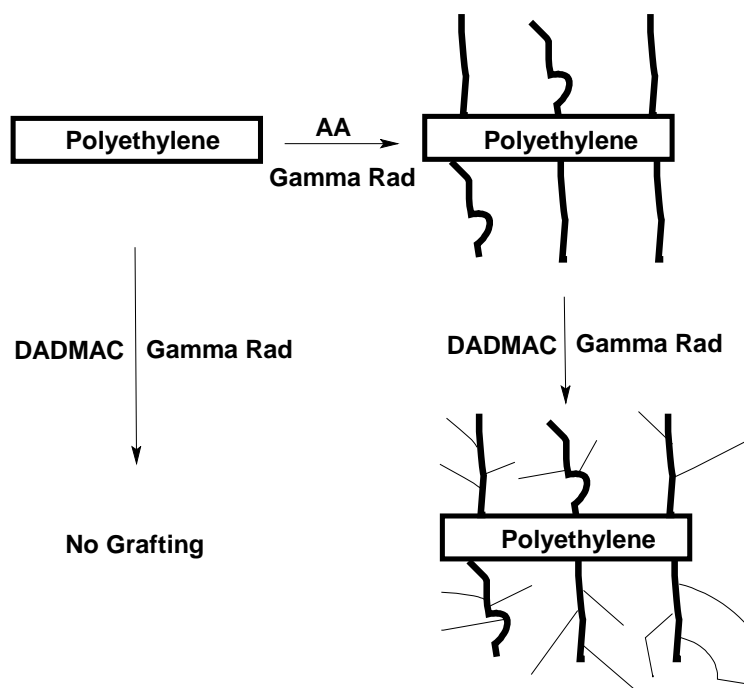
5.2.1 Experimental

5.2.1.1 Materials

Low density polyethylene (PE) films of thickness 80 μm were provided by Medi-Equip, India. Acrylic acid and DADMAC (65 % monomer solution) were purchased from Merck (India) Ltd and Fluka respectively. All the reagents were of analytical grade and used without further purification. Double distilled water (conductivity $< 1.5\mu\text{S}$) was used for all experiments. Gamma irradiation was carried out in a ^{60}Co gamma chamber, GC-4000A and GC-5000, (BRIT, India) at a dose rate of 0.26 kGyh^{-1} and 3.8 kGyh^{-1} respectively.

5.2.1.2 Grafting procedure

During the mutual radiation grafting process there is a competition between grafting of monomer on the substrate and homopolymerization of monomer in the solution. In order to achieve good yield of grafting it is necessary to suppress or inhibit homopolymerization by using certain additives. During preliminary investigation on grafting of DADMAC onto the surface of PE, various homopolymerization inhibitors like salts (NaCl, ZnCl_2 and LiCl), ammonia, acids, surfactants, Mohr's salt etc were tried, but no noticeable grafting was observed even at high radiation dose ($> 50\text{ kGy}$). This may be due to the inherently poor reactivity of allyl monomers compared to their vinyl counterparts [164]. Therefore, an indirect approach was adopted wherein grafting was done in two steps. In the first step acrylic acid (AA) was grafted onto PE film and in the second step DADMAC was grafted onto the AA-g-PE film. The procedure is shown in Scheme 5.1 and grafting details are discussed below.



Scheme 5.1: Grafting of DADMAC onto PE employing a two stage procedure

5.2.1.2.1 Acrylic acid grafting onto PE (AA-g-PE)

The functional PE films were prepared by γ -radiation induced mutual grafting of acrylic acid (AA) onto the surface of PE at room temperature. The PE films were washed in isopropanol to remove the surface contaminants and finally washed in distilled water and dried. The PE film (4 cm x 6 cm) was taken in a 60 ml glass vial containing 20 % (aqueous v/v) AA solution and sonicated for 30 minutes to remove the dissolved air. Mohr's salt was used at a concentration of 1 wt % to inhibit the homopolymerization of acrylic acid. The films were irradiated in sealed glass vials to various doses from 2 to 10 kGy. Grafting was confirmed from the IR spectrum and the grafting yield was calculated gravimetrically. The grafted films were treated with known quantity of NaOH solution to convert the free carboxyl group to its sodium salt. For complete conversion, excess of NaOH solution was used. The

degree of conversion, to the carboxylate anion, was calculated from the increase in weight of the film.

5.2.1.2.2 Diallyldimethylammonium chloride grafting onto AA-g-PE (DADMAC-g-AA-g-PE)

Grafting of DADMAC onto AA-g-PE films was carried out using the same procedure mentioned above. The AA-g-PE films (4 cm x 6 cm) with different degree of grafting were taken in a 60 ml glass vial containing different concentration of DADMAC aqueous solution and irradiated to various doses.

5.2.2 Characterization

5.2.2.1 Grafting Yield

The grafted PE films were washed repeatedly in hot distilled water to extract and remove the unreacted monomer and the homo-polymer. The grafted films were dried to constant weight and the grafting yield was determined gravimetrically using Eqn. 5.1.

$$\% \text{ Grafting} = \frac{\text{Weight after grafting} - \text{Initial weight}}{\text{Initial weight}} \times 100 \quad (5.1)$$

5.2.2.2 Equilibrium degree of swelling (EDS)

The equilibrium degree of swelling of the grafted films was determined gravimetrically. The grafted films, dried to constant weight, were immersed in excess distilled water at room temperature for 24 hours to attain equilibrium. The films were weighed after the excess water was removed with a filter paper and the EDS were calculated by Eqn. 5.2.

Weight of the swollen film - Initial weight

$$\text{EDS (\%)} = \frac{\text{Weight of the swollen film} - \text{Initial weight}}{\text{Initial weight}} \times 100 \quad (5.2)$$

5.2.2.3 Thermogravimetric analysis (TGA)

Thermo gravimetric analyses were carried out using Mettler TA 3000 thermal analysis system (TG 50). About 10 mg of the film was weighed into an alumina crucible and the thermal profiles were recorded from 50 °C to 800 °C at a heating rate of 10 °C/min under N₂ flow of 50 ml/min.

5.2.2.4 FT-IR spectra of the films

Jasco FT/IR-660 plus spectrometer was used to record the spectrum of the films from 500 cm⁻¹ to 3500 cm⁻¹ at a resolution 4 cm⁻¹. Averages of 50 scans were taken.

5.2.3 Results and discussion

For effective grafting of DADMAC, the surface of PE films was modified by radiation grafting of AA. The radiation induced grafting of AA onto PE has been studied by many workers [165, 166]. The grafting percentage of AA onto PE films as a function of absorbed dose, under the conditions of our experiment is shown in Fig. 5.1. The percentage grafting shows an S-shaped dependence on the absorbed dose. After an induction period up to a dose of 2 kGy, which is characterized by a comparatively low rate of grafting, the rate of the process rapidly increases and an acceleration of the grafting reaction is seen in the intermediate stage from 3.2 kGy to 6.3 kGy. Above the absorbed dose of about 6.3 kGy the grafting rate is slow and the grafting yield levels off.

AA grafted onto PE is present in the anionic form, due to the NaOH treatment, and the polyacrylate chains is expected to have strong affinity for the cationic DADMAC monomer.

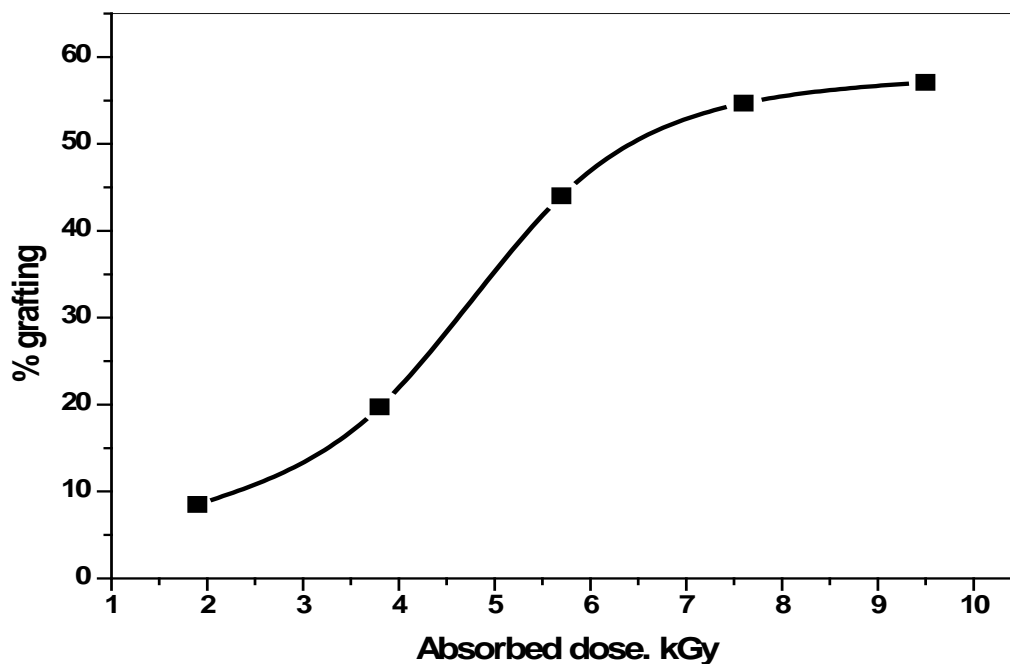
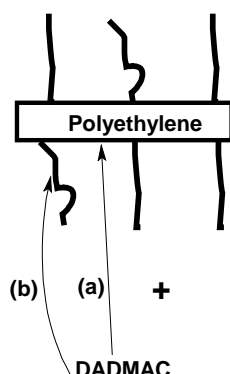


Fig. 5.1: Grafting percentage of AA onto PE films as a function of absorbed dose at an AA concentration of 20 % and dose rate of 3.8 kGy

When AA-g-PE film is irradiated in the presence of DADMAC, there are a number of reactions that can occur (Scheme 5.2). First of all, the DADMAC monomer can either (a) graft onto the PE backbone or (b) graft onto the already grafted polyacrylate chains. In the preliminary studies mentioned above, direct grafting of DADMAC onto PE was not observed. This possibility is further reduced when polyacrylate chains are present on the surface of PE, because the acrylate groups will show strong electrostatic attraction towards DADMAC monomer thereby preventing its access to the radical sites generated on the PE

backbone. Thus, the reaction (b) is much more probable than the reaction (a) and a comb type grafted structure can be expected [167].



Scheme 5.2: Different reaction modes of DADMAC

Secondly, there is a possibility that homopolymerization of DADMAC takes place in the first stage of irradiation and then the resulting polycation forms a complex with polyacrylate chains on the surface of PE films resulting in the increase in weight of the films. To rule out the possibility of polyelectrolyte complex formation, AA-g-PE films were equilibrated with commercially procured PDADMAC solution (low, medium and high molecular weight) for 24 hours. There was no significant change in the weight of the films indicating that polyelectrolyte complexes (PEC) are not formed on the surface of the films under these conditions. However, after the grafting of DADMAC onto AA-g-PE, the PDADMAC chains are bound to have strong electrostatic interaction with the negatively charged polyacrylate chains resulting in the formation of PEC.

5.2.3.1 Grafting yield

The grafting percentage of DADMAC onto AA-g-PE (30 % AA grafted) films as a function of absorbed dose at various DADMAC monomer concentration is shown in Fig. 5.2. The grafting yield increases considerably during the initial stages of irradiation, up to a dose of 15 kGy, after which the increase in grafting yield is not significant. The maximum degree

of grafting, at the various absorbed doses, was obtained at a DADMAC concentration of 10 %. At the highest monomer concentration of 25 %, the least percentage of grafting was obtained. Under the mutual grafting conditions, there is a competition between grafting and homopolymerization which takes place to a significant extent. Higher the monomer concentration, greater is the possibility of homopolymerization taking predominance over the grafting reaction. This accounts for the fact that lower DADMAC concentration of 10 % shows higher grafting yield compared to higher monomer concentration of 25 %. When DADMAC was used at the lowest concentration of 5 %, at all the absorbed doses, the grafting yield was found to be less than that obtained when 10 % DADMAC was used. This may be attributed to the diminished rate of the grafting reaction, and also the polymerization reaction at a lower monomer concentration.

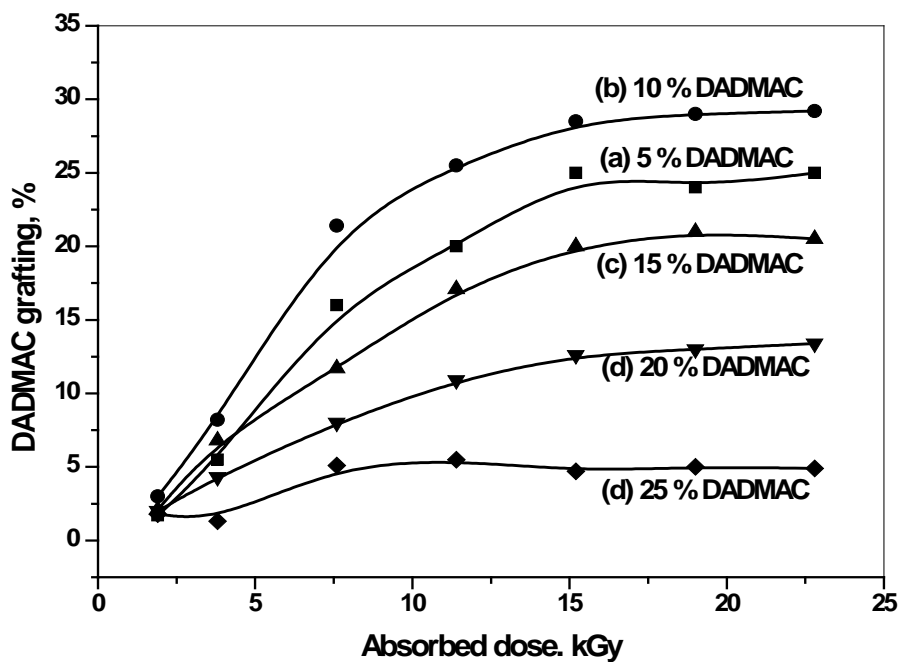


Fig. 5.2: Grafting percentage of DADMAC onto AA-g-PE (30 % AA grafted) films as a function of absorbed dose at various DADMAC monomer concentration

Fig. 5.3 shows the grafting percentage of DADMAC onto AA-g-PE films of different initial AA grafted composition, at a fixed absorbed dose of 15 kGy. It can be seen from the figure that higher the degree of initial AA grafting onto PE, the higher is the grafting of DADMAC onto the pre-grafted films. This is because as the acrylate chain density increases, the probability of the formation of radical sites on the polyacrylate chains is higher which facilitates the grafting of DADMAC.

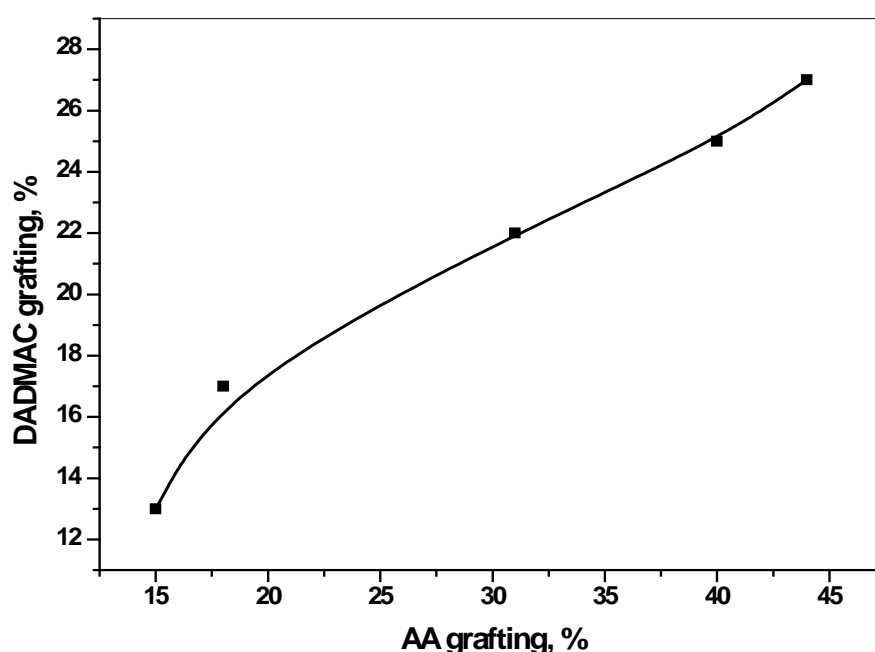


Fig. 5.3: Grafting percentage of DADMAC onto AA-g-PE films of different initial AA grafted composition, at a fixed absorbed dose of 15 kGy

5.2.3.2 Degree of conversion of the carboxyl group to its carboxylate anion and DADMAC grafting

The AA-g-PE films (30 %), with different degree of conversion, were irradiated to dose of 7.6 kGy in 20 % DADMAC solution. The percentage grafting as a function of degree of conversion of the carboxyl group to its carboxylate anion is shown in Fig. 5.4. For

effective grafting of DADMAC onto AA-g-PE film, the radical sites formed on polyacrylic acid backbone should be available to the monomer to initiate the grafting reaction. When polyacrylic acid is in the carboxyl form, the polymer chains prefer a more coiled conformation and there is a tendency for the polymeric radicals to undergo intra or inter chain crosslinking rather than reacting with the DADMAC monomer. As the degree of conversion increases, the charge density increases and polyacrylate chains attain a more extended conformation and the polymeric radical-radical reaction is suppressed to a great extent while the polymeric radical-monomer reaction is facilitated. Therefore the grafting yield increases linearly as more carboxyl group is converted into its Na salt.

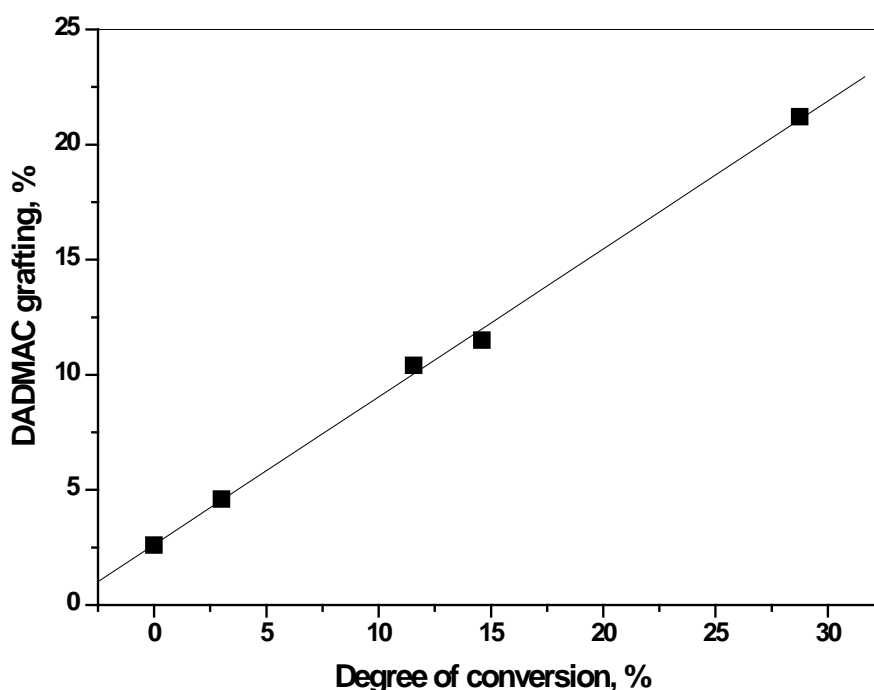


Fig. 5.4: Grafting percentage of DADMAC as a function of conversion degree of the carboxyl group to its carboxylate anion at an irradiated to dose of 7.6 kGy in 20 % DADMAC solution

5.2.3.3 Swelling studies

The presence of ionic groups is a decisive factor in the swelling behavior of polymeric films. When AA is grafted onto PE, the number of ionizable groups in the system increase and the degree of swelling increases correspondingly. For example, the EDS of PE film is almost negligible but after grafting AA (to an extent of 30 %) the EDS increased to about 50 %.

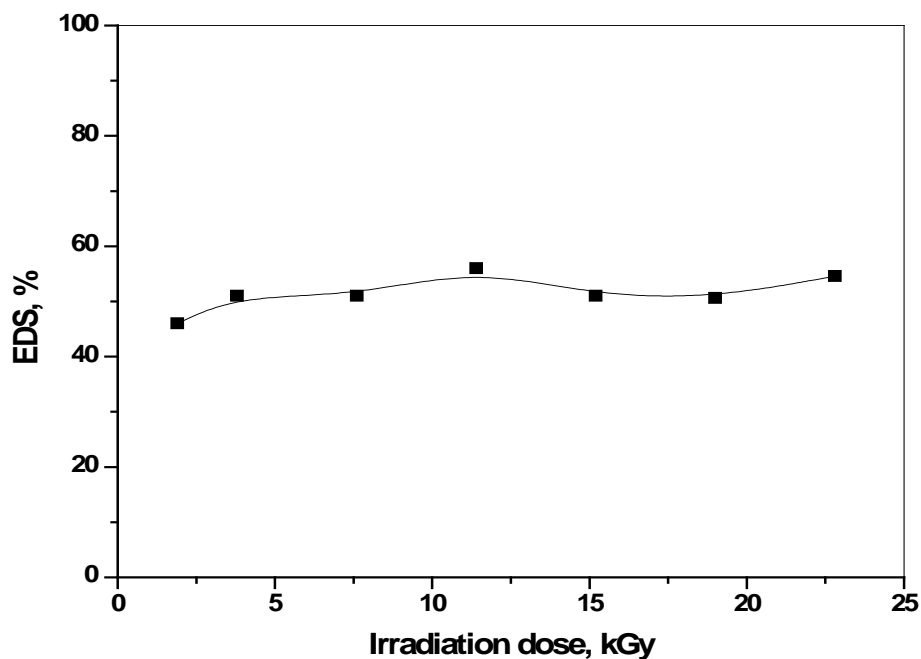


Fig. 5.5: Equilibrium degree of swelling of DADMAC grafted films as a function of irradiation dose

Further ionic groups are introduced when DADMAC is grafted onto the AA-g-PE films, but the EDS remain more or less constant at 50 % (Fig. 5.5). This is due to the formation of PEC of polyacrylate and PDADMAC on the surface of the film. The expected increase in swelling is offset by the formation of the PEC and the observed EDS (constant) is

due to the reduction in the number of free ionic groups that would have contributed to the swelling of the film.

5.2.3.4 Effect of dose rate

The effect of dose rates on the grafting yield of DADMAC is shown in Fig. 5.6. The effect of the dose rate on grafting yield is not very significant. A slightly higher grafting yield of 32 % could be obtained at the dose rate of 3.8 kGy/h compared to 29 % obtained at 0.26 kGy/h. This may be because, at higher dose rate, proportionately more homopolymerization occurs than grafting.

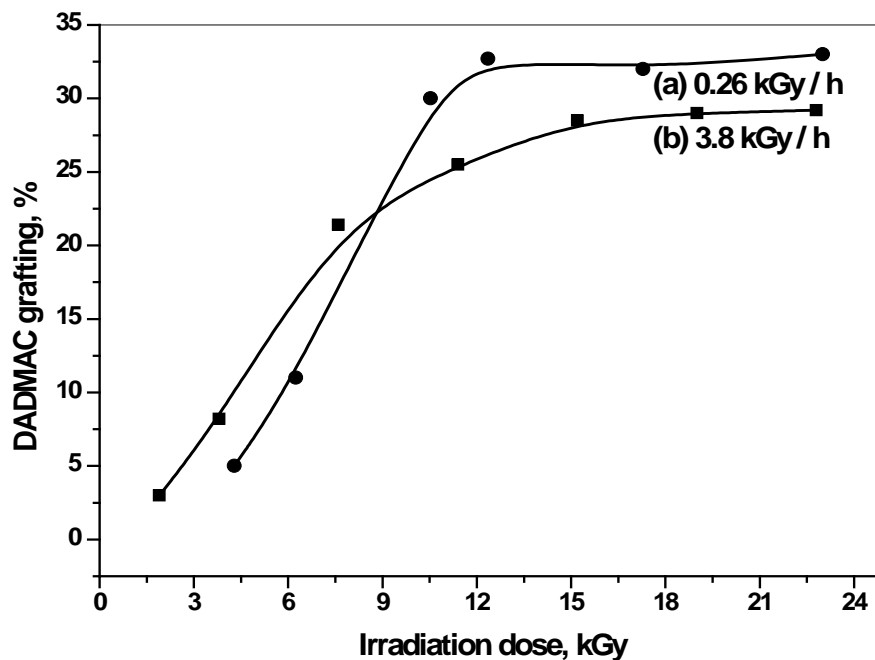


Fig. 5.6: Grafting yield of DADMAC, as a function of irradiation dose, at dose rates of (a) 0.26 kGy and (b) 3.8 kGy

5.2.3.5 FT-IR of the films

The FT-IR spectra of PE (a), AA-g-PE (b), pure PDADMAC) (c) and DADMAC-g-AA-g-PE (d) films are shown in Fig. 5.7. The PE film shows the characteristic peaks at 2924, 2854, 1462 and 721 cm^{-1} . After grafting with acrylic acid, the FT-IR spectra showed an additional peak at 1720 cm^{-1} due to the C=O stretching which confirms the grafting of AA onto PE. Pure PDADMAC shows the characteristic peaks at 1481 cm^{-1} and 1641 cm^{-1} . This is close to the characteristic band of PE (1462 cm^{-1}) and the band due to C=O (1720 cm^{-1}) from the grafted polyacrylic acid chain.

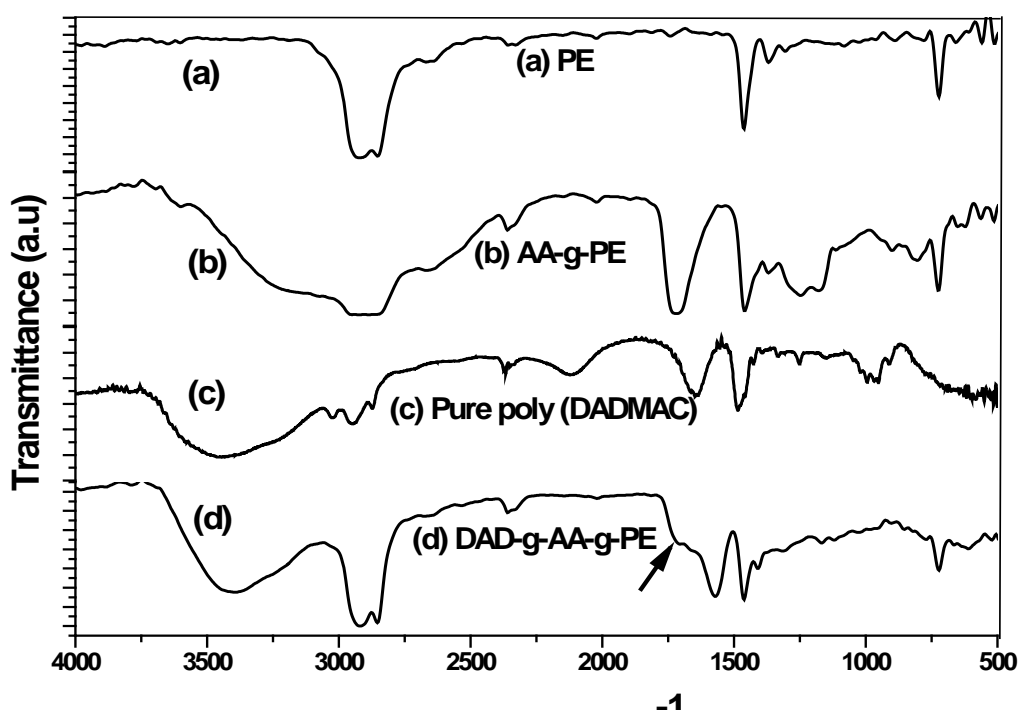


Fig. 5.7: FT-IR spectra of (a) PE, (b) AA-g-PE, (c) pure PDADMAC and (d) DADMAC-g-AA-g-PE

The spectrum of DADMAC-g-AA-g-PE shows a peak at 1570 cm^{-1} with a shoulder (shown by an arrow) at around 1721 cm^{-1} . The peak at 1570 cm^{-1} is due to the formation of

the carboxylate anion and the shoulder contains contribution from PDADMAC and the carboxyl group of polyacrylic acid.

5.2.3.6 Thermogravimetric analysis (TGA)

The TGA profiles of the original PE film, pure PAA and PDADMAC is show in Fig. 5.8. The PE film undergoes single step decomposition from 425 °C to 479 °C. TGA profile of PDADMAC shows two well defined steps [156]. The initial weight loss up to a temperature of around 150 °C is due to the loss of moisture from the polymer sample. The first step decomposition takes place over a broad temperature range from 287 °C to 355 °C, with a weight loss of 33 %. The second step degradation takes place over a relatively narrow temperature region from 435 °C to 467 °C with a weight loss of 67 %. TGA profile of polyacrylic acid shows two steps.

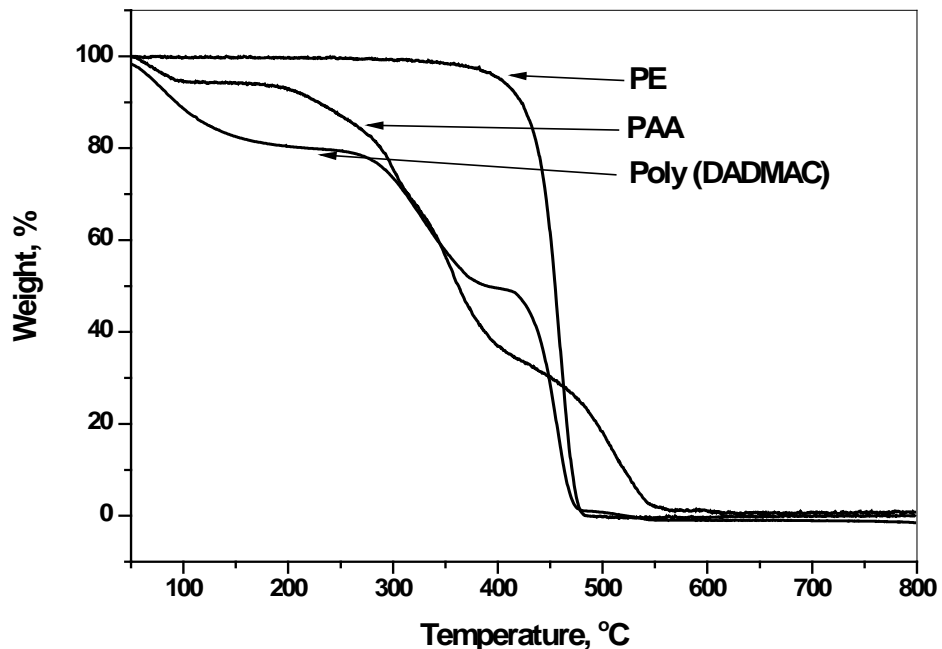


Fig. 5.8: TGA profiles of the original PE film, pure PAA and PDADMAC

The initial weight loss up to a temperature of around 120 °C can be attributed to the loss of moisture from the polymer sample. The first step is characterized by a weight loss of 57 % and the decomposition takes place from 184 °C to 385 °C. The second step degradation takes place over the temperature region between 385 °C and 560 °C with a weight loss of 43 %.

The TGA profiles of AA-g-PE film (b) and DADMAC-g-AA-g-PE film (c) is shown in Fig. 5.9. The thermal profile of original PE film (a) is also shown for comparison. The TGA profiles are divided into four regions, 50-150 °C (I), 150-425 °C (II), 425-472 °C (III) and 472-800 °C (IV). The weight loss in region I is due to the loss of absorbed moisture from the sample films. The pure PE film does not show any weight loss in this region since it is hydrophobic. Grafting of AA or AA and DADMAC onto the films makes it hydrophilic and it absorbs the atmospheric moisture.

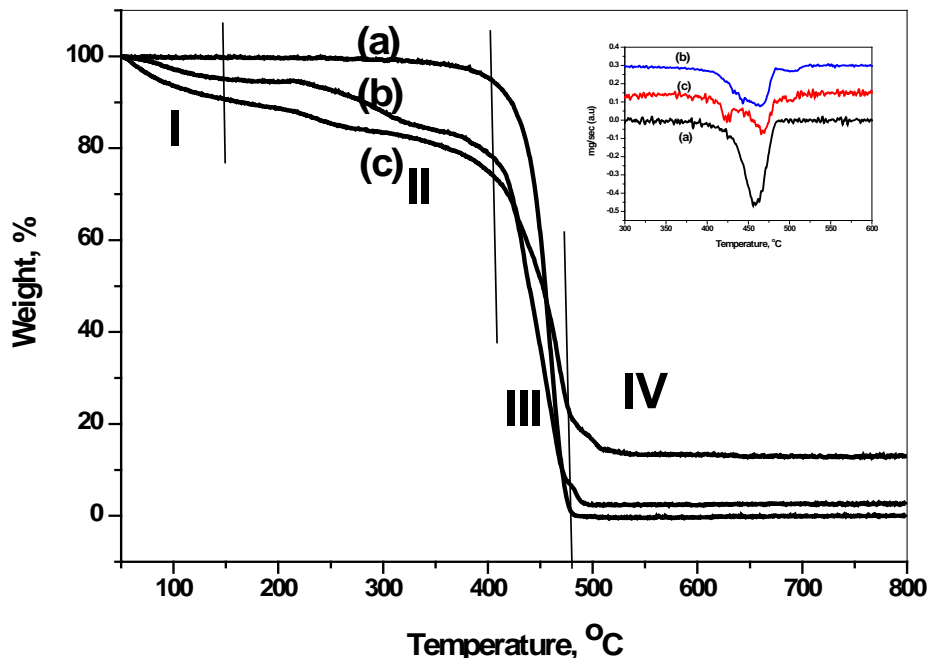


Fig. 5.9: TGA profiles of (a) original PE film, (b) AA-g-PE film and (c) DADMAC-g-AA-g-PE film

Therefore the grafted film shows a weight loss in the first region. It may be noted that the first step decomposition of polyacrylic acid (184 - 385 °C) and PDADMAC (287 - 355 °C) is complete before the decomposition temperature of PE (425 °C). Therefore the weight loss of the grafted films in the region II is due to the decomposition of the grafted side chains on the surface of PE. The AA-g-PE film shows a weight loss of 12 % while the DADMAC-g-AA-g-PE film shows a weight loss of about 18 %, before the decomposition of PE starts, which corresponds to the extent of grafting. The weight loss of the grafted films in the region III is due to contributions from two components, the grafted polymer chains and the PE backbone. In the IV region, after the complete decomposition of the PE backbone, a small weight loss is seen up to a temperature of 550 °C which can be attributed to the decomposition of the polyacrylic acid chains grafted on the PE. The decomposition temperature of PE was not significantly affected by the grafting of acrylic acid or DADMAC onto the surface of the film.

5.3 Part II: Gamma radiolytic encapsulation of PDADMAC in PES microcapsules

In second part of this chapter, a radiolytic process for encapsulating PDADMAC in the core of a preformed hollow polyether sulfone (PES) microcapsule, for the extraction of anions from aqueous solutions is described. PES microcapsules for the studies were prepared by the gel-sol phase inversion process. For preparation of the microcapsules, PES solution was first made by dissolving 37.5 g in 250 ml of N-methyl pyrrolidone by continuous stirring and keeping at room temperature for 4 h to eliminate the air bubbles in the solution. The polymer solution was gradually dropped through a glass dropper into a water coagulation bath maintained at a temperature of 30 ° C and further kept in water bath for a day to attain stability. Microcapsules of different physical characteristics such as the overall size, core structure and pore size can be synthesized by varying experimental conditions like

concentration of the polymer solution, temperature of the coagulation bath and certain additives.

DADMAC monomer was introduced inside the porous microcapsules by equilibrating in excess DADMAC solution and then polymerization was initiated by irradiation, to trap the polymer formed inside the capsule. The hollow capsules are permeable to water, ions and low molecular weight monomers but impermeable to high molecular weight polymers. When the Stokes radius of the polymer formed is more than the pore size of the microcapsule, it remains trapped in the core of the microcapsule. The microcapsules were washed in deionized water to remove unreacted DADMAC and oligomeric PDADMAC. The polymer in the core was converted to its hydroxide form (PDADMA-OH) by equilibrating in excess of NaOH solution and used for the anion exchange studies. Ion chromatography studies showed that the resultant microcapsule was able to take up and exchange some anions (F^- , Cl^- , Br^- , NO_3^{2-} and SO_4^{2-}) at relatively low concentrations.

5.3.1 Experimental

5.3.1.1 Material

PES having a molecular weight of 125000 (Gafone PES 3200P) was procured from Gharda Chemicals Limited, India. N-methyl pyrrolidone was purchased from E. Merck India Ltd and the monomer, diallyldimethylammonium chloride (DADMAC), 65 wt % was purchased from Fluka. Double distilled water (conductivity $< 1.5\mu S$) was used for all the experiments. The irradiation was carried out at a dose rate of 3.8 kGy h^{-1} respectively.

5.3.1.2 Degree of conversion

The degree of conversion was determined gravimetrically. The polymer formed after irradiation was precipitated and dried till the samples attained constant weight. The degree of conversion is given by Eqn. 5.3.

$$\text{Degree of conversion} = W_p / W_m \quad (5.3)$$

Where W_p is the weight of polymer formed and W_m is the initial weight of monomer in the solution.

5.3.1.3 Molecular weight determination (viscometry)

Intrinsic viscosity of the polymers measurements were carried out in 1 M NaCl solution using an Ubbelohde type viscometer at $24 \pm 1^\circ\text{C}$. The flow time for double distilled water was 61 seconds. The viscosity-average molecular weights were calculated using the Mark – Houwink – Sakurada equation (Eqn. 5.4).

$$\eta = 1.12 \times 10^{-4} M_v^{0.82} \quad (5.4)$$

5.3.1.4 Instrumentation

i) Thermogravimetric analysis (TGA)

The dynamic thermogravimetric analyses were carried out with Mettler thermogravimetric analyzer (TG 50) coupled with a Mettler TC 10A processor. A single microcapsule weighing approximately 35 mg were taken in an open alumina crucible and the degradation profiles were recorded from 35°C to 800°C at a heating rate of $10^\circ\text{C min}^{-1}$. The decomposition was carried out in an inert dynamic atmosphere of high purity nitrogen set at a flow rate of 100 ml min^{-1} .

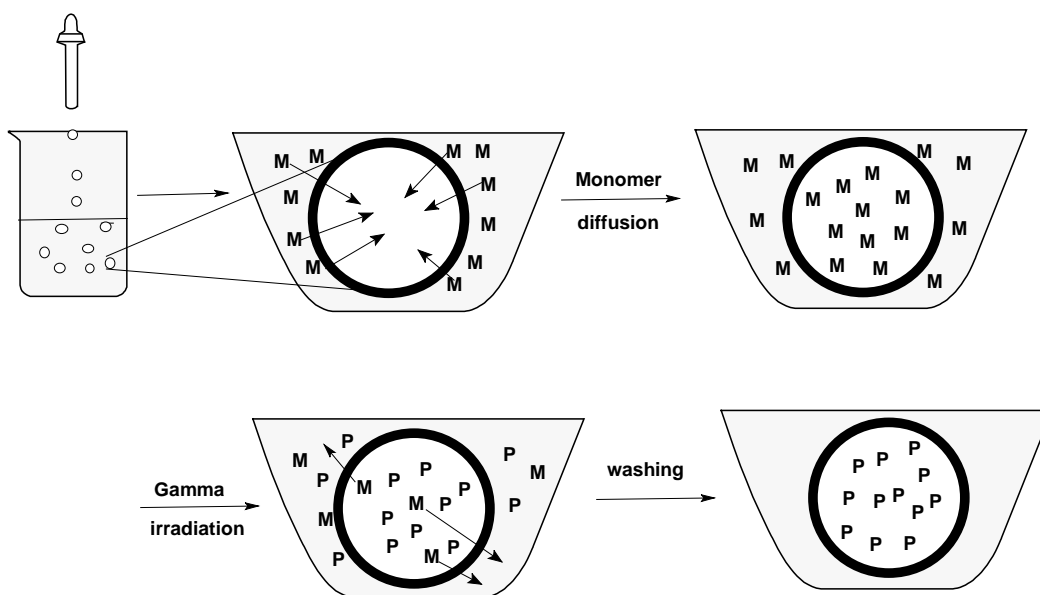
ii) Ion chromatography

All the analyses were conducted on Dionex ion chromatography equipment (DX-500) consisting of a gradient pump (GP 40), Rheodyne injection port, anion trap column (ATC), anion guard column (AG 11, 4mm), anion separating column (AS 11, 4mm), anion self regenerating suppressor unit (ASRS-ULTRA, 4mm), electrochemical detector (ED 40), UV/VIS absorbance detector (AD 20) and auto-sampler (AS 40). A Dionex Peaknet (version 5.01) chromatography workstation was used for system control and data collection. Sample loop of 10 μ L was used throughout the analyses. For the analysis, five microcapsules were equilibrated with 10 ml of standard anion solution for 24 hours, and the residual concentrations of the anions were determined using ion chromatography as mentioned above.

5.3.2 Results and discussion

In this study, PDADMAC was incorporated in the core of a preformed hollow polyether sulfone microcapsule using radiation processing for the extraction of anions from aqueous solutions. The hollow capsules are permeable to water, ions and low molecular weight monomers but impermeable to higher molecular weight polymers. The method reported here is general and is not limited to any particular polymer or application. Any polymer which can be synthesized by radiation polymerization from its respective monomer can be encapsulated in a microcapsule. The basic idea was to introduce the monomer into the porous microcapsules and initiate polymerization by radiation to trap the polymer formed inside the capsule. The Stokes radius or the hydrodynamic radius of a polymer will vary depending on its molecular weight and the nature of the solvent. When the Stokes radius of the polymer formed is more than the pore size of the microcapsule, it remains trapped in the core of the microcapsule. The concept is depicted in Scheme 5.3, the microcapsules are prepared by a gel-sol phase inversion method [168] and the monomer is introduced in the

core of the capsule and polymerized by gamma irradiation to form the final microcapsule containing the trapped polymer.



Scheme 5.3: The radiolytic encapsulation process

The microcapsules synthesized were equilibrated in 3 M DADMAC solution for 2 days and then exposed to gamma radiation (at a dose rate of 3.8 kGy/h) for 2 hours. Excess monomer was used to minimize the inhibitory effect of oxygen. It was observed that the microcapsules retained its physical structure under the conditions of irradiation, indicating its radiation stability.

The degree of conversion of the monomer and the molecular weight of the polymer formed could be easily determined by analyzing an aliquot from the solution. It can be safely assumed that the polymerization proceeds in a similar fashion within the capsule and the external monomer solution because the attenuation of gamma rays by the shell of the microcapsule is negligible. The average molecular weight of the polymer formed in the core of the microcapsule was determined viscometrically and found to 2.8×10^4 and the degree of conversion was found to be 0.4. By simply altering the irradiation condition it is possible to

prepare polymers of different molecular weights or even form a hydrogel within the microcapsule. In the present study, the reaction was stopped before the gelation point because hydrogels in the core would exert more swelling pressure on the capsule shell than a liquid core and hence more likely to deform and rupture the shell on repeated use. Moreover the kinetics is predictable to be faster in a liquid core than in a hydrogel core. The capsules were washed in deionized water to remove the unreacted monomer and low molecular weight polymer. The polymer in the core was converted to its hydroxide form (PDADMA-OH) by equilibrating in excess of 3.5 M NaOH solution and used for the anion exchange studies after thorough washing with deionized water. The anions from the external medium diffuse through the porous PES shell and exchange with the hydroxide ion of PDADMA-OH however the bulky polymer is retained in the capsule. The microcapsule could be repeatedly used after converting it back to the hydroxide form using NaOH.

Optical microscope images of the microcapsules are shown in Fig. 5.10. The average diameter of the beads was $4 \text{ mm} \pm 0.3 \text{ mm}$. The SEM image of a cross-section of the capsule is shown Fig. 5.11 which points to core-shell morphology, typical of the gel-sol phase inversion method and a porous morphology was clearly observed beneath the dense external skin layer.



Fig. 5.10: Typical optical image of the microcapsules

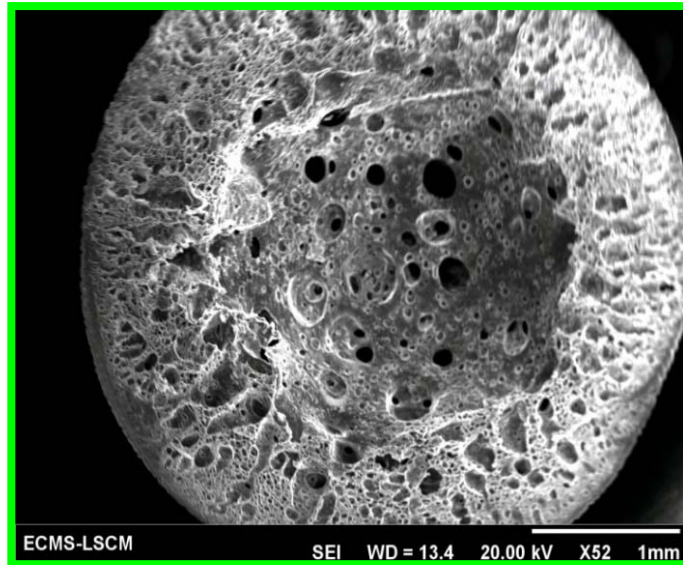


Fig. 5.11: SEM image of a cross-section of the microcapsule showing a core-shell morphology

TGA is a good technique to determine the pore volume of the capsules. By analyzing the microcapsules saturated with water and monitoring the weight loss associated with water, it was found that the open pores accounted for approximately 80 % of the total volume of the capsules.

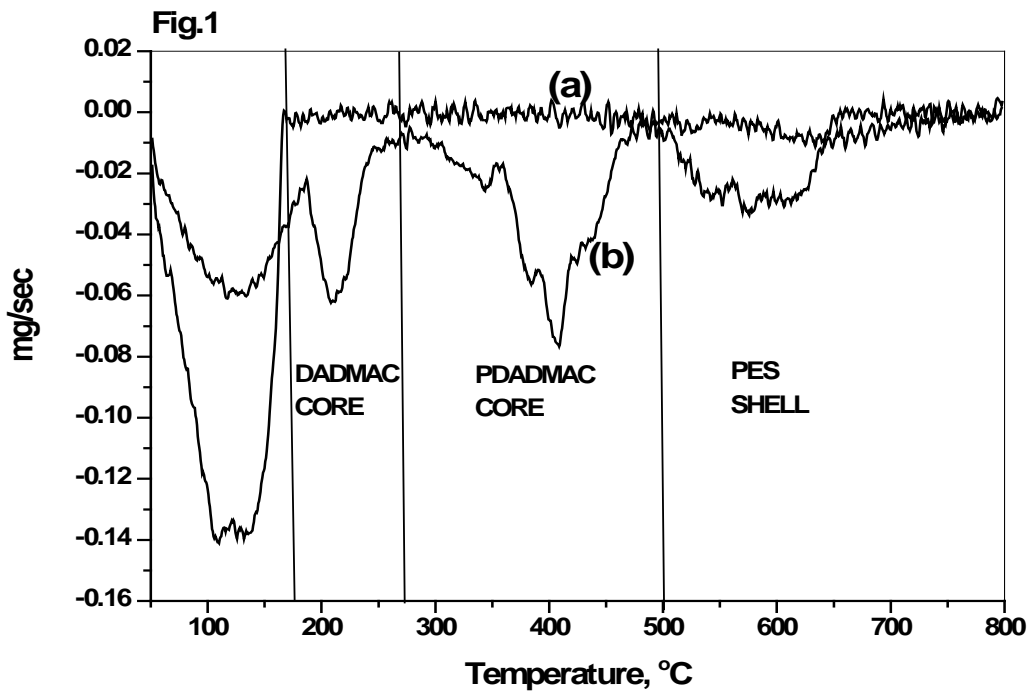


Fig. 5.12: DTG plots of (a) the pure PES microcapsule and (b) the microcapsule containing the monomer and polymer after gamma irradiation

Fig. 5.12 shows the DTG of the pure PES capsule and PES capsule containing the irradiated monomer solution. PES microcapsules show two steps (peak), the first peak in the temperature range 50 °C to 175 °C, is due to the loss of the solvent (NMP) and water while the second peak between 500 °C and 700 °C arises due the decomposition of the PES backbone. The microcapsule containing irradiated monomer shows three steps. The first step (175 °C -270 °C) is due to the residual monomer, NMP and water present in the core after irradiation. The core of the capsules also contains the polymer, PDADMAC, formed after irradiation which appears as the second peak in temperature range 270 °C to 500 °C [156]. The third step is due to the PES shell. Some of the NMP remains with PES as plasticizer and is lost on heating along with water. Overall, the result indicates synthesis of the polymer in the core of the microcapsule.

The microcapsules were equilibrated with solutions of different anions and the anion exchange was monitored with the help of ion chromatography. Table. 5.1 and Table. 5.1 show the results of the studies and provide indirect evidence for the encapsulation of the polymer in the microcapsule. A typical ion chromatograph for the mixed anion standard solution is shown in Fig. 5.13.

Table 5.1: Anion uptake by the microcapsule from mixed anion standards

	Fluoride	Chloride	Bromide	Nitrate	Sulfate
Initial conc(ppm)	0.89	8.28	9.23	7.75	7.39
Final conc(ppm)	0.67	6.54	6.27	4.65	1.82
% uptake	24	21	32	40	75

Table 5.2: Fluoride and Nitrate uptake by the microcapsule (separately)

	Fluoride	Nitrate
Initial conc (ppm)	10	10
Final conc (ppm)	7.7	2.3
% uptake	23	77

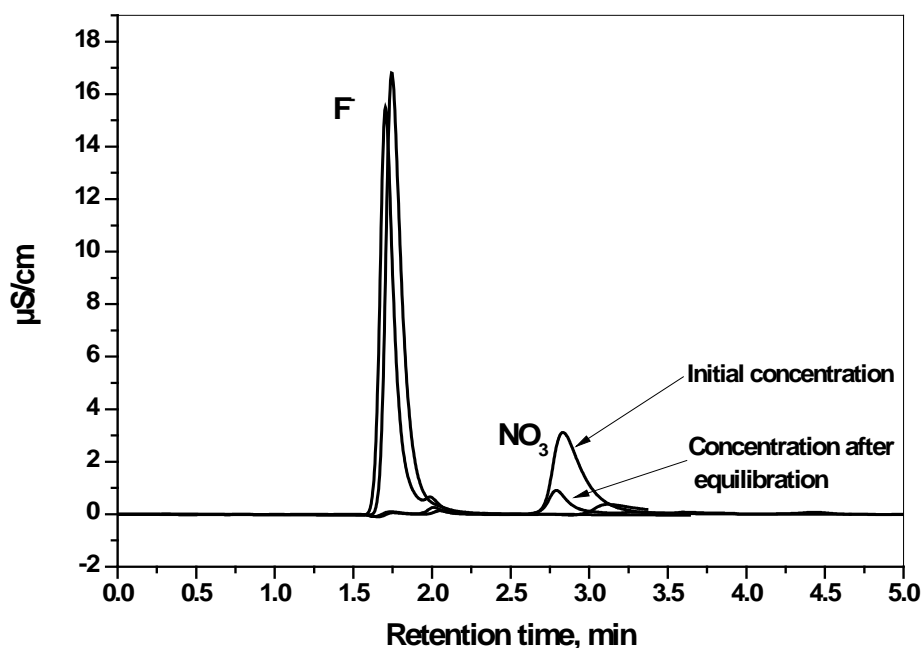


Fig. 5.13: Ion chromatograph for the typical mixed fluoride and nitrate ion standards

5.4 Conclusions

To take advantage of the properties imparted by the functional groups of PDADMAC for certain applications, the polymer was immobilized on a substrate by two methods, namely, a radiation grafting method and a radiolytic microencapsulation process. In the grafting procedure, the monomer acrylic acid was introduced between the polyethylene substrate and DADMAC, the monomer of our interest. The extent of grafting of these monomers could be varied over a wide range by adjusting process parameters like total absorbed dose, dose rate and monomer concentration. This control helps in tailoring the properties of the functional material for the desired application. The procedure reported has broader scope because, other than the system described here, many other monomers or a combination of monomers can, in principle, be anchored to a variety of polymeric substrates.

In the microencapsulation process, PES microcapsules were first produced by the sol-gel phase inversion procedure. DADMAC monomer was then allowed to diffuse into the core of the microcapsule and exposed to gamma radiation which initiates the in-situ polymerization of the monomer. The PDADMAC functionalized capsules was able to take up and exchange some anions like F^- , Cl^- , Br^- , NO_3^{2-} and SO_4^{2-} at relatively low concentrations. The morphology of the microcapsule and the degree of polymerization and subsequent crosslinking of the monomers can be easily controlled. So, the process could possibly be extended for the synthesis of a variety of functional microcapsules from different monomers.

Chapter 6: PDADMAC as the capping agent for synthesis of gold nanoplates

6.1 Introduction

Nanoscience and nanotechnology research is currently an area of intense scientific interest due to a wide variety of applications in industry and engineering. Nanoparticles have at least one dimension between 1 and 100 nm and acts as a bridge between bulk materials and atomic or molecular structures. At this length scale, the properties of a given material may deviate significantly from its bulk counterpart due to at least three important reasons: high surface-to-volume ratio, quantum confinement of electrons and electrodynamic effect. In heterogenous catalysis, for instance the enhancement in rate of chemical reactions is due to the increase in surface area of the nanoparticles. The high surface area also affects the phase stability in many cases, for example the melting point of metals is drastically reduced when the size of the particle is reduced. Quantum confinement effect is much pronounced in case of semiconductor nanoparticles and leads to interesting optical and electronic phenomenon whereas the electrodynamic effect such as localized surface plasmon resonance is dominant for metal nanoparticles.

Gold nanoparticles have attracted immense interest owing to their unique physical, chemical, biocompatible properties and promising applications in catalysis, sensing, bioimaging, photothermal therapy, drug delivery, nanoelectronics, and in the fabrication of photonic and plasmonic devices [169-172]. Majority of research so far has focused on the synthesis of isotropic nanoparticles (spherical and pseudo spherical) and a reasonable understanding has been developed about the relation between the size of the particles and its properties. During the past decade, researchers have focused on shape-controlled synthesis of

gold nanocrystals and made significant progress in this direction enabling the exploration of their shape-dependent properties [173-175].

For many applications it is desirable or sometimes necessary to have good control of the shape or morphology of the gold nanoparticles. Gold nanoparticles for instance, shows great potential in catalysis where the selectivity of the chemical reaction depends strongly on the shape of the particle. This is because the morphology or shape of the nanoparticles decides the facets exposed on a nanocrystal, for example the nanocube is exclusively bound by $\{100\}$ facets while the octahedron has exclusively $\{111\}$ facets exposed as shown in Fig. 6.1

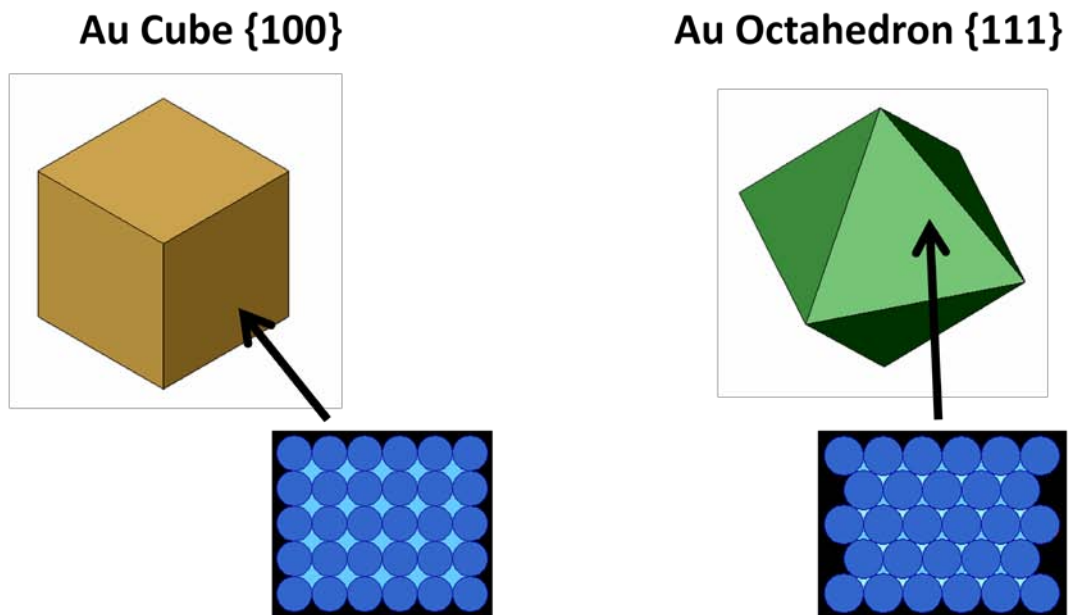


Fig. 6.1: The different facets of Au nanocube and Au octahedron

Since catalysis is a surface phenomenon and because the arrangement or packing of atoms on different facets is different the shape of nanoparticles profoundly affects the selectivity of the reaction [176-180]. Another interesting aspect of gold nanoparticles is that the particles can be readily conjugated by ligands, oligonucleotides, proteins and antibodies due to excellent affinity of gold surface for functional groups like thiol, phosphines and

amines. The gold nanoconjugates can enter living cells, depending on its size and shape and these conjugates shows promising applications as diagnostic or therapeutic agents in biotechnology.

Gold nanoparticles exhibit vivid colors resulting from the collective oscillation of the electrons in the conduction band known as the localized surface plasmon resonance absorption. The LSPR of gold nanocrystals depends on their size and shape [181-184]. For example, spherical nanoparticles of Au shows only one LSPR peak in the UV-visible spectrum which is not significantly affected by the size, whereas anisotropic particles such as nanorods and nanoplates show more than one resonance in the Visible/ NIR region which can be easily tuned across the spectrum. Fine control of nanoparticle shape results in absorption and scattering in the NIR region which is useful for cancer hyperthermia treatment and imaging application [185].

There are three main types of anisotropic nanostructures reported for gold nanoparticles [186-193]. These are 1D nanostructures like rods and wires having uniform cross section, 2D nanostructures such as triangular and hexagonal plates and highly faceted “platonic solids” which includes cubes, tetrahedron, octahedron, icosohedron etc. Among these structures, nanoplates are particularly interesting because of the high surface area to volume ratio and, the entire surface is essentially composed of a single crystal facet. Due to these features, they find applications in diverse areas like catalysis, biosensors, bio-diagnostics, photoluminescence, surface enhanced Raman scattering and imaging [170, 171, 193].

Gold nanoparticles are commonly synthesized by the solution based method wherein a reducing agent reduces the precursor metal salts in presence of capping agent which imparts stability to the colloidal system. In general, solution prepared gold nanoparticles are single crystalline with fcc structures compared to lithographically or electrochemically prepared

structures which are typically polycrystalline. Nanoparticles of desired size and distribution can be relatively easily synthesized by modulating experimental parameters like concentrations of the reactants, temperature, pH, seed concentration etc. The choice of the capping agent is not crucial for the synthesis of isotropic nanoparticles but in case of anisotropic nanoparticle it is important to select specific capping agent for good control of the shape [29-31]. The mechanism by which the capping agent directs anisotropic growth is not clear, however it is believed that the capping agent with certain functional groups interacts distinctively with the different facets of the growing seeds and induces anisotropic growth. For instance, cetyltrimethyl ammonium bromide (CTAB) has been extensively employed for synthesis of gold nanorods of various aspect ratios [30, 31].

In this chapter, the use of PDADMAC as a shape directing capping agent for the synthesis of gold nanoplates is discussed. Two methods were developed during the study. In the first procedure, the nanoplates were produced through gamma radiolytic reduction and in the second procedure gold was photolytically reduced by exposing the precursor solution to ambient sunlight. In general, both these methods are powerful and versatile for the synthesis of nanoparticles and nanocomposites. Here, reduction is brought about by transient radicals produced in-situ by ionizing radiation or excited states induced by light. Gold precursor is reduced to the zero valent state in presence of PDADMAC which further undergoes nucleation and growth. PDADMAC like CTAB contains the quaternary ammonium head group which can selectively interact with the different facets of gold seed which are formed as a result of nucleation and direct anisotropic growth resulting in the formation of nanoplates. Since no external reducing agents are used, the processes are much cleaner and the reaction also proceeds under milder condition like room temperature.

6.2 Experimental

Gold (III) chloride hydrate (Purity 99.999%) and Polydiallyldimethylammonium chloride (PDADMAC, $M_v \sim 100,000 - 200,000$) were purchased from Aldrich. Water used in all the experiments was purified by SG water system and the conductivity was less than 0.055 $\mu\text{S}/\text{cm}$. All glasswares were washed with chromic acid and thoroughly rinsed with deionized water.

UV-Visible spectra of the solution were recorded using Thermo, Evolution 300 spectrophotometer. Transmission electron microscopy (TEM) imaging was done using Zeiss Libra 120 electron microscope operating at an accelerating voltage of 120 keV and selected area electron diffraction (SAED) pattern was recorded using JEOL (Model: 200 FX) electron microscope. Scanning electron microscopy (SEM) images were recorded using SERON Technologies Inc., (Model: AIS 2100) operating at an accelerating voltage of 20 keV and energy-dispersive X-ray (EDX) analysis was performed with Oxford Instruments (Model: INCA E350) coupled to the SEM. X-ray powder diffraction studies were carried out with Philips X-ray diffractometer (Model PW 1729) using Cu $K\alpha$ radiation and X-ray photoelectron spectroscopy (XPS) investigations were carried with VG (CLAM-2) spectrometer, using Mg $K\alpha$ radiation. AFM (Model: NT-MDT Solver Next) images were recorded at a scanning rate of 0.5 Hz in semicontact mode. The optical microscope images were captured using Motic BA 400 optical microscope.

6.3 Part I: Size tunable synthesis of gold nanoplates by gamma irradiation in presence of PDADMAC as the capping agent

The synthesis of nanoparticles by gamma irradiation is a simple green process because external reducing agents are not required and the reduction is brought about by the transient species, e^-_{aq} and $\text{H}\cdot$, generated from the radiolysis of water. The size and shape of

the nanoparticles produced is known to be affected by the reduction rate of metal ions in solution, and in case of gamma irradiation this can be easily controlled by proper selection of dose rate employed for reduction. Due to these advantages, gamma radiation has been utilized for the synthesis of different types of nanoparticles employing a variety of capping agents [194-197], however, it is difficult to control the shape of the nanoparticles and mostly spherical or irregular nanoparticles are produced. Only recently a gamma radiolytic method was developed for the synthesis of gold nanoplates [198]. In the method, (3-aminopropyl) triethoxysilane (APTES) coated Fe_3O_4 nanoparticles was mixed with HAuCl_4 and exposed to gamma radiation to produce gold nanoplates. However, the disadvantage of the method is that Fe_3O_4 nanoparticles had to be first prepared in a separate step and later coated with (3-aminopropyl) triethoxysilane (APTES) for subsequent reaction with Au^{3+} .

Here we employ a gamma irradiation strategy for synthesis of single crystal gold nanoplates by employing PDADMAC as the capping agent. PDADMAC, an important polyelectrolyte, has in recent years been used as a capping agent for the synthesis gold nanoparticles under different experimental conditions [199, 200]. The method reported herein, does not require seeds or surfactants and the reduction occurs at room temperature. Importantly, the size of the nanoplates could be controlled from 500 nm to 5 μm by adjusting the concentration of Au^{3+} and PDADMAC in the solution.

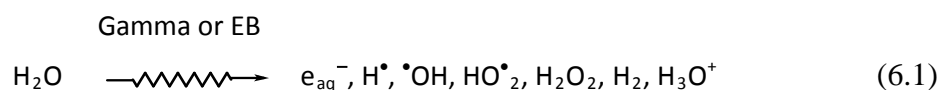
6.3.1 Synthesis of gold nanoplates

In a typical synthetic procedure, 100 μl of 10 mM HAuCl_4 solution and different amount of 0.1 M PDADMAC solution were added to water and the total volume was made to 10 ml. The concentration of Au^{3+} in the solution was fixed at 100 μM and the concentration of PDADMAC was varied to get different ratio (R) of Au^{3+} /PDADMAC. Different ratios were studied to determine the influence of PDADMAC on the shape of the nanoparticles produced. In the current work, the Au^{3+} /PDADMAC ratios investigated were 1:3, 1:4, 1:5

and 1:10. To synthesize the nanoparticles, the prepared solution was exposed to gamma radiation in a ^{60}Co gamma chamber (GC 5000, BRIT, India) at a dose rate of 2.2 kGyh^{-1} . A lower dose rate of 0.2 kGyh^{-1} was employed to investigate the influence of dose rate on the morphology of nanoparticles.

6.3.2 Results and discussion

Radiolytic reduction is an efficient method to produce metallic nanoparticles from the respective metal ions [194, 196]. When a dilute aqueous solution is irradiated, the direct effect of radiation is negligible and the effect mainly occurs via the important primary species produced as a result of water radiolysis (Eqn. 6.1).



The most important reducing species produced during radiolysis is the hydrated electron (e_{aq}^-), with a standard reduction potential of -2.87 V NHE and H^\bullet with a standard reduction potential of -2.3 V NHE . e_{aq}^- and H^\bullet are strong reducing agents which can easily reduce Au^{3+} to Au^0 , but OH^\bullet on the other hand is oxidizing ($+2.34 \text{ V NHE}$) in nature and can bring about the reverse oxidation of the gold atoms. Therefore, OH^\bullet is usually scavenged by using isopropyl alcohol, in which case isopropyl radical is generated which is also reducing in nature. However, the reduction of Au^{3+} is possible even without scavenging OH^\bullet , but under this condition, the overall yield of reducing species generated in the solution is lower and hence higher absorbed dose would be required for complete reduction [194, 195]. In this study, OH^\bullet radicals were not scavenged because we wanted to avoid additional steps or reagents. Our primary interest was the final shape or morphology of the nanoparticles rather than the kinetics of its formation under different conditions. In order to determine the radiation dose required for complete reduction of Au^{3+} to Au^0 in the solution, preliminary gamma irradiation studies were carried out and the appearance of the surface plasmon resonance band of gold nanoparticles ($\sim 520 \text{ nm}$) was monitored by UV-Vis

spectrophotometer. It was found that a dose of 2.5 kGy was sufficient to completely reduce Au^{3+} to Au^0 in presence of PDADMAC under the conditions of our experiments. Therefore, all subsequent synthesis of nanoparticles was carried out by irradiating the solutions to an absorbed dose of 2.5 kGy.

The colors of the nanoparticles solution after synthesis were visually observed and the optical properties were studied by UV-Visible spectroscopy. Gold nanoparticles are known to display intense color due to the surface plasmon resonance which depends on the size and shape of the nanoparticles [181, 182]. Spherical gold nanoparticles exhibits only one absorption band centered around 520 nm while anisotropic gold nanoparticles exhibit two or more resonance modes in the spectrum depending on the shape. Fig. 6.2 shows the UV-Vis spectra of the nanoparticle solutions synthesized at four different Au^{3+} /PDADMAC ratios.

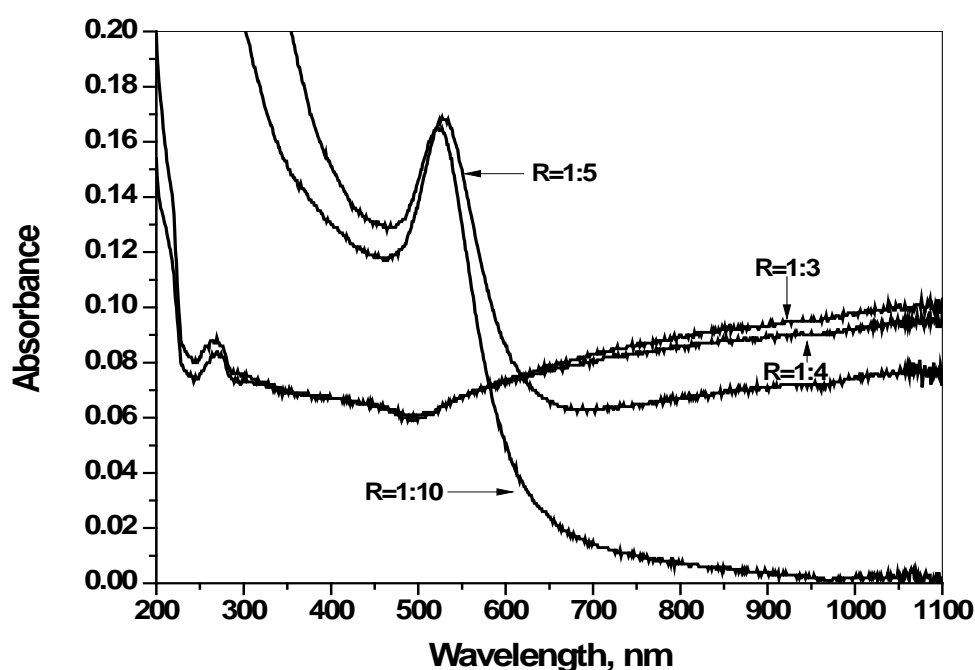


Fig. 6.2: UV-Visible spectrum of the gold nanoparticles synthesized at different Au^{3+} /PDADMAC ratios

At high PDADMAC concentration (R=1:10), the solution was red in color and only a single narrow absorption peak was observed at 522 nm. At R=1:5, the solution appeared reddish-purple in color and absorption peak red shifts to 530 nm. The spectrum shows only a single absorption peak, but there is appreciable absorption from about 600 nm to 1100 nm. At R=1:4, when the solution was exposed to gamma radiation, the faint yellow color of the solution disappears and shiny particles start to appear in the solution and the spectrum shows a continuous non-zero absorption in the entire UV-Visible region which further extends into near-infrared region. Similar spectrum has been reported for large nanoplates [201] and such absorption characteristic in the near-infrared region is useful for biomedical applications like hyperthermia treatment of tumors [193, 202]. The spectrum obtained for nanoparticle synthesized at R= 1:3 was akin to the spectrum obtained at R=1:4.

To confirm the actual size and shape of the nanoparticles synthesized, SEM/ TEM images of the samples were recorded and is shown in Fig. 6.3.

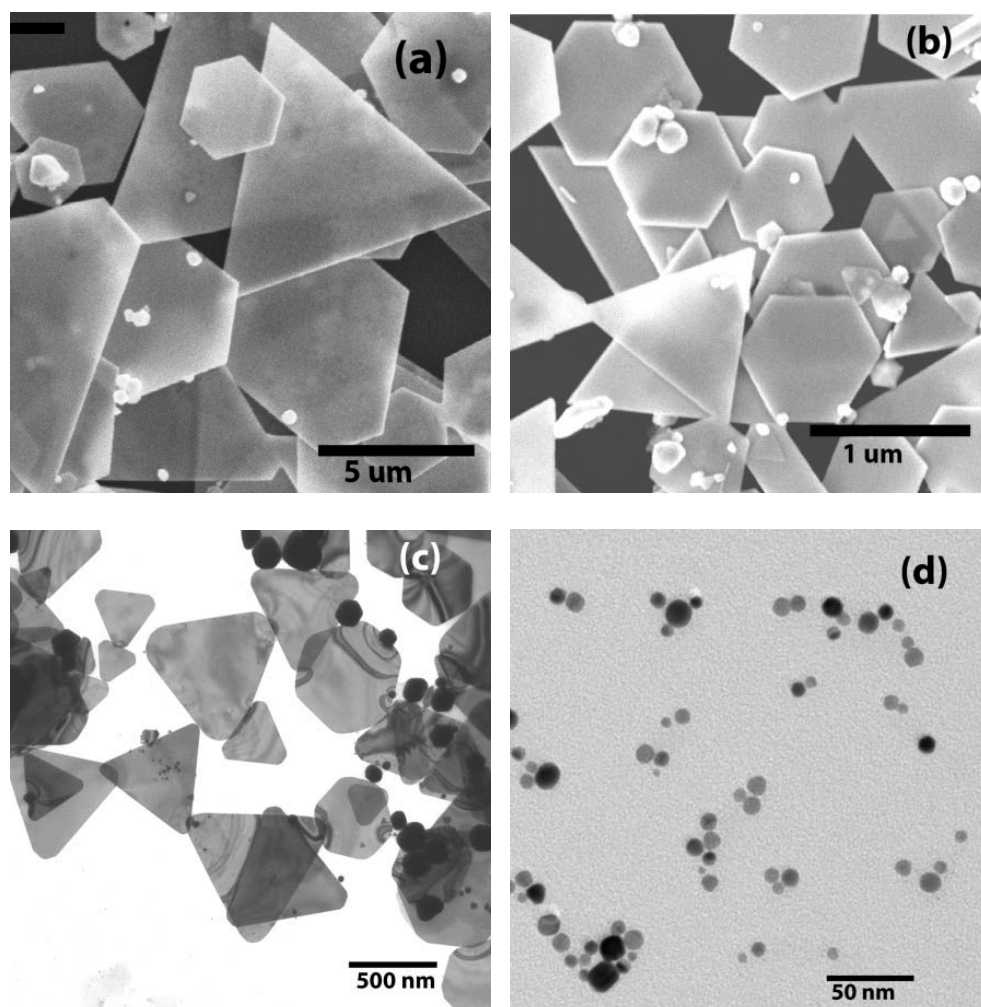


Fig. 6.3: Electron microscopy images of gold nanoparticles synthesized at different Au^{3+} /PDADMAC ratios. (a) SEM image at R=1:3; (b) SEM image at R=1:4; (c) TEM image at R=1:5; (d) TEM image at R=1:10

At Au^{3+} / PDADMAC ratio of R=1:3 (Fig. 6.3a), high yield of large hexagonal, truncated triangular and triangular nanoplates with average edge length of about 5 μm are obtained. Fig. 6.3b shows the SEM image of the nanoplates synthesized at R=1:4. Good yield of gold nanoplates comprising of hexagonal, triangular and truncated triangular shapes are obtained, and the size distribution is relatively narrow. The average edge length of the nanoplates is about 1 μm and the nanoplates seem to be very thin because electrons could pass through them and plates lying below were clearly visible. When the concentration of

PDADMAC is increased (R=1:5) smaller nanoplates are obtained, therefore TEM was used to record the image and is shown in Fig. 6.3c. The predominant shape of nanoplates formed was hexagonal and triangular with an average edge length of 500 nm. At the highest concentration of PDADMAC studied (R=1:10), there is a drastic change in the shape and only spherical nanoparticles are formed in the size range of 5-10 nm (Fig. 6.3d).

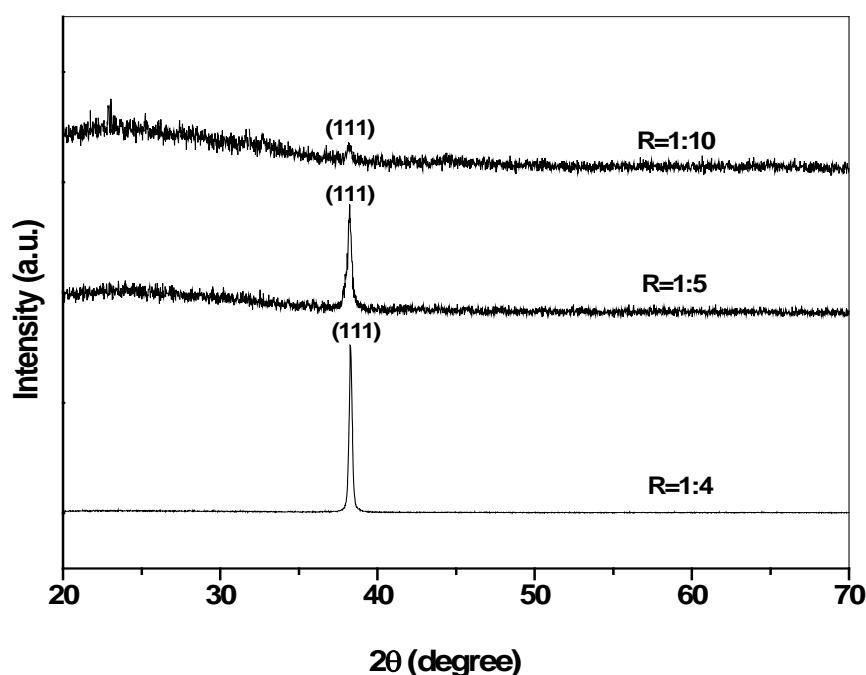


Fig. 6.4: XRD pattern of gold nanoparticles synthesized at different Au³⁺/PDADMAC ratios

The crystal structure of the nanoparticles was determined by powder XRD (Fig. 6.4) which gives information about the overall quality and purity of the sample. The XRD pattern of the nanoplates synthesized at R=1:5 and R=1:4 shows an extremely strong diffraction peak at 38.2 degrees, however, the peak obtained at R=1:5 is broader because the nanoplates are smaller than that obtained at R=1:4. No other peaks are observed in the entire scanning range suggesting that the nanoplates are single crystal fcc gold bound by {111} lattice planes [203, JCPDS Card No. 04-0784]. The XRD pattern obtained for large nanoplates synthesized at

R=1:3 (not shown) was almost identical to that obtained at R=1:4. The spherical nanoparticle formed at R=1:10 shows only one very weak peak at $2\theta = 38.1$ and since the overall intensity of the XRD pattern was poor, it was difficult to ascertain the exact crystalline nature of the nanoparticles. However, since the particles appear spherical in the TEM image and as the {111} diffraction was observed; the particles are probably small polyhedrons with most of the surfaces bound by the {111} lattice planes.

Further characterization of the gold nanoplates was carried out by EDX, XPS and SAED. For the purpose, the nanoplates synthesized at R=1:4 was chosen as representative among the nanoplates synthesized at different Au^{3+} / PDADMAC ratios. The elemental composition of the nanoplates was determined by EDX after drying a drop of the nanoparticle solution on a silicon wafer.

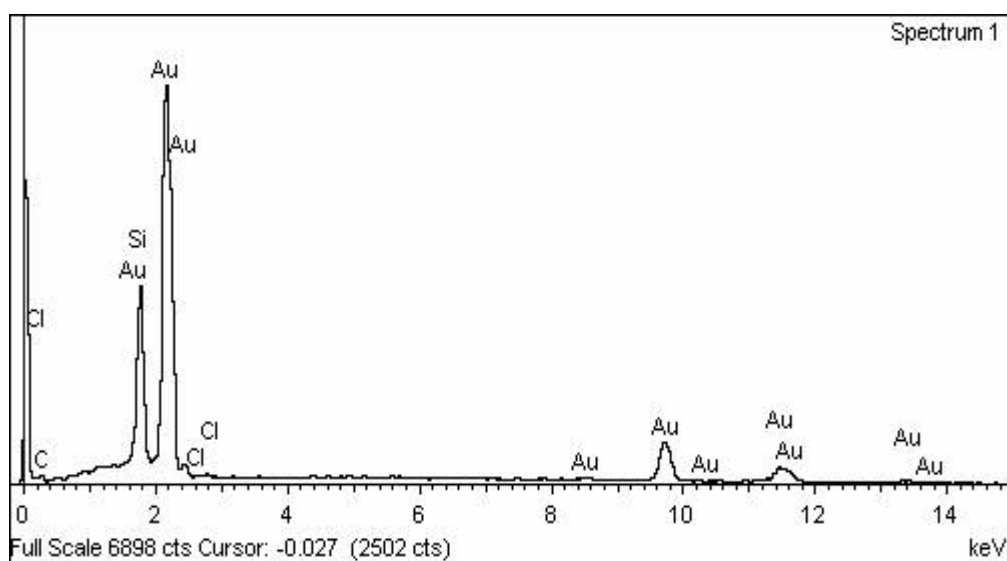


Fig. 6.5: EDX spectra of the nanoplates synthesized at R=1:4, deposited on a silicon wafer

Fig. 6.5 shows the EDX of the nanoplates and most of the peaks observed are due to Au, but peaks due to Si and Cl are also seen which originate from the background (Si wafer) and from PDADMAC. This reveals that the nanoplates are entirely composed of Au and stabilized by PDADMAC.

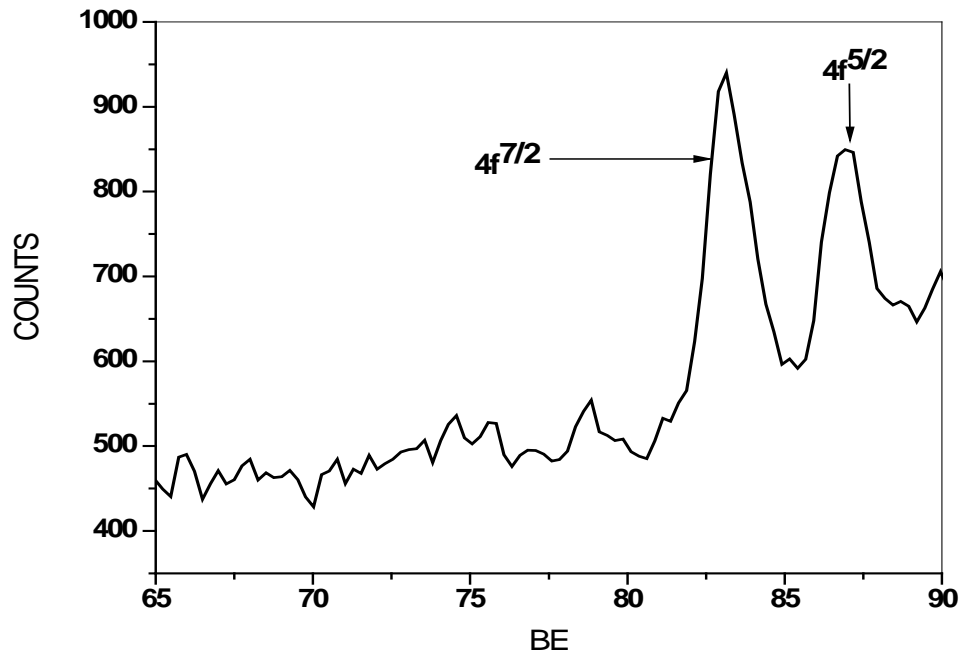


Fig. 6.6: XPS spectrum of gold nanoplates deposited on a silicon wafer

The XPS of the gold nanoplates is shown in Fig. 6.6 and the spectrum shows two peaks located at 83.3 and 87.6 eV which could be assigned to $4f^{7/2}$ and $4f^{5/2}$ of Au^0 oxidation state [203]. No peaks corresponding to Au^+ or Au^{3+} could be detected, indicating the complete reduction of gold.

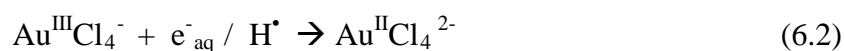


Fig. 6.7: SAED pattern obtained by aligning the electron beam perpendicular to the plane of a hexagonal nanoplate

Fig. 6.7 shows the SAED pattern obtained by aligning the electron beam perpendicular to the plane of a hexagonal nanoplate. The bright hexagonal pattern of spots obtained confirms that the gold nanoplates are single crystals with fcc structure and is bound by {111} lattice planes on the top and bottom [201]. This observation agrees well with the XRD results.

6.3.3 Probable mechanism of nanoplate formation

When ionizing radiation interacts with a dilute aqueous solution of metal ions the primary effects produced are excitation and ionization of water molecule resulting in the generation of primary transient species (Eqn. 6.1). Among the transient species generated, e^-_{aq} and H^\bullet are powerful reducing agents (with a standard reduction potential of -2.87 V NHE and -2.3 V NHE respectively which can reduce Au^{III} to Au^{II} (Eq. 6.2).





Au^{II} produced then disproportionate to Au^{III} and Au^{I} (Eqn. 6.3). Finally e^-_{aq} and H^\bullet brings about the reduction of Au^{I} to Au^0 (Eq. 6.4). The Au^0 formed can coalesce into clusters of higher nuclearity and finally to the metal nanoparticles (Eq. 6.5). The mechanism discussed above only describes the various steps of radiolytic reduction and does not give any indication about the shape or morphology of the nanoparticles formed. Surface-energy considerations are important in understanding and predicting the morphology of noble-metal nanocrystals. If the surface energy is isotropic (as for a liquid) then a sphere has the minimum the surface energy. However, in crystalline solids the surface energy is anisotropic and the energy-minimizing shape is found using the limiting planes of the lowest possible surface energy. From thermodynamic consideration, the surface energy of different crystallographic planes of a nanocrystal are different and the general sequence is $\gamma_{\{111\}} < \gamma_{\{100\}} < \gamma_{\{110\}}$ [204]. Although nanoplates are bound by lowest energy $\{111\}$ plane, their formation is less favoured compared to polyhedrons because of the relatively large surface area. According to Wulff theorem [205, 206], for fcc metals like gold, the predicted thermodynamic equilibrium shape is the truncated octahedron bound by low energy $\{111\}$ and $\{100\}$ planes. The truncated octahedron has 8 $\{111\}$ facets and 6 $\{100\}$ facets as shown in Fig. 6.8.

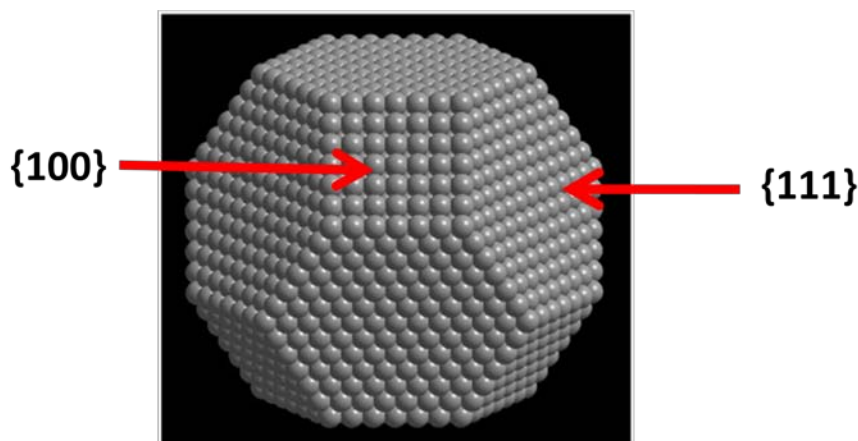


Fig. 6.8: Truncated octahedron showing the $\{111\}$ and $\{100\}$ facets

In order to account for the formation of anisotropic nanoplates rather than the octahedron various mechanisms has been proposed in the literature. Most notably, it has been proposed that the capping agent plays a key role in the asymmetric formation of nanoplates due to preferential or selective adsorption on the $\{111\}$ plane, thereby retarding the growth on this plane [207, 208]. However, there are many equivalent $\{111\}$ planes on the most stable octahedral seeds and introduction of selective capping agents need not necessarily result in anisotropic formation of nanoplates, instead, may result in the formation of polyhedrons.

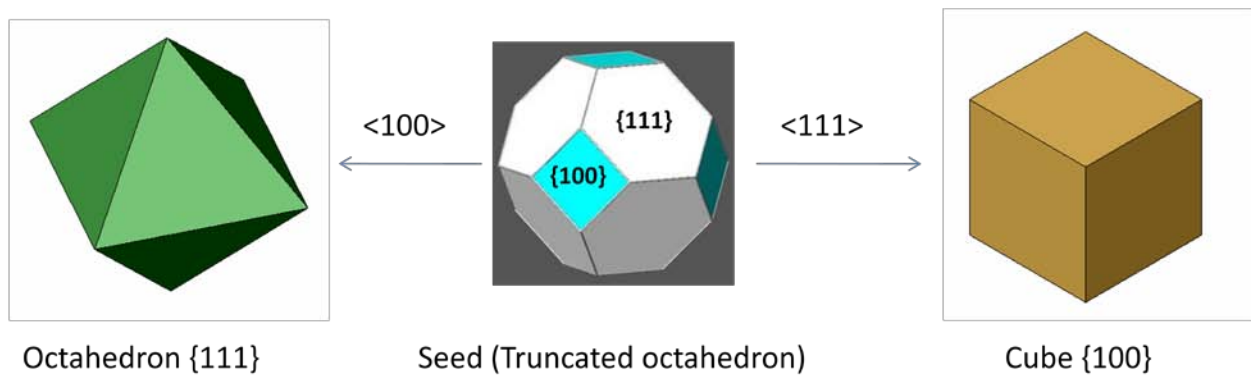


Fig. 6.9: Growth of octahedral seed along the $\langle 111 \rangle$ and $\langle 100 \rangle$ directions

For example, as shown in Fig. 6.9, if the $\{100\}$ facet of the truncated octahedron is blocked by a capping agent and growth takes place in the $\langle 111 \rangle$ direction then the resulting structure is a cube. On the other hand a regular octahedron results if growth takes place along the $\langle 100 \rangle$ direction by blocking the $\{111\}$ facet. Also during nucleation different types of seeds are formed and growth of these seeds may results in nanostructures of various morphologies without any preference for a particular type of structure. So, an alternative mechanism based on the crystallinity of the seed has been put forth which considers the formation of twins or stacking faults in the seeds during the nucleation stage, as the key factor responsible for anisotropic growth of nanoplates [209-211]. As a result of twinning, hexagonal plate-like seeds bound by the $\{111\}$ planes on the top and bottom are formed. The

plate like seeds has a convex and concave orientation shown as “A” and “B” in Fig. 6.10. There is a re-entrant groove on the A-type side of the seed where addition or growth takes place and this lateral growth results in the formation of nanoplates.

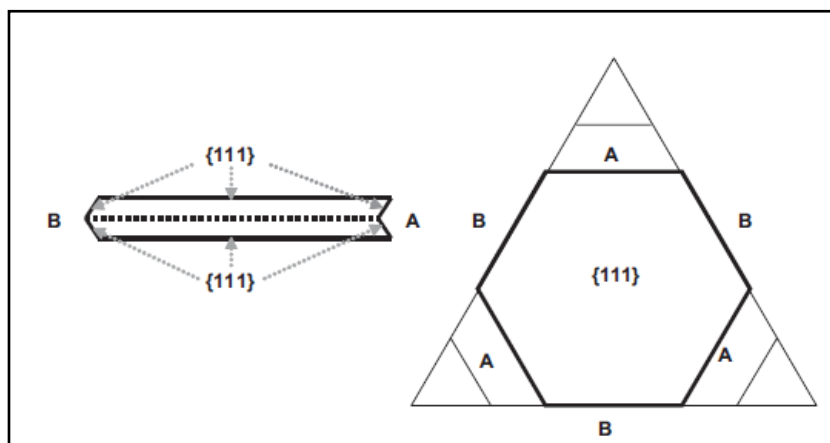


Fig. 6.10: Plate like seed showing the concave (A) and convex (B) sides

However, recent studies [212, 213] suggest that both the crystal structure of the seeds as well as selective binding of ligands is important for the formation of anisotropic nanoplates. When the concentration of Au atoms produced by radiolytic reduction reaches the supersaturation value, they will start to nucleate and form seeds of different crystalline nature like single crystal seeds, twinned seeds and multiply twinned seeds. To obtain a good yield of nanoplates, it is essential to have a large population of twinned seeds compared to single crystal seeds in the solution. In the system, the Cl^- released from PDADMAC along with the dissolved oxygen present in the solution can form O_2/Cl^- pair, which is a potent oxidative etchant for gold ($\text{Au}^0 \rightarrow \text{Au}^+$ or Au^{3+}) [214, 215]. The twinned seeds have lower stability and are susceptible to oxidation and dissolution. But if the capping agent has strong affinity for the twinned seeds, the stability order may be reversed and the single crystal seeds may be selectively removed by oxidative dissolution [216]. PDADMAC with its quaternary ammonium head group preferentially adsorbs on the {111} surface of the seeds [217-219], hence, twinned seeds having {111} plane is stabilized more compared to the single crystal

seeds having a combination of {111} and {100}. This results in the oxidative dissolution of the single crystal seeds and once the desired twinned seeds survive, PDADMAC further assist anisotropic growth by blocking the {111} plane of growing nanoplate, while permitting growth along <110> directions. The continuous addition of metal atoms to the exposed facets at the ends of the seed leads to the formation of gold nanoplates bound by {111} planes (Fig. 6.11).

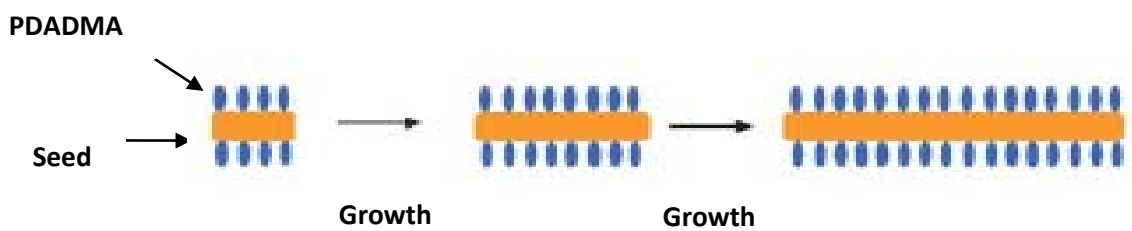


Fig. 6.11: Schematic illustration of facet blocking and lateral growth of gold nanoplates

As discussed before, the size and shape of the nanoparticles synthesized was significantly affected by Au^{3+} / PDADMAC ratio chosen. It has been reported that for a particular Au^{3+} concentration, the ratio of Au^{3+} to the capping agent determines the size of the nanoparticles formed, with lower ratio favoring the formation of small nanoparticles. That is, higher the concentration of capping agent, smaller is the size of the nanoparticles formed. We obtained similar variation in size of the gold nanoplates and our results are consistent with the previous reports [220]. When excess PDADMAC is used (R=1:10) there is high coverage on all the crystallographic facets of the seeds and hence there is no selective growth on any particular facets. This leads to isotropic growth resulting in the formation of small spherical gold nanoparticles.

The size and shape of the nanoparticles produced is reported to be affected by the reduction rate of metal ions in solution. To investigate the effect of dose rate on the morphology of gold nanoparticles, a precursor solution of fixed composition (Au:

PDADMAC, 1: 10) was exposed to gamma radiation at two different dose rates (2.2 kGy/hr and 0.2 kGy/hr). As can be seen from Fig. 6.12, lower dose rate results in the formation of nanoplates although the shapes are not very distinct. This is because lower reduction rate favors the nucleation of seeds with stacking faults which are considered essential for the formation of nanoplates.

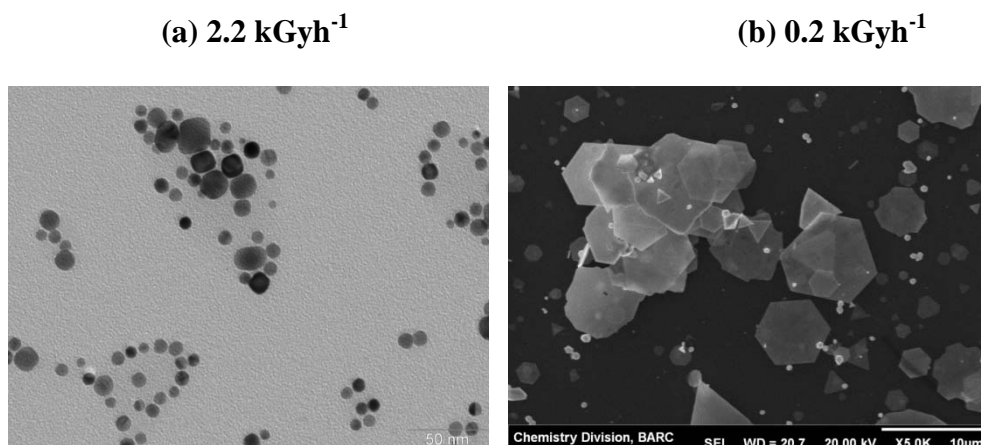


Fig. 6.12: Effect of dose rate on the shape of the nanoparticles (a) Spherical nanoparticles formed at 2.2 kGyh⁻¹ and (b) Nanoplates formed at 0.2 kGyh⁻¹

6.4 Part II: Photochemical synthesis of concave gold nanoplates employing PDADMAC as the capping agent

Most of the nanostructures like plates, cubes, plates, rods, wires octahedron and tetrahedron are usually bound by a convex surface involving low energy facets like {111}, {110} and {100}, thereby lowering the overall surface energy of the nanocrystals. On the contrary, concave (curving inwards from the surface) nanocrystals are bound by high energy facets comprising of large number of atomic steps and kinks. These nanocrystals reveal fascinating properties and shows immense potential for applications, especially in the field of catalysis [221, 222]. However, concave nanocrystals are energetically less favored

than convex nanocrystals, and therefore it is a challenge to develop new methods for their synthesis.

In general, there are two ways of producing a concave surface; i) oxidative etching of metal from specific sites and ii) controlled overgrowth on selective facets [223]. From a thermodynamic point of view, it is difficult to produce a concave surface by overgrowth, because even if a concave surface is generated during the initial stage, further growth would take place on the concave region due to the lower chemical potential of an atom on the concave surface, resulting in the disappearance of the newly formed concave surface. On the other hand, oxidative etching is relatively straightforward and effective strategy for the generation of concave surfaces on nanocrystals and etchants like Cl/O_2 , $\text{Fe}^{2+}/\text{Fe}^{3+}$ and $\text{Cu}^+/\text{Cu}^{2+}$ has been commonly used for generating concave surfaces on nanocrystals [224-226]. This strategy is particularly effective for generating single crystal polyhedrons because the precursor single crystal seeds are resistant to etching in the oxidative environment.

In the previous section of this chapter a process for the synthesis of gold nanoplates was discussed. There are several other methods reported for the synthesis of gold nanoplates with good control over the edge length and thickness, however, the synthesis of nanoplates having concave surface is very rare [227]. Compared to concave polyhedrons it is relatively difficult to produce nanoplates in an oxidative environment because the twinned seeds or seeds with stacking faults, considered crucial for the formation of nanoplates, have lower stability and undergoes oxidative dissolution very easily in the solution. In this report it is demonstrated how this limitation can be circumvented by using PDADMAC as the capping agent that selectively protects the twinned seeds and facilitates its anisotropic growth. Care should also be exercised while selecting the etchant, because a strong etchant may result in isotropic etching while a weak etchant may not attack the exposed surface of the nanocrystals.

Sunlight is non-polluting and renewable source of energy which has been recently harnessed for the synthesis of metal nanocrystals [228-230]. By using sunlight as a reducing agent, and thereby eliminating the use of chemical reducing agents, we are one step closer to a green synthetic procedure for preparing nanoparticles. In this part of the chapter, a sunlight irradiation strategy for the synthesis of concave gold nanoplates by employing PDADMAC as the capping agent is reported. PDADMAC selectively binds to the {111} facet of the twinned seeds and directs or controls the growth anisotropically, while the Cl^- released from PDADMAC, along with the dissolved oxygen present in the solution, aids oxidative etching. This etching occurs on the flat {111} facet of the nanoplates resulting in the formation of nanoplates with concave surfaces. Normal nanoplates bound by flat surfaces could also be prepared by subtle variation in the reaction conditions. The average intensity of direct solar radiation received at the earth's surface at noon time in India is approximately 1.0 kW/m^2 .

6.4.1 Synthesis of concave gold nanoplates

In a typical synthetic procedure for concave nanoplates, $200 \mu\text{l}$ of 10 mM HAuCl_4 solution and $200 \mu\text{l}$ of 0.1 M PDADMAC solution were added to 29.6 ml water. The concentration of Au^{3+} in the solution was $67 \mu\text{M}$ and the ratio of Au^{3+} : PDADMAC was fixed at 1:10. The solution was vortexed and exposed to sunlight for six hours. After irradiation, the faint yellow color of the solution disappears and shiny particles start to appear in the solution. The particles sediment at the bottom of the glass bottle due to their large size and were easily separated from the solution.

6.4.2 Results and discussion

In order to ascertain if the reduction of Au^{3+} occurs via photolytic route or by direct chemical means mediated by PDADMAC, the spectra of Au^{3+} under different experimental conditions was monitored by UV-Visible spectroscopy. PDADMAC being positively charged forms a stable complex with AuCl_4^- through strong electrostatic interaction [231] which

shows an absorption band at 324 nm (in absence of PDADMAC the peak appears at 295 nm).

Fig. 6.13(a) is the spectrum of the freshly prepared solution showing the absorption band at 324 nm attributed to Au^{3+} complex.

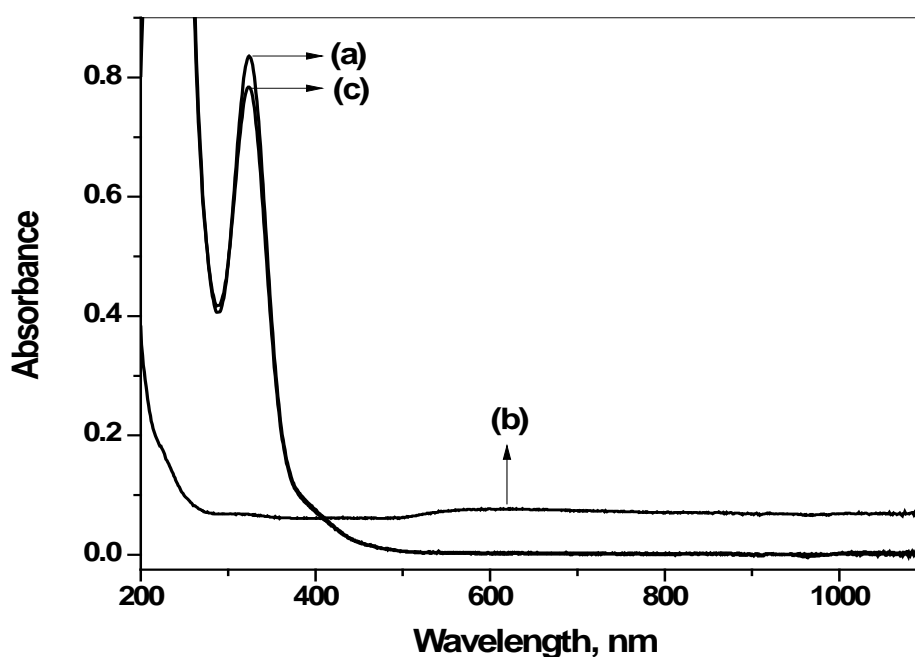


Fig. 6.13: (a) Spectrum of the freshly prepared solution; (b) Spectrum of the solution exposed to sunlight for six hours; (c) Spectrum of the solution kept in dark for six hours

On exposure to sunlight for six hours, the solution becomes colorless and the band at 324 nm disappears (Fig. 6.13(b)) confirming the reduction of Au^{3+} . The spectrum shows continuous non-zero absorption in the entire UV-Visible range which further extend into NIR region. The absence of absorption peak around 520 nm or any other specific peaks proves that small nanoparticles are absent in the solution after irradiation [181, 182]. Under identical conditions, when the solution is kept in dark for the same duration, no significant change in color or UV-Visible spectrum (Fig. 6.13(c)) is observed, proving that sunlight is essential for the reduction to take place and the mechanism is photolytic in nature.

Optical microscopy investigations were carried out after drying a drop of the

nanoplate solution on a glass slide. On the slide (and also on Si wafer used for SEM) the nanoplates exhibit the typical golden yellow color and metallic lustre of bulk gold. Fig. 6.14(a) shows the optical microscope images of the nanoplates captured using a 100 X objective lens. Very high yield of gold nanoplates comprising of hexagonal, triangular and truncated triangular shapes are obtained, and the size distribution is relatively narrow. The nanoplates appeared greenish-yellow in colour under white light illumination of the microscope. The average edge length of the nanoplates is 15 μm and the plates seem to be very thin because visible light could pass through them and plates lying below were clearly visible. On closer inspection, it was found that most of the nanoplates have darker edges (shown by arrows) and appear lighter towards the centre, indicating that the central part of the plate is thinner than the edges.

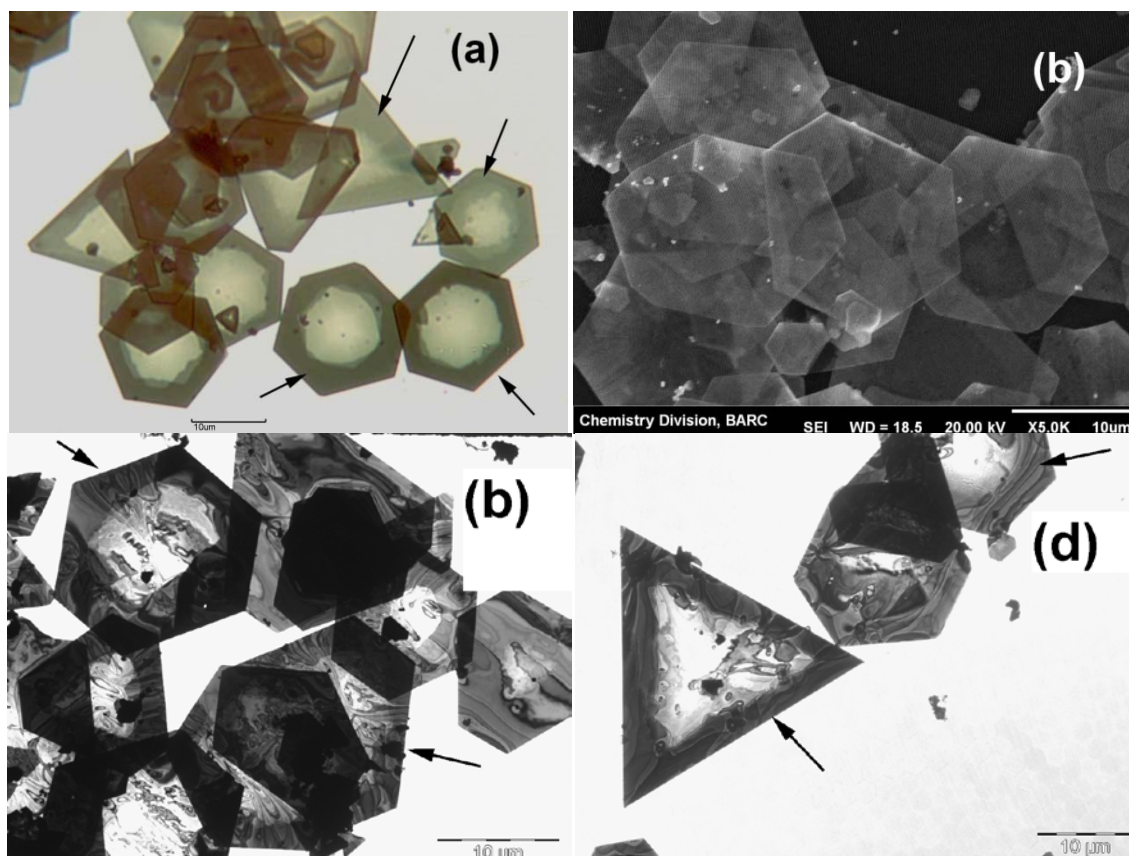


Fig. 6.14: (a) Optical microscope images of the concave nanoplates using 100 X objective lens (b) SEM image of the nanoplates (c) and (d) TEM image the nanoplates

The nanoplates were further characterized by SEM (Fig. 6.14(b)) and TEM (Fig. 6.14(c & d)) techniques. The images shows very low contrast characteristic, indicating that the nanoplates are thin and transparent to electrons. The contrast difference between the edge and the centre of the plates is also apparent, suggesting a thickness gradient across the nanoplate.

In order to confirm the three dimensional structure of the nanoplates, AFM imaging was carried out. Fig. 6.15(a) shows the 3D AFM image of a truncated nanotriangle.

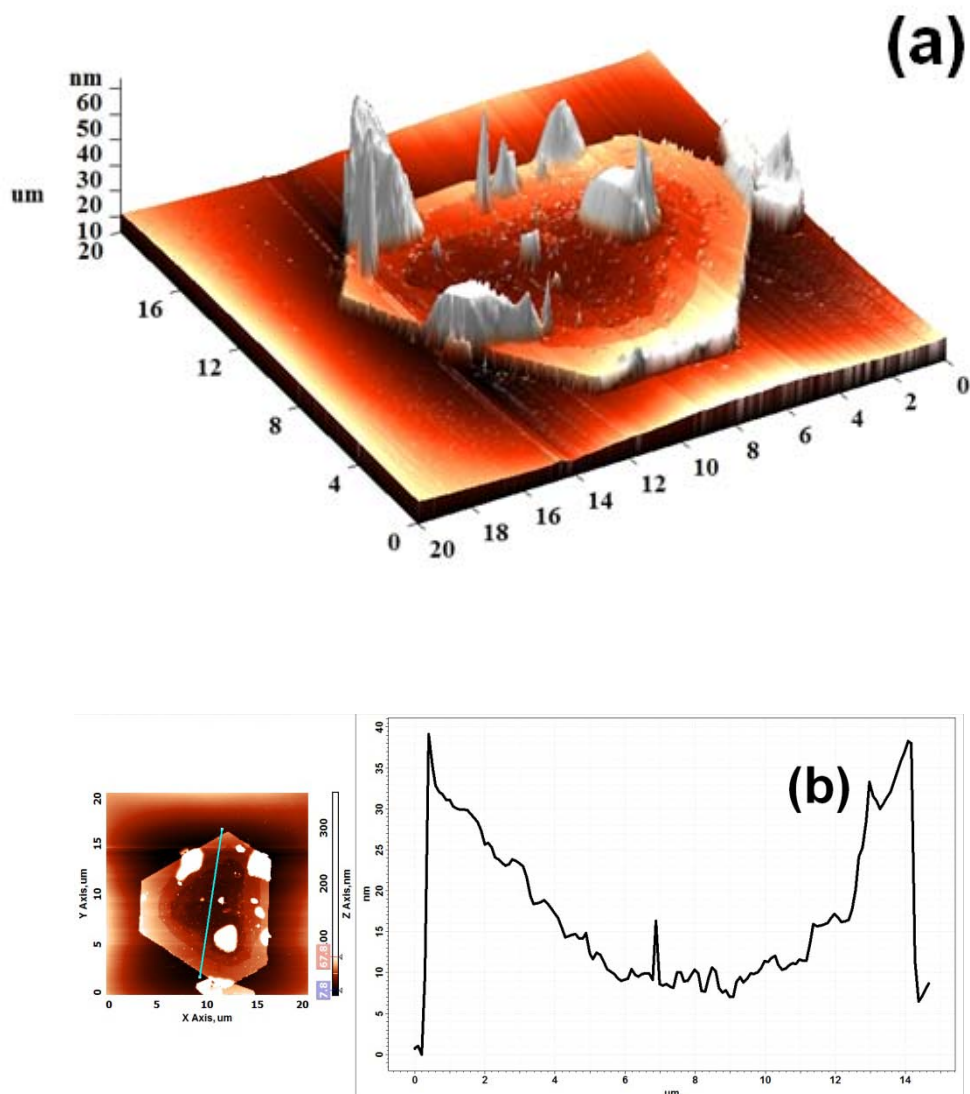


Fig. 6.15: (a) 3D AFM image of a truncated nanotriangle (b) section analysis across the nanoplate from one edge to the opposite edge

The section analyses were carried out to determine the thickness profile of the nanoplates. Some particles were found sticking to the nanoplates despite repeated washing with deionized water, therefore, the sections were carefully chosen to avoid interference from these particles. The section analysis across the particle (Fig. 6.15(b)), from one side to the other, clearly confirms the concavity of the nanoplates, which is consistent with the observation made by microscopy. Although the overall height profile is concave in nature,

small height variation or fluctuation is observed which may probably be due to the presence of atomic steps or kinks on the surface of the nanoplate. The thickness at the edge is about 40 nm, which progressively decreases towards the centre where the thickness is about 10 nm and this low thickness could be the reason for good transmission of visible light [232].

The crystal structure of the nanoplates was determined by powder XRD and SAED. As observed earlier for radiation synthesized nanoplates, the XRD pattern of the nanoplates (Fig. 6.16) shows only one very strong diffraction peak at 38.2 degrees which confirms that the gold nanoplates are bound by {111} lattice planes [201].

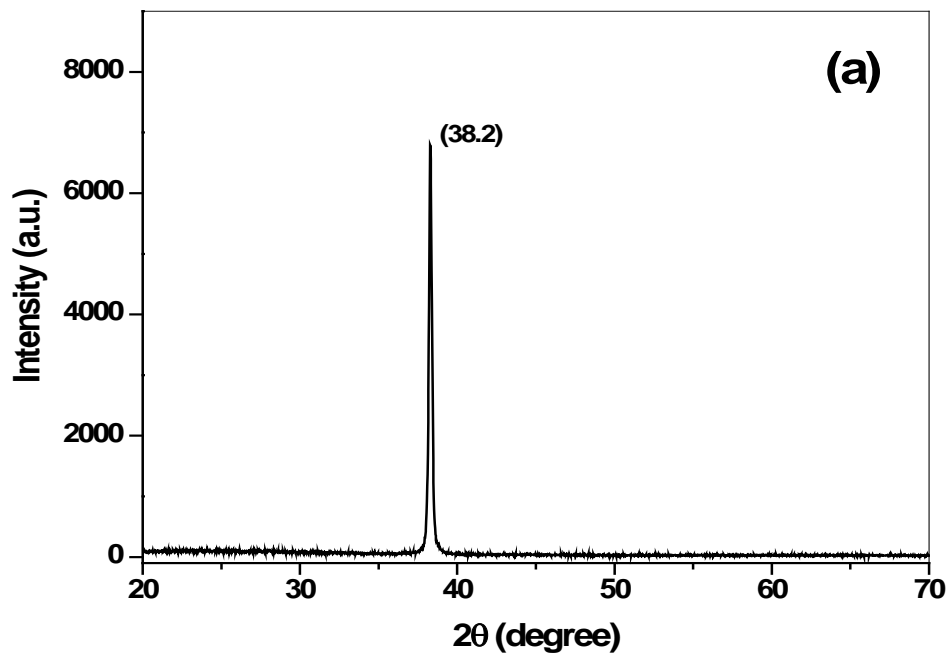


Fig. 6.16: XRD pattern of gold nanoplates

The SAED pattern (Fig. 6.16) obtained by aligning the electron beam perpendicular to the plane of a hexagonal nanoplate (inset) shows bright hexagonal pattern of spots (marked by circle) indicating that the nanoplates are bound by {111} lattice planes. This pattern is also similar to that seen earlier in the radiolytic method.

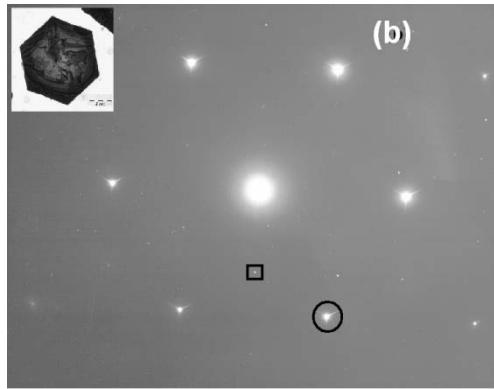


Fig. 6.17: SAED pattern recorded from a single hexagonal nanoplate (inset)

In addition, very faint spots (marked by square) corresponding to the $1/3\{422\}$ diffraction was also observed. These diffractions are forbidden for single crystal fcc metal and is attributed to the formation of stacking faults in the nanoplates which originates from the twinned seeds formed during nucleation [201, 209].

The EDX elemental analysis revealed that the nanoplates are entirely composed of Au and are stabilized by PDADMAC (Fig. 6.18).

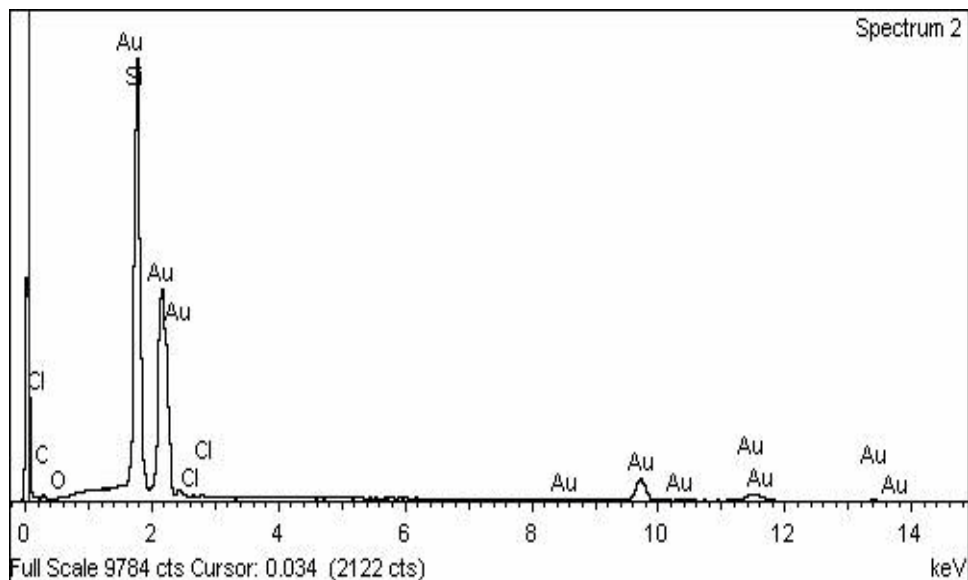


Fig. 6.18: EDX spectra of the nanoplates deposited on a silicon wafer

Two peaks were observed in the XPS spectrum of gold nanoplates (Fig. 6.19), corresponding to $4f^{7/2}$ and $4f^{5/2}$ (at 83.3 and 87.6 eV) of Au^0 oxidation state indicating the complete reduction of gold.

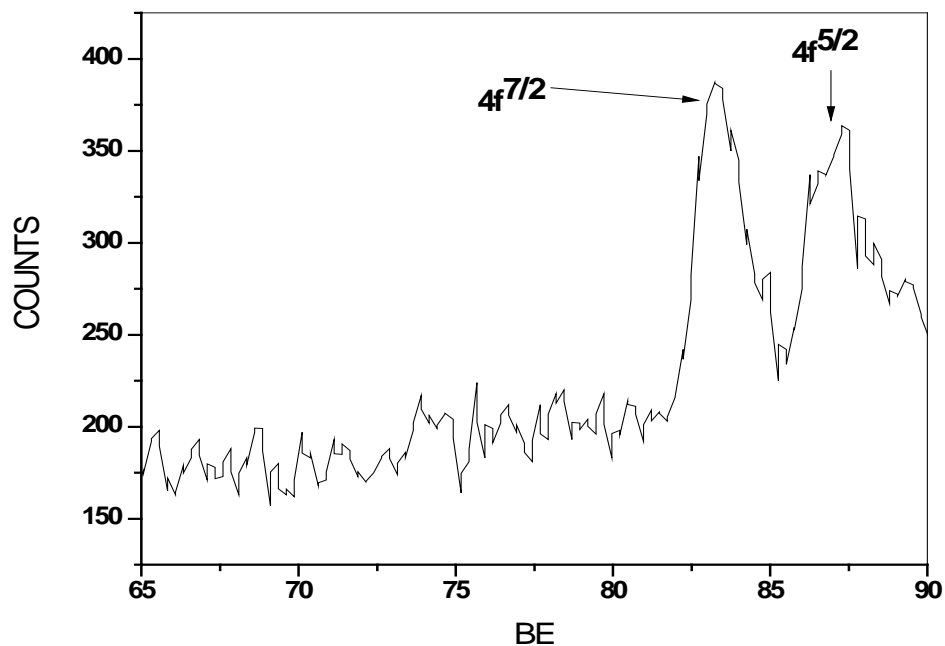
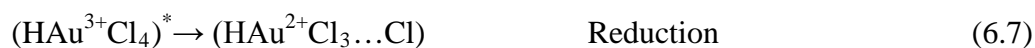
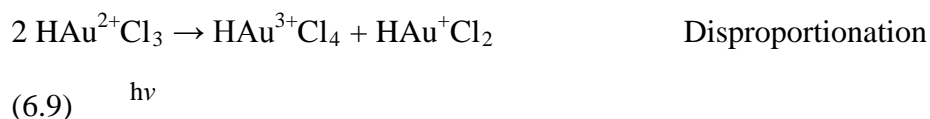


Fig. 6.19: XPS spectrum of gold nanoplates

6.4.3 Probable mechanism of concave nanoplate formation

The photochemical reduction of Au^{3+} has been studied by several researchers [233-236] and many mechanisms have been postulated. For example Kurihara et al. [235] have proposed the following mechanism:





The photolytic mechanism as in the case of radiolytic mechanism discussed previously, only describes the various steps (Eqn. 6.6 to Eqn. 6.11) involved in the reduction of $\text{Au}^{3+} \rightarrow \text{Au}^0$ and does not predict the shape of nanoparticles formed. The probable mechanism for formation of nanoplates has been described in the previous section. Since the system studied is the same (Au + PDADMAC), the explanation given for the formation of nanoparticles in radiolytic reduction is valid for the photolytic process as well.

The formation of concave surfaces may be explained by oxidative etching. Recently, concave gold nanoplates were synthesized in presence of sodium dodecyl sulfate employing glycine as the reducing agent [227] and an oxidative etching mechanism, mediated by O_2/Cl^- , was proposed by the researchers to explain the formation of concavities. The etching occurs preferentially at the centre due to its higher surface energy compared to the periphery and concave centres are produced in the nanoplates. In our system, with the availability of Cl^- and O_2 , the oxidative atmosphere generated is conducive for the formation of nanoplates with concave surface. The process is schematically depicted in Fig. 6.20.

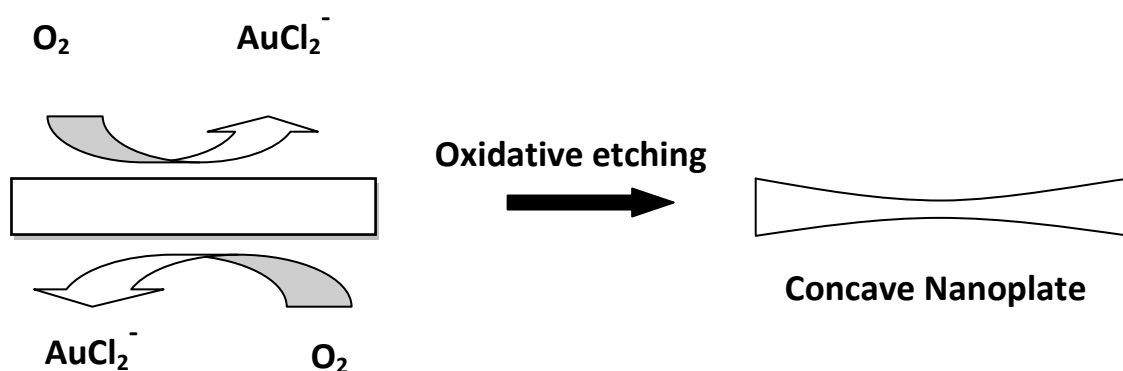


Fig. 6.20: Schematic presentation of the oxidative etching process on the {111} surface of gold nanoplates

However, it is important to realize that there exists a dynamic equilibrium between oxidation and reduction ($\text{Au}^{3+} \rightleftharpoons \text{Au}^0$), and the final shape or morphology of the nanoplates is determined by the relative rates of these processes. At relatively low concentration of Au^{3+} (67 μM), oxidation and reduction seems to proceed at comparable rates resulting in the formation of nanoplates with concave surface. To investigate the effect of Au^{3+} concentration on the morphology of nanoplates, the concentration of Au^{3+} was increased to 100 μM (Fig. 6.21a) and 200 μM , (Fig. 6.21b) while maintaining Au: PDADMAC ratio at 1:10.

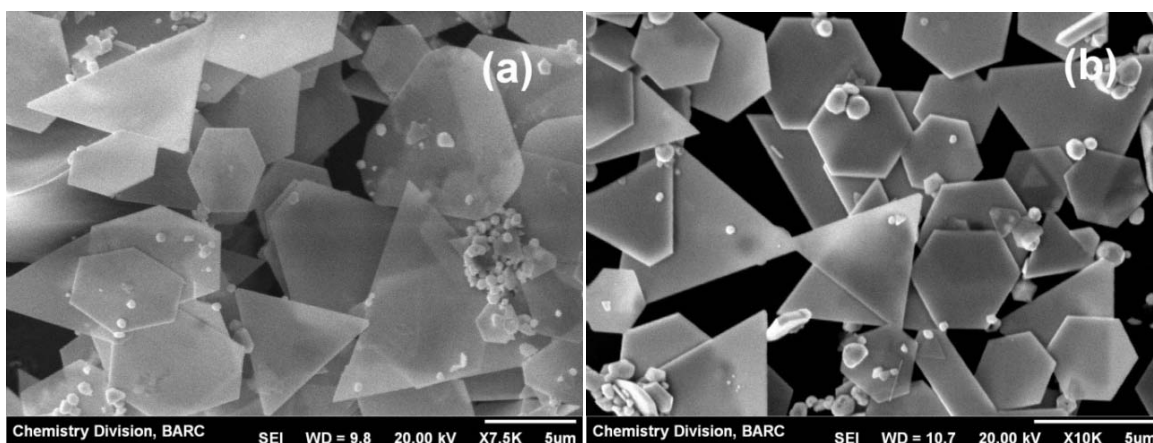


Fig. 6.21: SEM images of the nanoplates synthesized at different concentrations of Au and PDADMAC. (a) 100 μM Au and 1 mM PDADMAC; (b) 200 μM Au and 2 mM PDADMAC

Under these conditions, smaller nanoplates with average edge length of 10 μm and 5 μm are formed respectively, but, most importantly, these nanoplates did not exhibit the concave structure. When the concentration of Au^{3+} is increased to 100 μM and 200 μM , the equilibrium shifts towards the right and reduction proceeds at a much faster rate than oxidative etching, resulting in the formation of normal nanoplates. It may be noted that when

the concentration of Au^{3+} is increased we are also increasing the concentration of PDADMAC (fixed Au: PDADMAC ratio) which provides Cl^- to the solution and therefore the rate of backward oxidation reaction should increase. But, it has been reported that the presence of O_2 is important for the oxidation process in addition to the availability of Cl^- [225]. The concentration of dissolved O_2 in the solution remains more or less the same even when the concentration of Au^{3+} and PDADMAC is varied; therefore, the rate of backward reaction is limited by the amount of O_2 available in the solution and does not increase by the introduction of more Cl^- through PDADMAC. Hence, the forward reduction proceeds faster than the reverse oxidation and normal nanoplates are obtained. Although, it is difficult to quantify the rates of oxidation and reduction at this point of time, the delicate balance between the two processes decides the final structure of the nanoplates.

6.5 Conclusions

Two green strategies, namely, gamma irradiation strategy and photochemical strategy were developed for synthesis of gold nanoparticles. Here, the transients species produced by gamma radiolysis or the excited states formed during photolysis brings about the reduction of Au^{3+} to zero valent state obviating the need of any chemical reducing agent. In these studies, PDADMAC was employed as a capping agent that not only imparts stability to the colloidal system but also acts as shape-directing agent and dictates the ultimate shape of the synthesized nanoparticles. Spherical and non spherical gold nanoplates could be synthesized in excellent yield by adjusting reaction conditions like Au^{3+} /PDADMAC ratio and dose rate of irradiation. The photochemical method, which is similar to the radiolytic method, in addition to the synthesis of normal nanoplates, could also produce *concave* nanoplates by subtle variation in the process conditions.

References

- [1] Spinks J. W. T., Woods R. J. (1990) An introduction to Radiation Chemistry, 3rd edition, John-Wiley, New York-London-Sydney.
- [2] CRU Report (1980) Radiation Quantities and Units, ICRU Publications, 33.
- [3] CRU Report (1984) Radiation Dosimetry: Electron with energies between 1 and 50 MeV, ICRU Publications, 37.
- [4] Laughlin J. S., Gennes S. (1966) Radiation Dosimetry, 2nd Edition, Academic Press, New York, Vol.2.
- [5] Domen S. R. (1987) The dosimetry of Ionizing Radiation, Academic Press, New York, Vol 2.
- [6] Holm N.W., Berry R.J. (1970) Manual on Radiation Dosimetry, Marcel Dekker, New York.
- [7] Buxton G. V., Greenstock C. L., Hellman W. P. Ross A. B. (1988) J. Phys. Chem. Ref. Data. 17, 513.
- [8] Buxton G. V. (1968) Radiat. Res. Rev. 1, 209.
- [9] Hart E. J., Anbar M. (1970) The Hydrated Electron, Wiley Interscience, New York.
- [10] Wisenfield J. M., Ippen E. P. (1980) Chem. Phys. Lett. 73, 43.
- [11] Sworski T. J. (1954) J. Am. Chem. Soc. 76, 4786.
- [12] Chapiro A. (1962) Radiation Chemistry of Polymeric Systems, Interscience, John-Wiley, New York-London, New York.
- [13] Saito K., Sugo T. (2001) Radiation chemistry: present status and future trends, Elsevier Science, Amsterdam-London-New York-Oxford-Paris-Shanon-Tokyo, 671.
- Charlesby A. (1960) Atomic Radiation and Polymers, Pergamon Press, New York.
- [14] Uezu K., Saito K., Furusaki S., Sugo T., Ishigaki I. (1992) Radiat. Phys. Chem. 40, 31.
- [15] Eisenberg A. (1980) Ions in polymers Adv. in Chem. Ser. 187.

- Farhataziz, Rodgers M. A. J. (1987) *Radiation Chemistry*, VCH Pub. Inc., New York.
- [16] Samsonov G. V., Kuznetsova N. P. (1992) *Adv. Polym. Sci.* 104.
- Pikaev A. K., Woods R. J. (1994) *Applied Radiation Chemistry: Radiation Processing*, John-Wiley & Sons Inc., New York, 341.
- [17] Bensasson R. V., Land E. J., Truscott T. G. (1983) "Flash Photolysis and Pulse Radiolysis: Contributions to the Chemistry of Biology and Medicine", Pergamon Press, Oxford.
- [18] Tabata Y. (1991) "Pulse Radiolysis", (Eds. Tabata Y.) CRC Press, Boca Raton.
- [19] Keene J. P. (1972) *Quedeini del' Area di Ricera dell'Emilia Romagna* 1, 63.
- [20] Schmidt K. H., Buck W. L. (1966) *Science* 151, 70.
- [21] Smaller B., Remko J. R., Avery E. C. (1968) *J. Chem. Phys.* 48, 5174.
- [22] Schnabel W. (1986) *Radiat. Phys. Chem.* 28, 303.
- [23] Belloni J, Mostafavi M, Remita H, Marignier JL, Delcourt MO. (1998) *New J Chem*; 1239.
- [24] Sakamoto M, Fujistuka M, Majima T. (2009) *J Photochem Photobiol C: Photochem Rev*; 10: 33.
- [25] Mostafavi M, Douki T (2008) *Radiation Chemistry: From basics to applications in material and life sciences*. EDP Sciences 97.
- [26] Wishart J F, Rao B S M, (2010) *Recent Trends in Radiation Chemistry*, Singapore: Word Scientific 347.
- [27] Tatsul Sato and Richard Ruch, (1980) *Stabilization of colloidal dispersion by polymer adsorption*. Marcel Dekker Inc., New York,
- [28] D.H. Napper, (1983) *Polymeric Stabilization of Colloidal Dispersions*. Academic Press, London.
- [29] Y. Sun, B. Mayers, T. Herricks, Y. Xia, (2003), *Nano Lett.* 3, 955.

- [30] N. R. Jana, L. Gearheart, C. J. Murphy, (2001), *J.Phys. Chem. B* 105, 4065
- [31] Gou, L.; Murphy, C. J. (2005) *Chem. Mater.*, 17,3668.
- [32] Hopwood F. L., Philips J. T. (1938) *Proc. Phys. Soc. (London)* 50, 438.
- [33] Hopwood F. L., Philips J. T. (1939) *Nature* 143, 640.
- [34] Hopwood F. L. (1940) *British. J. Radiol.* 13,221.
- [35] Collison E., Dainton F. S., McNaughton G. S. (1957) *Trans. Faraday. Soc.* 53, 357.
- [36] Fox M., Alexander P. (1955) *J. Chim. Phys.* 52, 710.
- [37] Ballantine D. S., Manowitz B. (1956) *Brookhaven National Laboratories* 389 (T-73).
- [38] Khenokh M. A. (1941) *Zhur. Obschchel Khim.* 11, 776.
- [39] Khenokh M. A. (1947) *Zhur. Obschchel Khim.* 17, 1024.
- [40] Alexander P., Fox M. (1952) *Nature* 169, 572.
- [41] Alexander P., Fox M. (1953) *J. Chim. Phys.* 50, 415.
- [42] Alexander P., Fox M. (1954) *Trans. Faraday Soc.* 50, 605.
- [43] Charlesby A., Alexander P. (1955) *J. Chim. Phys.* 52, 694.
- [44] Charlesby A. (1960) *Atomic Radiation and Polymers*, Pergamon Press, New York.
- [45] Dole M. (1972) *The Radiation Chemistry of Macromolecules*, Academic Press, New York-London.
- [46] Farhataziz, Rodgers M. A. J. (1987) *Radiation Chemistry*, VCH Pub. Inc., New York.
- [47] Pikaev A. K., Woods R. J. (1994) *Applied Radiation Chemistry: Radiation Processing*, John-Wiley & Sons Inc., New York, 341.
- [48] Sanju Francis, Manmohan Kumar, Lalit Varshney (2004) *Radiat. Phys.Chem* 69, 481.
- [49] Y. K. Bhardwaj, Virendra Kumar, S. Sabharwal, (2003) *J. Appl. Polym. Sci*, 88, 730.
- [50] Virendra Kumar, N. K. Goel, Y. K. Bhardwaj, S. Sabharwal, L. Varshney, (2012) *Sep. Sci. Technol.* 47(13), 1937.

- [51] N. K. Goel, Virendra Kumar, Y. K. Bhardwaj, S. Pahan, S. Sabharwal, (2011) *J. Hazard. Mater.*, 193, 17.
- [52] Virendra Kumar, Y.K. Bhardwaj, S.N. Jamdar, N.K. Goel, S. Sabharwal (2006) *J. Appl. Polym. Sci.*, 102, 5512.
- [53] Y.K. Bhardwaj, H. Mohan, S. Sabharwal, A.B. Majali, (2000) *Radiat. Phys.Chem.* 58, 373.
- [54] Y.K. Bhardwaj, H. Mohan, S. Sabharwal, T. Mukherjee, (2001) *Radiat. Phys.Chem.* 62, 29.
- [55] V. Kumar, Y. K. Bhardwaj, S. Sabharwal, H. Mohan, (2003) *J. Radiat.Res.*, 44, 161.
- [56] V. Kumar, Y. K. Bhardwaj, S. Sabharwal, H. Mohan, (2004) *J. Radiat.Res.*, 45, 291.
- [57] N. K. Goel, V. Kumar, Y. K. Bhardwaj, J. Biswal, C. V. Chaudhari, K. A. Dubey, S. Sabharwal. (2009) *J. Biomat. Science: Polymer Edition.* 20 (5, 6) 785.
- [58] N. K. Goel, M. S. Rao, V. Kumar, Y. K. Bhardwaj, C. V. Chaudhari, K. A. Dubey, S. Sabharwal. (2009) *Radiat. Phys.Chem.* 78 (6), 399.
- [59] Muller W. (1990) *J. Chromtography.* 510, 133.
- [60] Matoba S., Tsuneda S., Saito K., Sago T. (1995) *Bio/Technology* 13, 795.
- [61] Kibay N., Katkai A., Sugo T., Egawa H. (1993) *J. Appl. Polym. Sci.* 49, 599.
- [62] Hori T., Hashino A., Omori A., Matsuda T., Takasa K., Watanabe K. (1997) *J. Membrane Sci.* 132, 203.
- [63] Iwata H., Saito K., Furusaki S., Sugo T., Okomoto J. (1991) *Biotechnol. Prog.* 7, 412.
- [64] Arai K., (1973) *Block and Graft Copolymers*, John Wiley, New York, 193.
- [65] Battaerd H. A. J., Tregear W. (1967) *Graft Copolymers*, Wiley Interscience, New York, 56.
- [66] Shukla S. K., Shrivatava D. (2003) *J., Polym. Mater.* 20, 207.

- [67] Menlo Park. (1983) Chemical economics handbook, Stanford Research Institute: 581.
- [68] Ottenbrite R M, Ryan W S Jr., (1980), Ind Eng Chem Prod Res Dev.19, 528.
- [69] Butler G B. (1992) Cyclopolymerization and Cyclocopolymerization; New York: Marcel Dekker.
- [70] McCormick C L. (1996), J Polym Sci., 34, 913.
- [71] Wandrey C , Hunkeler D., (1999) Adv .Polym. Sci., 145, 123.
- [72] Fricke H., Morse S. (1927) Am. J. Roentgenol. 18, 430.
- [73] Fricke H., Morse S. (1929) Philos. Mag. 7, 129.
- [74] Fricke H., Hart E. J. (1935) J. Chem. Phys. 3, 60.
- [75] Fielden E. M., Holm N.W. (1970) Manual on Radiation Dosimetry, Dekker, New York, 261.
- [76] ICRU Report 14 (1969) Radiation Dosimetry: X-rays and Gamma rays with maximum Photon Energies Between 0.6 and 50 MeV.
- [77] Fricke H., Hart E. J. (1969) Radiation Dosimetry, Second Edition” Acad., New York, Vol 1 Chap. 12.
- [78] Sehested K. (1970) Manual on Radiation Dosimetry (Eds. Holm N. W., Berry R.J.) Dekker, New York, 313.
- [79] American Society for testing and Materials Standards E, 1026.
- [80] Spinks J. W. T., Woods R. J. (1990) An Introduction to Radition Chemistry. Wiley Interscience New York.
- [81] ICRU Report 35 (1984) Radiation Dosimetry: Electrons with energies between 1 and 50 MeV.
- [82] Patterson L. K. (1987) Radiation Chemistry, Principles and Applications. VCH Publishers Inc., New York, 65.

- [83] Mukherjee T. (1997) Atomic Molecular and Cluster Physics, Narosa Publishers, New Delhi.
- [84] Fielden E. M. (1982) The Study of Fast Processes and Transient Species by Electron Pulse Radiolysis D.Riedel, Dordrecht, 49.
- [85] David B. Williams, Carter, C. Barry, (2009) Transmission Electron Microscopy, 2nd Ed., Springer Series.
- [86] L. Reimer, H. Kohl, (2008)Transmission Electron Microscopy- Physics of Image Formation, 5th Ed., Springer Series.
- [87] D. A. Skoog, F. J. Holler, T. A. Nieman, (1998). Principles of Instrumental Analysis, 5th Ed. Harcourt Brace & Company, USA.
- [88]http://en.wikipedia.org/wiki/Scanning_electron_microscope,<http://mse.iastate.edu/microscopy/>
- [89] Joseph Goldstein (2003). Scanning Electron Microscopy and X-Ray Microanalysis. Springer.
- [90] André Authier (2001), Dynamical Theory of X-Ray Diffraction, International Union of Crystallography & Oxford Science Publication.
- [91] B. E. Warren, (1990), X-Ray Diffraction, Dover Publications.
- [92] Joint Committee on Powder Diffraction Standards (JCPDS), International Centre for Diffraction Data (ICDD), Swarthmore, PA.
- [93] M. Hosokawa, K. Nogi, M. Naito, T. Yokoyama, (2007). Nanoparticle Technology Handbook, 1st Ed., Elsevier, Amsterdam, Netherlands.
- [94] Skoog; et al. (2007). Principles of Instrumental Analysis (6th Ed.). Belmont, CA: Thomson Brooks/Cole. 169.
- [95] Griffiths, P.; de Hasseth, J.A. (2007). Fourier Transform Infrared Spectrometry, 2nd ed. Wiley-Blackwell.

- [96] http://en.wikipedia.org/wiki/Fourier_transform_infrared_spectroscopy.
- [97] Small, Hamish (1989). Ion chromatography. New York: Plenum Press.
- [98] Tatjana Weiss; Weiss, Joachim (2005). Handbook of Ion Chromatography. Weinheim: Wiley-VCH.
- [99] Wunderlich, B. (1990). Thermal Analysis. New York: Academic Press. 137.
- [100] Dean, John A. (1995). The Analytical Chemistry Handbook. New York: McGraw Hill, Inc. 15.1
- [101] Coats, A. W.; Redfern, J. P. (1963). Analyst 88: 906.
- [102] http://en.wikipedia.org/wiki/Thermogravimetric_analysis
- [103] Rosiak J. M. (1994) J. Controlled Release 31, 9.
- [104] Naka Y., Kaetsu I., Yamamoto Y., Hayashi K. (1991) J. Polym. Sci., Part A 29, 1197.
- [105] Kaetsu I., Okubo H., Ito A., Hayashi K. (1972) J. Polym. Sci., Part A 10, 2203.
- [106] Barkalov I.M., Kiryushkin D.P., Pokidova T.S. (1979) Eur. Polym. J. 15, 761.
- [107] Ratner B., Miller I. (1975) J. Polym. Sci. Part A 10, 2425.
- [108] Carenza M., Palma G., Lora S., Filna F. (1976) Eur. Polym. J. 12, 665.
- [109] Hoffman A. S. (1981) Radiat. Phys. Chem. 18, 323.
- [110] Kaetsu I. (1981) Radiat. Phys. Chem. 18, 343.
- [111] Yoshida M., Omichi H., Kubota H., Katakai R. (1993) J. Intel. Mater. Sys. Struc. 4, 223.
- [112] Rosiak J. M. (1991) Radiation Effects on Polymers, American Chemical Society Symposium series 475, Washington DC, Chapter 17, 271.
- [113] Rosiak J. M., Olejniczak J., Pekala W. (1987) Polymers in Medicine 17, 85.
- [114] Leavitt F. C. (1961) J. Poly. Sci. 51, 349.
- [115] Fielden E. M. (1982) Study of Fast Processes and Transient species in Pulse Radiolysis, D. Riedel Publishing, Holland, 59.

- [116] Ellison D. H., Salmon G. A., Wilkinson, F. (1972) Proc. R. Soc. London Ser. A, 328, 23.
- [117] Swallow A. J. (1982) The study of fast processes and transient species by electron pulse radiolysis, D. Riedel Publishing Co. London 289.
- [118] Staudinger H, Heuer W, Berichte. (1934), 67, 1164.
- [119] Butler G B, Angelo R J, (1956). J. Am. Chem. Soc., 78, 4797.
- [120] Butler G B, Angelo R J, (1957). J. Am. Chem. Soc., 79, 3128.
- [121] Butler G B, Bunch R L, (1949). J. Am. Chem. Soc., 71, 3120.
- [122] Butler G B, Bunch R L, Ingley F L, (1952). J. Am. Chem. Soc., 74, 2543.
- [123] Butler G B, Goette R L, (1952). J. Am. Chem. Soc., 74, 1939.
- [124] Butler G B, Goette R L, (1954). J. Am. Chem. Soc., 76, 2418.
- [125] Butler G B, Ingley F L, (1951). J. Am. Chem. Soc., 73, 895.
- [126] Butler G B, Johnson R A, (1954). J. Am. Chem. Soc., 76, 713.
- [127] Matsumoto, A. (2001), Prog. Polym. Sci. 26, 189.
- [128] Butler, G. B. (1992).Cyclopolymerization and Cyclocopolymerization; Marcel Dekker: New York.
- [129] Tuzun, N. S.; Aviyente, V.; Houk, K. N. (2002) J. Org. Chem., 67, 5068.
- [130] Tuzun, N. S.; Aviyente, V. (2002), J. Phys. Chem. A 106, 8184.
- [131] Coates J (2000) Interpretation of infrared spectra, a practical approach. Encyclopedia of Analytical Chemistry. John Wiley & Sons Ltd, Chichester. 10815.
- [132] Khazaei A, Soudbar D, Sadri M, Mohaghegh S M S (2007). Iran. Polym. J. 16 (5) 309.
- [133] Xamena F X L, Areán C O, Spera S, Merlo E, Zecchina A (2004) Catal. Lett. 95 (1–2) 221.
- [134] Saveyna H, Pieter M S, Dentelc H S K, Martinsb J C, Van Der Meerena P (2008), Water Res. 42 2718.

- [135] Lancaster J E, Baccei L, Panzer H P (1976), *J. Polym. Sci Part C Polym. Lett.* 14, 549.
- [136] Assem Y, Greiner A, Agarwal S (2007), *Macromolecules* 28 1923.
- [137] Users Manual TA 3000 System. (1984) Mettler Instrument AG.
- [138] Users Manual. (2005).Mettler – Toledo GmbH
- [139] ASTM E 698. (1979 rev. 1993).
- [140] Kissinger H E. *Anal Chem.* (1957), 29, 1702.
- [141] Freeman E S, Carroll B., (1958), *J Phys Chem.*, 62, 394.
- [142] Coats A W, Redfern, J P., (1965), *J Polym Sci Polym Lett Edn.*, 33, 917.
- [143] Slovak V., *Thermochim. Acta.*,(2001), 372, 175.
- [144] Sawicka M, Storoniak P, Skurski P, Blazejowski J, Rak, J., (2006) *Chemical Physics.* 324, 425.
- [145] Blazejowski J, Kowalewska E., (1986) *Thermochim. Acta.* 105, 257.
- [146] Lubkowski J, Blazejowski J., (1990) *Thermochim. Acta.*, 157, 259.
- [147] Dokurno P, Lubkowski J, Blazejowski J., (1990), *Thermochim. Acta.*, 31, 165.
- [148] Skurski P, Jasionowski M, Blazejowski J., (1998), *J. Therm. Anal.*, 54, 189.
- [149] Blazejowski J, Krzyminski K, Storoniak P, Rak J., (2000), *J. Thermal Anal. Calorim.*, 60, 927.
- [150] ASTM Test Method E1356-03(2006). ASTM International.
- [151] DIN 53765: Prufung von Kunststoffen und Elastomeren, Thermische Analyse von Polymeren, Dynamische Differenzkalorimetrie (DDK).
- [152] Richardson M J., (1989), *Compr. Polymer Science.*, Vol 1, Pergamon, Oxford, 867.
- [153] Sanders J P, Gallagher P K., (2002), *Thermochim. Acta.*, 388, 115.
- [154] Matsumoto A. (2001), *Prog. Polym. Sci.* 26, 189.
- [155] Odian G. (1991).*Principles of polymerization.* 3rd Ed. New York: Wiley, 266.
- [156] Francis S et. al. (2007), *Eur. Polym. J.* 43, 2525.

- [157] Benita, S. (1996) *Microencapsulation: Methods and Industrial Applications*; Marcel Dekker, New York.
- [158] Kondo, A. (1979) *Microcapsule Processing and Technology*; Marcel Dekker, New York.
- [159] Chang, T. M. S. (1964). *Science*, 146, 524.
- [160] Mimura, H.; Ohta, H.; Akiba, K.; Wakui, Y.; Onodera, Y. (2002). *J. Nucl. Sci. Technol.* 39, 1008.
- [161] Mimura, H.; Ohta, H.; Akiba, K.; Onodera, Y. (2001). *J. Nucl. Sci. Technol.*, 38, 342-348.
- [162] Bucio, E., Burillo, G., (2007), *Radiat. Phys. Chem.* 76, 1724.
- [163] Yessica, S., Ramírez-Fuentes, Bucio, E., Burillo, G., (2007) *Nucl. Instr. Meth. Phys. Res. B* 265, 183.
- [164] Odian, G., (1991) *Principles of polymerization*, 3rd Ed. New York: Wiley.
- [165] Babkin, I, Yu., Gordeyev, Yu, M., Kitayev, K, N., Kovalev, B, A., (1980) *Polymer science U.S.S.R.* 22, 1908.
- [166] Grushevskaya, L, N., Aliev, R, E., Kabanov, V, Ya., (1990). *Radiat. Phys. Chem.* 36, 475.
- [167] Yoshida, R., Uchida, K., Kaneko, Y., Sakai, K., Kikuchi, A., Sakurai, Y., Okano, T., (1995) *Nature* 374, 240.
- [168] Guang-Jin Wang.; Liang-Yin Chu.; Ming-Yu Zhou.; Wen-Mei Chen. (2006). *J. Memb. Sci.*, 284, 301.
- [169] M. C. Daniel, D. Astruc, (2004), *Chem. Rev.* 104, 293.
- [170] A.J. Haes and R.P. Van Duyne, (2002) *J. Am. Chem. Soc.* 124, 10596.
- [171] K. Imura, T. Nagahara and H. Okamoto, (2006) *Appl. Phys. Lett.* 88, 23104.
- [172] X. Sun, S. Dong and E. Wang, (2004) *Angew. Chem. Int. Ed.* 43, 6360.

- [173] Andrea R. Tao, Susan Habas, and Peidong Yang (2008) *Small* 4, No. 3, 310.
- [174] Younan Xia, Yujie Xiong, Byungkwon Lim, and Sara E. Skrabalak *Angew. Chem. Int. Ed.*, 48, 60. (2009)
- [175] Millstone J E, Hurst S J, Metraux G S, Cutler J I, Mirkin C A (2009) *Small* 5:646.
- [176] T. S. Ahmadi, Z. L. Wang, T. C. Green, A. Henglein, M. A. El-Sayed, (1996), *Science* 272, 1924.
- [177] R. Narayanan, M. A. El-Sayed, (2005) *J. Phys. Chem. B* 109, 12663
- [178] A. Zecchina, E. Groppo, S. Bordiga, (2007) *Chem. Eur. J.* 13, 2440.
- [179] L. M. Falicov, G. A. Somorjai, (1985), *Proc. Natl. Acad. Sci. USA* 82, 2207.
- [180] A.-C. Shi, R. I. Masel, (1989), *J. Catal.* 120, 421.
- [181] S. Link and M.A. El-Sayed, (1999) *J. Phys. Chem. B.* 40, 4212.
- [182] M. A. El-Sayed, (2001), *Acc. Chem. Res.* 34, 257.
- [183] T. R. Jensen, L. Kelly, A. Lazarides, G. C. Schatz (1999), *J. Cluster Sci.* 10, 295.
- [184] J. P. Kottmann, O. J. F. Martin, D. R. Smith, S. Schultz, (2001), *Phys. Rev. B* 64, 235402.
- [185] Pinal C. Patel, and Chad A. Mirkin (2010), *Angew. Chem. Int. Ed.* 49, 3280.
- [186] J. Kim, S. Cha, K. Shin, J. Y. Jho, J. C. Lee, (2004), *Adv. Mater.* 16, 459.
- [187] F. Kim, J. H. Song, P. D. Yang, (2002), *J. Am. Chem. Soc.* 124, 14, 316.
- [188] B. D. Busbee, S. O. Obare, C. J. Murphy (2003), *Adv. Mater.* 15, 414.
- [189] W. O. Milligan, R. H. Morriss, (1964), *J. Am. Chem. Soc.* 86, 3461.
- [190] T. K. Sau, C. J. Murphy, (2004), *J. Am. Chem. Soc.* 126, 8648.
- [191] Y. G. Sun, Y. N. Xia, (2003) *Adv. Mater.* 15, 695.
- [192] G. S. Metraux, Y. C. Cao, R. C. Jin, C. A. Mirkin (2003), *Nano Lett.* 3, 519.
- [193] S. S. Shankar, A. Rai, B. Ankamwar, A. Singh, A. Ahmad, M. Sastry, (2004), *Nat. Mater.* 3, 482.

- [194] J. Belloni, M. Mostafavi, H. Remita, J.L. Marignier and M.O. Delcourt, (1998) *New J. Chem.* 22 1239.
- [195] J. Belloni, (2006) *Catal. Today* 113 141.
- [196] A. Henglein and D. Meisel, (1998) *Langmuir* 14 7392.
- [197] M. Treguer, C. De Cointet, H. Remita, J. Khatouri, M. Mostafavi, J. Amblard, J. Belloni and R.D. Keyzer, (1998) *J. Phys. Chem. B*, 102 4310.
- [198] Z.P. Qiao, Y. Xie, Y.T. Qian and Y.J. Zhu, (2000) *Mater. Chem. Phys.*, 62, 88.
- [199] Q. Jiang, Z. Jiang, L. Zhang, H. Lin, N. Yang, H. Li, D. Liu, Z. Xie and Z. Tian, (2011) *Nano Res.* 4, 612.
- [200] H. Chen, Y. Wang, and S. Dong, (2007) *Inorg chem.* 46 10587.
- [201] Kan C, Zhu X, Wang G (2009) *J. Phys. Chem. B.* 110:4651.
- [202] Shankar SS, Rai A, Ahmad A, Sastry M (2005) *Chem. Mater.* 17:566.
- [203] A. Miranda, E. Malheiro, E. Skiba, P. Quaresma, P.A Carvalho, P. Eaton, B.D. Castro, J.A. Shelnutt and E. Pereira, (2010) *Nanoscale* 2, 2209.
- [204] D.A. Porter and K.E. Easterling, (1981) *Phase transformation in metals and alloys*, Chapman and Hall: New York.
- [205] G.Z. Wulff, (1901) *Zeitschrift fuer Kristallographie und Mineralogie* 34, 449.
- [206] C. Herring, (1951) *Phys. Rev.* 82, 87.
- [207] Kawasaki H, Nishimura K, Arakawa R (2007) *J. Phys. Chem. C* 111:2683.
- [208] Lee J H, Kamada K, Enomoto N, Hojo J (2008) *Cryst. Growth Des.* 8 2638.
- [209] C. Lofton and W. Sigmund, (2005) *Adv. Funct. Mater.* 15 1197.
- [210] J. L. Elechiguerra, J. Reyes-Gasga and M. J. Yacaman, (2006) *J. Mater. Chem.* 16 3906.
- [211] B. Lim, P.H.C. Camargo and Y. Xia, (2008) *Langmuir*, 24, 10437.
- [212] Zhang Q, Li N, Goebel J, Lu Z, Yin Y (2011) *J. Am. Chem. Soc.* 133:18931.

- [213] Zhang H, Jin M, Xia Y (2012) *Angew. Chem. Int. Ed.* 51:7656.
- [214] Guo ZR, Zhang Y, Xu AQ, Wang M, Huang L, Xu K, Gu N (2008) *J. Phys. Chem. C* 112:12638.
- [215] Wang L, Wu X, Li X, Wang L, Pei M, Tao X (2010) *Chem Commun* 46:8422.
- [216] Xiong Y, Washio I, Chen J, Cai H, Li ZY, Xia Y (2006) *Langmuir* 22:8563.
- [217] Lee J H, Kamada K, Enomoto N, Hojo J (2008) *Cryst. Growth Des.* 8 2638.
- [218] Chen H, Wang Y, Dong S (2007) *Inorg chem.* 46:10587.
- [219] Jiang Q, Jiang Z, Zhang L, Lin H, Yang N, Li H, Liu D, Xie Z, Tian Z (2011) *Nano Res.* 4:612.
- [220] M. Tsuji, M. Hashimoto, Y., Nishizawa, Y., Kubokawa, M., Tsuji, T., 2005. *Chem. Eur. J.* 11, 440.
- [221] Tian N, Zhou ZY, Sun SG (2008) *J. Phys. Chem. C.* 112:19801.
- [222] Lee SW, Chen SO, Sheng WC, Yabuuchi N, Kim YT, Mitani T, Vescovo, Shao-Horn Y (2009) *J. Am. Chem. Soc.* 131:15669.
- [223] Zhang H, Jin M, Xia Y (2012) *Angew. Chem. Int. Ed.* 51:7656.
- [224] Wiley B, Herricks T, Sun Y, and Xia Y (2004) *Nano Lett.* 4:2057.
- [225] Xiong Y, Chen J, Wiley B, Xia Y, Aloni S, Yin Y (2005) *J. Am. Chem. Soc.* 127:7332.
- [226] Im SH, Lee YT, Wiley B, Xia Y (2009) *Angew. Chem. Int. Ed.* 44:7656-7673.
- [227] Wang L, Wu X, Li X, Wang L, Pei M, Tao X (2010) *Chem Commun* 46:8422.
- [228] Luo, Y (2007) *Mater Lett.* 61:2164.
- [229] Patil AB, Lanke SR, Deshmukh KM, Pandit AB, Bhanage BM (2012) *Mater Lett.* 79:1.
- [230] Pienpinijtham P, Han XX, Suzuki T, Thammacharoen C, Ekgasit S, Ozaki Y (2012) *Phys. Chem. Chem. Phys.* 14:9636.
- [231] Li C, Shuford KL, Chen M, Lee EJ, Cho SO (2008) *ACS Nano* 2:1760.
- [232] Carmichael ES, Gruebele M (2009) *J. Phys. Chem. C.* 113:4495.

[233] Han M Y and Quek C H (2000) *Langmuir* 16 362.

[234] Longenberger L and Mills G (1995) *J. Phys.Chem.* 16, 362.

[235] Kurihara K, Kizling J, Stenius P and Fendler J. H. (1983) *J. Am. Chem. Soc.* 105 2574.

[236] Eustis S, Hsu H and El-Sayed M A (2005) *J. Phys. Chem. B* 109 4811-4815.